8-2009

Nodulin 26-like Intrinsic Protein NIP2;1 and NIP7;1: Characterization of Transport Functions and Roles in Developmental and Stress Responses in Arabidopsis

Won-Gyu Choi
University of Tennessee - Knoxville

To the Graduate Council:

I am submitting herewith a dissertation written by Won-Gyu Choi entitled "Nodulin 26-like Intrinsic Protein NIP2;1 and NIP7;1: Characterization of Transport Functions and Roles in Developmental and Stress Responses in Arabidopsis." I have examined the final electronic copy of this dissertation for form and content and recommend that it be accepted in partial fulfillment of the requirements for the degree of Doctor of Philosophy, with a major in Biochemistry and Cellular and Molecular Biology.

Daniel M. Roberts, Major Professor

We have read this dissertation and recommend its acceptance:

Bruce McKee, Elizabeth Howell, Albrecht von Arnim

Accepted for the Council:

Carolyn R. Hodges

Vice Provost and Dean of the Graduate School

(Original signatures are on file with official student records.)

To the Graduate Council:

I am submitting herewith a dissertation written by Won-Gyu Choi entitled “Nodulin 26-like Intrinsic Protein NIP2;1 and NIP7;1: Characterization of transport functions and roles in developmental and stress responses in Arabidopsis” I have examined the final electronic copy of this dissertation for form and content and recommend that it be accepted in partial fulfillment of the requirements for the degree of Doctor of Philosophy, with a major in Biochemistry, Cellular and Molecular Biology.

Daniel M. Roberts, Major Professor

We have read this dissertation
and recommend its acceptance:

Bruce McKee

Elizabeth Howell

Albrecht von Arnim

Accepted for the Council:

Carolyn R. Hodges
Vice Provost and Dean of the
Graduate School

Nodulin 26-like Intrinsic Protein NIP2;1 and NIP7;1: Characterization of transport functions and roles in developmental and stress responses in Arabidopsis

A Dissertation Presented for

the Doctor of Philosophy

Degree

The University of Tennessee, Knoxville

Won-Gyu Choi

August 2009

ACKNOWLEDGEMENTS

I would like to express my deep appreciation for my mentor Dr. Daniel M. Roberts who has been more than just a principal investigator. I first came to know about him from his first graduate student Suk-Heung Oh, who interestingly happens to be my first boss during the pursuit of my Masters degree in Korea. The first few initial meetings with Dan were interesting in a way since I couldn't understand him due to my poor language skills in English. This however didn't stop him from transforming me into a good scientist as he saw one, all the time during these past seven years. All this was possible due to his exceptional patience and disciplined training that he imparted both inside and outside the working place, which now has become my first home. Among all the things that I learned from him, his saying about "Let the plants tell you what the results are rather than trying to see results that you might want to see" will especially enlighten me in the path to success. This wonderful journey and learning process has all been possible due to his trust and confidence in me.

I would like to thank my committee members, Dr. Bruce McKee, Dr. Liz Howell, and Dr. Albrecht von Arnim, who have been outstandingly supportive, instrumental and critical of all my works. All the committee meetings, individual attention and insightful advices have helped me build up a sound career not only constrained to science related objectives.

I would like to share a part of my successful career with my friends/labmates who kept the working atmosphere more like home. I still can't forget all the precious

time spent with Jim, Eric and Ian, who I guess today will also be remembering me in some way. A special thanks to Eric will always made sure to make each day a memorable one with all his amusing acts. Our cultural differences couldn't prevent us from sharing the knowledge of science and brotherhood. I would also like to thank my current labmates; Jin-Hwa, Pintu, and Ansul. They are simply awesome and mean more than good friends, and are my family. I will always continue to cherish the memories of all the priceless moments spent with them in the lab and outside. I must also thank Tian and John for sharing good moments and making things lighter. I wish them all the success in their careers.

Finally, I would like to thank my caring wife Su-Hwa and son Alex who have been patient and understanding during this developmental process. Without them it wouldn't have been possible for me to bring all this together.

ABSTRACT

Nodulin-intrinsic proteins (NIPs) are plant-specific, water and solute transporters with homology to soybean nodulin 26. In this study, it is shown that Arabidopsis *NIP2;1* (*AtNIP2;1*) expression is acutely stimulated upon waterlogging (70-fold in whole seedlings within 1 hr) and hypoxia (> 1000-fold in roots within 2 hr). Subcellular localization of a AtNIP2;1::YFP fusion protein shows localization to the plasma membrane. Analysis of AtNIP2;1 protein in *Xenopus* oocytes shows that it is a transporter of lactic acid, a fermentation end product. Experiments with T-DNA insertional mutants in the *AtNIP2;1* promoter showed that reduced *AtNIP2;1* expression induced higher lactic acid accumulation in roots compared to wild type, both under normoxic and hypoxic conditions. Under normal growth conditions, *atnip2;1* mutants grew normally but showed subtle changes in root morphology with increased numbers of lateral roots as well as increased primary root length and mass. Surprisingly, these T-DNA insertional mutants showed enhanced survival after severe hypoxia compared to wild type plants. Microarray analysis of a mutant (*atnip2;1-1*) and wild type roots showed that over 1300 transcripts were significantly upregulated in response to oxygen deprivation. Some genes were uniquely upregulated both under normoxia (54 genes) and hypoxia (14 genes) only in *atnip2;1-1* roots. Overall, the data suggest that *AtNIP2;1* is anaerobic-induced gene that encodes a lactic acid transporter, and may play a role in adaptation to lactic fermentation under anaerobic stress. Experiments with a second Arabidopsis NIP, *AtNIP7;1* revealed specific expression in flowers,

especially in developing pollen grains. A T-DNA insertional mutant (*atnip7;1-1*) showed no apparent defects in flower development under normal growth conditions. However, the mutant showed defects in pollen tube growth in the absence of boric acid, a known transport substrate for NIPs. Overall, these observations suggest that AtNIP7;1 might be involved in boric acid uptake necessary for pollen development in Arabidopsis.

COMPREHENSIVE ABSTRACT

Nodulin 26 intrinsic proteins (NIPs) are plant-specific, highly conserved water and solute transport proteins with structural and functional homology to soybean nodulin 26. *Arabidopsis thaliana* contains nine NIP genes. In the present work, focus has been placed on the two representative Arabidopsis NIPs: NIP2;1 (NIP subgroup I) and NIP7;1 (NIP subgroup II) with respect to their transport activity, tissue, cellular, and subcellular localization, and biological roles in Arabiopsis.

In experiments with AtNIP2;1, it is shown that *AtNIP2;1*, is exquisitely sensitive to water logging and hypoxia stress. Based on quantitative-PCR and promoter::GUS experiments, *AtNIP2;1* is expressed at a low basal level in the root tips, and the vascular bundle of differentiated roots. Transcript levels are elevated acutely and rapidly upon water logging of root or leaf tissues, increasing 70-fold in whole seedlings within the first hour of submersion. After this large initial increase, mRNA levels decline to steady state levels that remain over 10-fold higher by 6 hr post submersion. An even greater induction of *AtNIP2;1* expression was observed upon hypoxia challenge of Arabidopsis seedlings, with a 300-fold increase in *AtNIP2;1* transcript observed by 2 hr after the initiation of oxygen deprivation. GUS stain was predominant in root tissues with an even greater induction (> 1000-fold) of *AtNIP2;1* transcript observed within 2 hr post hypoxic treatment. Experiments with two T-DNA insertional mutants in the promoter of *AtNIP2;1* showed that the reduction of *AtNIP2;1* expression induced over accumulation of lactic acid compared to wild type under normoxic conditions as well as

during anaerobiosis. Under normal normoxic growth conditions, both mutants grew normally but showed subtle changes in root morphology and growth showing increased numbers of lateral roots as well as increased primary root length and mass. Surprisingly, these T-DNA insertional mutants showed increased survival rate (2-3 fold higher than wild type seedlings) after severe hypoxic treatment. The transcriptional profile of the roots of a knockout mutant (*atnip2;1-1*) and wild type plants showed that 54 genes were significantly upregulated in *atnip2;1-1* roots compared to wild type roots under normoxic conditions. Among the 54 genes, the majority (24 genes) appeared to be related to seed or late embryogenesis-induced genes, and six genes appeared to be significantly expressed in hypoxic wild type roots as well. Further analysis of microarray data sets showed that 14 unique genes were significantly upregulated (> 3-fold) only in hypoxic *atnip2;1-1* roots. Interestingly, among the 14 genes, three unique heat shock protein family were highly upregulated. Functional analysis of AtNIP2;1 expressed in *Xenopus* oocytes shows that the protein differs from soybean nodulin 26, showing minimal water and glycerol transport. Instead, AtNIP2;1 transports lactic acid, with a preference for the protonated acidic form of this weak acid. Overall, the data suggest that *AtNIP2;1* is anaerobic-induced gene that encodes a lactic acid transporter, and may play a role in adaptation to lactic fermentation under anaerobic stress.

Experiments with AtNIP7;1 revealed that *AtNIP7;1* is specifically expressed in flowers, especially expression is predominant in developing pollen grains. A T-DNA insertional knockout mutant of *AtNIP7;1* (*atnip7;1-1*) grows normally under normal standard LD conditions. Interestingly, although *atnip7;1-1* showed no apparent defects in flower development, the mutant showed a boric acid-dependent phenotype.

Specifically, *atnip7;1-1* pollen grains show defects of pollen tube growth in the absence of boric acid. Overall, these observations suggest that AtNIP7;1 might be involved in boric acid uptake during flower development in Arabidopsis and may have boric acid transport activity.

TABLE OF CONTENTS

LIST OF TABLES

TABLES **PAGE**

LIST OF FIGURES

FIGURE **PAGE**

FIGURE **PAGE**

FIGURE **PAGE**

FIGURE **PAGE**

LIST OF ABBREVIATIONS

AtNIP2;1, *Arabidopsis thaliana* Nodulin-like intrinsic protein 2;1; ***AtNIP7;1,*** *Arabidopsis thaliana* Nodulin-like intrinsic protein 7;1; **ar/R,** aromatic/arginine; **AQP,** aquaporin; **BCA,** bicinchoninic acid assay; ***CaMV35S*****,** cauliflower mosic virus 35S promoter; **cDNA,** complimentary DNA; **CDPK,** calcium dependent protein kinase; **CHIP,** channel-like intrinsic protein; **CV25,** synthetic peptide based on the 24 amino acids in the C-terminus of AtNIP2;1 protein sequence; **cRNA,** complementary RNA; **Ct,** comparative threshold cycle; **DEPC,** diethylpyrocarbonate; **DIC,** differential interference contrast; **DMSO,** dimethyl sulfoxide; **DTT,** dithiothreitol; $\mathbf{E_a}$, Arrhenius activation energy; **EDTA,** ethylenediaminetetraacetic acid; **ELISA,** enzyme-linked immunosorbent assay; **EM,** electron microscopy; **EtBr,** ethidium bromide; **GUS,** ß-glucuronidase; **KLH,** Keyhole Limpet Hemocyanin; **KO,** knock-out; **MAPK,** mitogen-activated protein kinase (see MPK); **MES,** 2-(*N*-morpholino) ethanesulfonic acid; **MIPs,** Major Intrinsic Proteins; **MOPS,** 3-(*N*-morpholino) propanesulfonic acid; **MS,** Murashige and Skoog basal medium; **NIP,** Nodulin-like intrinsic protein; **NPA,** asparagine-proline-alanine; **ORF,** open reading frame; **PBS,** phosphate buffered saline; **PCR,** polymerase chain reaction; $\mathbf{P_d}$, the diffusion permeability coefficient; **PI,** pre-immune; $\mathbf{P_f}$, the osmotic permeability coefficient; **PM,** plasma membrane; **PMSF,** phenylmethyl sulfonylfluoride; **PVDF,** polyvinylidene fluoride; **Q-PCR,** quantitative, realtime RT-PCR; **RT,** reverse transcriptase; **RT-PCR,** reverse transcription-polymerase chain reaction; **SDS-PAGE,** sodium dodecyl sulfate-polyacrylamide gel electrophoresis; **SEM,** standard error of the

mean; **SM,** symbiosome membrane; **WT,** wild-type; **X-Gluc,** 5-bromo-4-chloro-3-indoyl-ß-D-glucuronide; **YFP,** Yellow Fluorescent Protein

CHAPTER I

INTRODUCTION

Water movement across biological membrane through membrane protein channels

Water is commonly regarded as a fundamental component to life since all vertebrates, invertebrates, microbes, and plants are primarily composed of water. Water flux is crucial within biological systems for homeostatic processes such as maintaining water balance (or osmotic equilibrium), body temperature, generation of turgor pressure, cell volume regulation, and adaptation to osmotic stress (Vokes, 1987; Johansson et al., 2000). Water flow across biological membrane is often described by two distinct physiological terms. The two terms describing membrane permeability of water molecule are the diffusion permeability coefficient (P_d) and the osmotic permeability coefficient (P_f). P_d represents a measure of the water permeability across the phospho lipid bilayer under isoosmotic conditions and P_f reflects a measure of the water permeability exhibited in the presence of an osmotic gradient. The ratio of these two biophysical parameters is used to characterize the predominant pathway of water movement such as simple bilayer diffusion or facilitation by proteinacious membrane channels. The ratio of P_f/P_d is approximately one in simple diffusion, whereas the ratio of P_f/P_d is much greater than one if water moves across biological membranes through

proteinacious membrane channels (Agre et al., 1993; Tyerman, 1999; King et al., 2004). For example, the ratio of $P_f/P_d \geq 7$for tonoplast-enriched vesicles from wheat roots (Niemietz and Tyerman, 1997) and even larger than 7 for aquaporin 1 (AQP1) containing red blood cells (Henzler and Steudle, 1995).

In addition, diffusional water permeability through a lipid bilayer is affected by the membrane lipid organization and shows a high Arrhenius activation energy (E_a > 10 kcal/mol) (Cohen, 1975; Agre et al., 1993; Tyerman, 1999). In contrast to diffusional water transport, proteinacious membrane channel-mediated water permeability shows a reduction in Arrhenius activation energy (E_a < 5 kcal/mol) which is close to the rate of diffusional water movement in an aqueous environment (Agre et al., 1993; Johansson et al., 2000). The more rapid transport rate and lower energy cost of proteinacious channel-mediated transport of water is necessary to facilitate the rapid bulk movement of water associated with multiple physiological processes in animals and plants (Agre et al., 1993; Johansson et al., 2000). This led to the search for integral membrane channel proteins capable of mediating bulk water movement based on osmotic and pressure gradients at a reduced energy cost to allow rapid transport.

Aquaporins: the major intrinsic protein superfamily

The discovery of the aquaporin transport protein family first occurred with the findings of a major bovine lens cell membrane protein known as “MIP” (major intrinsic protein). The bovine MIP protein was initially presumed to function as a gap junctional protein channel (Gorin et al., 1984). More proteins related to bovine MIP were successfully identified by molecular cloning in other mammals (Zhang et al., 1990;

Preston and Agre, 1991; Smith and Agre, 1991; van Hoek et al., 1991; Van Hoek et al., 1992), and the structural similarity between this protein family was noted (Reizer et al., 1993).

The major breakthrough that led to the connection between MIPs and proteinaceous water channels was made by the laboratory of Peter Agre in 1992 (Preston et al., 1992). The Agre lab initially identified a 28-kDa protein that co-purified with the 32-kDa subunit of the human red blood cell Rh polypeptides (Agre et al., 1987; Saboori et al., 1988). Further study of the 28-kDa protein revealed that it is an integral membrane channel protein (Smith and Agre, 1991), and it was initially described as a channel-forming integral protein of 28-kDa or "CHIP28" (Preston and Agre, 1991). Sequence similarity to the previously described bovine lens MIP protein was also found (Preston and Agre, 1991). In a landmark study, Preston et al. (1992) demonstrated that the CHIP28 protein was a membrane water channel. The authors showed that *Xenopus laevis* oocytes injected with *in vitro* transcribed CHIP28 RNA exhibited the hallmarks of proteinaceous water transport activity, including enhancement of P_f by ~8 fold and reduction of activation energy ($E_a \leq 3$ kcal/mol) compared to control oocytes ($E_a >> 10$ kcal/mol). They also showed that the water permeability activity of CHIP28 was completely blocked by mercurial compounds, and that inhibition by mercurials was reversed by incubation with beta-mercaptoethanol. The CHIP28 water channel was subsequently renamed as aquaporin-1 (AQP1) and is recognized as the first characterized integral membrane water channel.

From these initial findings of MIPs and AQP1, additional MIPs were subsequently described in animal, plant and microbial species (Borgnia et al., 1999a).

A separate activity for these proteins in glycerol transport emerged with the observation that the bacterial glycerol facilitator GlpF shows sequence similarity to other MIPs (Sweet et al., 1990). Biochemical studies revealed that GlpF expressed in *Xenopus laevis* oocytes showed rapid and selective transport of glycerol with very low water permeability (Maurel et al., 1994). The functional properties of GlpF channel showed the hallmarks of MIP channels including inhibition of transport by mercurial compounds and exhibition of low activation energy (E_a = 4.5 kcal/mol) (Maurel et al., 1994).

Further structural and functional studies led to the classification of MIPs into two functional groups (Borgnia et al., 1999a). These two subgroups are aquaporin channel proteins that are specific for water transport and multifunctional aquaglyceroporin channel proteins that facilitate the flux of water as well as other small uncharged solutes such as glycerol and urea. For example, a total of 13 human AQPs have been discovered and are divided into these two groups according to their functional properties (Borgnia et al., 1999a; Sorani et al., 2008). The “orthodox” aquaporin subgroup are composed of AQP0 (AQP0 is the original bovine lens MIP), AQP1, AQP2, AQP4, AQP5, AQP6, and AQP8 (King et al., 2004; Sorani et al., 2008), and the aquaglyceroporin group are composed of AQP3, AQP7, AQP9, AQP10, AQP11, and AQP12A (Rojek et al., 2008; Sorani et al., 2008). The importance of some of these genes in transport physiology is apparent from the observation that defects in aquaporins are also associated with human disease and other phenotypes of abnormal water homeostasis (Sorani et al., 2008). For example, aquaporin 2 (AQP2) is involved in vasopressin-dependent concentration of urine (Deen et al., 1994) and mutation of

AQP2 is a major cause of autosomal dominant nephrogenic diabetes insipidus (NDI) (Mulders et al., 1998).

Structural topology and the conserved "hourglass fold" of the MIP superfamily

After AQP1 was functionally characterized (Preston et al., 1992), several attempts were taken to solve the membrane topology and structure of AQP1 by using biochemical and electron microscopic (EM) techniques (Preston et al., 1994), site directed mutagenesis (Jung et al., 1994), and projection of highly ordered two-dimensional (2D) crystals of reconstituted AQP1 in lipid bilayers (Mitra et al., 1994; Jap and Li, 1995). These early studies suggested that AQP1 forms a homotetramer with six transmembrane helices (H1-6 from N-terminus), five loops (loops A-E) with hydrophilic amino- and carboxyl termini exposed to the cytoplasmic side (Fig. 1.1). Two of the loop regions (loopB and E; Fig. 1.1) contain highly conserved asparagine-proline-alanine (NPA) sequence motifs that showed unusual hydrophobicity and were proposed to form part of the pore (Fig. 1.1). The AQP1 sequence and structure also show two-fold symmetrical structural repeat. Helices 1, 2, and 3 of the amino terminus with the first NPA motif show a two-fold symmetry with the helices 4, 5, and 6 and the other NPA motif (Fig. 1.1). Based on low resolution electron diffraction studies, it was suggested that the protein folds and forms a cluster of tilted α-helices with electron densities in the center that were proposed to be the NPA regions. Based on these initial studies, Jung et al. (1994) proposed that each AQP1 monomer forms a water channel pore and that the topology resembles an hourglass with wide cytosolic and extracellular vestibules that contracts within the pore at the center of the bilayer.

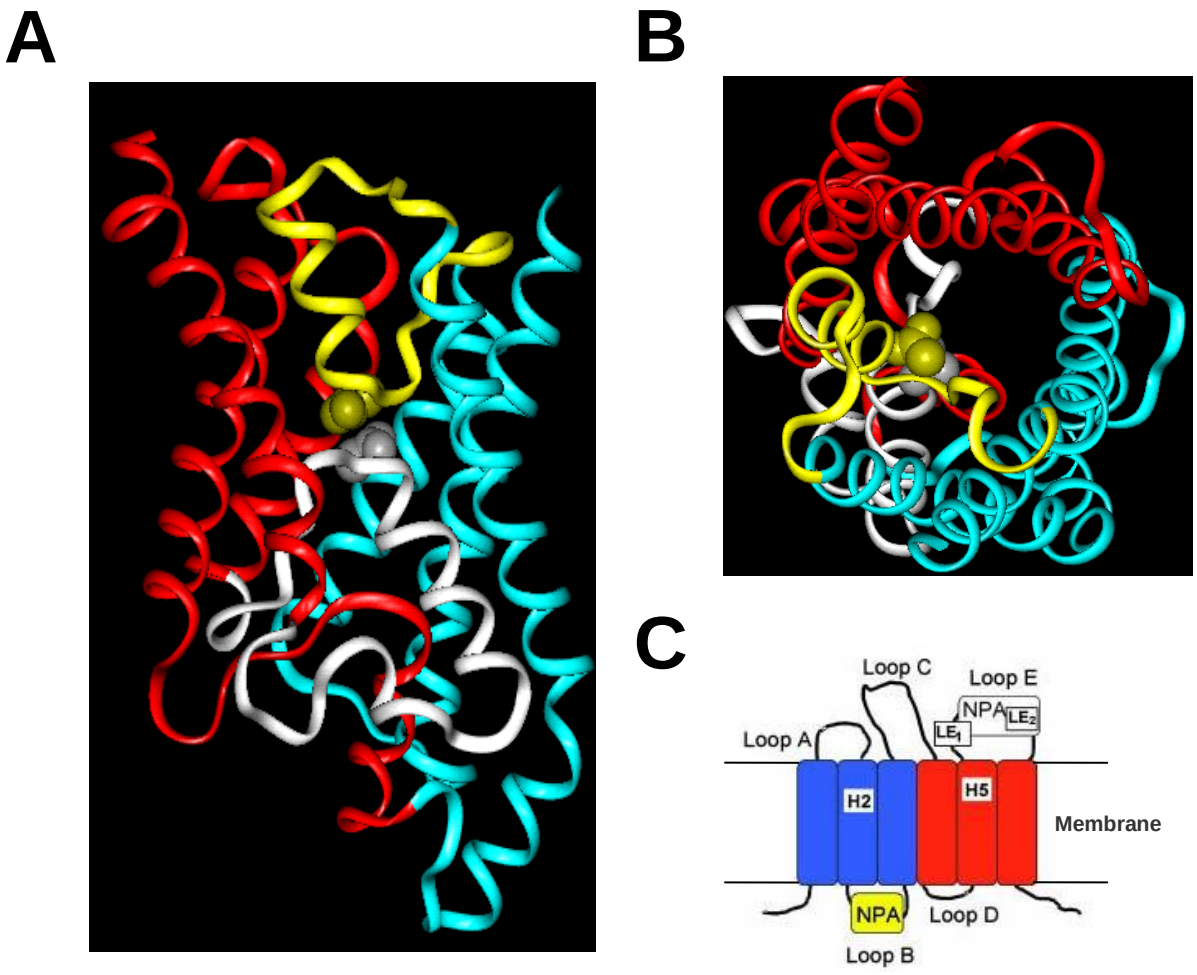

Figure 1.1. Structure and topology of AQP1. A-B. Monomer of the AQP1 shows hourglass shape structure viewed in plane with the membrane (**A**) or from the cytosolic side (**B**) (Wallace et al., 2002; Wallace and Roberts, 2004)(Sui et al., 2001; PDB ID, **1J4N**; models are from Wallace and Roberts, 2004) TM helices 1-3 are shown in blue, and TM helices 4-6 are shown in red. Two pseudo transmembrane helices form the central pore of the structure by the convergence two NPA motifs shown in yellow and white. Asn residues of the NPA region are shown in space filling. **C.** Membrane topology of the MIP superfamily. The highly conserved NPA motifs are shown in yellow and white boxes in loops B and E. The positions of the selective ar/R filter tetrad residues are shown at helix 2 (H2), helix 5 (H5), and loop E (LE_1 and LE_2), respectively.

The structural features of MIPs were better understood after the atomic structure of some MIPs were solved. The first atomic structure of an aquaporin to be solved was that of rat AQP1 isolated from red blood cells which yielded a structure of 3.8 Å resolution by cryo electron crystallography (Murata et al., 2000). After this initial electron crystallographic structure, eight additional MIP atomic structures have been solved by X-ray crystallography, including bovine AQP1 (bAQP1) (Sui et al., 2001), *E. coli* GlpF (Fu et al., 2000; Tajkhorshid et al., 2002), lens specific AQP0 (Gonen et al., 2004; Harries et al., 2004), archaebacterial AQPM (Lee et al., 2005), spinach plant SoPIP2;1 (Tornroth-Horsefield et al., 2006), brain water pore AQP4 (Hiroaki et al., 2006), and hAQP5 (Horsefield et al., 2008). The results of these high resolution structures of MIPs were remarkably consistent with the early predictions of the hourglass model. The X-ray structures show that MIPs consist of a homotetrameric structure with each monomer forming a single transport pore (Fig. 1.1). Each monomer consists of six transmembrane α helices form a right handed tilted α helical bundle (Fig. 1.1). The two NPA boxes form ½ helices that fold back into the membrane to form a seventh “pseudo” transmembrane α helix. The pore is formed at the center of these packed α helical structures.

The two subclasses of the MIP superfamily, aquaporins and aquaglyceroporins, have distinct functional properties even though they share a high degree of structural homology. This functional diversity of the MIPs comes from the selectivity filter aromatic/arginine (ar/R) region, which forms the narrowest constriction within the pore located approximately 8Å above from the NPA motifs towards the extracellular side of the membrane (Fu et al., 2000; Sui et al., 2001). The NPA motifs are contained in the

loops B and E, which fold back into the protein channel and converge at the pore center of the protein. The amide groups of the two Asn residues in the pore center form hydrogen bonds with transported water or glycerol molecules. As a result of the water orientation at the NPA center, the orientation of the neighboring water molecules are constrained, preventing proton flux through the pore via a “proton wire” (Fu et al., 2000; Sui et al., 2001). The AQP1 ar/R constriction region is composed of a tetrad of residues: phenylalanine 58 (F58), histidine 182 (H182), cysteine 191 (C191), and arginine 197 (R197) (Sui et al., 2001). These serve as a size selectivity filter (2.8Å in diameter; see Fig. 1.2), allowing water flux and excluding larger solutes (Sui et al., 2001). At the constriction region, residues H182 and R197, along with the carbonyl backbone oxygen of C191, form hydrogen bond contacts with transported water molecules. In addition, the adjacent cysteine 189 apprears to be the essential site of mercury inhibition, consistent with the proposal that this region is critical for transport (Preston et al., 1993; Zhang et al., 1993). Molecular dynamic (MD) simulation studies also suggest that there is a strong barrier for proton conduction, located near the NPA pore signature region as well as near the ar/R constriction region (de Groot et al., 2003), indicating that both the NPA and ar/R regions are critical for the functional properties of aquaporins.

In case of GlpF, a glycerol facilitator, the H182 and C191 residues of AQP1 are replaced by glycine (G) and phenylalanine (F) (Fu et al., 2000) (Fig. 1.2). These substitutions have critical effects on the characteristic of the ar/R region of GlpF. First, they increase the diameter of the ar/R region of the pore to about 4Å which accommodates larger solutes such as glycerol. Second, the hydrophobicity of the

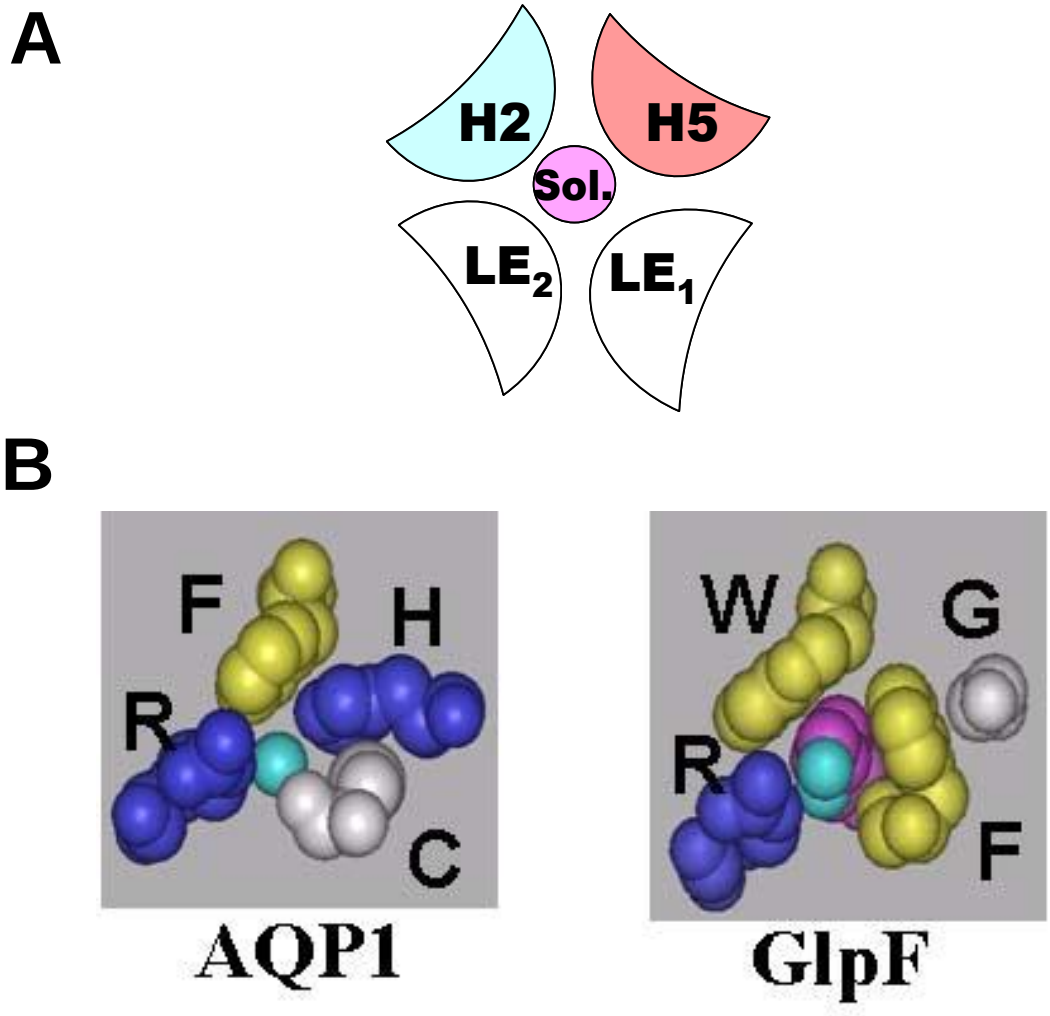

Figure 1.2. Comparison of the ar/R selectivity filter region of AQP1 and GlpF. A. Diagram of Ar/R tetrad model. The helix 2 (H2), helix 5 (H5), loop E_1 (LE_1), and loop E_2 (LE_2) indicate the positions where tetrad residues of the ar/R filter are located. **B.** Homology modeling of the side chains of the aromatic/arginine (ar/R) tetrad of AQP1 and GlpF viewed down the pore axis from the extracellular vestibule. The aqua sphere in AQP1 shows water molecule, whereas the bound glycerol is shown as a magenta (carbon backbone) and aqua (hydroxyl groups) molecue A, ala; C, cys; F, phe; G, gly; H, his; R, arg; V, val; W, trp.

selective filter region is increased with an aromatic wedge formed by the conserved tryptophan and phenylalanine residues. Increased size and hydrophobicity accommodate bulkier hydrophobic solutes such as glycerol as well as resulting in lower water permeation.

Phylogeny and diversity of the MIP superfamily in plants

Since their initial discovery, over 1000 MIP genes have been identified in a wide range of prokaryotic and eukaryotic species. Despite their diverse sequences, the MIP superfamily is proposed to adopt a conserved membrane topology and polypeptide fold (Johansson et al., 2000; Chaumont et al., 2005; Benga, 2009). While MIPs are wide spread and found in nearly all living organisms, the diversity within each organism varies. For example, analysis of bacterial species such as *E. coli* shows only two MIPs: AqpZ and GlpF, an aquaporin and aquaglyceroporin respectively (Heller et al., 1980; Borgnia et al., 1999a; Borgnia et al., 1999b; Calamita, 2000). As discussed above, the human genome contains genes encoding thirteen MIPs that also can be divided into aquaporin and aquaglyceroporin classes. Analysis of the ar/R regions of these proteins show that they possess one of the two classical ar/R motifs as shown in Fig. 1.2. In contrast, plants have a much greater number of MIPs with more diverse pore structures (Wallace and Roberts, 2004; Bansal and Sankararamakrishnan, 2007). For instance, 35 MIP family genes have been found in *Arabidopsis* (Johanson et al., 2001; Quigley et al., 2002), 36 genes have been identified in Maize (Chaumont et al., 2001), and 33 genes have been identified in rice (Sakurai et al., 2005). On the basis of sequence homology, plant MIPs have been classified into four subfamilies: the plasma membrane

intrinsic proteins (PIPs), the tonoplast intrinsic proteins (TIPs), the nodulin26-like intrinsic proteins (NIPs) and a small group named the small and basic intrinsic proteins (SIPs) (Johansson et al., 2000; Chaumont et al., 2005; Maurel et al., 2008). Among 35 genes of MIPs, for example, Arabidopsis contains 13 PIP genes, 10 TIP genes, 9 NIP genes, and 3 SIP genes of SIPs (Fig. 1.3).

In addition to phylogenetic diversity, the predicted ar/R selectivity filters in plant MIPs are also more diverse than animal and microbial MIPs. Based on computational studies and homology modeling, the ar/R selective filters in Arabidopsis MIPs are divided into 8 groups (Wallace and Roberts, 2004), showing ar/R combinations that diverge from classical aquaporins and aquaglyceroporin ar/Rs as shown in Fig. 1.2. In addition, other model plant species such as rice and maize are even more diverse in the ar/R groups showing an additional ninth group which is not found in Arabidopsis MIPs (Bansal and Sankararamakrishnan, 2007). These observations suggest that plant MIPs may have additional transport functions besides water and glycerol.

Analysis of the global expression of Arabidopsis MIPs (Alexandersson et al., 2005) shows that the major MIPs in most plant tissues are the PIP and TIP proteins. The PIPs and TIPs were initially distinguished by their distinct subcellular localization showing that the PIPs are mainly localized in the plasma membrane and TIPs reside mainly in the tonoplast, respectively (Maurel and Chrispeels, 2001; Chaumont et al., 2005; Maurel, 2007; Maurel et al., 2008). Although, most of the PIPs are preferentially expressed on the plasma membrane, some PIPs such as *Zea mays* PIP1s are localized on internal membranes and require hetero-oligomerization for PM localization (Zelazny et al., 2007; Zelazny et al., 2009). For instance, ZmPIP1 is retained in the ER when

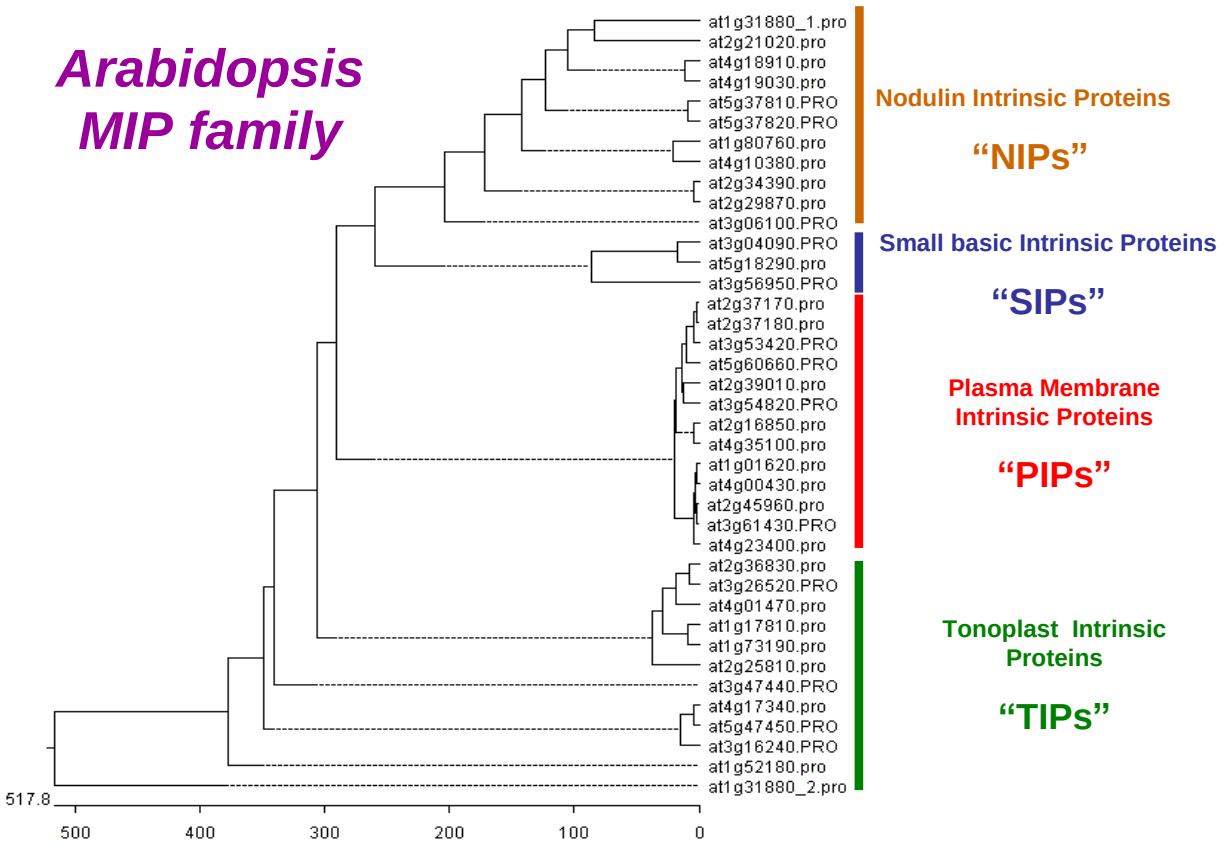

Figure 1.3. The phylogenetic tree of the Arabidopsis MIP family. The 35 full-length MIP subfamily members from the Arabidopsis genome were aligned by the ClustalW algorithm and assembled into a phylogenetic tree using the DNAstar software. The four plant MIP subgroups are indicated to the right of the tree. The members of each subfamily are indicated by their Arabidopsis Genome Initiative (AGI) number. The axis below the tree indicates the relative number of amino acid substitutions. The subfamily designations are based on the nomenclature of Johanson et al. (2001).

transiently expressed in maize protoplasts, whereas ZmPIP2s are normally targeted to the PM. When ZmPIP1s and PIP2s are co-expressed in maize cells, ZmPIP1s form a hetero-oligomer with ZmPIP2 and are trafficked from the ER to the PM suggesting that localization of some MIPs is regulated by protein trafficking.

PIPs form the largest subfamily of plant MIPs, and provide a major pathway for cellular water transport in plants and exhibit a ar/R filter structure typical of orthodox, water-selective aquaporins (Wallace and Roberts, 2004; Chaumont et al., 2005; Bansal and Sankararamakrishnan, 2007; Maurel et al., 2008). They are the only plant MIPs to have the water-selective aquaporin ar/R and have been experimentally shown to transport water and no other solutes. The water-selective transport activity of plant PIPs is also regulated by posttranslational modifications such as phosphorylation and pH gating (Chaumont et al., 2005; Maurel et al., 2008). All plant PIPs contain a highly conserved phosphorylation site in the loop B (Chaumont et al., 2005; Tornroth-Horsefield et al., 2006; Maurel, 2007), and it has been shown that phosphorylation stimulates PIP water transport activity. The atomic structure of SoPIP2;1 shows that phosphorylation of loop B could trigger the opening of the channel by regulating loop D which also contains the site for pH sensing (Tornroth-Horsefield et al., 2006).

The tonoplast membrane of vacuoles is the preferential expression location of the TIPs. Based on immunocytochemical studies using isoform-specific anti-TIP antibodies, it has been shown that the isoforms of the TIPs can be co-expressed in distinct types of vacuoles in the same cell (Maurel and Chrispeels, 2001; Chaumont et al., 2005; Maurel et al., 2008). For example, TIP1 and TIP2 isoforms are preferentially localized to the large lytic vacuoles (Jauh et al., 1998), and AtTIP1;1 is accumulated in

intravacuolar invaginations made of a double tonoplast membrane (Saito et al., 2002). Based on the computational studies of homology modeling of the ar/R filters, TIPs apprear to have high diversity within the pore selectivity regions (Wallace and Roberts, 2004; Bansal and Sankararamakrishnan, 2007). For example, Arabidopsis TIPs show the three distinct ar/R selectivity filters that differ from the classical ar/R constriction filters of aquaporin and aquaglyceroporin (Wallace and Roberts, 2004). TIPs in rice and maize show even higher diversity showing the additional four ar/R constriction filters which are not found in Arabidopsis TIPs (Bansal and Sankararamakrishnan, 2007). Biochemical analyses have demonstrated that the functional properties of TIPs are distinct from PIPs and they transport other substrates such as urea (Liu et al., 2003), and ammonia (Loque et al., 2005), besides showing water permeability (Chaumont et al., 1998). Molecular genetic evidence also shows that Arabidopsis TIP1;1 is capable of transporting reactive oxygen species such as hydrogen peroxide (Bienert et al., 2007). Similar to PIPs, there is evidence that the functional properties of TIPs can be regulated by posttranslational modifications such as phosphorylation. For example, multiple phosphorylations have been shown in α-TIP on serine redidues (Ser 7, Ser 23, and Ser 99) by using *in vitro* kinase assays, and its water permeability is enhanced when *Xenopus laevis* oocytes expressing α-TIP are exposed to cAMP, suggesting phosphorylation by protein kinase A in oocytes (Maurel et al., 1995). In addition, direct evidence by mass spectrometry analysis shows that *Phaseolus vulgaris* PvTIP3;1 is phosphorylated on serine residues within the N- and C-terminal regions (Daniels and Yeager, 2005).

Less is known about the SIP family, but biochemical experiments using specific anti-SIPs antibodies and transient expression of green fluorescent protein (GFP) fused SIPs in protoplasts show all the three SIP homologs in Arabidopsis are mainly localized in the endoplasmic reticulum (ER) (Ishikawa et al., 2005). Based on sequence similarity, the SIP family is subdivided into two subgroups: SIP1 and SIP2 which are conserved in plant species with other MIP subfamilies (Chaumont et al., 2001; Johanson et al., 2001; Quigley et al., 2002). Based on homology modeling, each SIP subgroup possesses distinct putative ar/R selectivity filters from other plant MIPs. Functional analysis has demonstrated that Arabidopsis SIP subgroup I (AtSIP1;1 and AtSIP1;2) has water transport activity (Ishikawa et al., 2005), but other SIP transport substrates remain to be determined.

The NIP (Nodulin 26-like Intrinsic Protein) family represents a structurally and functionally unique, plant specific MIP class. Since NIPs are the major focus of the present work, the history and background of this family is presented below in more detail.

Nodulin 26: an archetype of the NIPs

Nodulin 26 (Nod26) belongs to a subset of nodulin proteins. Nodulins are plant proteins that show root nodule-specific expression, and which are involved in the development, structure, maintenance and overall metabolism of symbiotic nitrogen-fixing root nodules (Legocki and Verma, 1980). Nodules are formed upon infection of legume roots by *Rhizobium* bacteria, which during the nodule organogenesis process invade a specialized plant cell (the infected cell). Bacterial nitrogen fixation takes place within this cell. Within the infected cell, the bacteria become enclosed in a specialized

organelle, known as the symbiosome. The encapsulated bacteria are separated from plant cell cytosol by the plant-derived SM. Nod26 is the major proteinacious component of the SM and constitutes 10-15% of the SM protein mass (Fortin et al., 1987; Weaver et al., 1991; Dean et al., 1999). The identification of Nod26 as a member of the MIP family was made based on structural comparisons with bovine lens MIP (Sandal and Marcker, 1988; Shiels et al., 1988). Functional studies revealed that Nod26 is a multifunctional aquaglyceroporin with a high glycerol transport rate and low intrinsic water permeability, and it was the first aquaglyceroporin to be described (Rivers et al., 1997; Dean et al., 1999). Homology modeling shows that the structure of the ar/R constriction filter of Nod26 is distinct from AQP1 and GlpF, with Val and Ala residues substitution in helix 5 (H5) and loop E_1 positons respectively, resulting in increased pore size and hydrophobicity of this region (Wallace and Roberts, 2004). It was suggested that an aliphatic side chain in the H5 position of the ar/R selectivity filter accounts for glycerol transport and also for a low water transport rate (Wallace et al., 2002; Wallace and Roberts, 2005). Biochemical evidence shows that Nod26 is a major phosphorylation target of a SM bound calcium-dependent protein kinase (CDPK) (Weaver et al., 1991). Phosphorylation of Nod26 occurs on Ser 262 within the cytosolic C-terminal tail (Weaver and Roberts, 1992). When native Nod26 is reconstituted into the liposome vesicles and phosphorylated by CDPK, an increase in liposome P_f occurs suggesting that the water permeability of the protein might be regulated by phosphorylation (Guenther et al., 2003). In addition, the water permeability of Nod26 expressed in *Xenopus laevis* oocytes is stimulated by low pH (Choi and Roberts, 2007), suggesting potential pH-dependent gating of Nod26 similar to other aquaporins. In

addition to transport of water and glycerol, work by Niemietz and Tyerman (2000) suggests that a NH_3 transport activity on symbiosome membranes may also be mediated by Nod26. This may be part of the efflux pathway for fixed nitrogen through the symbiosome.

The NIP subfamily of plant MIPs

Since the initial discovery of nodulin 26 (Fortin et al., 1987), it has become clear that a large number of "Nodulin 26-like" Intrinsic Proteins (NIPs) are found in all land plants from mosses to angiosperms (Wallace et al., 2006). For example, multiple NIPs are found in the sequenced genomes of several plant species such as Arabidopsis, maize, rice and the moss *Physcomitrella patens* (Chaumont et al., 2001; Johanson et al., 2001; Sakurai et al., 2005; Danielson and Johanson, 2008)

In *Arabidopsis*, there are nine members of the NIP subfamily (Johanson et al., 2001). Based on sequence homology and modeling of the ar/R tetrad, Wallace and Roberts divided the nine Arabidopsis NIPs into two subgroups, subgroup I and subgroup II (Wallace and Roberts, 2004). NIP subgroup I in Arabidopsis is composed of six genes encoding AtNIP1;1, AtNIP1;2, AtNIP2;1, AtNIP3;1, AtNIP4;1, and AtNIP4;2 showing an identical ar/R selectivity filter as the classical archetype protein soybean Nod26. NIP subgroup II contains three genes (*AtNIP5;1, AtNIP6;1, and AtNIP7;1*) showing a distinct configuration of the ar/R constriction region that differs from the ar/R tetrad in Nod26 and other NIP subgroup I proteins. In NIP subgroup II, an Ala substitution for a Trp residue (typical of NIP subgroup I) at the helix H2 position of the ar/R filter results in a wider predicted pore, suggesting that NIPs subgroup II

may have different functional properties than NIP subgroup I. This indeed appears to be the case as will be described in the next section.

A larger phylogenetic analysis of NIP genes from a variety of plant species shows that all have representative members of both subgroup I and subgroup II (Wallace et al., 2006), and may even have greater diversity within the NIP subgroup II. For example, in maize, there are four NIP genes (*ZmNIP1;1, ZmNIP2;1, ZmNIP2;2,* and *ZmNIP3;1*) (Chaumont et al., 2001). Based on sequence homology and modeling of the ar/R region, *ZmNIP1;1* is most closely related to *Nod26* and belongs to NIP subgroup I, whereas *ZmNIP3;1* belongs to NIP subgroup II (Bansal and Sankararamakrishnan, 2007). However, ZmNIP2;1 and ZmNIP2;2, while similar to Arabidopsis NIP II proteins, posses a modified ar/R filter with a Gly and a Ser substitution at position H2 and H5 of the ar/R tetrad respectively, compared to Trp (H2) and Val (H5) (NIP I), and Ala (H2) and Ile (H5) (NIP II). This suggests a more recent segregation in NIP evolution (Bansal and Sankararamakrishnan, 2007), and it has been proposed that two different pore classes (NIP II_a and II_b) may be present in some plant species (reviewed in Wallace et al., 2006).

In the case of rice, there are 13 members of the NIP subfamily, that show a similar sequence diversity of the ar/R constriction region based on phylogenetic analysis (Sakurai et al., 2005; Bansal and Sankararamakrishnan, 2007). Among 13 OsNIPs, seven NIPs appear to be closely related to the two Arabidopsis NIP subgroups (NIP subgroup I, OsNIP1;1, OsNIP1;2, OsNIP1;3, OsNIP1;4, and OsNIP1;5; NIP subgroup II_a, OsNIP3;1 and OsNIP3;3). A third NIP subgroup shows ar/R regions with smaller residues (Gly/Ala/Ser/Cys) at both positon of H2 and H5 of the ar/R tetrad

from the two NIP subgroups in Arabidopsis (i.e. similar to NIP subgroup II_b), suggesting that these NIPs are likely to have the widest ar/R diameter (Bansal and Sankararamakrishnan, 2007). The functional significance of this observation became apparent with the genetic characterization of a representative of the third NIP class, OsNIP2;1 (Ma et al., 2007) as discussed below in the next section.

Since the discovery and functional characterization of the first aquaporin from plants (γ-TIP) (Maurel et al., 1993), the functional properties of several plant MIPs have been characterized. These studies have revealed that plant MIPs are important not only in biophysical processes of water transport, but have other transport activities including the transport of other uncharged small metabolites such as glycerol, urea, and ammonia (Chaumont et al., 2005) Thus, the higher number and structural diversity of the plant MIPs apparently lead to a higher functional diversity compared to the animal and microbial MIPs. In the next section, these distinct functional properties of various NIP proteins are summarized.

Functional and physiological properties of the NIPs

As discussed above, soybean Nod26 is a symbiosome-specific protein that forms an aquaglyceroporin with a low water permeability that is stimulated by phosphorylation (Rivers et al., 1997; Dean et al., 1999; Niemietz and Tyerman, 2000; Guenther et al., 2003). Given its multifunctional transport properties (water, glycerol and ammonia), multiple potential biological roles in symbiosis ranging from osmoregulation of the infected cell (based on the high concentration of nodulin 26 and the fact that it is the major organelle in the infected cell [Udvardi and Day, 1997]) to the

efflux of ammonia (Niemietz and Tyerman, 2000). Other nodulin 26 orthologs are present in the symbiosome membranes of other legumes including *Lotus japonicus* (Guenther and Roberts, 2000) and *Medicago truncatula* (Catalano et al., 2004), suggesting that this is a common symbiosis protein. Functional characterization of *Lotus* intrinsic membrane protein 2 (LIMP2 ro LjNod26) in *Xenopus* oocytes shows that it possesses nearly identical transport properties as soybean nodulin 26 including the ability to transport glycerol, and a low but significant water permeability (Guenther and Roberts, 2000). In addition, *in vitro* kinase analysis also shows that the C-terminus of LjNod26 is the target for phosphorylation mediated by CDPK (Guenther and Roberts, 2000; Guenther et al., 2003). In fact nearly all NIP subgroup I proteins have a conserved CDPK phosphorylation site within their carboxyl terminal domains (Table 1.1), suggesting that this may be a common calcium-dependent regulatory site in these proteins.

The first functional characterization of non-legume NIPs came from the analysis of *Arabidopsis* AtNIP1;1 and 1;2, representative of NIP I subgroup (Weig et al., 1997; Weig and Jakob, 2000). It was found that expression of these proteins in *Xenopus* oocytes and yeast resulted in the formation of an aquaglyceroporin channel, similar to nodulin 26 (Weig and Jakob, 2000). Similar nodulin 26-like gene products were subsequently identified from the suspensor ligament of loblolly pine embryo (Ciavatta et al., 2001) as well as seed coats of pea (Schuurmans et al., 2003). Similar to *nodulin 26* and *AtNIP1;1*, all of these genes have been shown to encode functional aquaglyceroporins. However, the biological function of NIP I proteins, and whether water and glycerol are their sole substrates remains unknown.

Table 1.1 Conserved CDPK phosphorylation sites in the carboxyl termini of representative NIP Subgroup I proteins

Protein	Peptide Sequence
Soybean Nod26	I-T-K-S-A-**S-**F-L-K
Lotus japonicas Nod26 (LIMP2)	I-T-K-N-V-**S-**F-L-K
AtNIP1;1	I-T-K-S-G-**S-**F-L-K
AtNIP1;2	I-T-K-S-G-**S-**F-L-K
AtNIP2;1	F-S-K-T-G-**S-**S-H-K
AtNIP4;1	L-T-K-S-A-**S-**F-L-R
AtNIP4;2	L-T-K-S-A-**S-**F-L-R
ZmNIP3;1	I-T-K-S-T-**S-**F-L-K
OsNIP1;1	T-K-L-S-G-**S-**F-L-K

A table showing a list of putative phosphorylation sites of representative NIP I proteins from deduced amino acid sequences in the rice, corn, and *Arabidopsis thaliana* genomes. The putative CDPK phosphorylation epitope (hydrophobic – X – basic – X – X – Ser/Thr) is shown with the predicted phosphorylated residue underlined.

In contrast to NIP I proteins, genetic and biochemical functional data have provided a clearer picture of the function of NIP II_b proteins. For example, work with a rice mutant, that shows defective silicon uptake shows that the defective gene codes for *OsNIP2;1*. Subsequent analysis of OsNIP2;1 in *Xenopus* oocytes shows that it is a metalloid transporter that mediates the uptake of H_4SiO_4 (pK_{a1}=9.84, pK_{a2}=13.2 at 25°C) from soil, a critical nutrient that prevents lodging ("falling over") in rice (Ma et al., 2007). This protein shows localization in the plasma membrane on the distal side of both the exodermis and endodermis of roots, and aids in mediating the uptake of silicon from the soil (Ma et al., 2007). Similar to OsNIP2;1, Lsi6, another member of NIP subgroup II_b in rice, displays silicon distribution in the shoots of rice and shows polar localization in the xylem parenchyma cells of the leaf sheath and leaf blades (Yamaji et al., 2008). Genetic evidence shows knockout of *Lsi6* does not affect the uptake of silicon in the roots, but results in disordered silicon depositon in the shoots of rice, suggesting that this silicon transporter is similar to OsNIP2;1 in terms of silicon transport activity, but plays a distinct physiological role because of different cellular localization (Yamaji et al., 2008).

The findings of Ma et al. (2007) suggest that the transport of uncharged metalloid compounds such as silicic acid (H_4SiO_4) might be a characteristic of NIP II proteins. This was further supported by studies of the NIP II_a proteins in Arabidopsis. For example, Fujiwara's laboratory identified an Arabidopsis mutant that showed defective growth under boric acid limiting conditions (Takano et al., 2006). Subsequent cloning of the gene responsible showed that it is the NIP II_a protein, AtNIP5;1. Recent biochemical and genetic evidence show that Arabidopsis NIP5;1 is

selectively expressed in the roots and shows selective uptake of boric acid (H_3BO_3) in *Xenopus* oocytes (Takano et al., 2006). T-DNA knock-out of *AtNIP5;1* shows root growth defects during development under boron deficient conditions (Takano et al., 2006). Boric acid is a critical nutrient for growth because of its incorporation into, and crosslinking of, the rhamnogalacturonan II pectic polysaccharide in the cell wall (O'Neill et al., 2004). Green fluorescent protein (GFP) tagged NIP5;1 also shows plasma membrane localization in root epidermal, cortical and endodermal cells where it is proposed to aid in boric acid uptake and vascular loading of this nutrient (Takano et al., 2006).

Subsequent work by Tanaka et al. (2008) showed that another NIP II_a protein, AtNIP6;1 is selectively expressed in the shoot, but not in roots and its transcript is accumulated under boric acid deprivation condtions. Biochemical experiments reveal that NIP6;1 also has selective boron uptake activity based on functional analysis using *Xenopus laevis* oocytes expression system and plasma membrane subcellular localization by using GFP-tagged NIP6;1 expression (Tanaka et al., 2008). T-DNA insertional Knock-out of the *AtNIP6;1* gene causes defective leaf growth under boron limiting conditions (Tanaka et al., 2008). Together, it has been proposed that NIP5;1 and NIP6;1 play separate roles in boron transport across the biological membrane in the roots and the shoot because of selective cellular expression patterns (Tanaka et al., 2008).

Goals of this thesis research

Expression analyses in model organisms such as Arabidopsis, rice and maize suggest that multiple NIP genes are present in non-legume species and are in general expressed at a much lower level compared to most other plant MIPs (Chaumont et al., 2000; Johanson et al., 2001; Sakurai et al., 2005). In addition, they are often expressed in specialized cells and organs suggesting that NIP transport activities may be prevalent in a more defined set of cells in the plant (Wallace et al., 2006). While functions are emerging for some NIP proteins (e.g. AtNIP5;1 and AtNIP6;1 as metalloid transporters), there is much to be learned about the biological functions of most NIPs. In the present research project, focus has been placed on representative Arabidopsis NIPs of the two NIP pore families that have unknown functions: NIP2;1 (NIP subgroup I) and NIP7;1 (NIP subgroup II) with respect to their transport activity, tissue, cellular, and subcellular localization, and biological roles in Arabiopsis.

CHAPTER II

MATERIALS AND METHODS

Plant materials and general growth conditions

Arabidopsis thaliana ecotype Columbia 0 seeds were surface sterilized with 50% (v/v) ethanol for 1 minute, and then with 50% (v/v) sodium hypochlorite (bleach) containing 0.1% (v/v) Tween 20 for 15 minutes. The seeds were rinsed five times with sterile distilled water and were planted on 1/2 strength Murashige and Skoog (MS) agar medium supplemented with 0.4% (w/v) phyto agar and 1.5% (w/v) sucrose (Cat # M9274; Sigma-Aldrich, St. Louis, MO). The seeds were stratified at 4°C for 2 days, and were then transferred to a growth chamber and were grown under cool white fluorescent lights (76-100 µmol m^{-2} s^{-1}) with a long day (LD) cycle of 16 hr light/8 hr dark at 22°C. Twelve day old seedlings were transplanted to Pro-Mix soil (Premier Horticulture Inc., Dorval, Quebec), and were grown under cool white fluorescent lights (76-100 µmol m^{-2} s^{-1}) at 22°C under the LD cycle. Arabidopsis plants that were grown for seed harvest were grown in a growth chamber under LD conditions until they set seeds and were allowed to completely dry in the growth chamber without watering for a week. Seeds were harvested from dried siliques by using a 200 mesh stainless steel screen.

Arabidopsis plants that were used for protoplast generation were grown in a growth chamber as above but under short-day conditions of 8 hr light/16 hr dark at 22°C in order to delay flowering and generate more leaf material per plant.

For etiolated growth, Arabidopsis seeds were planted on the grid A line of square Petri dish plates (gridded 100 X 100 X 15mm plates; Fisher Scientific, Pittsburgh) containing 1/2 strength MS agar medium supplemented with 0.4% (w/v) phyto agar and 1.5% (w/v) sucrose. The plates were wrapped with aluminum foil and were then placed in an opaque plastic container. Seeds were stratified at 4°C for 2 days and were grown in darkness for 2 weeks at 22°C.

For pollen tube germination experiments, plants were grown under standard LD conditions. Pollen tube germination was done as described previously (Hicks et al., 2004) with slight modificaitions. Briefly, pollen grains were harvested from fully opened flowers of 6-wk old plants and were germinated on 10% (w/v) sucrose, 1mM $CaCl_2$, 1 mM $Ca((NO)_3)_2$, 1 mM $MgSO_4$, 0.5% (w/v) agar and either the presense of 0.01% (w/v) boric acid or the absence of boric acid. Germination was allowed to proceed at 22°C for 10 hours in a humidified atmosphere. Germinated pollen tube was imaged using a LEICA MZ16FA microscope equipped with a DFC 420 color camera and the Application Suite software (Leica Microsystems Inc., Bannockburn, IL, USA). The size of pollen grains and the length of pollen tubes were measured using the NIH Image J software (National Institutes of Health).

Stress experimental conditions

For oxidative stress, Arabidopsis seeds were germinated on sterile filter paper and were grown on 1/2 strength MS agar medium with 1.5% (w/v) agar under the standard LD conditions. At two weeks, the filter paper with seedlings was transferred onto freshly prepared 1/2 strength MS agar containing 10 mM H_2O_2. Seedling samples were harvested at intervals over 24 hr and were immediately frozen in liquid nitrogen, and then stored at -80°C until isolation of total RNA.

For flooding and hypoxia treatments, Arabidopsis seeds were germinated on the grid A line of grided square Petri dish plates containing full strength MS agar medium supplemented with 0.8% (w/v) phyto agar and 3% (w/v) sucrose. Plants were grown vertically under the standard LD conditions at 22°C for 10 days prior to flooding treatment. The roots of the seedlings were subjected to flooding stress by submergence in sterile water to the grid B line. Seedlings were harvested at intervals over 24 hr and were immediately frozen in liquid nitrogen, and then stored at -80°C until isolation of total RNA.

For hypoxia treatment, vertically grown 2-wk old seedlings were placed into an anaerobic jar (BD Cat.# 260626; BD Diagnostic Systems, NJ, USA) and were subjected to anaerobic conditions by using a BD BBL GasPak 100 Systems with a BBL dry anaerobic indicator strip (BD Cat.# 271051; BD Diagnostic Systems, NJ, USA). Based on the indicator strip, anaerobic conditions are established after 60 minutes in the jar. Seedling samples were then harvested at various intervals over 24 hr and were immediately frozen in liquid nitrogen, and then stored at -80°C until isolation of total RNA. For survival analysis after anaerobic treatment, seedlings were exposed to

oxygen deprivation by using the anaerobic jar conditions described above, were returned to normoxic conditions and were grown under standard LD conditions for an additional two weeks prior to scoring for survival.

For preadaptation experiments, vertically grown 2-wk old seedling samples were placed in an anaerobic jar and were subjected to a brief anaerobic episode for 3 hr using the GasPak 100 system as described above. Seedling samples were then allowed to recover by returning for the growth chamber under normoxic conditions for 16 hr. Recovered “pre-adapted” seedlings were then subjected to full anoxic stress and were scored for survival as described above.

To determine L-lactate concentration in tissue samples, vertically grown 2-wk old seedlings were subjected to hypoxic-treatment in an anaerobic jar as described above. The seedling samples submerged into MS media were flushed with air for 24 hr as normoxic control or nitrogen gas as a 24 hr hypoxia-treatment. The normoxia and hypoxia-treated tissue samples were dissected into shoot and root tissues and were ground in liquid nitrogen using a mortar with a pestle. L-lactate was then extracted from the ground tissue powder to determine lactate content in Arabidopsis tissues as described below.

Total RNA isolation and first-strand cDNA synthesis

Total RNA was isolated from tissue samples (~200 mg) by using the Plant RNA Purification Reagent (Invitrogen, Carlsbad, CA) according to the manufacturer’s instructions. Briefly, the tissues samples were ground into fine powder in a mortar with a pestle cooled with liquid nitrogen. Total RNA was isolated from the resulting tissue

powder by incubation in 500 µL of Plant RNA Purification Reagent at room temperature for 10 minutes. Samples were then centrifuged at 10,000 x g at room temperature for 10 minutes to remove cell debris. The supernatant was transferred to a new sterile tube containing 300 µL of chloroform and 125 µL of nuclease-free 4 M NaCl prepared in 0.1% (v/v) diethylpyrocarbonate (DEPC) treated deionized water. The resulting mixture was centrifuged at 13,000 x g, 4°C for 10 minutes. The aqueous phase was transferred to a new sterile tube and the RNA was precipitated by addition of an equal volume of 100% isopropanol, and incubation at either -20°C for 2 hr or at -80°C for 30 minutes. The precipitated RNA was collected by centrifugation at 13,000 x g, 4°C for 10 minutes. The pellet was washed with 70% (v/v) ethanol prepared in DEPC-treated water, and was then dried in a SpeedVac SVC100 system equipped with a refrigerated condensation trap RT100 (Savant Instruments, Inc., Farmingdale, NY). The pellets were resuspended in 100 µL of DEPC-treated water. The RNA concentration and purity was determined by absorbance at 260 nm (A_{260} = 1.0 corresponds to an RNA concentration of 40 µg/mL) and the A_{260}/A_{280} ratio (RNA was considered pure when the A_{260}/A_{280} ratio is between 1.8 and 2.0). The integrity of the purified RNA was assessed by observation of the 18S and 28S ribosomal RNA bands after electrophoresis on 1% (w/v) agarose gels containing 0.3 ng/mL ethidium bromide and 1X Tris-acetate EDTA (TAE) buffer (Sambrook and Russell, 2001).

Genomic DNA from the total RNA samples was removed by RNase-free DNase I treatment using the TURBO DNA-*free*™ kit (Cat# 1907; Ambion, Austin, TX) according to the manufacturer's instructions. Briefly, 25 µL of total RNA was incubated with 2 units of TURBO DNA-*free*™ enzyme at 37°C for 40 minutes. The reaction was

terminated by the addition of 5µL of DNase Inactivation Reagent followed by incubation at room temperature for 2 minutes. The concentration, purity and integrity of the total RNA samples were assessed by spectrophotometry and agarose gel electrophoresis as described above.

Total RNA samples (2-4 µg) were reverse transcribed into first-strand cDNA with the SuperScript^{TM} First-Strand Synthesis System for RT-PCR (Invitrogen, Carlsbad) in 40 µL of final reaction volumes (50-100 ng of total RNA/µL) according to the manufacturer's instructions. First-strand cDNA was then synthesized by incubation of the reaction at 25°C for 15 minutes, 42°C for 90 minutes, and 72°C for 15 minutes. The residual total RNA in the resulting first-strand cDNA samples was removed by incubation of the reactions with 1 µL of *E.coli* RNase H at 37°C for 30 minutes. The first-strand cDNA samples were then stored at -20° until use. To monitor the quality of the resulting first-strand cDNA samples, the *Arabidopsis Actin2* (*ACT2*) or *ubiquitin10* (*UBQ10*) reference gene was amplified by RT-PCR or Q-PCR as described in subsequent sections.

Molecular cloning techniques

The *AtNIP2;1* promoter::GUS reporter construct was generated as described previously (Choi and Roberts, 2007). Briefly, a DNA fragment corresponding to 1098 bp of the *AtNIP2;1* gene upstream of the transcriptional start site was amplified from wild type Arabidopsis genomic DNA by PCR using gene-specific primers (Newgus3-F and Newgus3-R; Table 2.1) with *Hind*III and *Pst*I sites introduced for cloning. The PCR amplified *AtNIP2;1* promoter fragment (1098bp) was digested with *Hind*III and *Pst*I at

Table 2.1. Sequences of primers used for cloning of GUS-fusion, YFP C-terminal-fusion and *Xenopus* oocyte expression constructs.

Name	Direction	Sequence (5' to 3')[a]	Comments[b]
Newgus3-F	Forward	GGCAAGCTTAAATCCTTCCTCCTCCATCTTCC	*Hind*III
Newgus3-R	Reverse	GGCCTGCAGTCATCCGTTTTTCTTTTTGTCCG	*Pst*I
NIP2;1FNCOI	Forward	CCATGGATGACATATCAGTGAGCAA	*Nco*I
NIP2;1RNCOI	Reverse	CCATGGACAGAGGAAGATCGGTAAC	*Nco*I
Bgl-II-nip2;1F	Forward	AGATCTGATGACATATCAGTGAGC	*Bgl*II
Bgl-II-nip2;1R	Reverse	AGATCTTCACAGAGGAAGATCGGT	*Bgl*II
FLAG epitope	Forward	GATCCGAATTCATGGACTACAAAGACGACGA CGACAAAA	*BamH*I
FLAG epitope	Reverse	GATCTTTTGTCGTCGTCGTCTTTGTAGTCCAT GAATTCG	*Bgl*II

[a]All primer sequences are in the 5' to 3' direction.

[b]Underlined portions of the sequences represent restriction sites or in the case of the FLAG epitope, restriction site overhangs.

37°C overnight and was cloned into the *Hind*III and *Pst*I sites of pCAMBIA1391Z (Hajdukiewicz et al., 1994) upstream of a promoterless *GUS* reporter gene. The resulting construct was transformed into *E. coli* strain DH5α. Transformants with the *AtNIP2;1* promoter::GUS insert was assessed by plamid purification and restriction enzyme digestion with *Hind*III and *Pst*I.

For subcellular localization of AtNIP2;1 in Arabidopsis mesophyll protoplasts, a cDNA encoding the full length AtNIP2;1 ORF was amplified from first-strand cDNA sample of the 2 hr anoxic treated roots using gene specific primers (NIP2;1FNCOI and NIP2;1RNCOI; see Table 2.1) with *Nco*I sites introduced for cloning into expression vector pBS (Subramanian et al., 2004) in frame with a C-terminal yellow fluorescence protein (YFP) tag downstream of the Cauliflower Mosaic Virus (CaMV) 35S promoter. The resulting construct was transformed into *E. coli* DH5α and plamids were subjected to restriction enzyme digestion with *Sac*I to determine the presence of insert and the correct orientation.

For the preparation of transgenic Arabidopsis expressing the AtNIP2;1::YFP fusion, a cassette consisting of the CaMV 35S promoter-AtNIP2;1::YFP fusion from the expression construct described above was excised by restriction enzyme digestion with *BamH*I and *Kpn*I, and was cloned into the *BamH*I and *Kpn*I sites of the pBIN19 plant binary vector (Frisch et al., 1995). The presence of the cloned 35S promoter-AtNIP2;1::YFP fusion cassette in pBIN19 vector was assessed by restriction enzyme digestion with *BamH*I and *Kpn*I and its orientation was verified by *Sac*I digestion.

For *Xenopus laevis* oocyte expression a cDNA encoding the full length *AtNIP2;1* ORF was amplified from root total RNA from 6 wk old Arabidopsis by RT-PCR

amplification using the gene specific primers (Bgl-II-nip2;1F and Bgl-II-nip2;1R; see Table 2.1) with *Bgl*II sites. The following PCR parameters were used: 94°C for 5 minutes; followed by 35 cycles of : 94°C for 30 seconds, 55°C for 30 seconds, 72°C for 90 seconds; with a final elongation cycle of 72°C for 7 minutes. The amplified cDNA fragment was cloned into the *Bgl*II restriction site of a modified *Xenopus* expression plasmid pX*β*G-ev1-FLAG containing a sequence to introduce an in-frame N-terminal fusion of the FLAG epitope (MDYKDDDDK) as described in Wallace and Roberts (2005). The cassette contains cohesive ends complementary to *Bgl*II or *BamH*I overhangs at the 5' and 3' end. This cassette also contains an *EcoR*I restriction site at the 5' end, followed by the coding sequence for the FLAG epitope. A FLAG-tag fusion of soybean nodulin 26 was generated in the same vector (Wallace and Roberts, 2005). Capped cRNA was generated by in vitro transcription of *Xba* I-linearized pX*β*G-ev1-FLAG constructs by using the mMESSAGEmMACHINE T3 kit (Ambion, Austin) as previously described (Guenther et al., 2003; Wallace and Roberts, 2005; Choi and Roberts, 2007). The cRNA integrity was assessed by gel electrophoresis on 1% (w/v) agarose gels containing 0.3 ng/mL ethidium bromide in 1X TAE buffer (Sambrook and Russell, 2001) and was quantitated by measuring absorbance at A_{260} as well as measuring the A_{260}/A_{280} ratio for purity.

Quantitative Real-Time RT-PCR (Q-PCR)

Q-PCR expression experiments for flooding stress, etiolation, and oxidative stress was done by using an ABI Prism 7000 Sequence Detection System, and analyses were performed with the ABI Prism 7000 SDS software (PE Applied

Biosystems, Foster City). Q-PCR expression experiments for hypoxic-treated root and leaf/shoot tissues were done on a Bio-Rad IQ5 real-time PCR detection system, and analyses were performed with the Bio-Rad Optical System software version 1.0 (Bio-Rad Laboratories, Inc., Hercules, CA). Gene-specific and internal control primers are described in Table 2.2. cDNA proportional to 10-100 ng of the starting total RNA was combined with 500 nM of each primer and 12.5 µL of the 2XABsolute SYBR Green fluorescein dUTP Mix (ABgene USA, Rochester, NY) in a final volume of 25 µL. Q-PCR reactions were performed using the following parameters: 1 cycle of 5 min at 50°C, 1 cycle of 10 min at 95°C, and 45 cycles of 30 sec at 95°C, 45 sec at 45°C, and 45 sec at 72°C in a 96-well optical PCR plate (ABgene USA, Rochester, NY). The *Arabidopsis UBQ10* gene was used as an internal reference for standardization as described previously (Czechowski et al., 2004; Choi and Roberts, 2007).

Quantitation of expression of the gene of interest was calculated using the comparative threshold cycle (Ct) method as described previously (Pfaffl, 2001; Schmittgen and Livak, 2008). ΔCt was calculated using following equation:

$$\mathbf{\Delta Ct = Ct_{(target)} - Ct_{(reference)}} \quad \text{(Eq. 1)}$$

where $Ct_{(target)}$ is Ct value of gene of interest , and $Ct_{(reference)}$ is Ct value of the *AtUBQ10*. Relative expression was calculated by using the calculated ΔCt values and the following equation;

$$\mathbf{Relative\ expression = 2^{-\Delta Ct}} \quad \text{(Eq. 2)}$$

ΔΔCt values were calculated using the following equation;

$$\mathbf{\Delta\Delta Ct = \Delta Ct_{(sample)} - \Delta Ct_{(calibrator)}} \quad \text{(Eq. 3)}$$

where $\Delta Ct_{(sample)}$ represents the expression value of the sample, and $\Delta Ct_{(calibrator)}$ is the

Table 2.2. Sequences of primers used for quantitative RT-PCR experiments.

Name	Direction	Sequence (5' to 3')[a]	Comments[b]
QPCR-AtNIP1;1F	Forward	AATCCTTTTCCTCTTCTT	5'UTR
QPCR-AtNIP1;1R	Reverse	TCATCCTTGAGATTCAC	Exon 1
QPCR-AtNIP1;2F	Forward	AGTGTGTGAAAAGAGAAA	5'UTR
QPCR-AtNIP1;2R	Reverse	TTGTTGTTGTTGTTCGTC	Exon 1
RTNIP21F	Forward	CCGCCATTGCCGTGAA	Exon 2
RTNIP21R	Reverse	CCCCAAACCACAGCAATCC	Exon 2
RTnip22F	Forward	ACCGTCAATACCAAACGC	Exon 3
RTnip2;2-R2	Reverse	AAGATGCAAGGAGGATTG	3'UTR
QPCR-AtNIP3;1F	Forward	ACACAAAGGTCTGAAAAG	5'UTR
QPCR-AtNIP3;1R	Reverse	CGCGCTCCATGTTCG	Exon 1
QPCR-AtNIP4;1F	Forward	AATTTGTTTCTAAGAACAAAT	5'UTR
QPCR-AtNIP4;1R	Reverse	TCCTCCTTGGCAATC	Exon 1
QPCR-AtNIP4;2F	Forward	TCACATCCACATTTTTCT	5'UTR
QPCR-AtNIP4;2R	Reverse	ATTCCTCCTTGGCTAT	Exon 1
RTNIP71F	Forward	CATCTCTGGCGCCCATCT	Exon 2
RTNIP71R	Reverse	CCGCCAAAGACAGCGAAA	Exon 2
QPCR-AtAdh1F	Forward	AAGTTCTTCACTGTTGAT	5'UTR
QPCR-AtAdh1R	Reverse	AGCAACCTCCACTTC	Exon 1
QPCR-AtLdh1-F	Forward	ATGGAGAAGAACGCATCGAC	Exon 1
QPCR-AtLdh1-R	Reverse	AAGGATCGGAGTTGTGGATC	Exon 1
QPCR-Pdc1F	Forward	AGTGAACTCAAACCTTC	5'UTR
QPCR-Pdc1R	Reverse	TGTTGCGACGGTGCC	Exon 1
QPCR-AtGLB1-For	Forward	GTTGTGAAATATTATGGAGA	5'UTR & Exon 1
QPCR-AtGLB1-Rev	Reverse	CTTCATGACACTCCAAGACT	Exon 1
QPCR-AtCML38-For	Forward	GAGTTATGATTAGTGCTTTTGA	Exon
QPCR-AtCML38-Rev	Reverse	ACAACAACAACAACAACAATG	3'UTR
QPCR-HSP70-For	Forward	GATGTTGCGGTTACTGCTACTG	Exon
QPCR-HSP70-Rev	Reverse	GCGAATTGTGTTCTGCAAAATGTCT	Exon

Name	Direction	Sequence (5’ to 3’)[a]	Comments[b]
QPCR-HSP25.3P-For	Forward	CCTCAACAACGCTTAACCATGGA	Exon
QPCR-HSP25.3P-Rev	Reverse	TCGTCCTCATTGGTGACAAAGG	Exon
RTubq10F	Forward	CACACTCCACTTGGTCTTGCGT	Exon
RTubq10R	Reverse	TGGTCTTTCCGGTGAGAGTCTTCA	Exon

[a]All primer sequences are in the 5’ to 3’ direction.

[b]5’UTR, 3’UTR, and Exon indicate priming region of each primer indicated. 5’UTR and 3’UTR show 5’ untranslated region (UTR) and 3’ untranslated region (UTR), espectively. Each primer set of AtNIP subgroup I is specific for the corresponding genes and used for Q-PCR analysis. RTubp10F and RTubq10R are the primer set for *AtUBQ10* gene, an endogenous reference consistently expressing gene through all the tissues tested. *AdhI* and *PdcI* are used as an endogenous reference for the hypoxia induced genes.

expression value of the sample to which other samples in the data set are normalized. Each $\Delta Ct_{(calibrator)}$ and its value for individual Q-PCR experiment is indicated in the Figure legends and a table for the ΔCt values of each individual Q-PCR result. The obtained ΔΔCt values including the calibrator were normalized by using the following equation;

$$\textbf{Normalized Expression} = 2^{-\Delta\Delta Ct} \quad \text{(Eq. 4)}$$

Reduction of gene expression was calculated by using the Normalized expression values and following equation;

$$\textbf{Reduced Expression} = -(1/2^{-\Delta\Delta Ct}) \quad \text{(Eq. 5)}$$

Plant transformation and mutant characterization

Agrobacterium tumefaciens strain GV3101 (Koncz and Schell, 1986) was transformed with plant expression binary vectors by electrophoation. Electrocompetent *Agrobacterium* were generated from a mild logarithmic phase culture by centrifugation at 10,000 g for 5 minutes at 4°C. The pelleted cells were resuspended in ice cold sterile water and were washed three times. The final cell pellet was resuspended in sterile 10% (v/v) glycerol. Electrocompetent *Agrobacterium* was placed in a BioRad Gene Pulser cuvette with 100 ng of purified plant binary plasmids and were electroporated using the following operational settings: 250 volts; Resistance 200 Ω; Capacitance 25 μFD. Transformants were identified by selection on LB agar containing 50 μg/mL kanamycin.

Transgenic Arabidopsis plants were generated by using the floral dip method (Clough and Bent, 1998). Briefly, inflorescences of 4-wk old Arabidopsis were submerged into mid-logarithmic cultures (A_{600} = 0.8) of *Agrobacterium tumefaciens* in

5% (w/v) sucrose and 0.05% (v/v) Silwet-L77 (Lehle Seeds, Round Rock, TX) for 1 minute. The plants were then returned to a tray, and were covered with clear plastic to prevent desiccation of inflorescences. The plants were kept overnight in a growth chamber set to LD conditions and were then washed 3-5 times with distilled water to remove residual sucrose from leaves. The plants were grown and allowed to set seed under standard LD conditions.

For selection of transformants expressing the AtNIP2;1 promoter::GUS construct, seeds were surface sterilized as described above in the "**Plant materials and growth conditions"** section, and germinated on 1/2 strength MS agar containing 50 µg mL^{-1} hygromycin. Seedlings showing resistance to hygromycin were then transplanted to Pro-Mix soil, and were grown under LD conditions until the plants set seed. F1 generation seeds were harvested from individual transformants and were used for histochemical analyses as described below.

Transgenic Arabidopsis transformed with the AtNIP2;1::YFP construct under the control of the **ca**uliflower **m**osaic **v**irus (**CaMV**) 35S promoter were germinated and selected on 1/2 strength MS agar medium containing 50 µg mL^{-1} kanamycin. F1 generation seeds from kanamycin resistant plants were then harvested from individual plant and were used for subcellular localization experiments.

For subcellular localization experiments, transient expression of AtNIP2;1::YFP was done in mesophyll protoplasts prepared from 3-wk old *Arabidopsis* Col_0 wild type plants by the protocol described in (Sheen, 1995; Yoo et al., 2007). For transformation, protoplasts were resuspended (2 X 10^5 protoplasts/mL) in 0.4 M mannitol, 15 mM $MgCl_2$, 4 mM MES-NaOH pH 5.7, and were transformed with 10 µg of pBS-35S-YFP

containing the AtNIP2;1::YFP construct by the procedure of Yoo et al. (2007). Protoplasts were cultured at room temperature for 18 hr in 1 ml of 154 mM NaCl, 125 mM $CaCl_2$, 5 mM KCl, 2 mM MES-NaOH pH 5.7. Transformed protoplasts were observed using a Leica DMRE laser scanning confocal microscope with filter settings of 507-532 nm for YFP and 588-716 nm for chloroplasts. Microscopy was done at the University of Tennessee Analytical Microscopy Facility (Knoxville, TN, U.S.A).

AtNIP2;1::YFP was also visualized in primary root tissues from 7-d old T_1 generation of stable transgenic Arabidopsis lines over expressing AtNIP2;1::YFP C-terminal fusion as described above using an Axiovert 200M microscope (Zeiss) equipped with a YFP fluorescence filter setting (Chroma, filter set 52017) of 500-530 nm. Images were captured with a digital camera (Hamamatsu Orca-ER) controlled by the Openlab software (Improvision).

Characterization of T-DNA insertion mutants of *AtNIP2;1* and *AtNIP7;1*

Two T-DNA insertional mutants (WiscDsLox233237_22k and Salk_023890) with insertions in the *AtNIP2;1* gene were obtained and characterized. T_1 generation seed of WiscDsLox 233237_22k (we refer to as *atnip2;1-1*) and T_3 generation seed of Salk_023890 (we refer to as *atnip2;1-2*) strains were obtained from the Arabidopsis Biological Resource Center (ABRC). One T-DNA insertional muant (Salk_042590) with an insertion in the *AtNIP7;1* gene was characterized. T_3 generation seed of Salk_042590 (we refer to as *atnip7;1-1*) strain was obtained from the ABRC.

For characterization of *atnip2;1-1*, seeds were surface sterilized and grown on a selection plate containing ½ MS agar medium with 200 µM glufosinate-ammonium.

Twelve day old antibiotic-resistant seedlings were transplanted onto Pro-Mix soil and were selected again by spraying with 1:1000 diluted “Basta” containing 300 µM glufosinate-ammonium followed by growth under LD conditions. Plants were allowed to set seed, and seeds were harvested from individual antibiotic resistant plants. Genotyping was done by further antibiotic selection as discussed above and homozygous lines were selected for further study.

For PCR genotyping, genomic DNA was extracted from 2-wk old *atnip2;1-1* seedings which showed 100% antibiotic resistance using the *Wizard* Genomic DNA purification kit (Cat.# A1120; Promega, Madison, WI) according to the manufacturer’s instructions. The T-DNA insertion site and the genotype of T_2 generation of the mutant were analyzed by using PCR-based genotyping with the following PCR parameters: 94°C for 5 minutes; followed by 30 cycles of: 94°C for 30 seconds, 66°C for 30 seconds, 72°C for 90 seconds; with a final elongation cycle of 72°C for 7 minutes. The gene specific primers of the *AtNIP2;1* gene, and the left border T-DNA primer used for genotyping are shown in Table 2.3. The amplified *T-DNA/AtNIP2;1* PCR product was then cloned into the pCR2.1-TOPO vector (Invitrogen) and transformed into the TOP10 *E. coli* strain (Invitrogen) to map the exact location of T-DNA insertion by using sequencing analysis.

For characterization of *atnip2;1-2*, seeds were germinated on regular ½ strength MS agar medium and were grown under LD condition for harvesting seeds as described above. Genomic DNA was extracted from 2-wk old *atnip2;1-2* seedings and the T-DNA insertion site and the genotype of T_5 generation of the second allele were analyzed by

using PCR based genotyping with the same PCR parameters described above for T-DNA insertional positional mapping in *atnip2;1-1*.

For characterization of *atnip7;1-1*, seeds were germinated and grown as described above. Genomic DNA was extracted from 6-wk old plants and the T-DNA insertion site and the genotype of T_5 generation of the *atnip7;1-1* were then analyzed by using PCR based genotyping with the PCR parameters: 94°C for 5 minutes; followed by 30 cycles of : 94°C for 30 seconds, 58°C for 30 seconds, 72°C for 90 seconds; with a final elongation cycle of 72°C for 7 minutes. The *AtNIP7;1* gene specific primers and the left border T-DNA primer were used for genotyping (Table 2.3). The amplified *T-DNA/AtNIP7;1* PCR product was cloned into the pCR2.1-TOPO vector (Invitrogen) and transformed into the TOP10 *E. coli* strain (Invitrogen) to map the exact location of T-DNA insertion by using sequencing analysis as described above.

Affymetrix microarray analysis

Global transcript analysis of wild type and *atnip2;1*-1 knock-out Arabidopsis seedlings under normoxic and hypoxic conditions was done by microarray analysis using the Affymetrix Arabidopsis ATH1 genome arrays (Affymetrix, Santa Clara, CA) and was performed at the University of Tennessee, Knoxville Affymetrix Core Facility.

Vertically grown seedlings of 2-wk old wild type Arabidopsis and *atnip2;1-1* were placed in a GasPak anaerobic jar and were subjected to 4 hr of hypoxia or normoxic (negative controls) as described above. After treatment, Arabidopsis seedlings were

Table 2.3. Sequences of primers used for T-DNA insertional mutants

Name	Direction	Sequence (5' to 3')[a]	Comments
AT3RP	Forward	CGGGTCGACCTGTGTCTTTTG	
AT3LP	Reverse	ACCCAGAAGGAGATGACCCGA	
NIP7.1LP	Forward	TTCATACGAATTTCGCTTCAC	
NIP7.1RP	Reverse	ACCTGCTTTAAGCTGCGTTTC	
LBb1	Forward	GCGTGGACCGCTTGCTGCA	Salk T-DNA left border primer
p745	Forward	AACGTCCGCAATGTGTTATTAAGTTGTC	Wisconsin T-DNA left border primer

[a]All primer sequences are in the 5' to 3' direction. .

dissected into shoot and root tissues and were frozen in liquid nitrogen. Total RNA was then isolated as described above.

To check the integrity of the RNA and to verify the anaerobic conditions, 2 µg of the resulting total RNA samples were reverse transcribed into first-strand cDNA with SuperScript™ First-Strand Synthesis System for Q-PCR analysis as described above. To monitor the quality and anaerobic conditions of the resulting first-strand cDNA samples, *ubiquitin10* (*UBQ10*), a reference gene, and alcohol dehydrogenase (*Adh1*), a standard anaerobic polypeptide gene, were amplified by Q-PCR with the gene specific priemrs for *UBQ10* and *Adh1* (Table 2.2) as described above.

Arabidopsis ATH1 Genome Array chips containing ~24,000 genes were purchased from Affymetrix (Santa Clara, CA). Eleven pairs of oligonucleotide probes are used to measure the transcription level of each sequence represented. The probe sets were designed in collaboration with The Institutes for Genome Research (TIGR). The Affymetrix protocol for One-Cycle cDNA synthesis and labeling was followed using a TargetAmp 1-round amplification kit for biotin labeling cRNA (Epicentre Biotechnologies). First, 500ng of each total RNA sample was converted into single stranded cDNA using SuperScript III (Invitrogen) and a T7-Oligo (dT) primer. Second strand cDNA was then synthesized using dNTPs, Second Strand Reaction Buffer, *E. coli* DNA Ligase, and *E. coli* DNA polymerase I. After purification, the cRNA was fragmented to a size ranging from 35 to 200 bases using fragmentation buffer at 94°C for 35 minutes. Fifteen micrograms of the fragmented cRNA was mixed into a hybridization cocktail containing hybridization buffer, the B2 oligo (grid alignment control that forms a grid around the array to determine the boundary after hybridization) and

DMSO (Affymetrix). The solution was hybridized to GeneChips at 45°C for 16 hours. After hybridization, the cocktail was removed from the GeneChips and was stored for potential future analyses. Using an Affymetrics Fluidics 450 wash station (Affymetrix Fluidics Protocol FS450_004), the GeneChip was washed and stained with streptavidin-phycoerythrin according to manufacturer's instructions (Molecular Probes). The GeneChips were immediately scanned with a GeneChip 7G High-Resolution Scanner. The individual GeneChip scans were quality checked for the presence of the control genes *UBQ10* and *Adh1*, and for background signal values. The probe signal intensities were further analyzed using the Affymetrix® Microarray suite software (MAS 5.0). Normalization of the raw data and estimation of signal intensities was done using the GC-Robust Multichip Average (GC-RMA) algorithm (Bolstad et al., 2003).

For statistical analysis, the average expression values and *p*-values (one way ANOVA) were calculated using the Partek Genome suite™ (Partek GS; Partek Inc., Missouri, USA) software. For comparison of changes in gene expression between arrays, the Partek Genome suite™ software was also used. The genes that are significantly up regulated or down regulated were selected by setting a cut-off value of two-fold change and a *p*-value of less than 0.05 (95% confidence). Functional categorization of the expressed genes was done by using the Wilcoxon Rank Sum algorithm in a "ImageAnnotator 3.0.0.RC1" of the Mapman software (Thimm et al., 2004; Usadel et al., 2005), a user-driven tool that displays gene expression data from Arabidopsis Affymetrix arrays onto diagrams of metabolic pathways or other processes.

Expression and transport analyses in *Xenopus* oocytes

Stage V and VI *Xenopus* oocytes were prepared as previously described (Dean et al., 1999) and microinjected with 46 nL of 1 µg/µL of cRNAs or with RNase-free water as a negative control using a Drummond "nanoject" automatic injector (Drummond Scientific Company, Broomall). The oocytes were cultured for 72 hr in 96 well microtiter plates at 16°C in Ringers solution (96 mM NaCl, 2 mM KCl, 5 mM $MgCl_2$, 5 mM HEPES-NaOH pH 7.6, 0.6 mM $CaCl_2$, 200 mosmol/kg) supplemented with 100 µg/mL penicillin-streptomycin. Media was removed and replenished every 24 hr until the oocytes were assayed.

The osmotic water permeability (P_f) of the oocytes was measured by the standard oocyte swelling assay as previously described (Guenther et al., 2003; Wallace and Roberts, 2005). Measurements were done at 18˚C upon hypoosmotic challenge with 30% (60-70 mosmol/kg) Ringers solution. Swelling was measured by video microscopy on a Nikon Alphaphot YS microscope equipped with a Pro-Series High Performance CCD camera. Images were captured using the NIH Image software as described in (Wallace and Roberts, 2005). An initial oocyte swelling rate [$(dV/V_0)/dt$] in 30% diluted (60-70 mosmol/kg) Frog Ringers solution from its original osmolarity (200 mosmol/kg) was used to determine the water permeability coefficient (P_f) by using the following equation:

$$\mathbf{P_f = \frac{V_0(dV/V_0)dt}{(S_{real}/S_{sphere})V_w(osm_{in} - osm_{out})}} \quad \text{(Eq. 6)}$$

where $\mathbf{V_0}$ is the surface area of the oocyte at time 0, $\mathbf{osm_{in}}$ is the osmolarity in the oocyte, $\mathbf{osm_{out}}$ is the osmolarity of the bath media used for swelling assay, $\mathbf{V_w}$ is the

partial molar volume of water (18 cm^3/mol), $\mathbf{S_{real}}$ is the actual surface area of the oocyte, and $\mathbf{S_{sphere}}$ is the area calculated by assuming a sphere. $\mathbf{S_{real}/S_{sphere}}$ is taken as 9 for the water permeability measurements (Zampighi et al., 1995; Rivers et al., 1997).

Glycerol and urea permeability measurements of *Xenopus* oocytes were performed by radioisotopic uptake assay as in (Wallace and Roberts, 2005). Assays were performed at 22°C for 10 minutes and oocytes were washed twice in 6 mL of ice cold Ringers solution containing 20 mM of the test solute without radioisotope. Lactic acid transport experiments in oocytes were done by a similar approach except that ^{14}C labeled lactic acid was used. The assay buffer consisted of a modified Ringers solution containing 20 mM lactic acid (12 μC_i/mL ^{14}C labeled lactic acid [Sigma-Aldrich, St. Louis]) in a base buffer of 75 mM NaCl, 2 mM KCl, 5 mM $MgCl_2$, 5 mM Tris-succinate, 0.6 mM $CaCl_2$ (200 mosm/kg). Assay incubations were done at 22°C for 10 min and oocytes were washed twice with 6 mL of ice cold Ringers solution without isotope. Sensitivity to mercurials was determined by preincubating oocytes in Ringers solution containing 1 mM $HgCl_2$ for 10 min prior to assay, essentially as previously described (Rivers et al., 1997). After isotopic uptake assays, oocytes were lysed with 300 µL of 10% (w/v) SDS and scintillation counting was done in 10 mL of Scintsafe (Fisher Scientific, Pittsburgh) by using a Beckman LS6500 Multi-Purpose Scintillation Counter (Beckman Coulter, Fullerton).

For activation energy (E_a) measurements, the lactic acid direct uptake experiments were performed at various termperature ranging from 5 to 24°C. Natural logarithms of the ^{14}C-lactate uptake rate (nmol/min^{-1} $oocyte^{-1}$) collected at these

temperatures were plotted against the inverse of the absolute temperature (K), and linear regression analysis was used to fit the data to the Arrhenius equation as follows:

$$\mathbf{ln(^{14}C\text{-}lactate\ nmol/min^{-1}\ oocyte^{-1}) = (-\ E_a/R)(1/T) + ln(A)} \qquad \text{(Eq. 7)}$$

where $\mathbf{E_a}$ is the activation energy for lactate transport, **R** is the universal gas constant, **T** is the absolute temperature (K), and **A** is the Arrhenius pre-exponential factor.

Ethanol, boric acid, and lactic acid permeability measurements of *Xenopus* oocytes were performed by oocyte swelling assays as described previously (Wallace and Roberts, 2005; Tanaka et al., 2008). Briefly, measurements were done by incubating oocytes in an isoosmotic (200 mOsm/kg) modified Ringers-based solution containing 100 mM testing solute molecules instead of NaCl. The permeabiliy of the test solutes was determined by the initial oocyte swelling rate $(dV/V_0)/dt$, due to uptake of the test solute creating an osmotic gradient and water uptake (Wallace and Roberts, 2005).

Immunochemical Techniques

To generate a site-directed antibody (Ab) against AtNIP2;1, a synthetic peptide composing the amino acid sequence of the predicted carboxyl terminal cytosolic domain of AtNIP2;1 (CHKMLPSIQNAEPEFSKTGSSHKRV; refered to as CV25) was synthesized (GenScript Co., Scotch Planis, NJ). The synthetic CV25 peptide was engineered with an additional cysteine at the amino terminus to facilitate coupling to carrier proteins. For antibody production, CV25, was coupled to m-maleimidobenzoyl-N-hydroxysuccinimide ester (MBS)-activated keyhole limpet hemocyanin (KLH) according to the manufacturer's protocols (Pierce Endogen Chemicals). The coupling

efficiency was monitored by the decrease in free sulfhydryl groups as assayed by Ellman's Reagent (Ellman, 1959). The KLH-CV25 conjugate was purified by gel filtration on Sephadex G25 in 137 mM NaCl, 2.7 mM KCl, 9.6 mM NaH_2PO_4, 1.5 mM K_2HPO_4, pH 7.2 (PBS). For immunization, 100 µg of KLH-CV25 conjugate was diluted into 225 µL of PBS and was emulsified 1:1 with Titermax-Gold adjuvant (TiterMax USA, Inc., GA). The emulsified mixture was injected subcutaneously into New Zealand White female rabbits. The immunization was repeated after 1 week with an additional injection of 100 µg of KLH-CV25 conjugate in 225 µL of PBS and Titermax-Gold adjuvant (emulsified 1:1 mixture). Subsequent booster injections of the antigen were periodically repeated (an additional 4 times over six weeks) with 100 µg of the KLH-CV25 conjugate in 450 µL of PBS. Blood was harvested from immunized rabbits and processed for sera as described in Harlow and Lane (1998). As a negative control, pre-immune sera was harvested prior to immunization. Western blotting and ELISA assays were used to monitor antibody production in collected sera as described in (Weaver et al., 1991; Guenther et al., 2003).

For affinity purification of AtNIP2;1 Ab, an affinity support consisting of the CV25 peptide antigen coupled to ω-aminohexyl-agarose (Sigma-Aldrich) was prepared by using the heterobifunctional crosslinking reagent MBS (Pierce Endogen Chemicals) according to manufacturer's instructions. The coupling efficiency was assayed by using Ellman's reagent as described above. Antibodies were purified from antisera as described by Harlow and Lane (1998). Briefly, 50 mL of 1:10 diluted antisera in PBS pH 7.5 was adsorbed to CV25 peptide agarose resin (1 g) in 10 mM Tris-HCl, pH 7.5. The column was washed with 10 mM Tris-HCl, pH 7.5 and the adsorbed antibodies were

eluted sequentially with 100 mM glycine-HCl, pH 2.5, and then with 100 mM triethylamine, pH 11.5. Eluents were neutralized with 1 M Tris-HCl pH8.0, and were concentrated on a Centricon YM-30 (Cat.# 4208; Millipore Co., MA, USA). The buffer was exchanged into PBS by using the Centrion filter. The final concentrated product was stored at -80°C.

Western blots for FLAG-tagged proteins in *Xenopus* oocytes were done as in (Wallace and Roberts, 2005). Oocytes lysates were prepared as described previously (Mulders et al., 1998). Lysates (10 µg total protein) were resolved by SDS-PAGE on 12.5% (w/v) polyacrylamide gels and proteins were transferred to Immobilon-P polyvinylidene fluoride membrane (PVDF; Millipore Corporation, Bedford, MA, U.S.A). Blotted membranes were blocked for 2 hr in 10% (w/v) nonfat dry milk (NFDM) and 2% (v/v) goat serum in PBS pH 7.2. Monoclonal anti-FLAG M2 antibody (1:1000; Stratagene, La Jolla, CA, U.S.A) and peroxidase-labeled horse anti-mouse IgG (H+L) secondary antibody (1:2000; Vector Laboratories, Inc., Burtingame, CA, U.S.A) incubations were performed for 1 h at 37℃in 2% (w/v) NFDM and 0.5%(v/v) goat serum in PBS pH 7.2. Chemiluminescent detection was done by incubation of membrane with 10 mL of 1.25 mM luminol, 0.2 mM *p*-coumaric acid, and 0.009% (v/v) hydrogen peroxide in 0.1 M Tris-HCl pH 8.5, followed by autoradiography.

For immunodetection of AtNIP2;1 in the roots of Arabidopsis plants, total protein was extracted from the root sample as described previously (Ishikawa et al., 2005) with slight modifications. Arabidopsis tissues were frozen and ground in liquid nitrogen into a fine powder, and were resuspended and vortexed in ice-chilled 50 mM Tris-Acetate pH 7.5, 250 mM sorbitol, 2 mM EGTA, 2 mM DTT, 1 mM phenylmethylsulfonyl fluoride

(PMSF), 5 µg/mL leupeptin, 5 µg/mL pepstatin A (1 mL buffer/0.2 mL of tissue powder). Cell debris was removed by filtration through Miracloth (Cat# 475855; Calbiochem, EMD Chemicals Inc., Darmstadt, Germany), and the extract was centrifuged at 8,000 g, 4°C for 20 minutes in a Sorvall SS-34 rotor. The microsomal fraction was obtained by centrifugation of the 8,000 g supernatant at 100,000 g, 4°C for 1.5 hr in a Beckman type 50 Ti rotor. The pellet was then resuspended in 1 mL of 50 mM Tricine-KOH pH 7.5, 5% (w/v) sucrose, 1 mM EGTA, 2 mM EDTA, and was centrifuged at 100,000, 4°C for 1 hr in a Beckman type 50 Ti rotor. The pellet was then resuspended in pre-chilled 100 µL of resuspension buffer and was stored at -80°C until use. Western blots were performed using affinity purified anti-AtNIP2;1 antibodies and the protocol of (Guenther et al., 2003).

Histological and Histochemical Techniques

Two week old Arabidopsis seedlings were used for cell viability determination using the fluorescein diacetate (FDA) staining assay as described previously (Hirayama et al., 2004) with slight modifications. Typically, 10-12 two week old seedlings were stained by submergence in 50 mL of deionized (DI) water containg 0.2 µg FDA for 10 minutes at room temperature. Stained seedling samples were washed twice with DI water, and were aligned on a MS-agar plate for microscopy. The fluorescence signal of the seedlings was observed using a LEICA MZ16FA microscope equipped with a DFC 420 color camera and the Application Suite software using filter setting of excitation 450-490 nm and emission 520 nm (Leica Microsystems Inc., Bannockburn, IL, USA).

GUS staining was done on Arabidopsis seedlings as described in Jefferson et al. (1987) with slight modifications. Tissues were incubated for 8-16 hrs at 37˚C in 0.1 M potassium phosphate pH 7.0, 0.1% (w/v) Triton X-100, 0.4 mM $K_3[Fe(CN)_6]$, 0.4 mM $K_4[Fe(CN)_6]$) and 0.9 mM 5-bromo-4-chloro-3-indolyl-β-D-glucuronidase (X-Gluc; Rose Scientific, Ltd, Edmonton, Alberta, Canada). Seedlings were cleared with 70% (v/v) ethanol at room temperature and were mounted in 50% (w/v) glycerol. GUS stained tissues were observed and imaged using a Nikon ECLIPSE E600 microscope equipped with Micropublisher 3.3 cooled and QCapture 2.60 software (QImaging Corporation, Burnaby, BC, Canada).

To determine cellular localization, GUS-stained root tissues were dehydrated and embedded in Technovit 7100 resin (Heraeus Kulzer GmbH, Germany) at room temperature according to the manufacturer's instructions. GUS-stained tissues were dehydrated twice in 96% ethanol for 30 minutes, and were then pre-infiltrated with 50% base liquid Technovit 7100 in 96% ethanol for 2 hr. Infiltration of the tissues was done by submerging pre-infiltrated tissues in 1% (w/v) hardener I solution in base liquid Technovit 7100 for 2 hr. The tissue samples were then polymerized in a solution containing 1% (w/v) hardener I solution and 6.25% (v/v) of hardener II in base liquid Technovit 7100 at room termperature for overnight. Tissue blocks were cross sectioned to 2.5 µm thickness with a Reichert OMV3 microtome equipped with a glass knife and were mounted in 50% (w/v) glycerol. GUS staining was then observed and imaged using a Nickon ECLIPSE E600 microscope equipped with Micropublisher 3.3 cooled and QCapture 2.60 software (QImaging corporation, Burnaby, BC, Canada).

In situ hybridization

For *in situ* hybridization, a 350 bp fragment of the *AtNIP7;1* gene was amplified from the Arabidopsis flower cDNA sample using the gene specific primers (ISN71F (forward primer): 5'-CGCTGGATTATCTGTGGTGGTC-3' and ISN71R (reverse primer): 5'-TGACTGTTCCAATCACGAACCC-3') with the following PCR conditions: 94°C for 5 minutes; followed by 30 cycles of : 94°C for 30 seconds, 57°C for 30 seconds, 72°C for 40 seconds; with a final elongation cycle of 72°C for 7 minutes. The amplified PCR product was cloned into the pCR2.1-TOPO vector (Invitrogen), and was transformed into the TOP10 *E. coli* strain (Invitrogen) to generate the sense and anti-sense NIP7;1 probes. The orientation of the 350bp PCR products of relative to the T7 promoter of the pCR2.1-TOPO vector was analyzed by restriction enzyme digestion with *Rsa*I and *EcoR*I, and was verified by sequencing. Digoxigenin (DIG)-labeled sense and antisense NIP7;1 RNA probes were prepared using the T7 RNA polymerase using DIG RNA labeling mix (Cat.# 1 277 073; Roche Diagnostics Corporation, Indianopolis, IN) according to the manufacturer's instructions (Roche Diagnostics Corporation, Indianopolis, IN). Labeling efficiency and quantitation of the DIG-labeled NIP7;1 RNA probes was determined in a spot test with a DIG-labeled RNA control (Cat.# 1 585 746; Roche Diagnostics Corporation, Indianopolis, IN) provided according to the manufacturer's instructions (Roche Diagnostics Corporation, Indianopolis, IN).

To test expression of *AtNIP7;1*, flowers of 6-wk old wild type Arabidopsis were fixed in 4% (w/v) paraformaldehyde in PBS, pH 7.5, and were paraffin embedded. The flower tissue blocks were then sectioned to 10 µm thickness with a Sorvall JB-4A microtome equipped with tungsten knife. The flower tissue sections were mounted on

poly-L lysine-coated glass slides and were hybridized with the DIG-labeled NIP7;1 antisense (test) and sense (negative control) probes according to the "Nonradioactive *In Situ* Hybridization Application Manual" (https://www.roche-applied-science.com/PROD_INF/MANUALS/InSitu/InSi_toc.htm; Roche Diagnostics Corporation, Indianopolis, IN). The hybridization signal was detected by incubation with anti-DIG-alkaline phosphatase followed by colorimetirc staining with nitroblue tetrazolium (NBT)/5-bromo-4-chloro-3-indolyl-phosphate (BCIP). Staining was observed and imaged using a Nickon ECLIPSE E600 microscope equipped with Micropublisher 3.3 cooled and QCapture 2.60 software (QImaging corporation, Burnaby, BC, Canada).

Other analytical techniques

To determine L-lactate concentration in Arabidopsis tissues, tissue samples were frozen in liquid nitrogen and were ground in a mortar with a pestle. The ground tissue was extracted and assayed for lactate as described previously (Bergmeyer, 1974) with slight modifications. Briefly, ground tissue was extracted in two volumes of 1N perchloric acid, and was neutralized with potassium carbonate on ice. Ten microliters of each neutralized extract sample were added into a 96-well plate containing 240 µL of 100 mM glycine, 50 mM hydrazine and 100 µM beta-nicotinamide-adenine dinucleotide (β-NAD, pH 9.0). Twenty units of L-lactic dehydrogenase (LDH) from rabbit muscle (Sigma-Aldrich Inc., St Louis, Mo, U.S.A) was added and the mixture was incubated at 37°C for 2 hr. The enzyme reaction was terminated by heating at 65°C for 5 minutes, and NADH production was assayed by the change in absorbance at

340 nm. To determine the lactate content of the tissue sample, a standard curve in which L-lactate was varied and the LDH activity was measured was generated as described previously (Bergmeyer, 1974). All plasmids generated in this study were transformed into *E. coli* DH5α strain and the sequence was verified by automated DNA sequencing using a Perkin Elmer Applied Biosystems 373 DNA sequencer at the University of Tennessee Molecular Biology Research Facility (Knoxville, TN). Protein quantitation was done by using the BCA (Pierce Endogen Chemicals), or Bradford assay (Bradford, 1976). SDS-polyacrylamide gel electrophoresis was performed using the buffer system of Laemmli (1970). Free sulfhydryl groups on peptides was determined by using Ellman's reagent (Ellman, 1959).

CHAPTER III

RESULTS

Expression of *AtNIP2;1* in Arabidopsis tissues under normal conditions

In order to investigate expression of *AtNIP2;1* in Arabidopsis tissues, total RNA was isolated from various organs of six-week old Arabidopsis and was analyzed by quantitative RT-PCR (Fig. 3.1). Prior to analysis, standard PCR was done using the internal reference gene *Arabidopsis actin 2* to monitor cDNA quality and amplification efficiency in all five tissues tested (Fig. 3.1A). The results of Q-PCR showed that *NIP2;1* transcript was detectable in all the tissues tested, but the expression levels were 40-fold higher in roots compared to stems, flowers, leaves, and siliques (Fig. 3.1B). Expression analysis of *AtNIP2;1* promoter::GUS transgenic plants supports the findings of Q-PCR and show that the *AtNIP2;1* promoter drives the expression of GUS mainly in root tissues (Fig. 3.2A). Expression predominantly occurs within the root cap and within the vascular cylinder of mature cells within the zone of cell specialization of the primary root, but appears to be lacking in the zone of cell division and elongation (Fig. 3.2B and C). Additionally, staining is absent in emerging, elongating lateral roots (Fig. 3.2B).

To determine the cellular localization of *AtNIP2;1* in mature roots, expression of the *AtNIP2;1 promoter-GUS* transgene was examined in the cross-sections of the roots

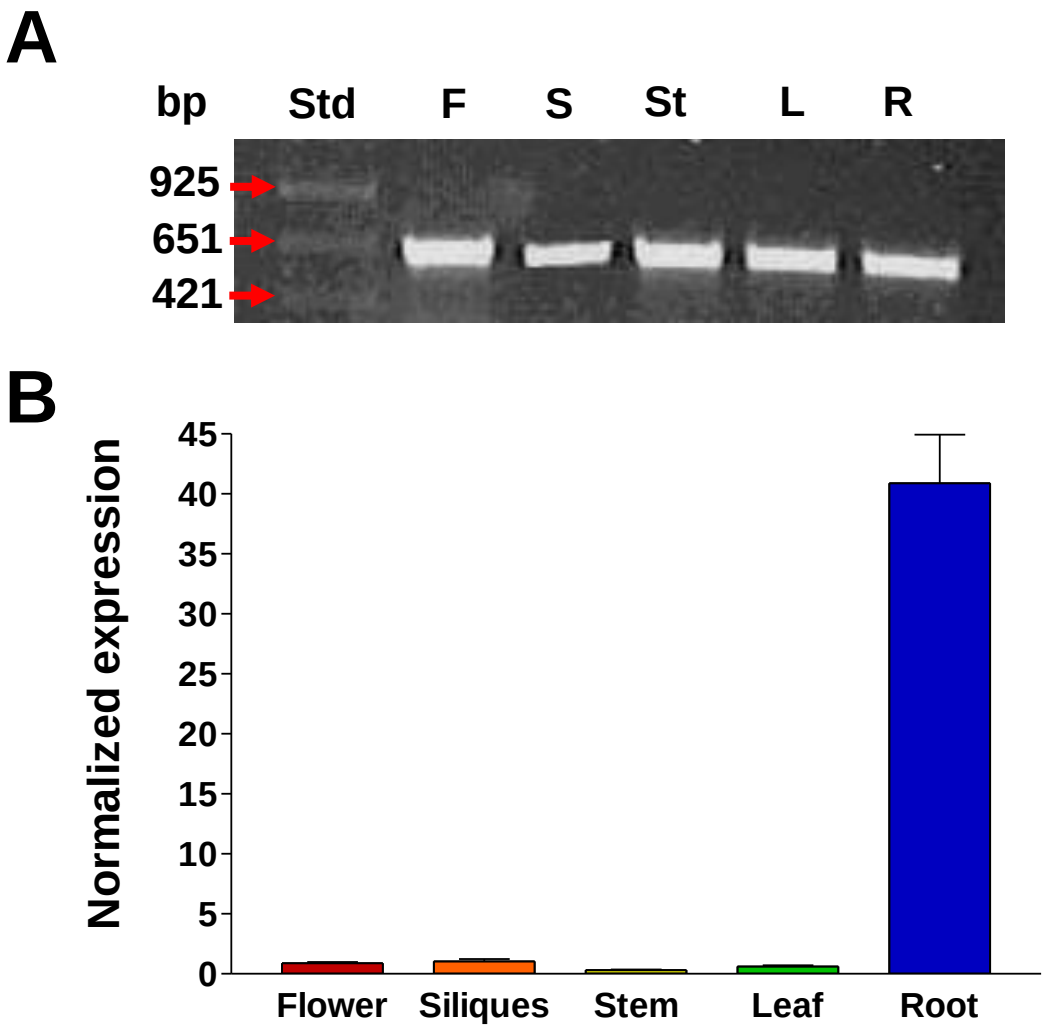

Figure 3.1. Expression of *AtNIP2;1* in various tissues of wild type Arabidopsis under standard growth conditions. Total RNA (100 ng) isolated from the indicated organs of 6 wk old Arabidopsis plants was used for semi-quantitative RT-PCR and real-time quantitative RT-PCR (Q-PCR) analyses as described in **Materials and Methods**. **A.** RT-PCR amplification of *Arabidopsis Actin 2* (*ACT2*) as an internal reference gene and a loading control. **Std** and **bp** represent DNA molecular standard marker and the molecular weights of the DNA molecular standard marker in base pairs. Abbreviations of **F, S, St, L,** and **R** indicate flower, siliques, stem, leaf, and root. **B.** Q-PCR analysis for the expression of *AtNIP2;1* in indicated organs of 6-wk old wild type Arabidopsis plants under normal growth conditions. The expression was normalized to the *AtNIP2;1* expression in siliques. Error bars show the SEM of three biological replicates.

Figure 3.2. GUS staining analysis of *AtNIP2;1* promoter::GUS transgenic Arabidopsis seedlings under normal growth conditions. GUS staining of two-week old Arabidopsis expressing the *AtNIP2;1 promoter-GUS* transgene was performed as described in the **Materials and Methods**. **A.** 2-wk old whole seedlings grown under normal LD light cycle conditions. Scale bar is 1.0 mm. **B and C.** The differentiated mature root region 2 cm from the root tip (**B**) and the root tip (**C**) regions. Scale bars are 100 µm.

A

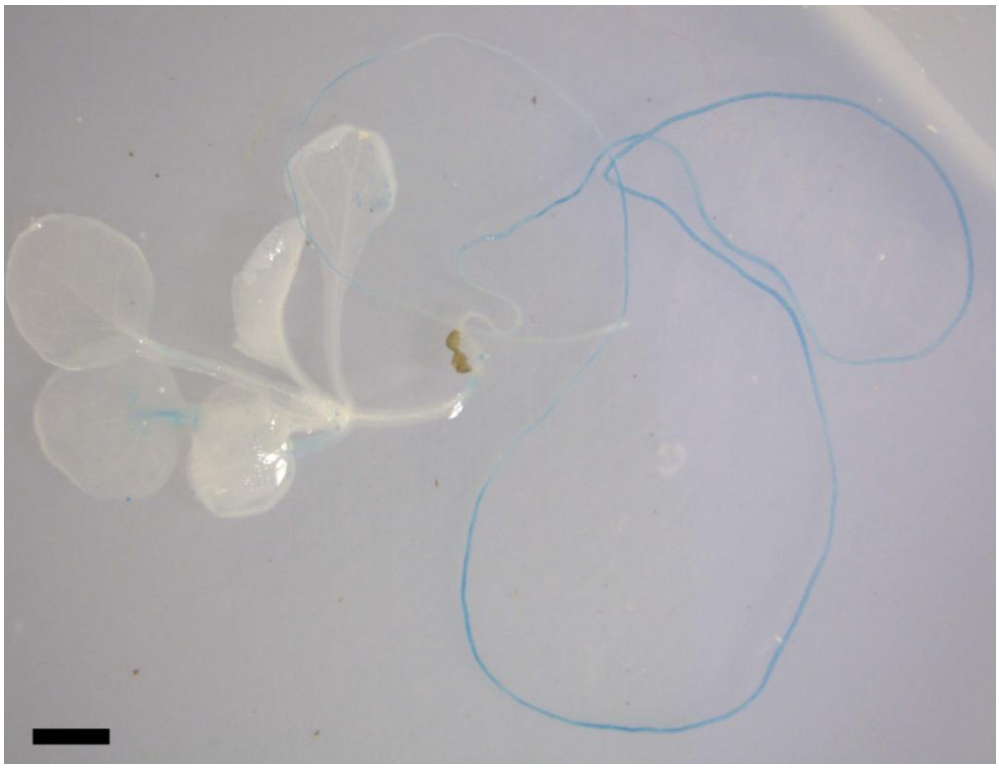

B

C

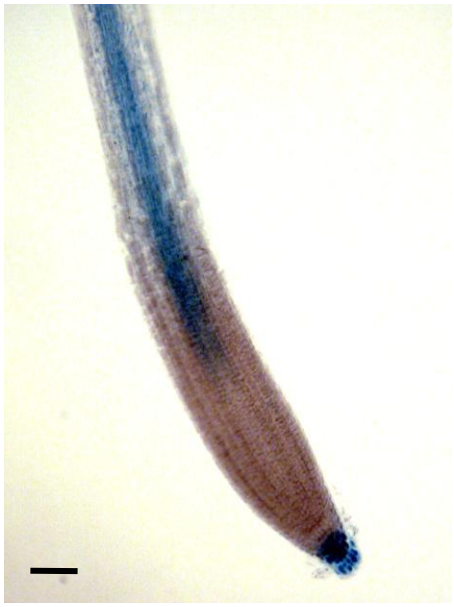

of 2-wk old Arabidopsis plants after GUS staining. Analysis of the cellular localization of GUS staining in the cross-sections of the unstressed roots showed that staining is predominant in the pericycle, phloem and companion cells within the stele, with little or no GUS signal apparent in xylem, endodermal, cortical and epidermal cells (Fig. 3.3).

Expression of *AtNIP2;1* in response to etiolation, oxidative, and flooding stress

Although *AtNIP2;1* is detectable by sensitive assays such as Q-PCR, overall its expression, similiar to most NIPs, is much lower than other plant MIPs (Alexandersson et al., 2005; Wallace et al., 2006). Since a number of plant MIPs are responsive to various environmental stress signals, analysis of *AtNIP2;1* expression in response to a series of various environmental stimuli using the Q-PCR and GUS staining approaches was under taken.

Most treatments surveyed had only modest effects on *AtNIP2;1* expression levels. For example, expression of *AtNIP2;1* was increased 2.5-fold in response to growth in complete darkness (etiolation) (Fig. 3.4), a result that was supported by GUS staining analysis (Fig. 3.4C 'Etiolated'). Little GUS expression was detected in the shoot of 2-wk old Arabidopsis under normal long day (LD) growth conditions (Fig. 3.4C 'Green').

In addition to etiolation, *AtNIP2;1* expression was also stimulated by oxidative stress achieved by applying an exogenous solution of 10 mM hydrogen peroxide (Fig. 3.5). Transcripts of the *AtNIP2;1* gene were increased over five-fold at 2 hr based on Q-PCR analysis, and declined to basal expression level at 24 hr (Fig. 3.5B). However, the most

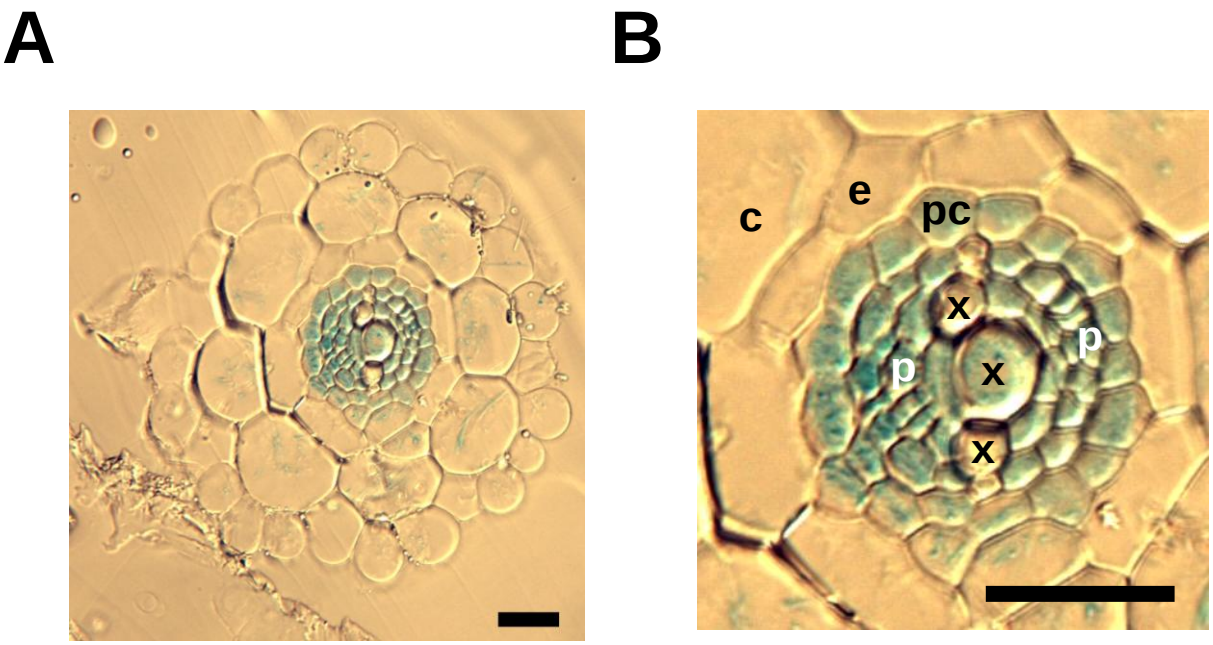

Figure 3.3. Cellular localization of *AtNIP2;1* in the roots under normal growth conditions. Two-wk old *AtNIP2;1pro*::GUS transgenic seedlings were grown under normal LD conditions and were stained for the reporter enzyme GUS. The GUS stained roots were then transverse sectioned (2 µm thickness) and were analyzed. **A.** Cellular localization of *AtNIP2;1* expression in the root transverse sections under normoxic conditions. **B.** Closer view of the stele region of the root section shown in the panel **A**. Each cell type of the stele was indicated according to the morphological study of Dolan et al. (1993). 'c' and 'e' represent cortex (c) and endodermis (e). 'pc' and 'p' indicate pericycle cells (pc) and phloem (p). 'x' represents meta-xylems (x). The scale bars show 20 µm.

Figure 3.4. Expression of *AtNIP2;1* in response to etiolation. WT and *AtNIP2;1pro*::GUS transgenic seedlings were grown under normal LD conditions or in complete darkness for 2 weeks. Q-PCR and GUS staining analyses were done as described in the **Materials and Methods**. **A.** Comparison of *AtNIP2;1* expression under normal growth conditions and darkness by using Q-PCR analysis. The expression was normalized to the *AtNIP2;1* expression in green seedlings. Error bars show the SEM of four biological replicates. **B.** RT-PCR amplification of *ACT2* as an internal reference gene to monitor cDNA quality and a loading control. **C.** GUS staining analysis of 2-wk old Arabidopsis *AtNIP2;1pro*::GUS transgenic seedlings grown under normal LD growth conditions (Green) and in darkness (Etiolated).

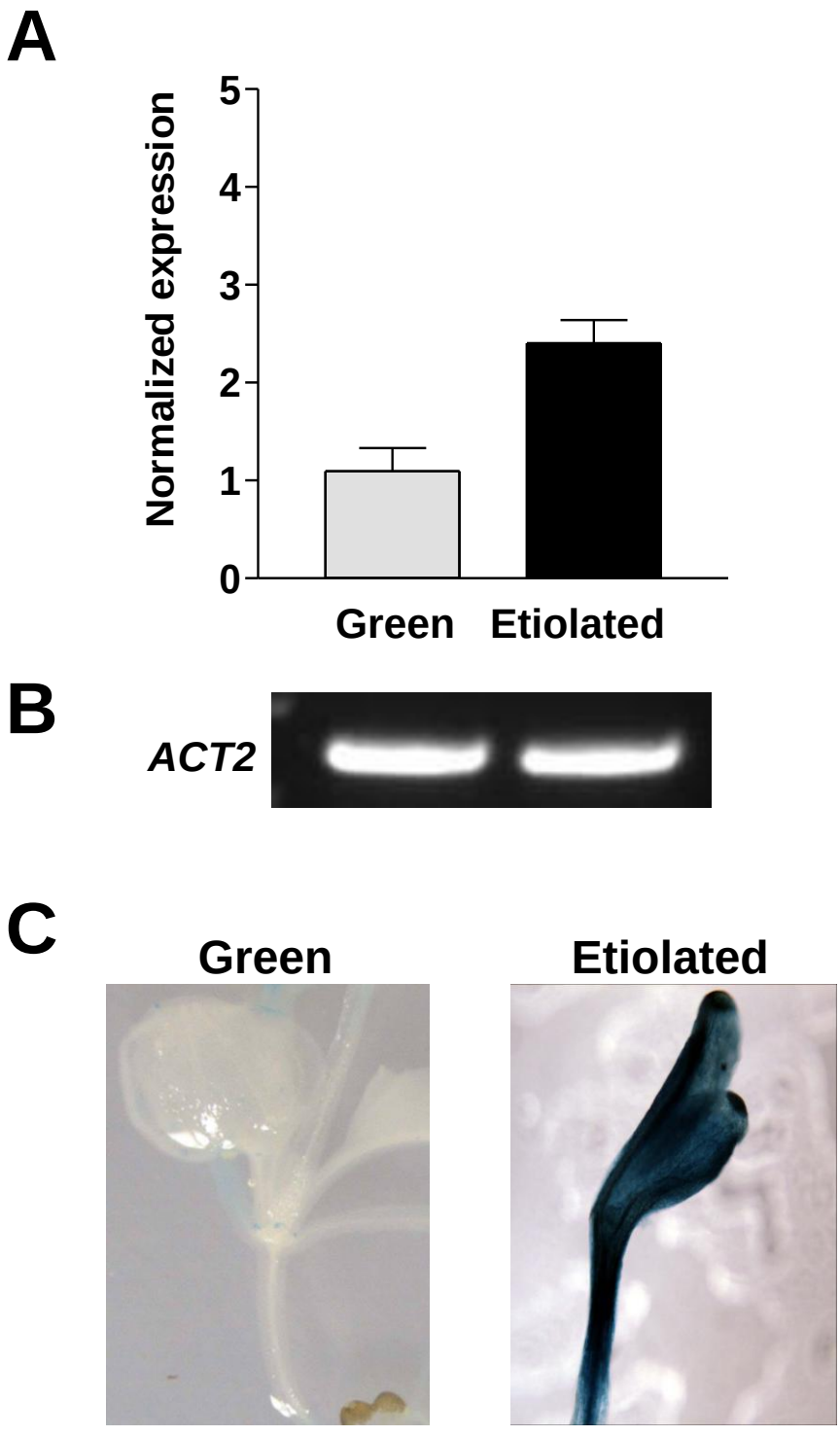
A
Normalized expression
5
4
3
2
1
0
Green
Etiolated
B
ACT2
C
Green
Etiolated

acute induction of *AtNIP2;1* expression was observed in response to flooding stress (Fig. 3.6 and 3.7).

Flooding stress was achieved by complete submergence of the root regions of 2-wk old seedlings as shown in Figure 3.6. Upon waterlogging of the roots of 2-week old young seedlings, a rapid 70-fold increase in *AtNIP2;1* transcript level was observed within 1hr after root submergence as assayed by Q-PCR (Fig. 3.7A). Expression subsequently decreased by 6 hr post flooding, but still remained between 10 to 20 fold higher than the control transcript levels (Fig. 3.7A). This pattern of *AtNIP2;1* regulation is also observed in the GUS staining pattern of flooding stressed *AtNIP2;1* promoter*::*GUS transgenic Arabidopsis (Fig. 3.7B). After submersion, GUS expression rapidly increased at 1 hr, peaked with high expression apparent not only in the vascular cylinder, but also in cortical cells and lateral roots (Fig. 3.7B). Similar to the Q-PCR results, GUS expression declined after this point, reaching a stable but elevated level at 6 hr (Fig. 3.7B)

Regulation of *AtNIP2;1* expression by anaerobiosis

Waterlogging of roots results in severe oxygen deficit due to the low diffusion co-efficient of oxygen in water (van Dongen et al., 2003). To test whether elevation of *AtNIP2;1* in response to flooding is part of the response of the plant to oxygen deficit, ten day old Arabidopsis seedlings were subjected to severe hypoxia by using an anaerobic jar. These tissues were then analyzed for *AtNIP2;1* expression, along with the expression of two established anaerobic polypeptide transcripts (*Pdc1* and *Adh1*

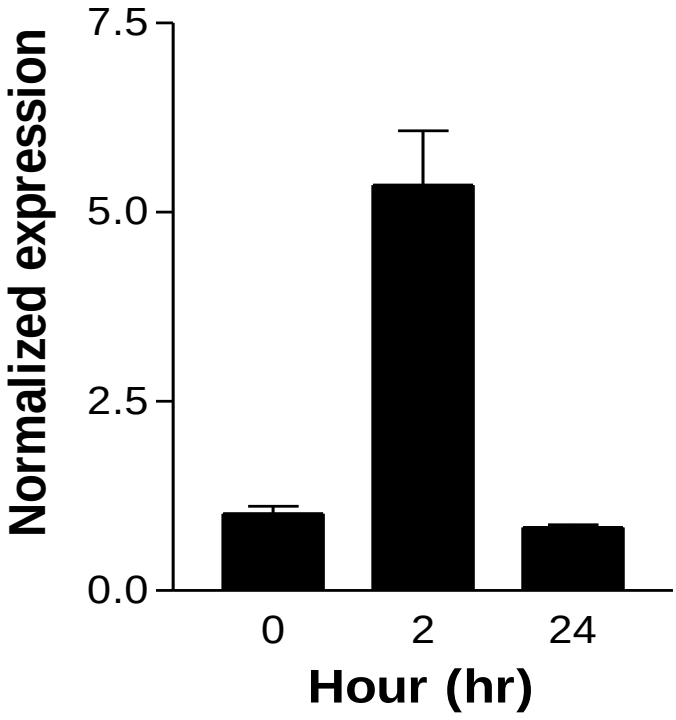

Figure 3.5. Effects of oxidative stress on *AtNIP2;1* expression in 2-wk old Arabidopsis plants. Q-PCR analysis of the expression of *AtNIP2;1* in response to 10 mM H_2O_2 treatment. Total RNA (100 ng) isolated from 2-wk old wild type Arabidopsis plants was used for Q-PCR analyses. Error bars show the SEM of four biological replicates.

A

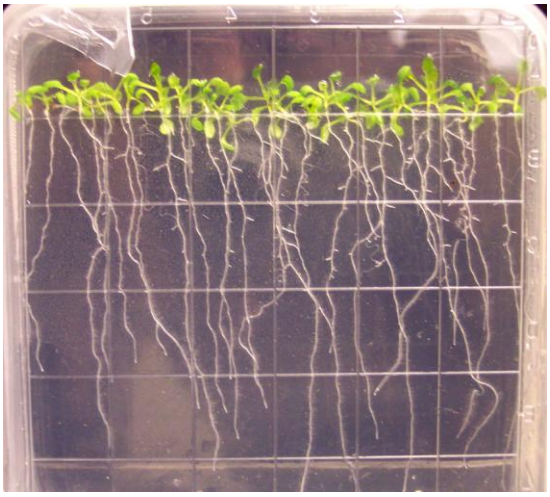

B

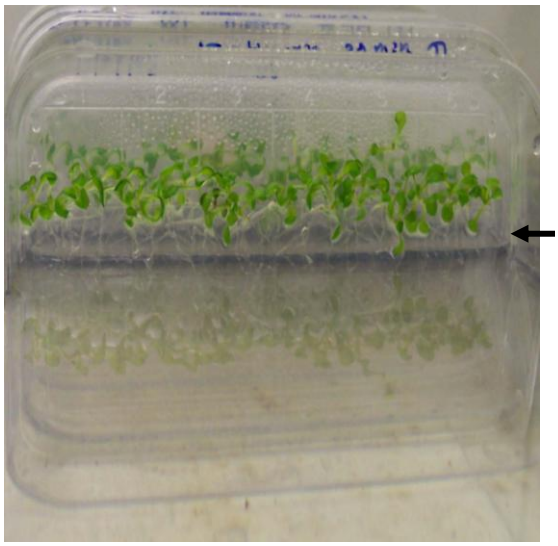

Figure 3.6. Waterlogging stress of 2-wk old Arabidopsis seedlings. Two-wk old wild type Arabidopsis plants were subjected to flooding stress by submerging only the root region of seedlings in water acclimated in a LD conditioned growth chamber. **A.** Two-wk old wild type Arabidopsis seedlings on a 1X strength MS agar plant just before submergence in water. **B.** Submerged Arabidopsis plants of the panel **A**. Arrow indicates water label on the plate showing that water label is below the shoot of seedlings.

Figure 3.7. *AtNIP2;1* expression in 2-wk old Arabidopsis seedlings in response to waterlogging. A. Two-week old Arabidopsis seedlings were subjected to flooding stress by complete immersion of the root region as described in the Methods. Total RNA (100 ng) was isolated for whole seedlings and was used for Q-PCR analysis of *AtNIP2;1* and *UBQ10* expression. Error bars represent the SEM of eight biological replicates. **B.** GUS staining of two-week old seedlings expressing the *AtNIP2;1 promoter-GUS* construct was carried as described in the **Materials and Methods**. Staining for GUS expression was carried out at 0 hr, 1 hr and 6 hr after submersion of the roots. The scale bar indicates 100 µm.

A

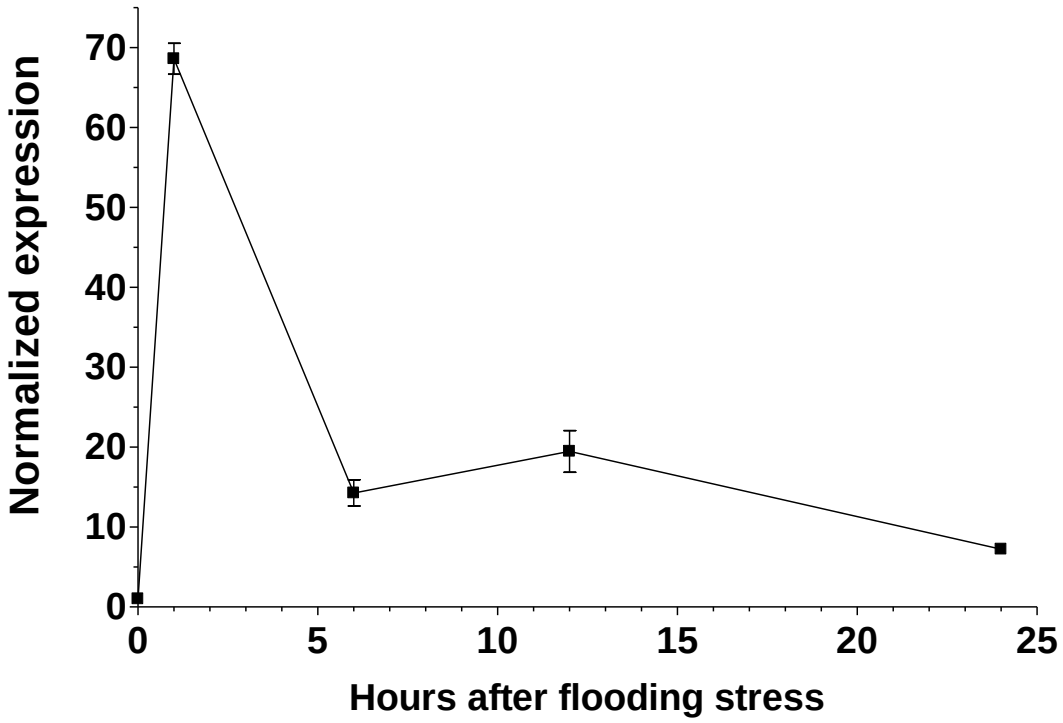
Normalized expression
70
60
50
40
30
20
10
0
0
5
10
15
20
25
Hours after flooding stress

B

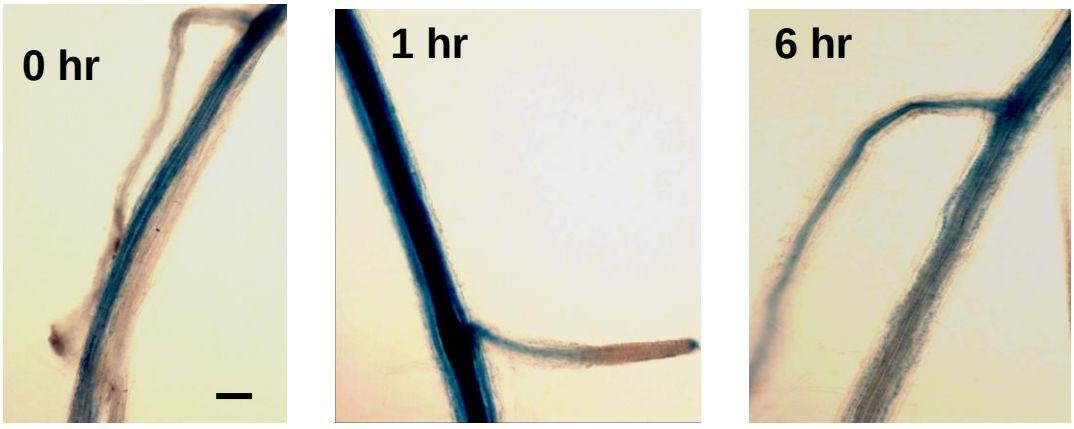
0 hr
1 hr
6 hr

encoding pyruvate decarboxylase 1 and alcohol dehydrogenase 1, respectively), by Q-PCR (Fig. 3.8). Severe hypoxic treatment of ten day old Arabidopsis seedlings showed an even greater stimulation of *AtNIP2;1* expression compared to waterlogged plants. At 30 min after the onset of hypoxia/anoxia, *AtNIP2;1* exhibits an increase in expression that parallels that of *Pdc1* (Fig. 3.8A) and *Adh1* (Fig.3.8B), and by 2 hr the expression of *AtNIP2;1* is increased 300-fold compared to control levels (Fig. 3.8).

AtNIP2;1 is a member of a multigene subfamily of Arabidopsis NIPs (Johanson et al., 2001; Wallace et al., 2006). To determine whether this sensitivity to waterlogging/oxygen deprivation is a common response among the NIP subfamily, or whether it is specific for *AtNIP2;1*, Q-PCR was performed on flooding and hypoxia-stressed seedlings using transcript specific probes for all members of the NIP subgroup I (*AtNIP1;1*, *AtNIP1;2*, *AtNIP2;1*, *AtNIP3;1*, *AtNIP4;1* and *AtNIP4;2*). As shown in Figure 3.9, low but detectable signal was observed for all NIPs in 10-day old Arabidopsis seedlings, except *AtNIP4;1*, which is expressed at an exceedingly low level based on microarray and Q-PCR data (Alexandersson et al., 2005). Although *AtNIP1;1* showed a slight increase in expression in response to flooding stress, all other NIP transcripts showed little or no change in response to flooding or anoxia stress compared to *AtNIP2;1* (Fig. 3.9). This argues that even though *AtNIP2;1* belongs to a closely related gene family (Arabidopsis NIP subgroup 1) (Wallace et al., 2006), *AtNIP2;1* is the only NIP subgroup I gene to show this selective rapid and acute responsiveness to oxygen deprivation (Fig. 3.9).

To determine the tissue distribution of *AtNIP2;1* expression in response to oxygen deprivation, two week old Arabidopsis seedlings were subjected to severe

Figure 3.8. *AtNIP2;1* expression in response to hypoxia treatment. Ten day old Arabidopsis seedlings were subjected to hypoxia in anaerobic flasks as described in the **Materials and Methods**. Total RNA (10 ng) isolated from root tissue was analyzed for *AtNIP2;1*, *Pdc1*, and *Adh1* expression by Q-PCR. **A.** Time course of *AtNIP2;1* (filled squares) and *Pdc1* (open squares) expression after the onset of hypoxia. **B.** Histogram comparing *AtNIP2;1*, *Adh 1* and *Pdc 1* after 2 hr of hypoxia (cross hatched bars) and normoxia controls (filled bars). The expression was normalized to the *AtNIP2;1* expression in normoxic seedlings. Error bars indicate SEM of four biological replicates (*AtNIP2;1* and *Pdc 1*) or three biological replicates (*Adh 1*).

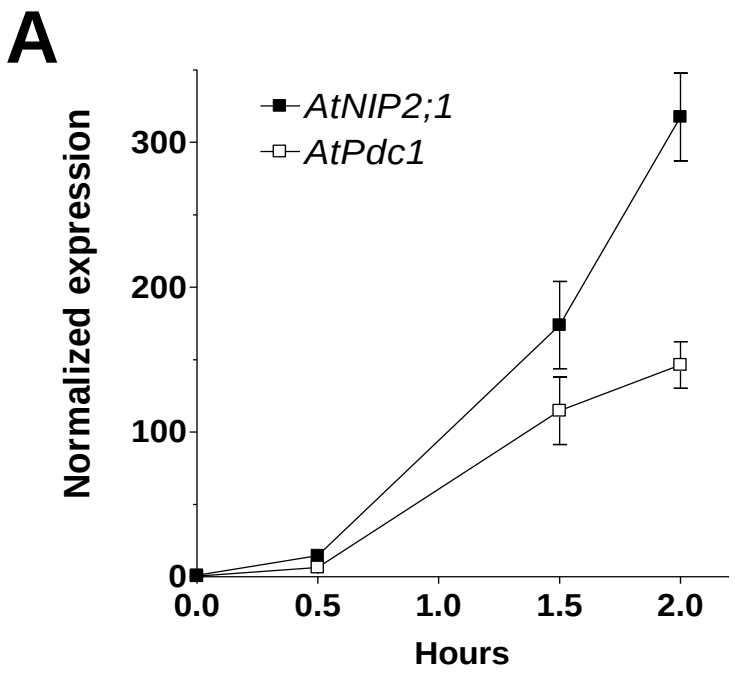
A
AtNIP2;1
AtPdc1
Normalized expression
300
200
100
0
0.0
0.5
1.0
1.5
2.0
Hours

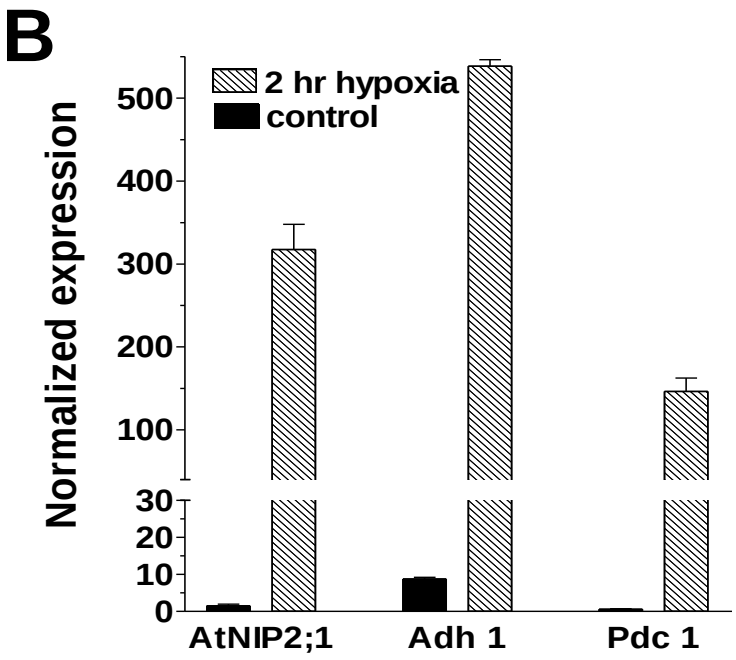
B
2 hr hypoxia
control
Normalized expression
500
400
300
200
100
30
20
10
0
AtNIP2;1
Adh 1
Pdc 1

Figure 3.9. Comparison of AtNIP subgroup 1 transcript levels in response to flooding and anoxia. Flooding or anoxia stress was administered as described in Figure 3.6 and 3.7 respectively using 2-wk old Arabidopsis seedlings. Q –PCR analysis was performed on total RNA (10 ng) using primer sets specific for the AtNIP transcripts indicated as described in the **Materials and Methods**. **A.** Expression of AtNIP transcripts in response to 1 hr flooding (crosshatched bars) compared to untreated controls (solid bars). **B.** Expression of AtNIP transcripts in response to 2 hr hypoxia-treatment (crosshatched bars) compared to untreated controls (solid bars). The expression was normalized to the *AtNIP2;1* expression in normoxic control. Error bars show SEM of four biological replicates (*AtNIP2;1*) or three biological replicates (other transcripts).

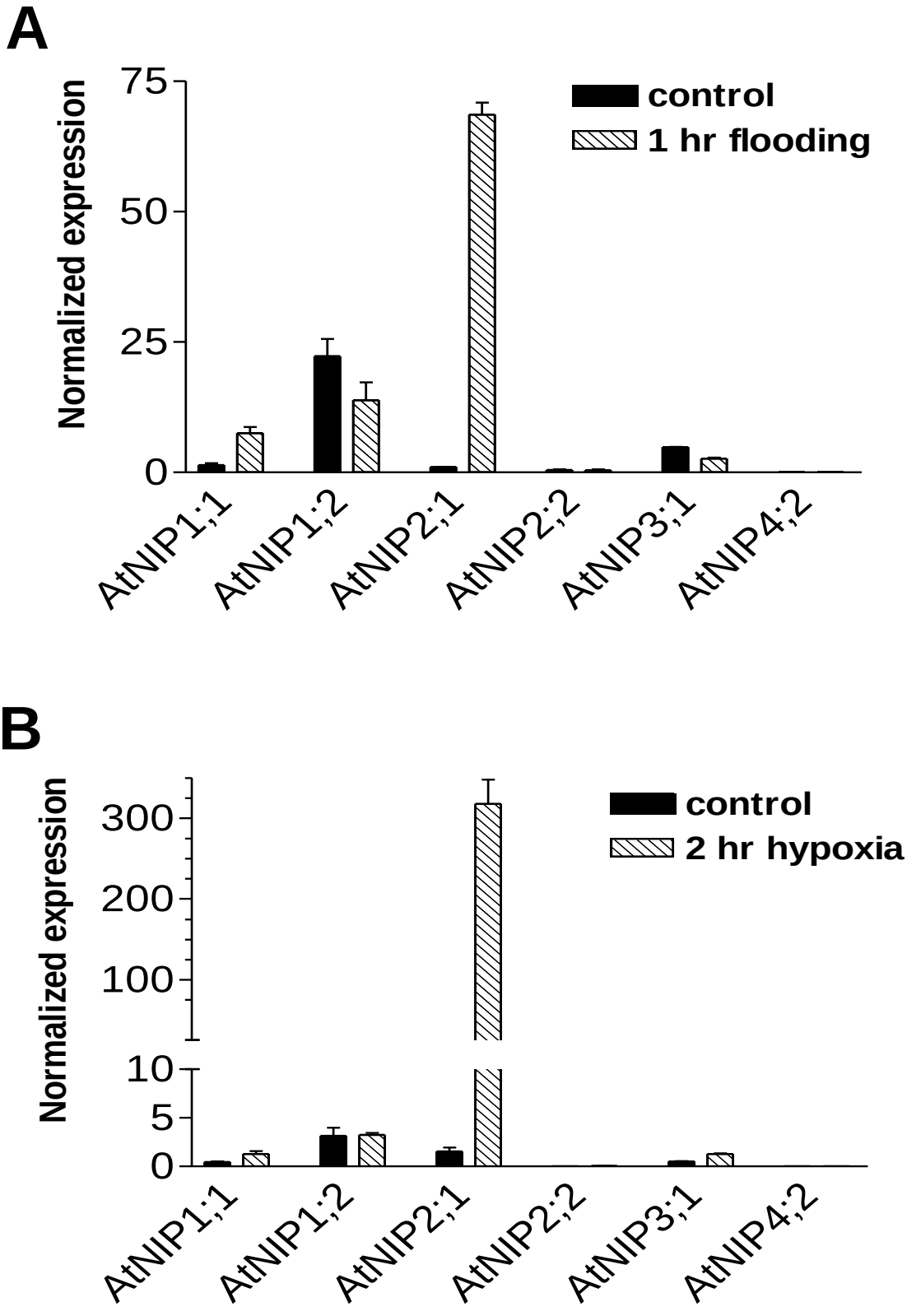
A
Normalized expression
75
50
25
0
control
1 hr flooding
AtNIP1;1
AtNIP1;2
AtNIP2;1
AtNIP2;2
AtNIP3;1
AtNIP4;2
B
Normalized expression
300
200
100
10
5
0
control
2 hr hypoxia
AtNIP1;1
AtNIP1;2
AtNIP2;1
AtNIP2;2
AtNIP3;1
AtNIP4;2

hypoxia as described above and were dissected into shoot and root tissues for RNA isolation and Q-PCR analysis. *AtNIP2;1* transcript levels are elevated predominantly in root tissues with a >1000 fold increase in *AtNIP2;1* transcript observed within two hours after the onset of anaerobiosis (Fig. 3.10A). *AtNIP2;1* transcript levels then showed a sharp decline by 12 hr but still remained over 100-fold elevated relative to normoxic controls (time 0, Fig. 3.10A). Hypoxia also induced AtNIP2;1 expression in shoot tissues, but with a lower overall expression (40-fold relative to basal levels) compared to roots. In addition, the time course of accumulation in shoots lagged behind root tissues and expression did not peak until 12 hr post treatment (Fig. 3.10A 'Inserted graph').

Identical patterns of *AtNIP2;1* expression were observed with *AtNIP2;1::GUS* promoter fusion plants subjected to the same oxygen deprivation regime (Fig. 3.10B). Analysis of the cellular localization of GUS staining under normoxic conditions shows that expression is limited to the roots (Fig. 3.10B) with little staining detected in shoot tissues (Fig. 3.10B). As discussed above, cross-sections of unstressed (normoxic) roots showed that staining is predominant in the pericycle, phloem and companion cells within the stele, with little or no GUS signal apparent in xylem, endodermal, cortical and epidermal cells as described in Fig. 3.3 (Fig. 3.11A). At 4 hr after the induction of hypoxia, root tissues show a large increase in GUS staining within the cells of the stele as well as the appearance of the GUS signal in the cortex, epidermis and root hairs (Fig. 3.11B). Similar to the Q-PCR result, this staining peaked at 4 hr post anoxic treatment and then decreased by 12 hr post treatment (Fig. 3.11B), although the expression at these later time points was still much higher than the basal expression in the unstressed roots (Fig. 3.11B). In comparison to roots, increases in GUS expression

Figure 3.10. Distinct *AtNIP2;1* expression patterns in *Arabidopsis* roots and shoots in response to oxygen deficit. Two-week old *Arabidopsis* seedlings were subjected to anoxia as described in the **Materials and Methods**. Total RNA (10 ng) isolated from the root and shoot tissues was used for Q-PCR. The ΔCt value of *AtNIP2;1* obtained from 0 hr of shoot sample was used as the calibrator for ΔΔCt and $2^{-\Delta\Delta Ct}$ calculations. **A.** Time course of *AtNIP2;1* expression in the root (filled squares) and the shoot (open squares) tissues after the onset of anoxia treatment. Inserted graph shows a rescaled view of *AtNIP2;1* expression in the shoot. Error bars indicate the SEM of three to six biological replicates. **B.** GUS staining analysis of two-week old *Arabidopsis* expressing the *AtNIP2;1 promoter*::GUS transgene subjected to severe hypoxia as in panel **A**. Scale bars are 1.0 mm.

A

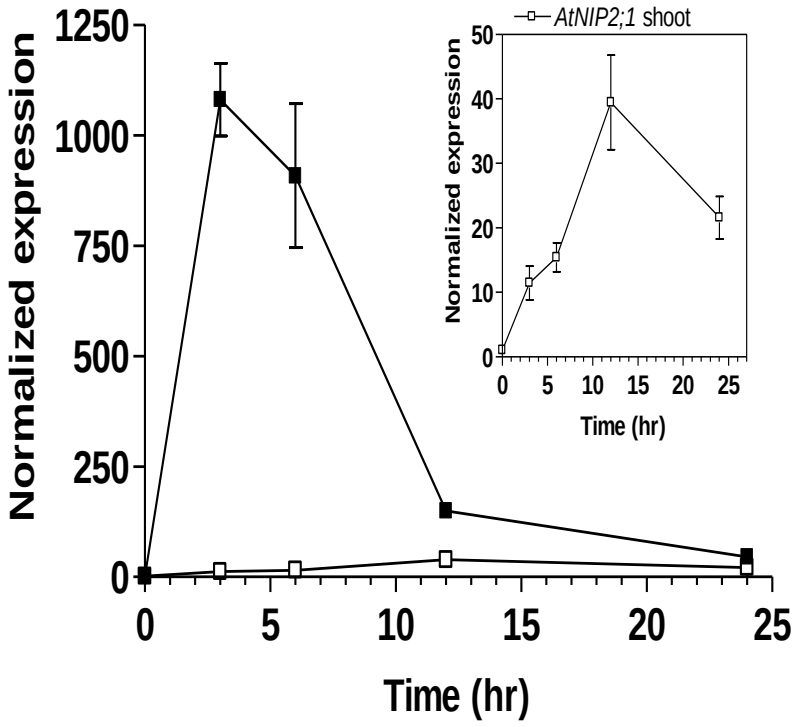
Normalized expression
1250
1000
750
500
250
0
0
5
10
15
20
25
Time (hr)
AtNIP2;1 shoot
Normalized expression
50
40
30
20
10
0
0
5
10
15
20
25
Time (hr)

B

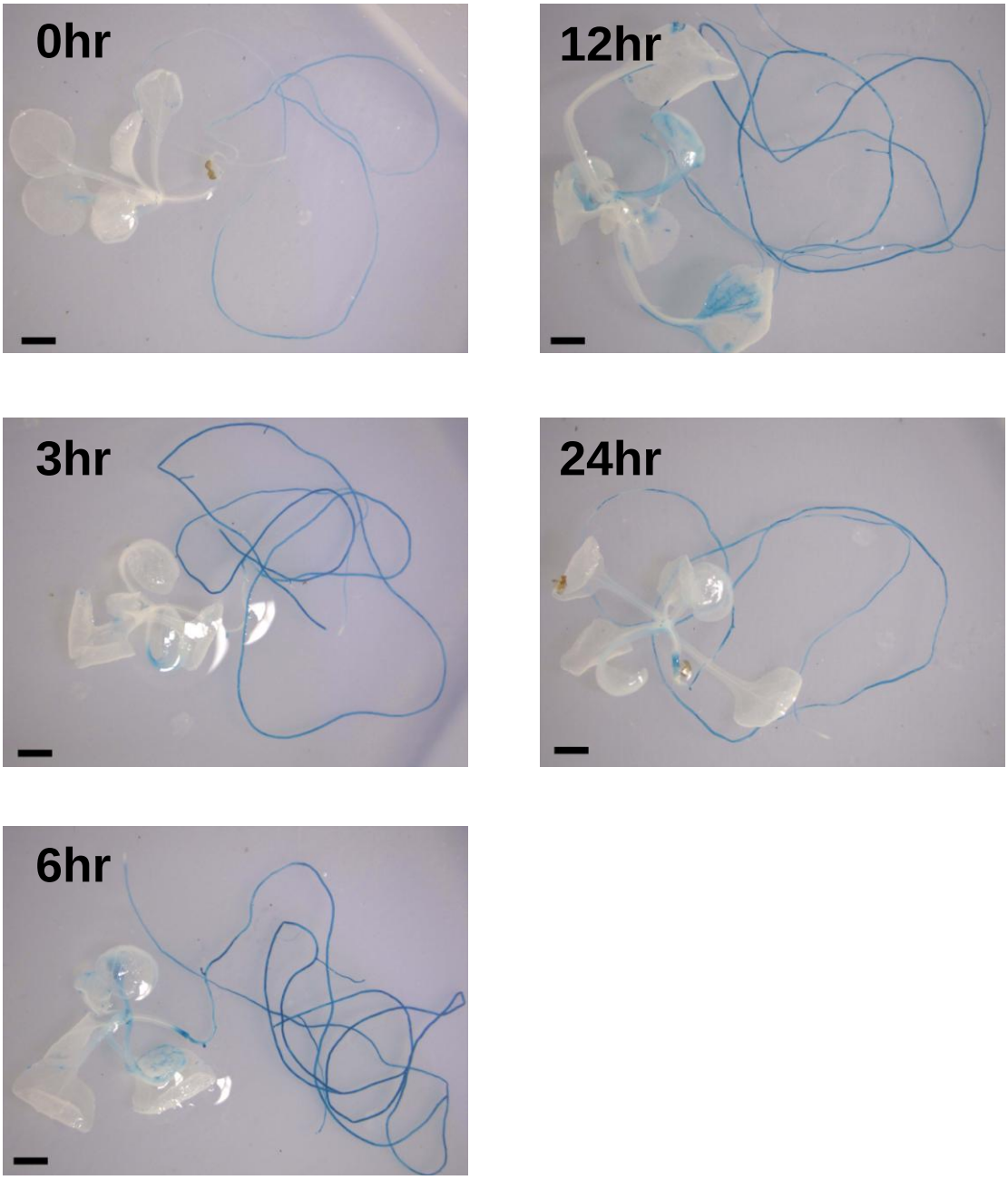

Figure 3.11. Cellular localization of *AtNIP2;1* in the roots and shoots of hypoxia stressed Arabidopsis. Two-week old *AtNIP2;1pro*::GUS transgenic seedlings were subjected to hypoxia and the GUS staining pattern was analyzed. **A.** Transverse section of the normoxic root. Each cell type of the stele was indicated as showed in the Figure 3.3. 'c' and 'e' represent cortex (c) and endodermis (e). 'pc' and 'p' indicate pericycle cells (pc) and phloem (p). 'x' represents meta-xylems (x). **B.** Cellular localization of *AtNIP2;1* expression in the root transverse sections in response to 0 hr (as normoxic control), 4 hr and 12 hr hypoxic treatment. The scale bars indicate 20 micrometers. **C.** GUS staining pattern of the shoot in response to 0 hr (as normoxic control) and 12 hr hypoxia. The scale bars show 1.0 mm.

A

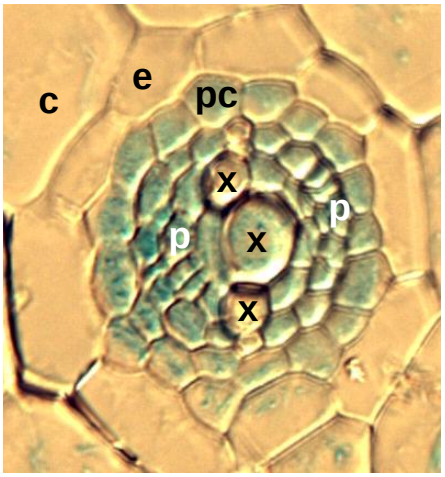

B

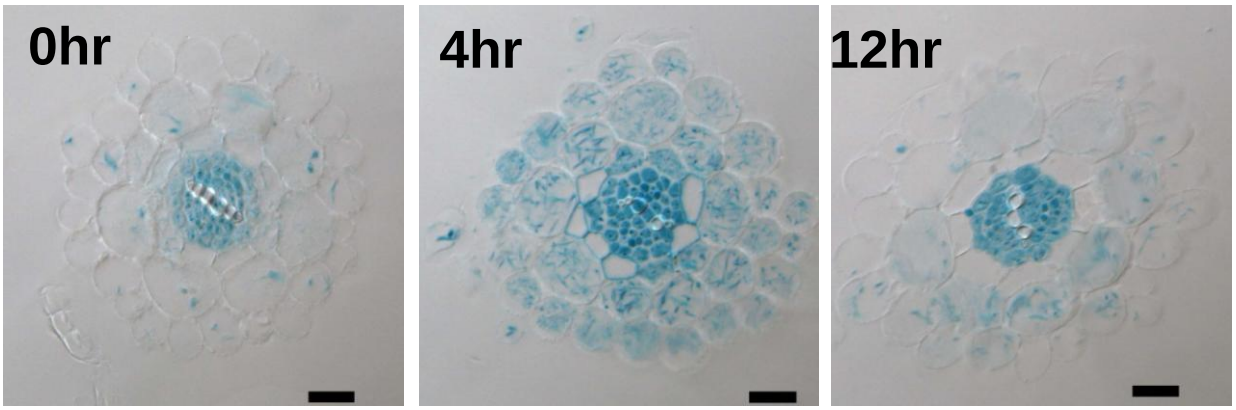

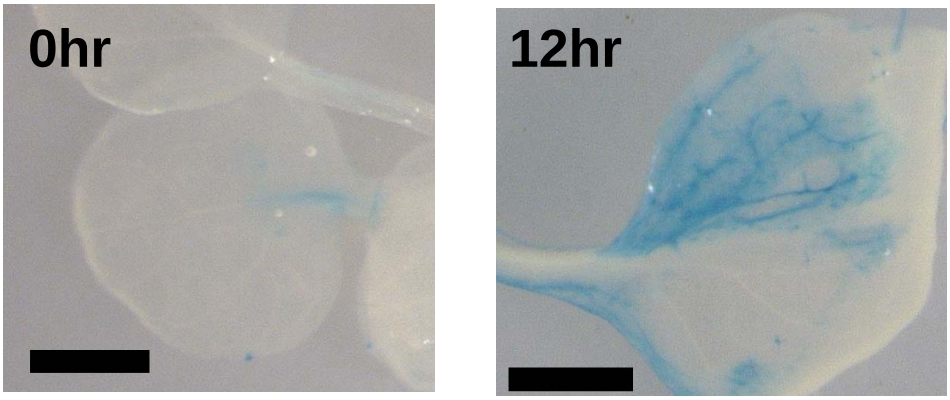

in shoots were less acute and were restricted mainly to the vascular tissues of leaves (Fig. 3.10B and 3.11C). Overall, these data show that *AtNIP2;1* is an Anaerobic Polypeptide that shows root-selective expression.

Subcellular localization of AtNIP2;1 in Arabidopsis

To determine the subcellular localization of AtNIP2;1, carboxyl terminal YFP fusion constructs were generated and were used to transiently transform *Arabidopsis* mesophyll protoplasts as well as produce stably transformed transgenic Arabidopsis plants (Fig. 3.12 and 3.13). Transient expression of AtNIP2;1-YFP in protoplasts results in a uniform expression around the cell periphery of protoplasts with a localization distinct from the cytosolic compartment visualized with endogenous fluorescence from chloroplasts (Fig. 3.12B). This pattern is consistent with plasma membrane localization. In contrast, controls with YFP alone show localization inside the cell and within the nucleus (Fig. 3.12A). In addition, CaMV35S-driven expression of AtNIP2;1::YFP was analyzed in stable transgenic Arabidopsis. In root epidermal (Fig. 3.13A) and root hair (Fig. 3.13B) cells expression of AtNIP2;1::YFP fussions showed a similar pattern of localization at the cell periphery consistent with the results observed in protoplasts. Overall, the pattern suggests a plasma membrane localization.

Functional characterization of AtNIP2;1 transport in *Xenopus* oocytes

The next question that was addressed is “what is the transport activity of AtNIP2;1 and what role does it play in adaptation to hypoxia”? To determine its transport properties, AtNIP2;1 was expressed as an amino terminal FLAG-tagged fusion in *Xenopus laevis* oocytes and was compared to the prototypical NIP soybean

Figure 3.12. Subcellular localization of AtNIP2;1::YFP fusion proteins in Arabidopsis mesophyll protoplasts. Transient expression of the AtNIP2;1::YFP C-terminal fusion in *Arabidopsis* mesophyll protoplasts was done as described in the **Materials and Methods**, and localization was analyzed by laser-scanning confocal fluorescence microscopy. '**DIC**' represents Optical Differential Inference Contrast (DIC) image for intact mesophyll protoplasts. '**Chlorophyll**' and '**YFP**' indicate chlorophyll auto-fluorescence (588-716 nm) signal (Chlorophyll) and YFP-fluorescence (507-532nm) signal (YFP), respectively. '**Merge**' represents merged image of '**Chlorophyll**' and '**YFP**' signal images. **Panel A.** YFP expression in mesophyll protoplasts. **Panel B.** AtNIP2;1::YFP expression in mesophyll protoplasts.Size bars are 16 µm.

A

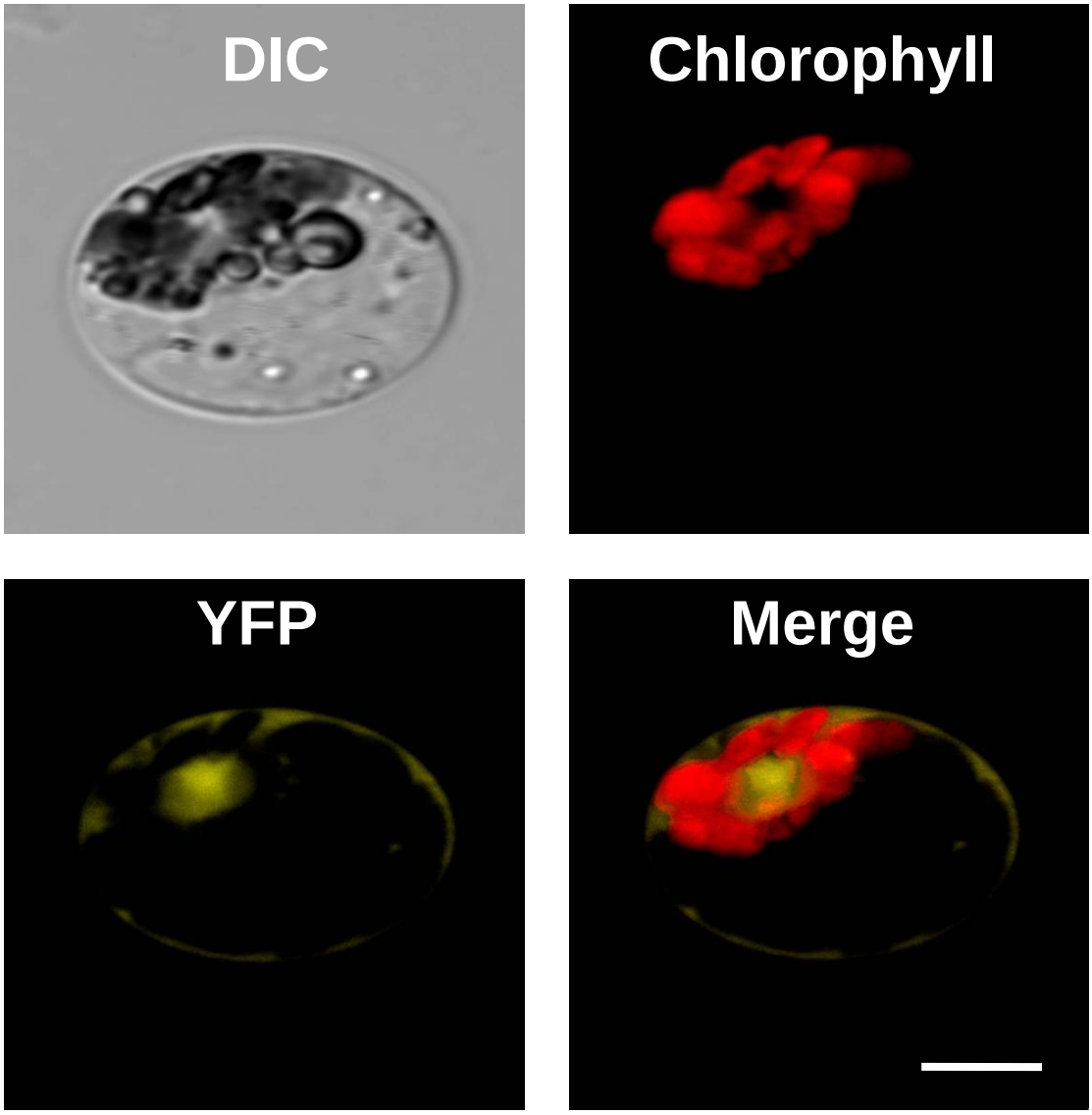

B

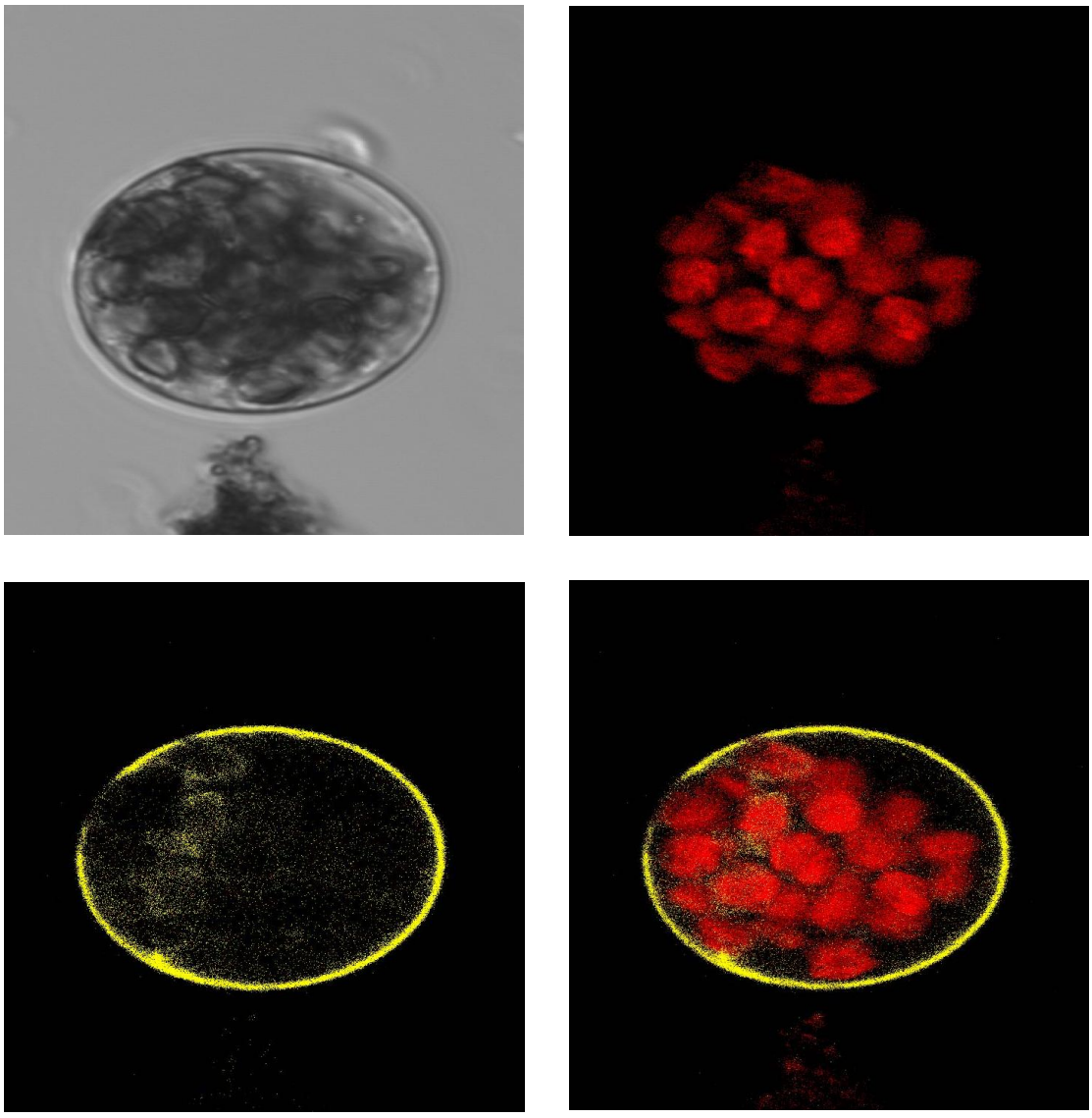

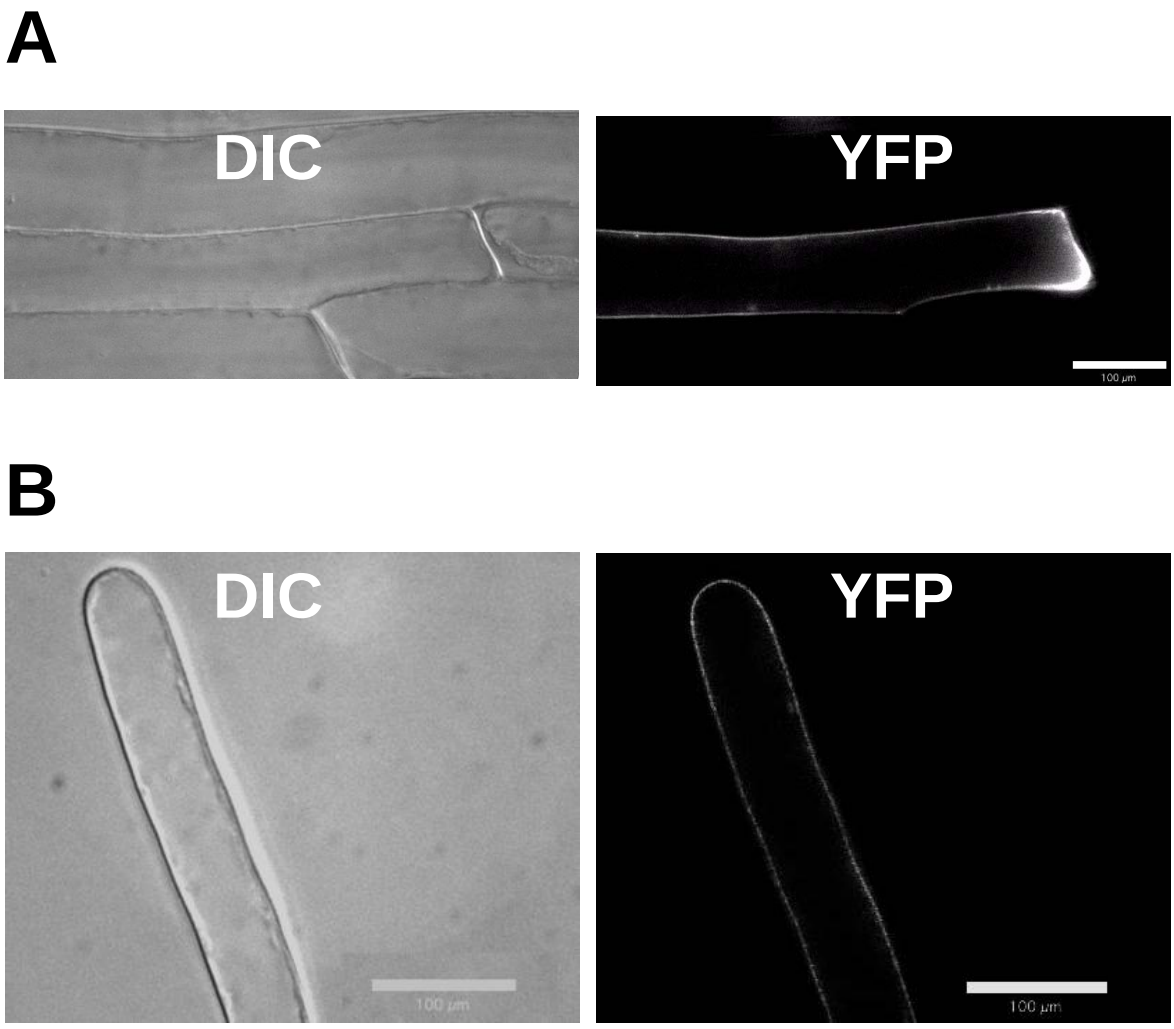

Figure 3.13. Subcellular localization of AtNIP2;1 in the roots of transgenic Arabidopsis expressing AtNIP2;1::YFP fusions. Stable transgenic Arabidopsis overexpressing AtNIP2;1::YFP fusions were generated as described in the **Materials and Methods**. Subcellular localization of AtNIP2;1::YFP fusions was analyzed by fluorescence microscopy equipped with YFP filter. **A.** Subcellular localization of AtNIP2;1::YFP in mature primary root epidermal cells (~2 cm from the root tip) of 7 day old seedlings. **B.** AtNIP2;1::YFP localization in a root hair. '**DIC**' represents Optical Differential Inference Contrast (DIC) image. '**YFP**' indicates YFP-fluorescence signal (YFP), respectively. Size bars show 100µm.

nodulin 26. Inititial experiments investigated the aquaporin activity of the two proteins in swelling assay pioneered by Preston et al. (1992). Injection of AtNIP2;1 results in expression of the protein in oocytes at approximately the same level as soybean nodulin 26 (Fig. 3.14). Analysis of the water permeability of AtNIP2;1 expressing oocytes showed only a slight increase in osmotic water permeability (P_f = 0.99 x 10^{-4} cm/s at pH 7.6) compared to control oocytes (0.46 x 10^{-4} cm/s). This water permeability is significantly lower than that observed with control oocytes expressing soybean nodulin 26 (1.93 x 10^{-4} cm/s at pH 7.6) (Fig. 3.15A). Interestingly, nodulin 26 showed an enhanced P_f in response to lower pH (4.6 x 10^{-4} cm/sec at pH 5, Fig. 3.15A), consistent with previous observations of pH-dependent gating stimulating the transport of some aquaporins (Nemeth-Cahalan and Hall, 2000). The water permeability of AtNIP2;1 remained low throughout the pH range although a slight elevation of P_f is observed at pH 4 (Fig. 3.15A). Water flux through AtNIP2;1 and nodulin 26 were both inhibited by 1 mM Hg^{2+} (Fig. 3.15B), consistent with previous observations suggesting protein facilitated water transport (Rivers et al., 1997). The data of the water permeability analysis of AtNIP2;1 showing low intrinsic water permeability suggests, therefore, that AtNIP2;1 may differ from its archetype Nod26 and have alternative substrates.

Given the observation that *AtNIP2;1* is elevated in response to flooding and anoxic stress (Fig. 3.7 and 3.8) and that water is not a likely substrate for this channel protein (Fig. 3.15), an alternative transport activity supporting adaptation to low oxygen conditions such as flooding was considered. Flooding stress in plants results in oxygen deficit which induces a rapid metabolic shift from aerobic respiration to lactic acid fermentation as proposed in the Davies-Roberts pH stat model (Fig. 3.16).

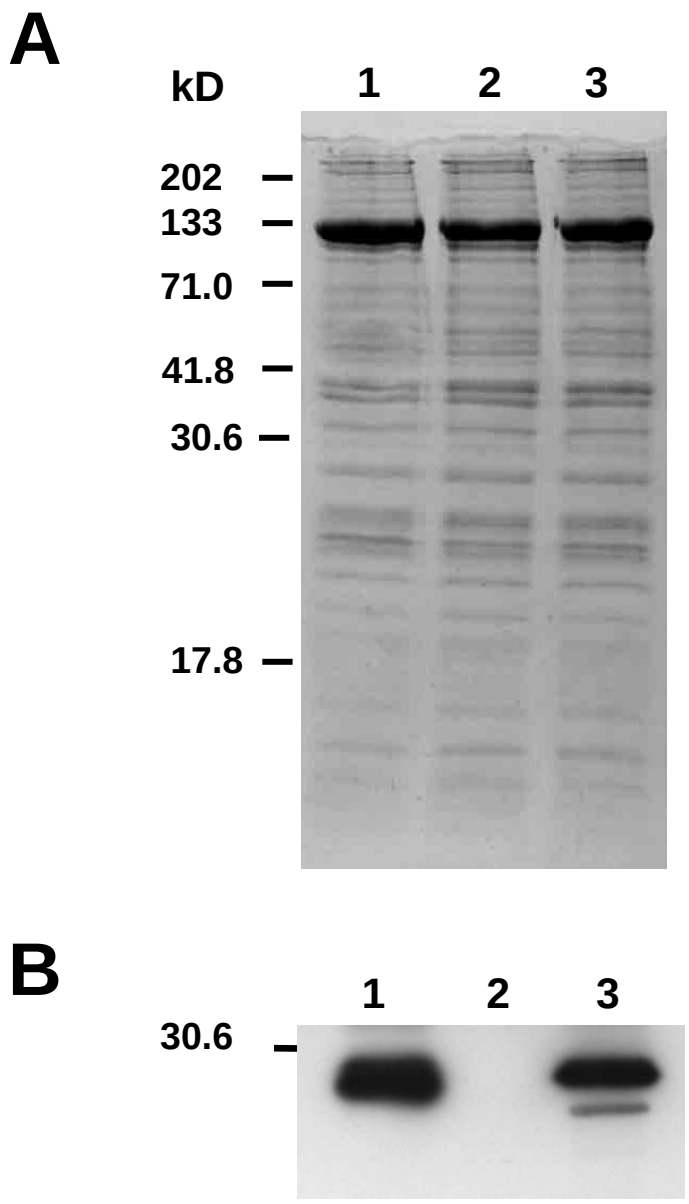

Figure 3.14. Western blot analysis for Nod26 and AtNIP2;1 expression in *Xenopus* oocytes. Oocyte lysates were extracted from oocytes expressing Nod26 (positive control), no MIPs (water injected; negative control), and AtNIP2;1 protein as described in the **Materials and Methods**. **A.** Coomassie blue staining of 12.5% SDS-PAGE. B**.** Western blot analysis of oocyte lysates (16 µg protein) using α-FLAG monoclonal antibody. **lane 1,** AtNIP2;1F-injected oocytes; **lane 2**, control oocytes injected with RNase-free water; **lane 3**, Nod26F-injected oocytes. '**kD**' shows the molecular weight of protein molecular weight standards.

Figure 3.15. Osmotic water permeability (P_f) of AtNIP2;1 in *Xenopus* oocytes. *Xenopus* oocytes were injected 46nL of 1ng/nl FLAG-tagged *AtNIP2;*1 (*AtNIP2;1F*) or FLAG-tagged *Nod26* (*Nod26F*) cRNA or with 46nl of RNase free water (control). Oocytes were cultured for three days and were assayed for water permeability by using the swelling assay as described in the **Materials and Methods**. **A.** Comparison of the osmotic water permeability co-efficient (P_f) of oocytes expressing AtNIP2;1 and soybean Nod26, and control oocytes as a function of the pH of the bath solution. **B.** Effects of $HgCl_2$ (1 mM) on the P_f of AtNIP2;1 (left) and Nod26 (right). Error bars indicate SEM (n = 5 to 9).

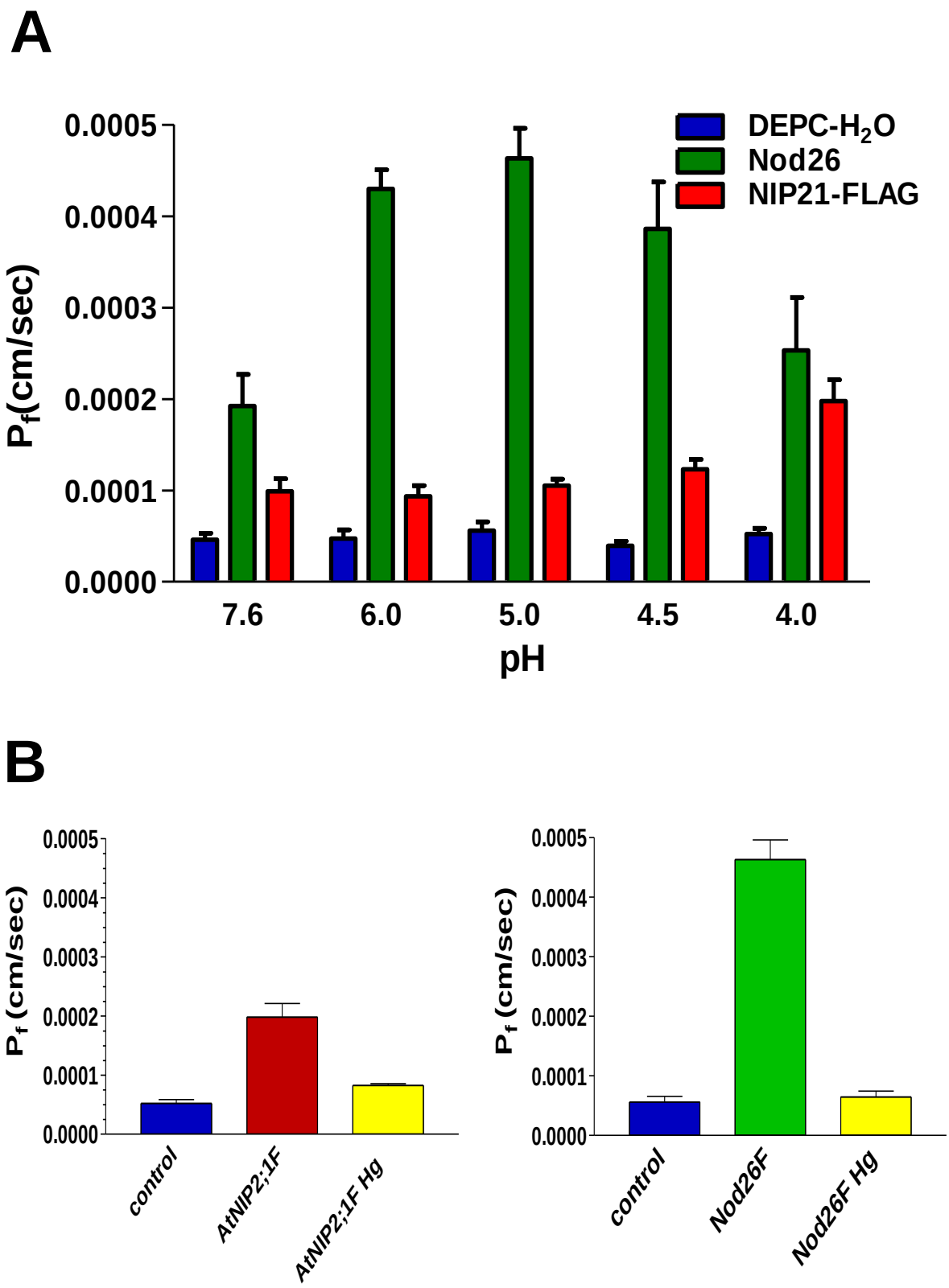
A
0.0005
0.0004
0.0003
0.0002
0.0001
0.0000
Pf(cm/sec)
DEPC-H2O
Nod26
NIP21-FLAG
7.6
6.0
5.0
4.5
4.0
pH
B
0.0005
0.0004
0.0003
0.0002
0.0001
0.0000
Pf (cm/sec)
control
AtNIP2;1F
AtNIP2;1F Hg
0.0005
0.0004
0.0003
0.0002
0.0001
0.0000
Pf (cm/sec)
control
Nod26F
Nod26F Hg

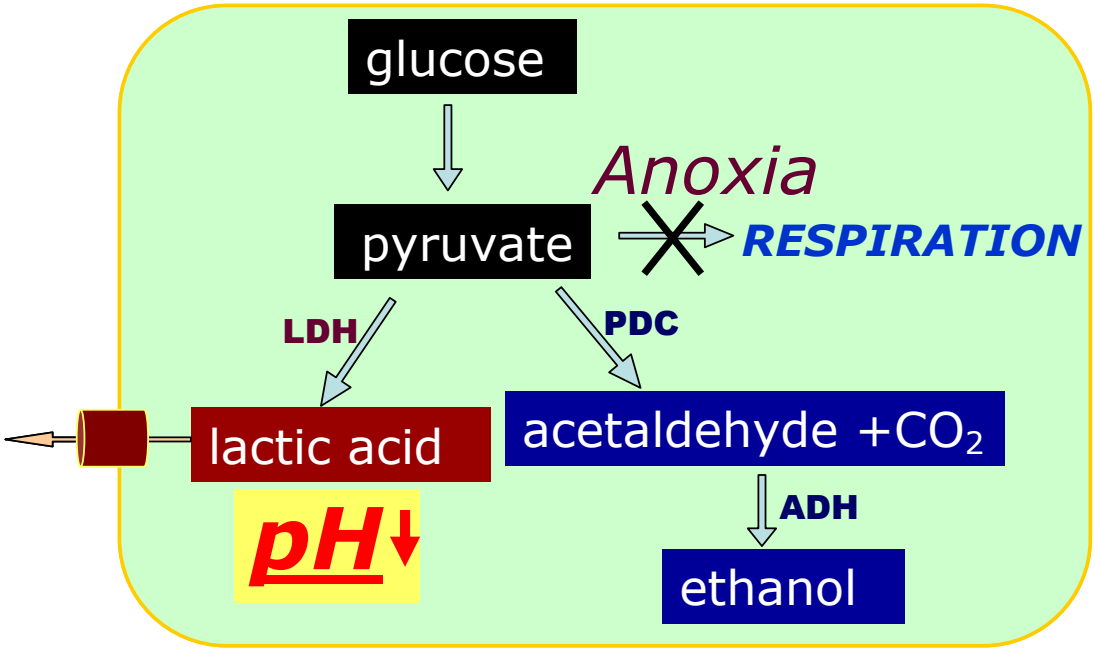

Figure 3.16. The Davies-Roberts pH stat model for adaptation of plant roots to oxygen deprivation. In response to anoxia, energy catabolism is disrupted due to the lack of oxygen to support respiration. Under these conditions glycolysis is the principal source of ATP production. To sustain glycolytic flux, NADH needs to be recycled by lactic acid fermentation. However, this leads to an accumulation of H^+ in the cytosol leading to acidosis. To prevent this, plants switch to alcoholic fermentation and lactic acid efflux is stimulated (Davies et al., 1974; Roberts et al., 1984).

As part of the adaptation to this altered metabolic flux, and to avoid cytosolic acidification, several plant species acquire the ability to transport lactate/lactic acid out of the cytosol (Felle, 2005). An examination of protonated lactic acid (MW= 90.1 and van der Waals volume= 48.0 cm^3/mol) reveals similarities in solute size and dimension to other NIP transport substrates such as glycerol (MW= 92.1 and a van der Waals volume= 51.4 cm^3/mol) (Fig. 3.17).

To test the hypothesis that AtNIP2;1 might be involved in transport activities associated with anaerobic adaptation, the *Xenopus* oocyte expression system was used to analyze the transport behavior of the protein. The results showed that oocytes expressing AtNIP2;1 show an enhanced rate of uptake of ^{14}C-labeled lactic acid from the bath solution which is dependent on pH (Fig. 3.18A). Further, the pH dependence of the transport rate of ^{14}C-lactic acid parallels the calculated concentration of protonated lactic acid (Fig. 3.18B), suggesting that the acid form is the substrate for transport through the AtNIP2;1 channel. Control oocytes show uptake of ^{14}C-lactate at lower pH, albeit at a much lower rate compared to AtNIP2;1-expressing oocytes (Fig. 3.18A) and with unsaturable kinetics.

To verity that lactic acid transport is mediated and facilitated by the AtNIP2;1 membrane channel, we tested inhibition by mercurial compounds, and determined the Arrhenius activation energy. Similar to findings with water and glycerol transport through other NIPs, AtNIP2;1 lactic acid transport is completely inhibited by $HgCl_2$ as shown in Figure 3.19 (panel A), suggesting that lactic acid transport is channel mediated and is not due to simple diffusion through the bilayer. Further, analysis of the activation energy of transport in uninjected and AtNIP2;1-expressing oocytes was

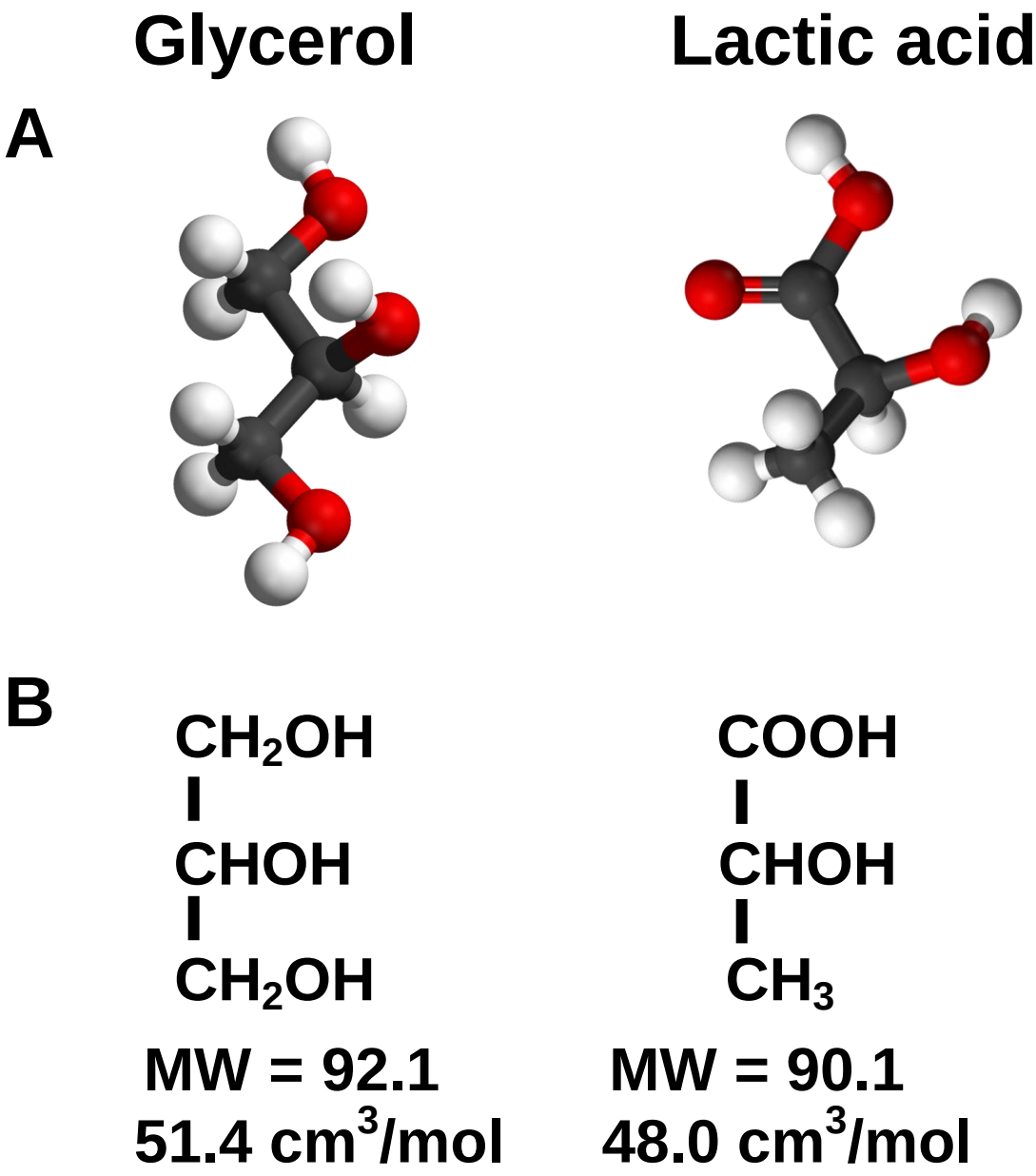

Figure 3.17. Comparison of chemical properties of glycerol and lactic acid. A. structure of glycerol and lactic acid. Gray atoms show carbon and the red and white atoms indicate oxygen and hydrogen, respectively. **B.** Molecular formula of glycerol and lactic acid, respectively. "cm^3/mol" is the unit of van der Waals volume.

Figure 3.18. Lactic acid transport by AtNIP2;1 in *Xenopus* oocytes. Flag-tagged AtNIP2;1 (AtNIP2;1F) -expressing oocytes were tested for the uptake of lactic acid by incubation in bath solutions containing modified Frog Ringer's solution with ^{14}C-labeled lactic acid (20 mM) as described in the **Materials and Methods**. **A.** ^{14}C-labeled lactic acid transport rate of control or AtNIP2;1F-expressing oocytes as a function of the media pH. Error bars show SEM (n = 3). **B.** Lactic acid uptake rate of AtNIP2;1F-expressing oocytes as a function of pH. ^{14}C-lactic acid uptake was performed as in part A with the exception that the bath solution was buffered to the pH value indicated. The uptake by AtNIP2;1F oocytes was corrected by subtracting the basal lactic acid uptake by water-injected control oocytes. The solid line shows the concentration of the protonated lactic acid as a function of pH based on the Henderson-Hasselbach equation. Error bars show SEM (n = 3).

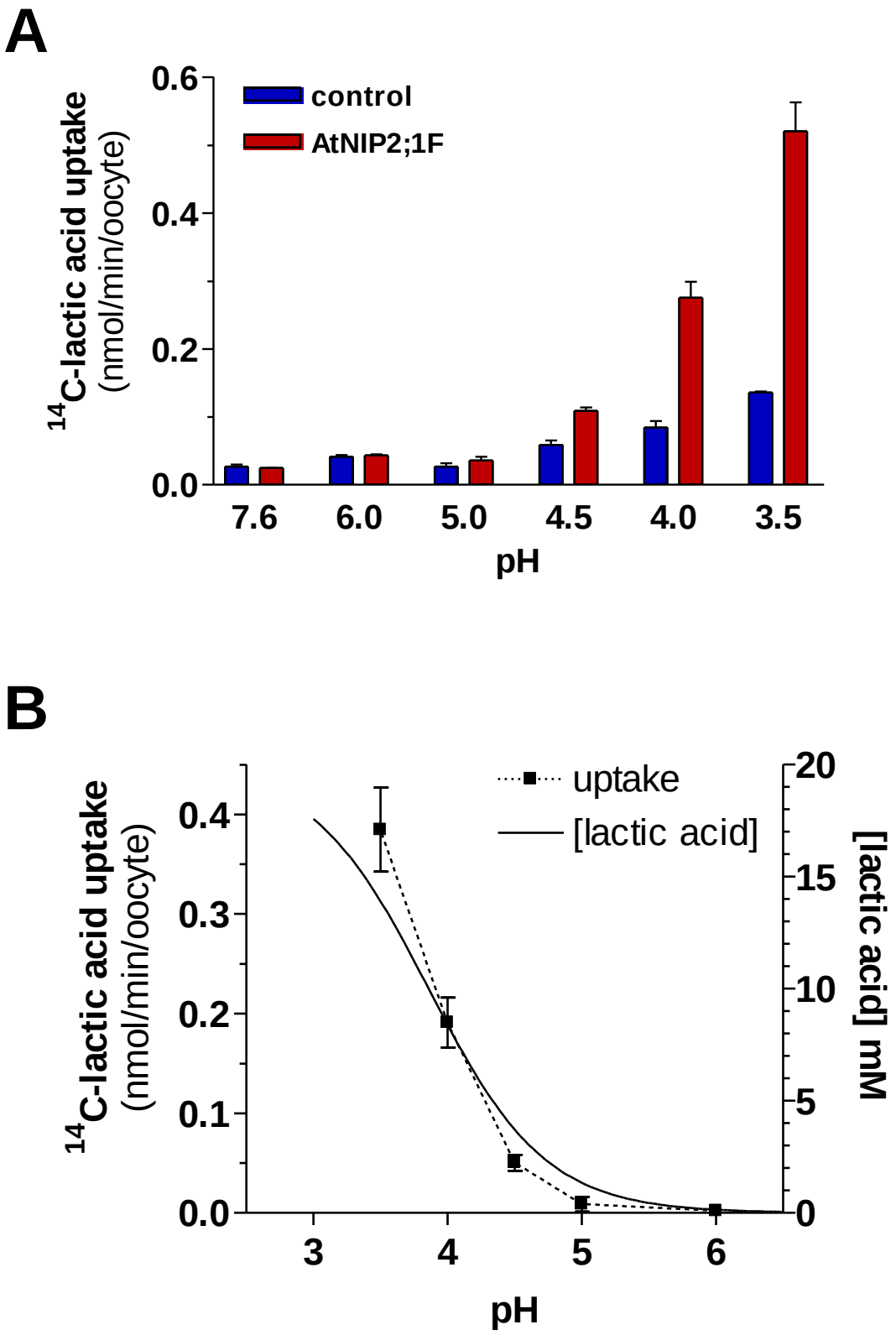
A
0.6
0.4
0.2
0.0
control
AtNIP2;1F
14C-lactic acid uptake
(nmol/min/oocyte)
7.6
6.0
5.0
4.5
4.0
3.5
pH
B
uptake
[lactic acid]
0.4
0.3
0.2
0.1
0.0
20
15
10
5
0
[lactic acid] mM
14C-lactic acid uptake
(nmol/min/oocyte)
3
4
5
6
pH

Figure 3.19. Lactic acid transport by AtNIP2;1 shows the hallmarks of facilitated transport. A. Effects of Hg^{2+} on the ^{14}C-lactic acid uptake by AtNIP2;1F. Ooctyes were preincubated with 1 mM $HgCl_2$ for ten min prior to assay of lactic acid uptake. Error bars show SEM (n = 3). **B.** Arrhenius plot of lactic acid transport through control and AtNIP2;1 oocytes (n=6).

A

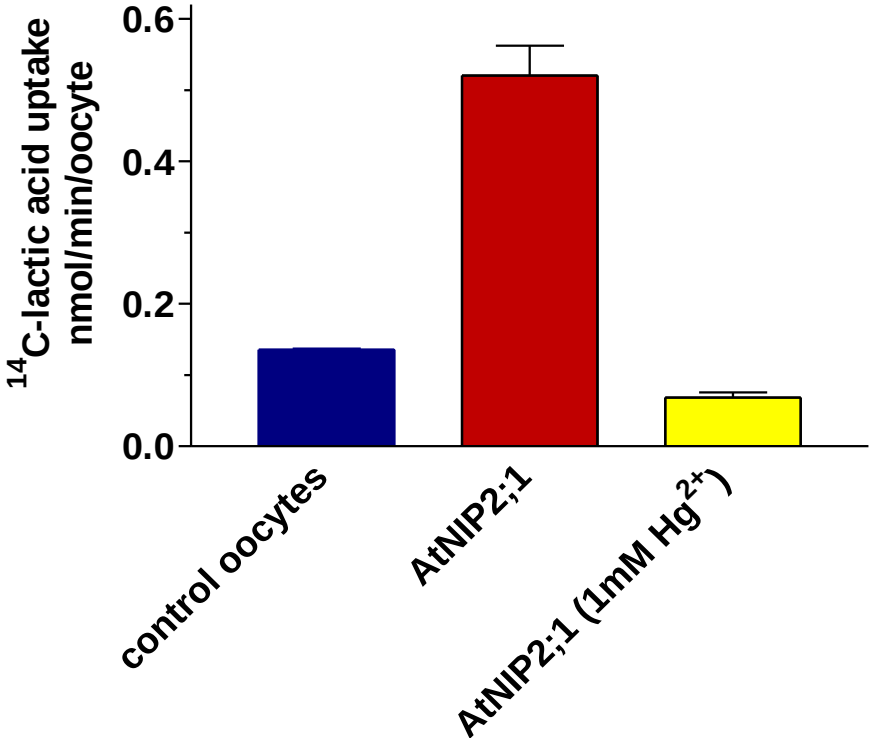
^{14}C-lactic acid uptake
nmol/min/oocyte
0.6
0.4
0.2
0.0
control oocytes
AtNIP2;1
AtNIP2;1 (1mM Hg^{2+})

B

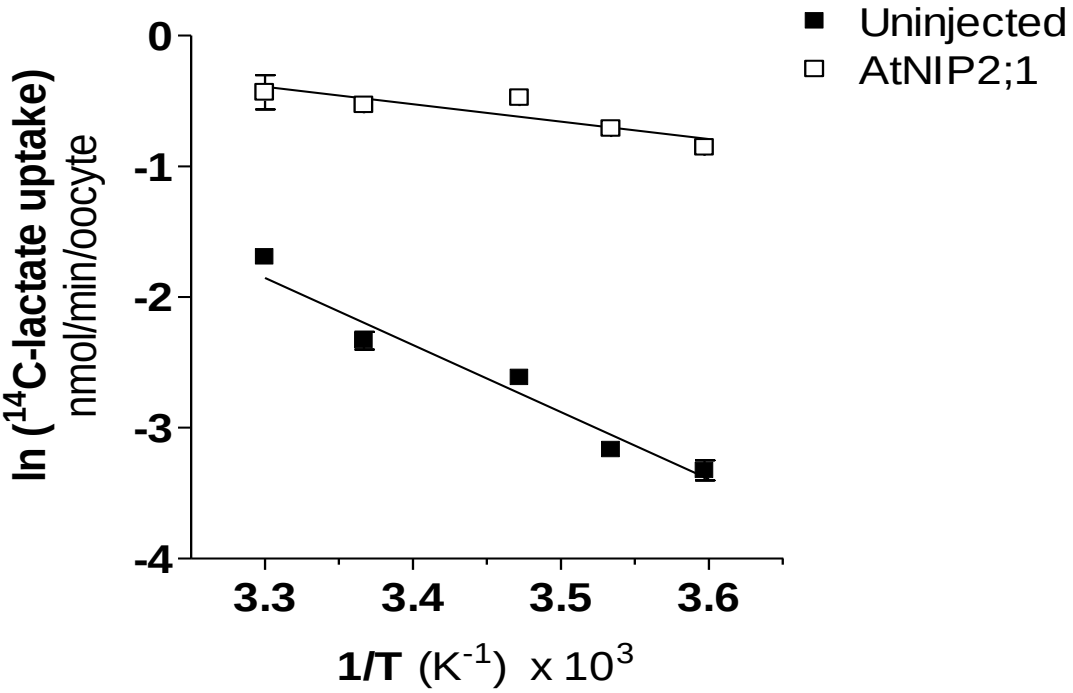
Uninjected
AtNIP2;1
ln (^{14}C-lactate uptake)
nmol/min/oocyte
0
-1
-2
-3
-4
3.3
3.4
3.5
3.6
1/T (K^{-1}) x 10^3

analyzed by Arrhenius plot (Fig. 3.19B). Calculation of the Arrhenius activation energy showed that AtNIP2;1 lowers the activation energy of lactic acid uptake (E_a = 4.02 kcal/mol) compared to uninjected oocytes (E_a = 15.1 kcal/mol), consistent with facilitated transport of water and solutes through aquaporin/glyceroporin channels (Agre et al., 2002). As a final note, transport through AtNIP2;1 shows saturable kinetics (apparent $K_{0.5}$ = 34.7 mM) in contrast to lactic acid transport in control uninjected oocytes, which show a slow and unsaturable rate. Overall, the results strongly suggest transport of lactic acid through a channel mechanism provided by the AtNIP2;1 protein.

Interestingly, in contrast to soybean nodulin 26, AtNIP2;1-expressing oocytes showed minimal transport of glycerol (Fig. 3.20B). Other NIP transport substrates such as urea (Wallace and Roberts, 2005) and boric acid (Takano et al., 2006) are also not transported in oocytes expressing AtNIP2;1 (Fig. 3.21; Table 3.1). In addition, the ability of AtNIP2;1 to transport ethanol, a product of ethanolic fermentation product during oxygen stress (Sachs et al., 1980) was evaluated. As shown in Table 3.1, the permeability of AtNIP2;1 oocytes to ethanol is essentially not different than that of negative control oocytes (water-injected), indicating that AtNIP2;1 is not involved in facilitating ethanol diffusion across the biological membrane. Conversely, Nod26-expressing oocytes were indistinguishable from negative control oocytes (water-injected) with respect to ^{14}C-lactic acid uptake (Fig. 3.20A), but Nod26 showed ^{3}H-labeled glycerol transport activity, respectively (Fig. 3.20B).

Overall, the data of functional analysis support the contention that AtNIP2;1 is a selective transporter of the protonated form of lactic acid as an alternative transport substrate rather than common NIPs substrates such as glycerol, boric acid and urea,

Figure 3.20. Comparison of the glycerol and lactic acid uptake by AtNIP2;1 and soybean nodulin 26. A. ^{14}C-labeled lactic acid uptake at pH 4.0 by oocytes expressing AtNIP2;1F or Nod26F, or control oocytes injected with RNase-free water was done as described in Fig. 3.18. **B.** ^{3}H-labeled glycerol uptake by oocytes expressing AtNIP2;1F or Nod26F, or control oocytes injected with RNase-free water was done as described in the **Materials and Methods**. Standard assays were done at pH 7.6, however the uptake by AtNIP2;1 was also performed at pH 4.0. The error bars show SEM (n=3).

A

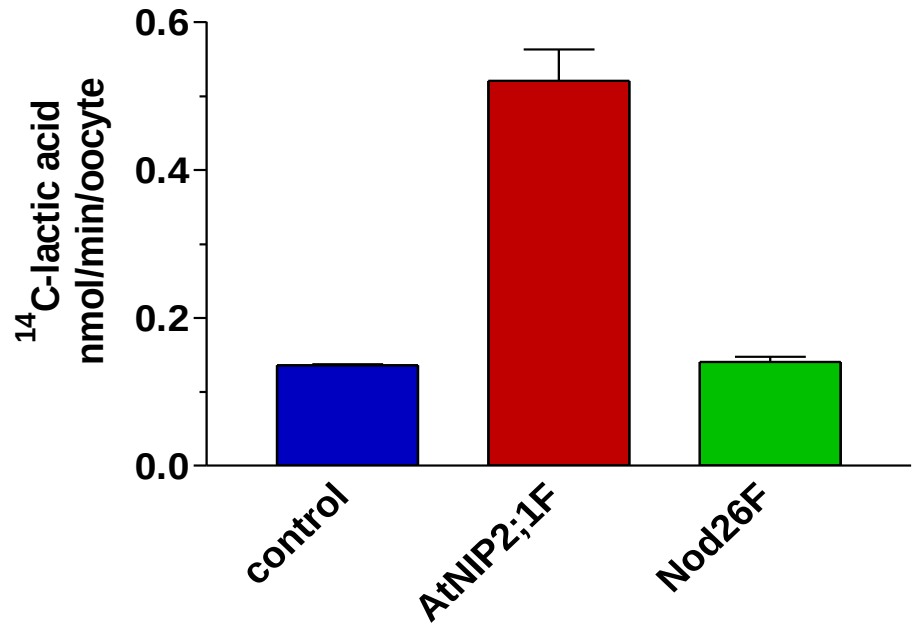
0.6
0.4
0.2
0.0
14C-lactic acid
nmol/min/oocyte
control
AtNIP2;1F
Nod26F

B

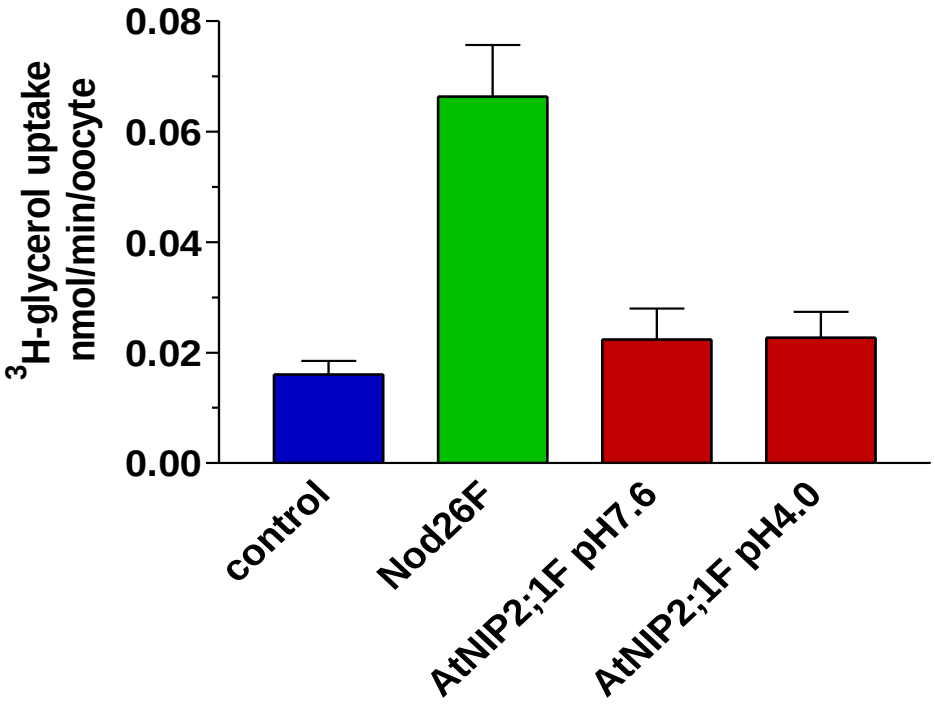
0.08
0.06
0.04
0.02
0.00
3H-glycerol uptake
nmol/min/oocyte
control
Nod26F
AtNIP2;1F pH7.6
AtNIP2;1F pH4.0

Table 3.1. Analysis of the solute permeability of AtNIP2;1 by *Xenopus* oocyte swelling assays

Solute[a]	Transport rate[b]	
	Control	AtNIP2;1
Boric acid	**0.115** (SEM=0.019, n=8)	**0.123** (SEM=0.014, n=8)
Ethanol	**0.195** (SEM=0.027, n=7)	**0.200** (SEM=0.029, n=9)
Lactic Acid	**0.033** (SEM = 0.006, n=7)	**0.327** (SEM=0.030, n=9)

[a]Assays were performed in isoosmotic modified Ringers solution, pH 4.0 with 100 mM of the indicated solute as described in the Experimental Procedures section. Upon incubation in the indicated solution, the uptake of solute was monitored by the rate of swelling as water follows the solute into the oocyte due to an osmotic gradient (Wallace and Roberts, 2005).

[b]The transport rate was determined by measuring the rate of oocyte swelling upon transfer from Ringers solution into the modified Ringers solution with the indicated substrate. The rates represent the $(dV/V_o)sec^{-1}$ $x10^3$.

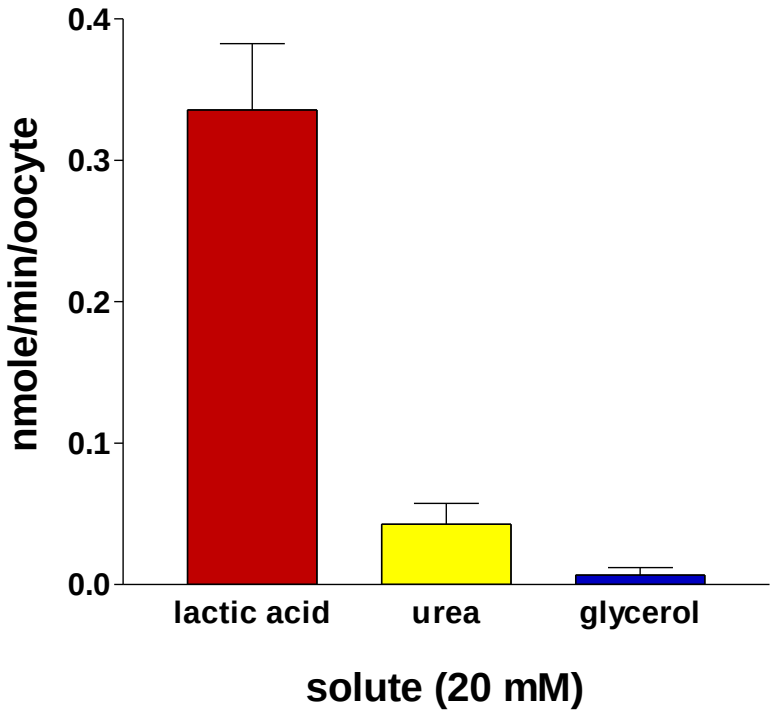

Figure 3.21. Analysis of the selectivity of AtNIP2;1 using *Xenopus* oocyte expression system. Transport activity of AtNIP2;1 was tested for common NIPs substrates indicated. Oocytes were assayed in 20 mM of the indicated radiolabeled substrate at pH 4.0 and the uptake by AtNIP2;1F oocytes was corrected by subtracting the basal uptake by water-injected control oocytes. The error bars show the SEM (n = 9 for lactic acid, n=10 for urea, n=3 for glycerol).

suggesting that AtNIP2;1 differs from other NIPs.

Characterization of two promoter T-DNA insertion mutants of *AtNIP2;1*

To investigate the potential role of AtNIP2;1 in adaptation to hypoxia, two mutants (WiscDsLox233237_22k and Salk_023890) with T-DNA insertions in the *AtNIP2;1* gene were obtained from the ABRC. A PCR-based genotype approach was used to characterize the WiscDsLox233237_22k mutant (Fig. 3.22). Gene specific primers were designed to flank the predicted insertion site as shown in Figure 3.22B. PCR was done on genomic DNA isolates with the two gene specific primers and the T-DNA left border primer. Amplification shows a single amplification product of ~400 bp, and no wild type amplification product, consistent with a homozygous T-DNA insertion mutant. This conclusion was further supported by antibiotic selection showing 100% resistance to 300 µM glufosinate-ammonium. Sequencing of the insertion site revealed that this mutant contains a T-DNA element in the promoter region at a position -30 bp upstream from the initiator ATG (Fig. 3.22B).

The second T-DNA insertional mutant allele (Salk_02890) was predicted to have a putative T-DNA insertion site in exon 1 of the *AtNIP2;1* gene. However, detailed PCR genotyping revealed an unusual insertion. Initial PCR with the T-DNA left border primer and the AT3RP forward primers yielded a 500bp product as predicted from an insertion into exon I (Fig. 3.23A). This was verified by TOPO-TA cloning of the PCR fragment and DNA sequencing. However, PCR with wild type primers flanking the putative site of insertion consistently yielded a wild type product even after several

Figure 3.22. Characterization of T-DNA insertional mutant of *AtNIP2;1* from the Wisconsin mutant collection (WiscDsLox233237_22K). T-DNA insertion mutants were obtained from the ABRC and were characterized by using PCR-based genotyping. The T-DNA insertion site of this mutant was obtained by sequencing analysis. **A.** Genomic DNA PCR mapping for T_2 generation line of WiscDsLox233237_22K. WT and Mu indicate the genomic DNA samples of WT and T_2 generation of WiscDsLox233237_22K. Lane 1 and 3 show *AtNIP2;1* PCR products resulting from AT3RP and AT3LP primers. Land 2 and 4 represent T-DNA PCR products resulting from AT3RP and T-DNA p745 primers. AT3RP and AT3LP represent *AtNIP2;1* specific forward and reverse primers. T-DNA p745 shows T-DNA left border primer of *pDS-Lox* T-DNA. **B.** A diagram of sequencing of PCR result showing the T-DNA insertion site in the promoter region of *AtNIP2;1*.

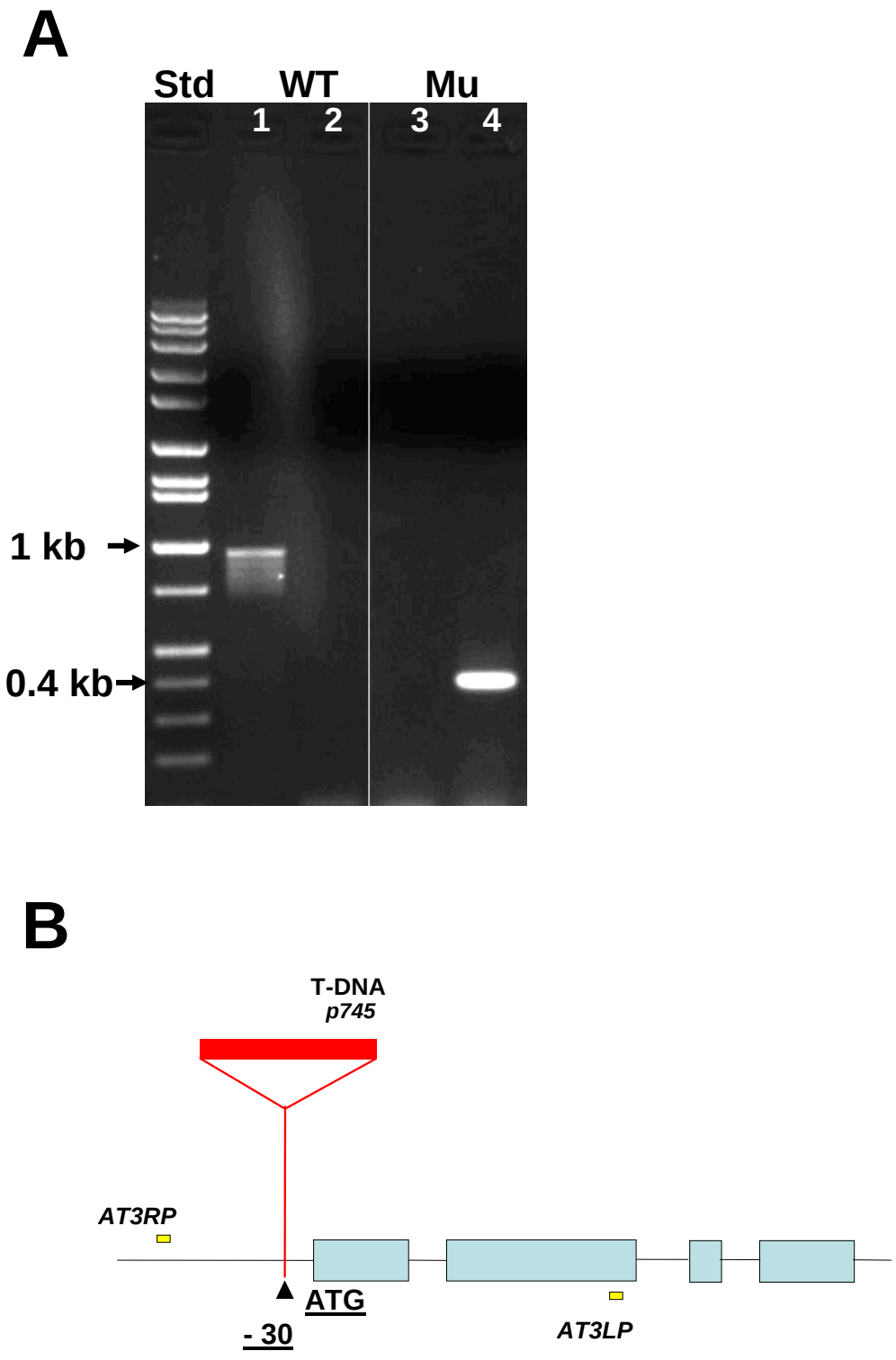
A
Std
WT
Mu
1
2
3
4
1 kb
0.4 kb
B
T-DNA
p745
AT3RP
ATG
- 30
AT3LP

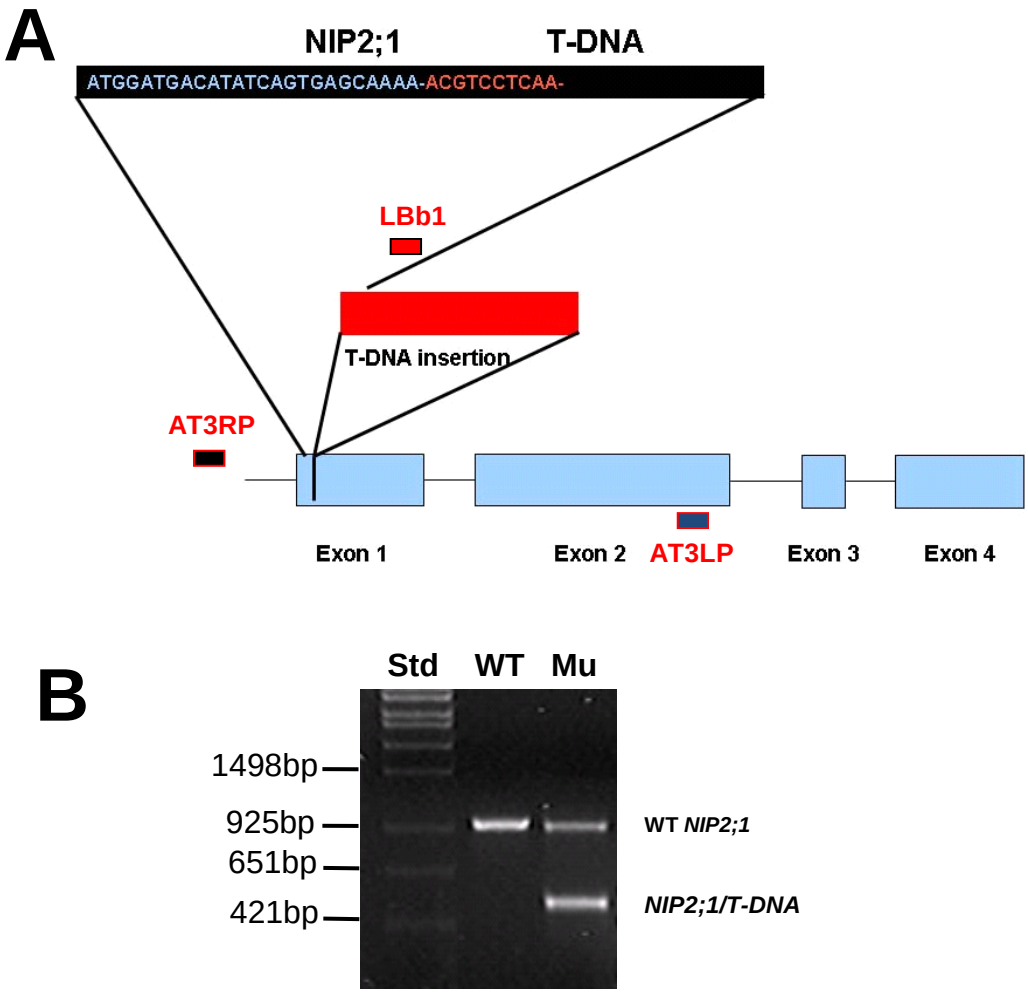

Figure 3.23. PCR genotyping of T-DNA insertional mutant of *AtNIP2;1* from the Salk collection (Salk_023890). A. A diagram of sequencing result showing predicted T-DNA insertion position in the *AtNIP2;1* gene. AT3RP and AT3LP show *AtNIP2;1* specific forward and reverse primers. LBb1 represents T-DNA left border primer of Salk T-DNA (Table 2.3). The T-DNA insertion position is shown in red box. T-DNA flanking sequences are colored in blue (*AtNIP2;1*) and red (Salk T-DNA). **B.** PCR-based genotyping result of wild type (WT) and T-DNA insertional mutant of *AtNIP2;1* (Mu). Std shows DNA molecular marker. "WT *NIP2;1*" indicates PCR product of the wild type *AtNIP2;1* gene. "*NIP2;1/T-DNA*" shows PCR product of T-DNA flanking region.

generations (Fig. 3.23B). Segregation ratios for this pattern were 100% and therefore it was not likely the result of a heterozygous state.

A clue to the reason for the strange genotyping pattern came from PCR for the Salk_023890 genomic DNA with the left border T-DNA primer and the gene-specific reverse primer AT3LP. This yields an unexpected high molecular weight product (Fig. 3.24). Sequencing of this product showed a normal *AtNIP2;1* gene sequence within the coding regions and an unexpected T-DNA insertion site at -410 bp in the 5' promoter region of the gene (Fig. 3.24). This confusing result suggests that both gene-specific forward and reverse primers can generate a product with the T-DNA left border primer sequences. A model for how this might occur is shown in Fig. 3.24C. Upon insertion of the T-DNA element a portion of the T-DNA and exon I were duplicated and inserted. If this model is valid then the Salk_023890 mutant should contain an uninterrupted conding region in the *AtNIP2;1* gene. RT-PCR of root RNA isolated from the T_5 generation of this insertional mutant showed a normal full length *AtNIP2;1* product (Fig. 3.23B), suggesting that basal expression of the *AtNIP2;1* was not suppressed by T-DNA insertion. Thus both T-DNA insertional mutants apparently contain the T-DNA element in the promoter region of the gene.

To determine whether the promoter based-insertions would have any effect on *AtNIP2;1* expression, the promoter region of *AtNIP2;1* was first analyzed for the presence of anaerobic response elements (ARE). AREs are essential *cis*-acting elements for the induction of expression of the anaerobic polypeptide genes. By using web-based software and manual inspection of the sequences, analysis of the promoter

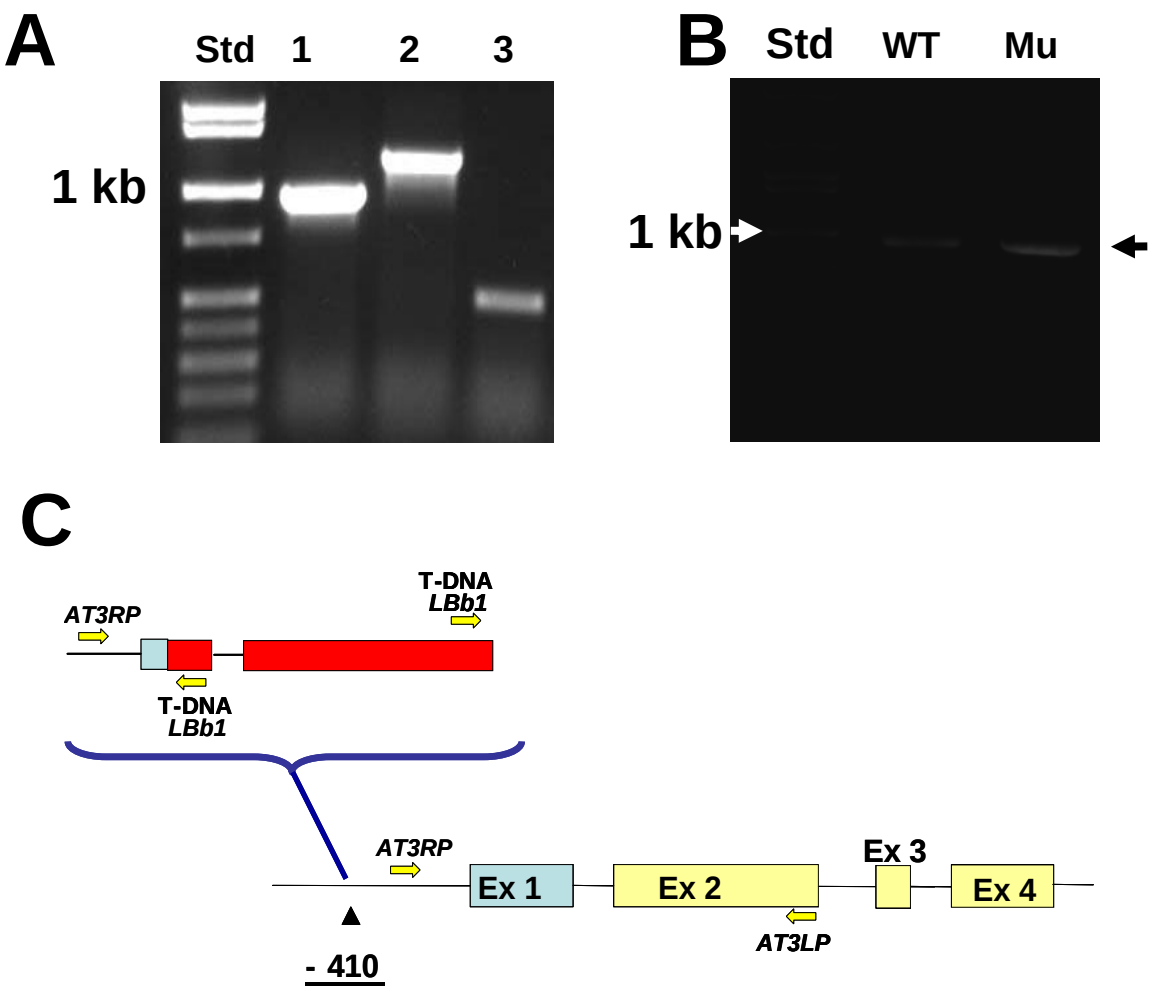

Figure 3.24. Characterization of T-DNA insertional mutant of *AtNIP2;1* from the Salk collection (Salk_023890). A. Genomic DNA PCR mapping for a T_5 generation line of Salk_02890. Lane 1 shows *AtNIP2;1* PCR product resulting from AT3RP and AT3LP primers. Lane 2 represents T-DNA PCR product resulting from AT3LP and T-DNA LBb1 primers. Lane 3 indicate T-DNA PCR product resulting from AT3RP and T-DNA LBb1 primers. **B.** RT-PCR result for full-length *AtNIP2;1* amplification using RNA from normoxic 2 week old Arabidopsis plants. WT and Mu represent the cDNA samples of WT and T_5 generation of Salk_02890. Black arrow indicates full-length *AtNIP2;1* PCR products. **C.** A diagram showing the predicted T-DNA insertion in the promoter region of *AtNIP2;1* that would lead to the observated PCR-genotyping pattern.

region of the *AtNIP2;1* gene reveals the presence of six AREs. Among the six AREs, four are identical to the GT-motifs found in *Adh1* gene of *Zea mays* (Walker et al., 1987; Olive et al., 1990) and two are identical to the GT-motifs found in *Adh1* of *Arabidopsis thaliana* (Dolferus et al., 1994) (Fig. 3.25). Based on the T-DNA insertional sites of the mutants and *cis*-acting elements analysis, the T-DNA element of the WiscDsLox233237_22k mutant is inserted in a position that completely disrupts all six AREs (Fig. 3.26A). On the other hand, the T-DNA element in the Salk_023890 mutant is inserted in a position that interrupts only two AREs (Fig. 3.26A). Homozygous lines of the two mutant alleles were analyzed for *AtNIP2;1* expression by Q-PCR (Fig. 3.26B) to further verify the results of *cis*-acting element analysis in the promoter region of the *AtNIP2;1* gene.

Consistent with the site of insertion of the T-DNA element within the promoter, the roots of 2 week old WiscDsLox233237_22k mutant plants completely lose the ability to express *AtNIP2;1* in response to hypoxia stress (Fig. 3.26B), but the Salk_023890 mutant plants showed that it is still capable of responding to hypoxia stress albeit with a 30-fold reduction in peak *AtNIP2;1* expression compared to WT plants (Fig. 3.26B). Based on the results of Q-PCR analysis, we treated the WiscDsLox233237_22k allele as a “knockout” mutant for *AtNIP2;1*, and refer to it as a *atnip2;1-1*. The other mutant allele of *AtNIP2;1* was treated as a “knockdown” mutant, and we refer to it as a *atnip2;1-2*. Western blot analysis of root microsomal fractions using a site-directed AtNIP2;1 antibody showed that AtNIP2;1 protein levels are induced in wild type roots by 6 hr hypoxic stress whereas no protein signal was detected in the roots of *atnip2;1-1* plants(Fig. 3.27B). Thus, the T-DNA insertion within the *atnip2;1-1* promoter results in

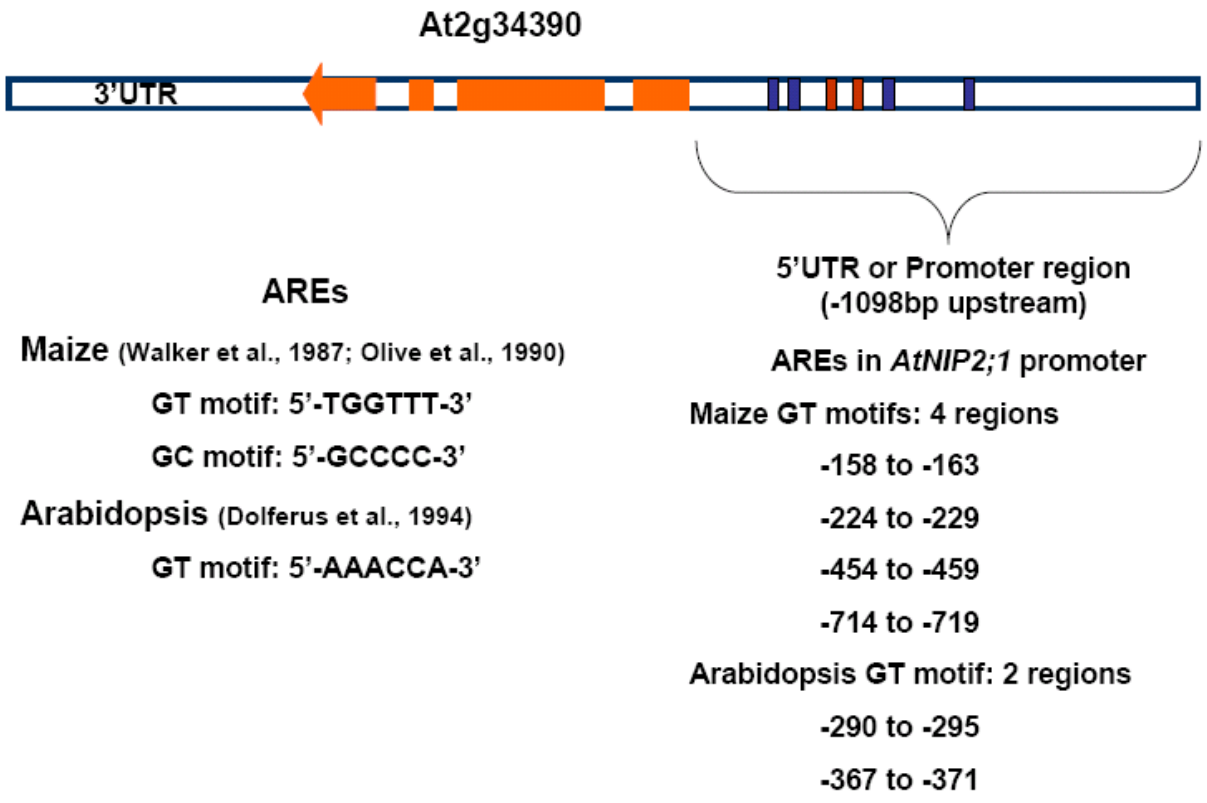

Figure 3.25. Promoter analysis of *AtNIP2;1* for *cis*-acting anaerobic regulatory elements. The promoter sequence (-1098 bp from initiator ATG) of *AtNIP2;1* was analyzed for Anaerobic Response Element (ARE) by using web based analysis software "PlantCARE" (http://bioinformatics.psb.ugent.be/webtools/plantcare/html/). The six AREs obtained from "PlantCARE" analysis were then confirmed by manual analysis based on the published literature (Walker et al., 1987; Olive et al., 1990; Dolferus et al., 1994). The blue and red boxes represent maize GT motifs and Arabidopsis GT motifs or AREs found in maize and Arabidopsis of the promoter region of the *AtNIP2;1* gene.

Figure 3.26. Characterization of two T-DNA insertion mutants of *AtNIP2;1.* A. Diagram of the *AtNIP2;1* gene showing the site of T-DNA insertion in *atnip2;1-1* (WiscDsLox233237_22k) and *atnip2;1-2* (Salk_023890) mutant alleles. Black filled boxes including filled arrowhead box represent the 4 exons of *AtNIP2;1*. Gray filled rectangular boxes and gray lines indicate T-DNA and T-DNA insertion site within *AtNIP2;1* promoter region. Open rectangular boxes indicate AREs typical of those reported in *Zea mays* (Walker et al., 1987; Olive et al., 1990). Diagonal filled rectangular boxes show AREs typical of those reported in *Arabidopsis* (Dolferus et al., 1994). **B.** Comparison of Q-PCR results for *AtNIP2;1* expression in the roots of 2 wk-old WT Col-0, *atnip2;1-1* and *atnip2;1-2* seedlings during anoxic treatment. The ΔCt value of *AtNIP2;1* expression in normoxic WT roots was used as a calibrator for $\Delta\Delta$Ct calculations. Error bars are SEM of three to five biological replicates.

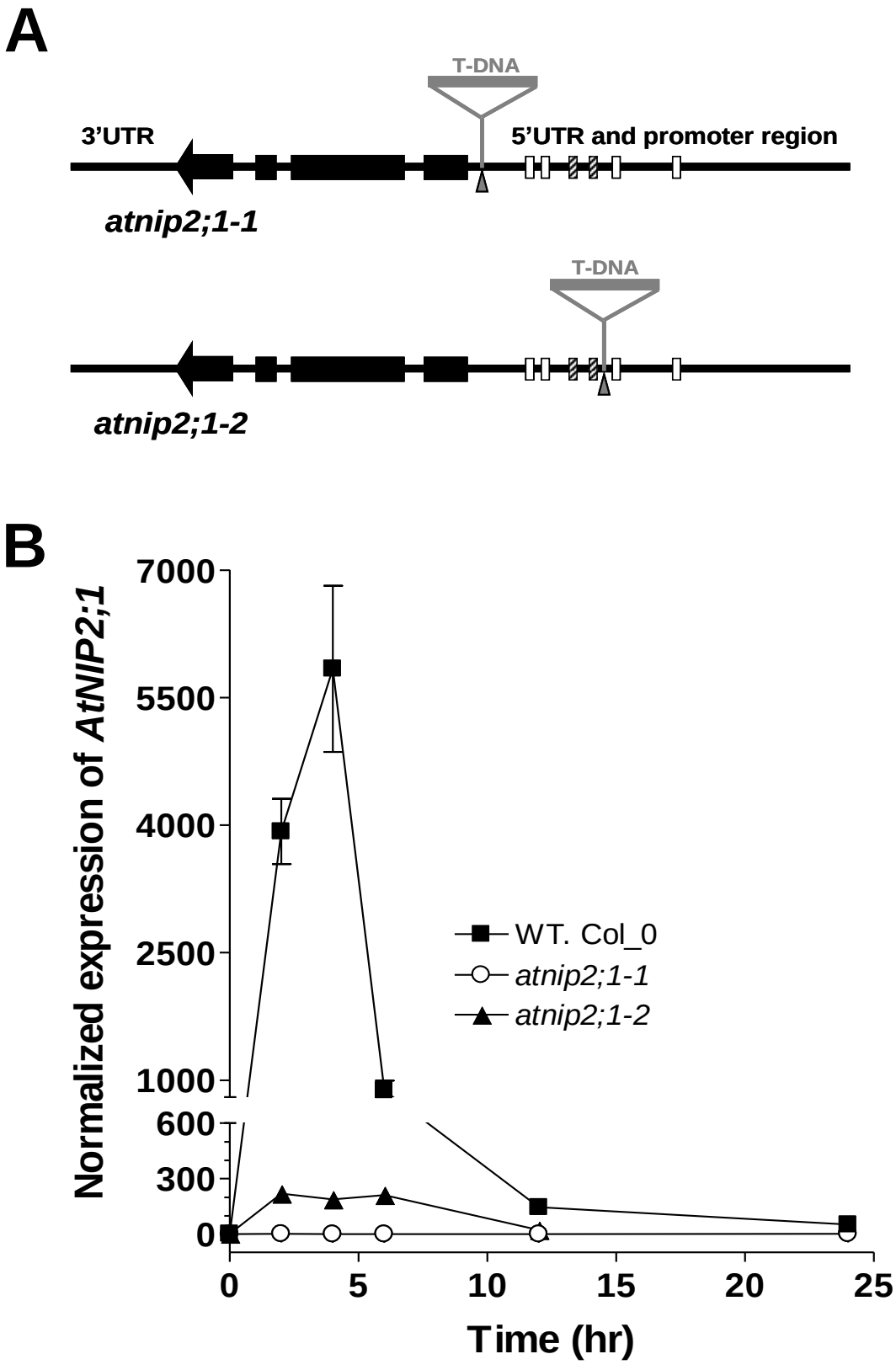
A
T-DNA
3'UTR
5'UTR and promoter region
atnip2;1-1
T-DNA
atnip2;1-2
B
Normalized expression of AtNIP2;1
7000
5500
4000
2500
1000
600
300
0
0
5
10
15
20
25
Time (hr)
WT. Col_0
atnip2;1-1
atnip2;1-2

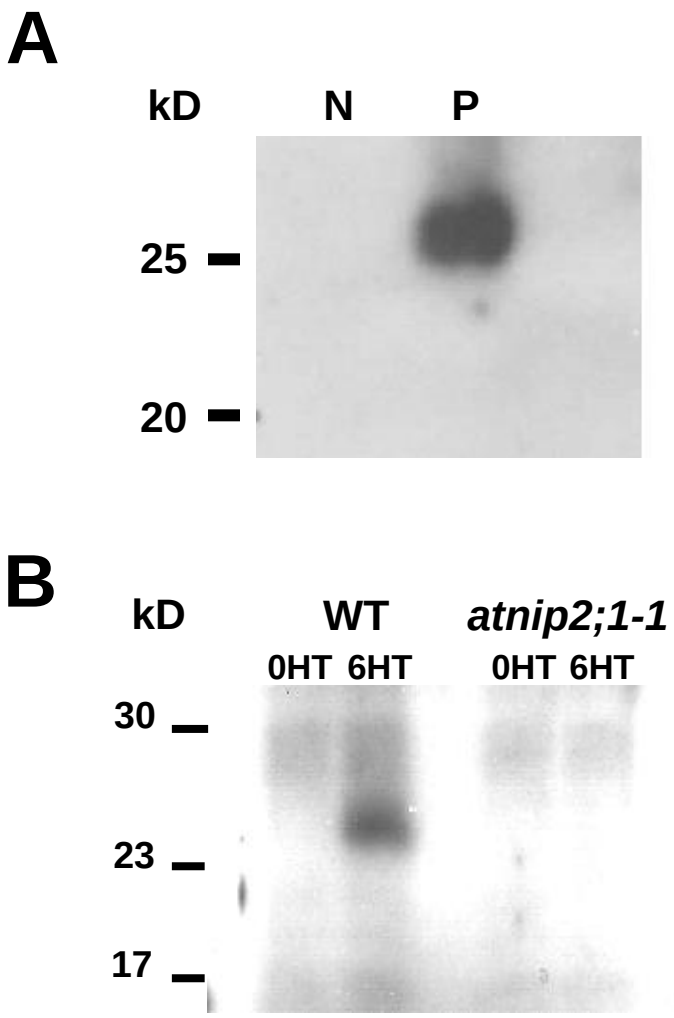

Figure 3.27. Western blot analysis of AtNIP2;1 expression in *Xenopus* oocytes expressing AtNIP2;1 and the roots of Arabidopsis plants. Western blot analysis was done with the oocyte lysate samples and the root samples of Arabidopsis using anti-AtNIP2;1. **A.** AtNIP2;1 expression in oocytes injected with AtNIP2;1 cRNA, positive control (P), and with water, negative control (N) using aniti-AtNIP2;1 Ab. Oocyte lysate (10 µg/lane) were resolved by SDS-PAGE on a 12.5% gel and were analyzed by Western blot with site-directed AtNIP2;1 antibodies as described in the **Materials and Methods**. **B.** AtNIP2;1 Western blot of wild type and *atnip2;1-1* roots. Root extracts (10 µg/lane) were resolved by SDS-PAGE on a 15% gel and were analyzed by Western blot. **0HT**, microsomal fraction of the normoxic roots; **6HT**, microsomal fraction of the 6hr hypoxic/anoxic-treated roots.

complete loss of RNA transcription and protein expression under normal and hypoxic conditons.

Effect of a reduction in *AtNIP2;1* expression on root development under normoxic conditions

Analysis of two T-DNA insertional mutants showed that both sets of mutant plants grow normally except for subtle alterations in root growth under standard normoxic growth conditions. At two weeks of growth, *atnip2;1-1* and *atnip2;1-2* show increased emergence of lateral roots compared to wild type plants (Fig. 3.28). More careful quantitation shows that *atnip2;1-1* plants show an increased number of lateral roots that were increased 2-fold (average of 101 seedlings was 19.6; *p*-value is <0.0001) compared to wild type seedlings (average of 105 seedlings was 10.6) (Table 3.2). Wet weights (gram fresh weight (g F.W)) of the roots of *atnip2;1-1* plants were also slightly increased showing 1.3-fold greater than wild type plants (Table 3.2).

Effect of reduced *AtNIP2;1* expresson on lactate accumulation in Arabidopsis mutants

As discussed above, functional assays of *Xenopus* oocytes that express AtNIP2;1 protein are capable of transporting lactic acid (Choi and Roberts, 2007). This led to the hypothesis that the role of the AtNIP2;1 transporter in hypoxic roots may be to serve as a lactic acid channel that may facilitate an efflux of cytosolic lactic acid produced during early fermentation in tissues subjected to oxygen deprivation (Xia and Saglio, 1992). To test this hypothesis, we investigated the effects of the loss of

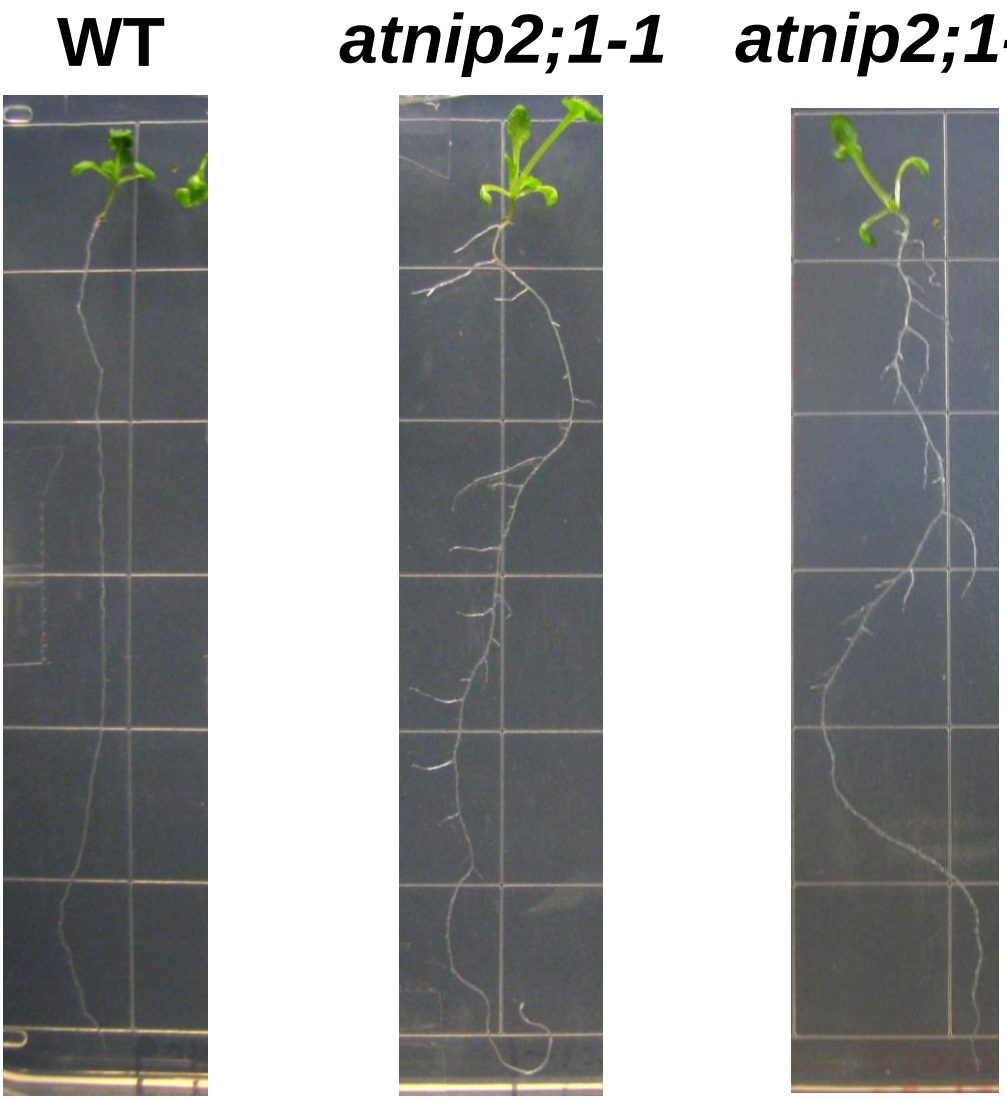

Figure 3.28. Comparison of primary root and lateral root growth of 2-wk old wild type and *atnip2;1* plants under normoxic conditions. Representative 2-wk old seedlings of WT, *atnip2;1-1*, and *atnip2;1-2* were grown vertically under standard LD conditions as descbribed in the **Materials and Methods.**

Table 3.2. Comparison of root mass and lateral root growth of 2-wk old wild type and *atnip2;1-1* plants under normoxic conditions

	WT. Col_0			*atnip2;1-1*			Student *t*-tests
	Mean[c]	SEM	N[d]	Mean	SEM	N[d]	*p*-value
[Shoot F.W.[a]] mg/plant	3.21	0.210	554	3.76	0.285	454	0.1493
[Root F.W.] mg/plant	0.84	0.052	554	1.07	0.047	454	0.0096*
Root length (cm)	8.05	0.103	105	8.86	0.100	101	<0.0001*
Number of L.R.[b]	10.6	0.52	105	19.6	0.75	101	<0.0001*

[a]Fresh weight (F.W.) of root and shoot tissues of 2-wk old seedlings grown under normal condition (long day (LD) light cycle (16 hr light/8 hr darkness) at 22°C.

[b]Number of lateral roots (L.R.) of individual 2-wk old seedlings.

[c]The mean weight per plant was determined from weights of batches of 31 to 35 plants.

[d] Number of total seedlings analyzed from six separate experiments.

*Student *t*-tests P values showing significant differences (P<0.05) between WT. Col_0 and *atnip2;1-1* plants.

AtNIP2;1 on the endogenous lactic acid levels in the roots of two week old wild type and *atnip2;1-1* seedlings under normoxic and hypoxic conditions.

In wild type Arabidopsis, the basal levels of lactic acid are low (Fig. 3.29B). However, upon hypoxic challenge, lactic acid levels steadily increase, reaching a maximum level by twelve hours post hypoxia. Arabidopsis has a single lactate dehydrogenase (*Ldh1*) gene which shows a spike of increased expression (10-12 fold) within two hours after the onset of hypoxia (Fig. 3.29A). These observations are consistent with the stimulation of lactic acid fermentation at the early stages of oxygen deprivation.

Analysis of *atnip2;1-1* seedlings under identical conditions show that hypoxia induces a similar increase in *Ldh1* expression (Fig. 3.29A). However, the accumulation of lactic acid is distinct from wild type. Basal levels of lactic acid were over 20-fold higher than wild type and accumulated to higher levels during hypoxic treatment (Fig. 3.29B). These data suggest that a reduction in transcription and translation of the *AtNIP2;1* gene results in the accumulation of higher levels of lactic acid within normoxic and hypoxic Arabidopsis roots, consistent with the proposed role of AtNIP2;1 for the transport of this substrate in response to hypoxia-induced lactic acid fermentation.

Effect of reduced expression of *AtNIP2;1* on survival of *Arabidopsis* to oxygen deprivation

To investigate the effects of the reduction in *AtNIP2;1* expression on survival to oxygen deprivation, two week-old T-DNA insertion mutant seedlings and wild type Arabidopsis seedlings were subjected to oxygen deprivation for 48 hr in an anaerobic

Figure 3.29. Comparison of *AtLdh1* expression and lactate levels in the roots of *Arabidopsis* in response to hypoxia. A. Total RNA (10 ng) isolated from root tissues of hypoxia treated 2-wk old WT. Col_0 (green square boxes) and *atnip2;1-1* (red triangles) was used for Q-PCR analysis for *AtLdh1* expression. The average ∆Ct value of the 0hr *AtLdh1* values in the WT. Col_0 shoot was used as the calibrator for ∆∆Ct calculations. Error bars show the SEM of five to six biological replicates. **B.** Lactate concentrations in the WT.Col_0 and *atnip2;1-1* roots subjected to the hypoxia treatments described in the **Materials and Methods**. Error bars represent SEM of three biological replicates.

A

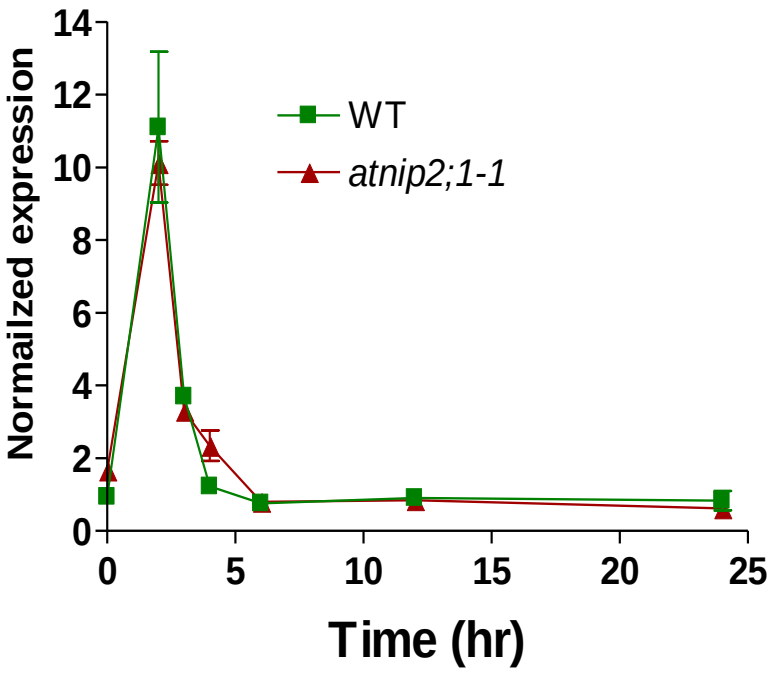
Normailzed expression
14
12
10
8
6
4
2
0
0
5
10
15
20
25
Time (hr)
WT
atnip2;1-1

B

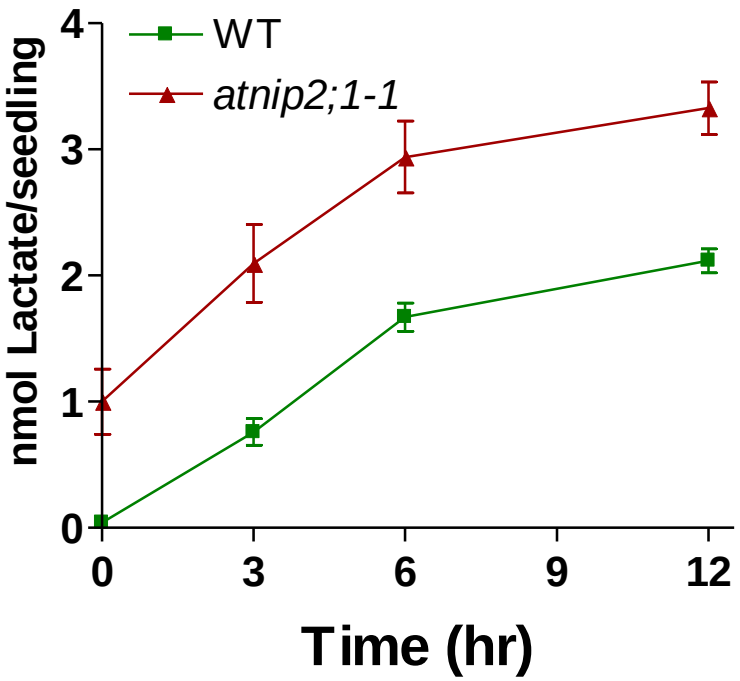
nmol Lactate/seedling
4
3
2
1
0
0
3
6
9
12
Time (hr)
WT
atnip2;1-1

jar by the standard approaches described in previous sections, and were stained with the vital dye fluorescein diacetate (FDA) (Hirayama et al., 2004). FDA is commonly used as a vital stain for living cells since it diffuses freely through the lipid bilayer membrane and is hydrolyzed in living cells resulting in a fluorescent signal due to accumulation of fluorescein. Staining of wild type and *atnip2;1-1* plants after a 48 hr treatment show that wild type plants have a greater susceptibility to anaerobic stress, particularly within the apical regions of the roots which are known to be more susceptible to anoxic stress (Van Toai et al., 1995). In comparison, *atnip2;1-1* plants show stronger FDA staining throughout the length of the root system (Fig. 3.30), suggesting, surprisingly, that these plants may be more tolerant to low oxygen stress.

To test this hypothesis further, the survival of wild type and the T-DNA insertional lines in response to anaerobic stress was tested. After a 48 hr treatment in the anaerobic jar, seedlings were returned to standard LD growth conditions under normal oxygen conditions, and were allowed to recover and grow for two weeks prior to scoring for survival (Fig. 3.31). Exposure of wild type Arabidopsis seedlings to this stress resulted in arrest of root growth, chlorosis of leaves, and ultimately the death of most of the seedlings with a 22.5% survival rate observed (Fig. 3.31). However, in comparison both *atnip2;1-1* and *atnip2;1-2* seedlings showed an enhanced ability to withstand this treatment (Fig. 3.31A). The survival rate of *atnip2;1-1* (66.8%, 3 fold higher than wild type seedlings) was greater than that found in *atnip2;1-2* (46.8%, 2 fold higher than wild type seedlings), which is consistent with the comparative reduction of *AtNIP2;1* expression in these two mutant lines in response to oxygen deprivation (Fig. 3.26).

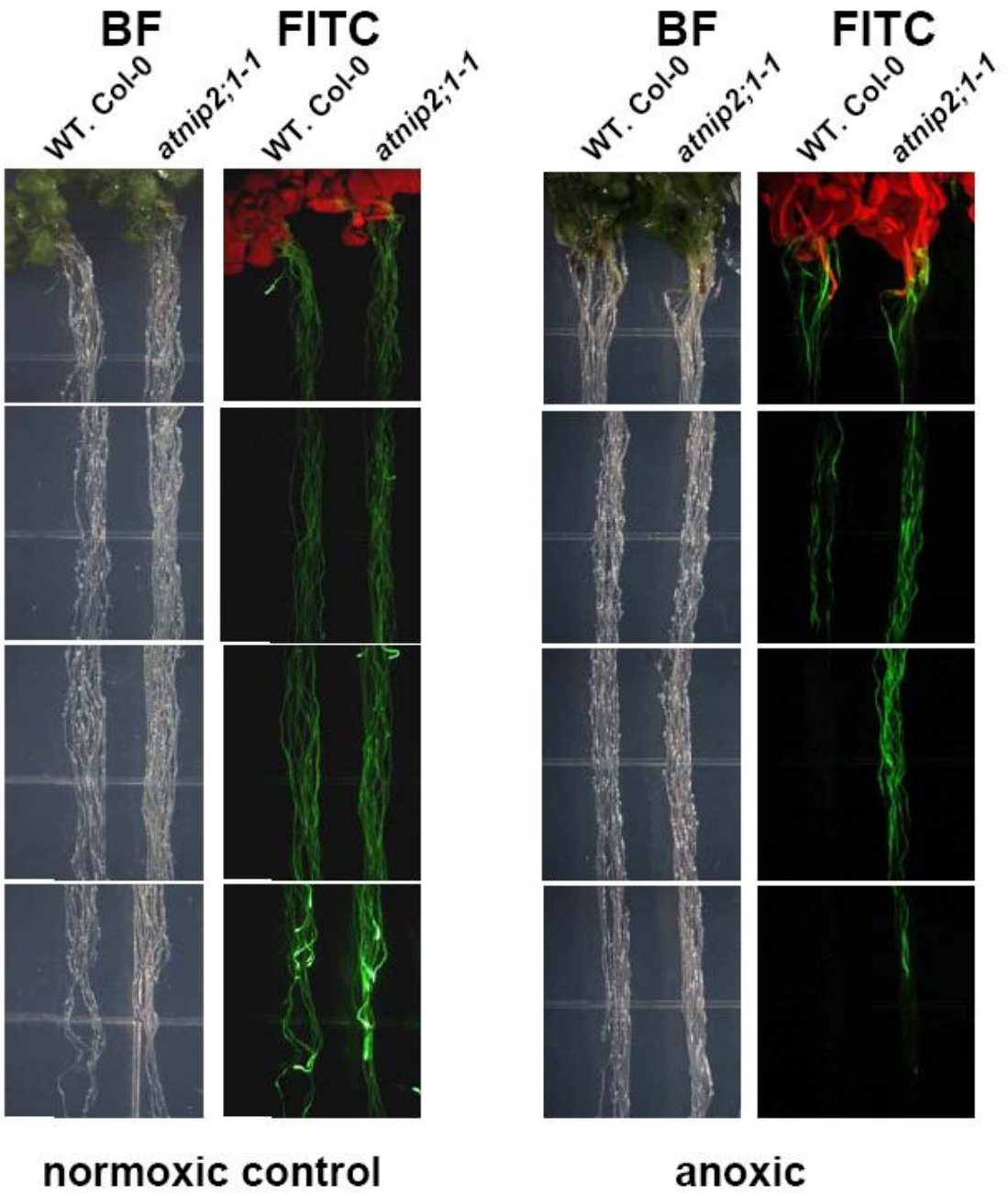

Figure 3.30. Comparison of the root viability of WT and *atnip2;1-1* plants after exposure to hypoxia. Two-wk old plants were exposed to hypoxic conditions in an anaerobic jar for 48 hr and were then stained with the viability stain fluorescein diacetate for the root viability determination as described in the **Materials and Methods**. **BF** shows bright field images and **FITC** shows the fluorescence signal using the fluorescein isothiocyanate (**FITC**) filter set.

Figure 3.31. Effects of oxygen deprivation on survival of WT and T-DNA insertional mutants in anaerobic flasks. A. Two week old, vertically-grown *atnip2;1-1* (*nip2;1-1*), *atnip2;1-2* (*nip2;1-2*) and WT seedlings were subjected to 48 hr hypoxia (48 hr HT) in an anaerobic jar (right panel) or 48 hr normal oxygen conditions (normoxic control; left panel), and were allowed to recover and grow under normal LD conditions for an additional two weeks. **B.** Histogram showing the % survival of wild-type Col_0, *atnip2;1-1* and *atnip2;1-2* mutants in response to anoxic stress administered as described above. Error bars show the SEM of six to nine experiments with each containing 10 to 40 seedlings.

A

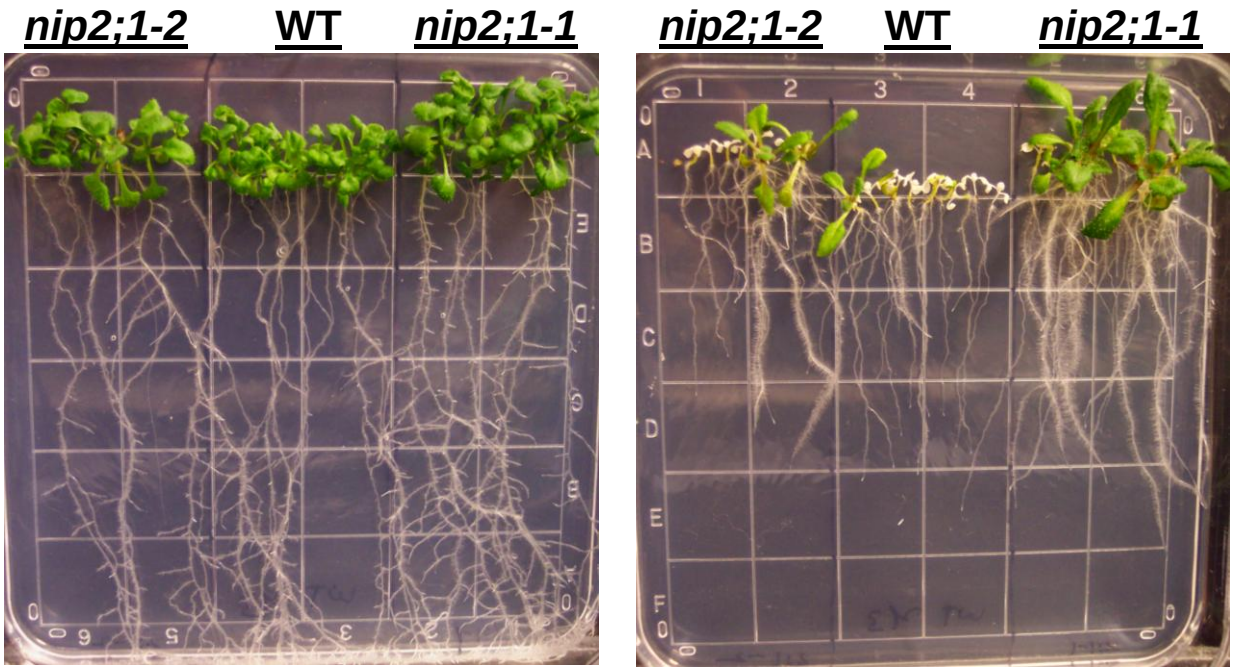
nip2;1-2
WT
nip2;1-1
nip2;1-2
WT
nip2;1-1
Normoxic
48 hr HT

B

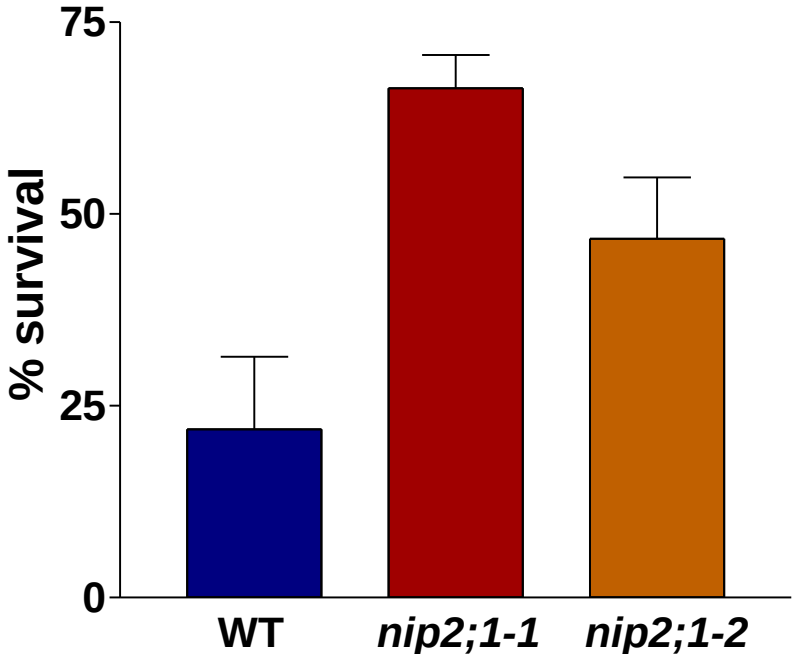
75
50
25
0
% survival
WT
nip2;1-1
nip2;1-2

The procedure used to induce hypoxia in anaerobic jas relies on the consumption of O_2 and the production of CO_2, diriven by a GasPak. To determine whether the observations were due to anoxia rather than elevated CO_2, a separate protocol employing the flushing of sealed flasks with nitrogen gas was used to induce severe hypoxia. Under these conditions a similar survival phenotype for *atnip2;1-1* plants was observed, arguing that the effect is due to an anaerobic signal (Fig. 3.32).

Previous experiments suggest that pre-adaptation of Arabidopsis plants to mild hypoxia prior to the administration of severe hypoxia enhances survival (Ellis et al., 1999). To test the effects of "pre-adaptation", two-wk old WT and *atnip2;1* plants were administered a brief 3 hr hypoxic episode and were allowed to recover for one day prior to exposure to the full 48 hour anoxic stress regime described above. Analysis of the survival of WT and *atnip2;1-1* plants revealed that both "pre-adapted" WT and *atnip2;1-1* seedlings acquire high resistance to oxygen deprivation and were indistinguishable in their ability to survive 48 hr anoxic stress (Fig. 3.33). One possible explanation of the data is that the reduction of *AtNIP2;1* expression in non-adapted *atnip2;1-1* mutants causes a partial "pre-adaptation" state that allows greater survival to anaerobic stress.

Transcript profiling in the roots of WT and *atnip2;1-1* under hypoxia

To gain insight into the basis for the subtle root developmental phenotypes and the increased resistance to anoxic stress associated with the *atnip2;1-1* T-DNA mutant, we investigated the global changes in the Arabidopsis transcriptome by using microarray analysis. For this approach, vertically grown two-wk old WT seedlings and *atnip2;1-1* seedlings were used. Total RNA was isolated in triplicate from the roots of

Figure 3.32. Effects of anoxia on survival of WT and T-DNA insertional mutants using N_2 flushing. **A.** Two week old, vertically-grown *atnip2;1-1* and WT seedlings were subjected to 24 hr hypoxia (24 hr AT) in an anaerobic jar (right panel) or 48 hr normal oxygen conditions (normoxic control; left panel) by continuous flushing with N_2 gas, and were allowed to recover and grow under normal LD conditions for an additional two weeks. **B.** Histogram showing the % survival of wild-type Col_0 and *atnip2;1-1* mutants in response to hypoxic stress administered as described above. Error bars show the SEM of five experiments with each containing 15 to 18 seedlings.

A

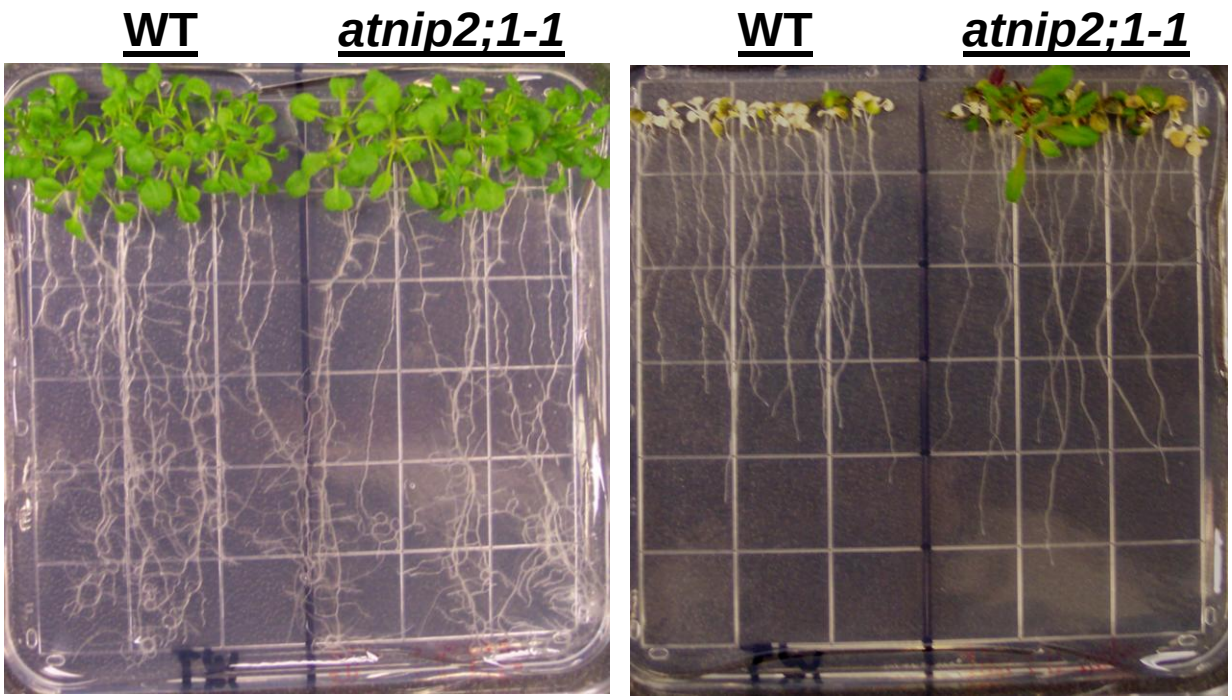
WT
atnip2;1-1
WT
atnip2;1-1
Normoxic control
24 hr N_2

B

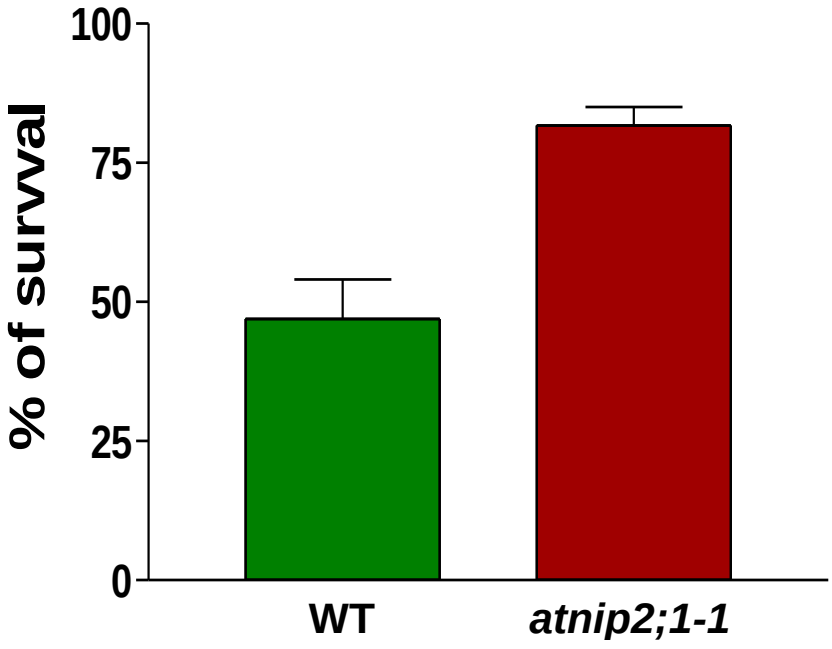
100
75
50
25
0
% of survval
WT
atnip2;1-1

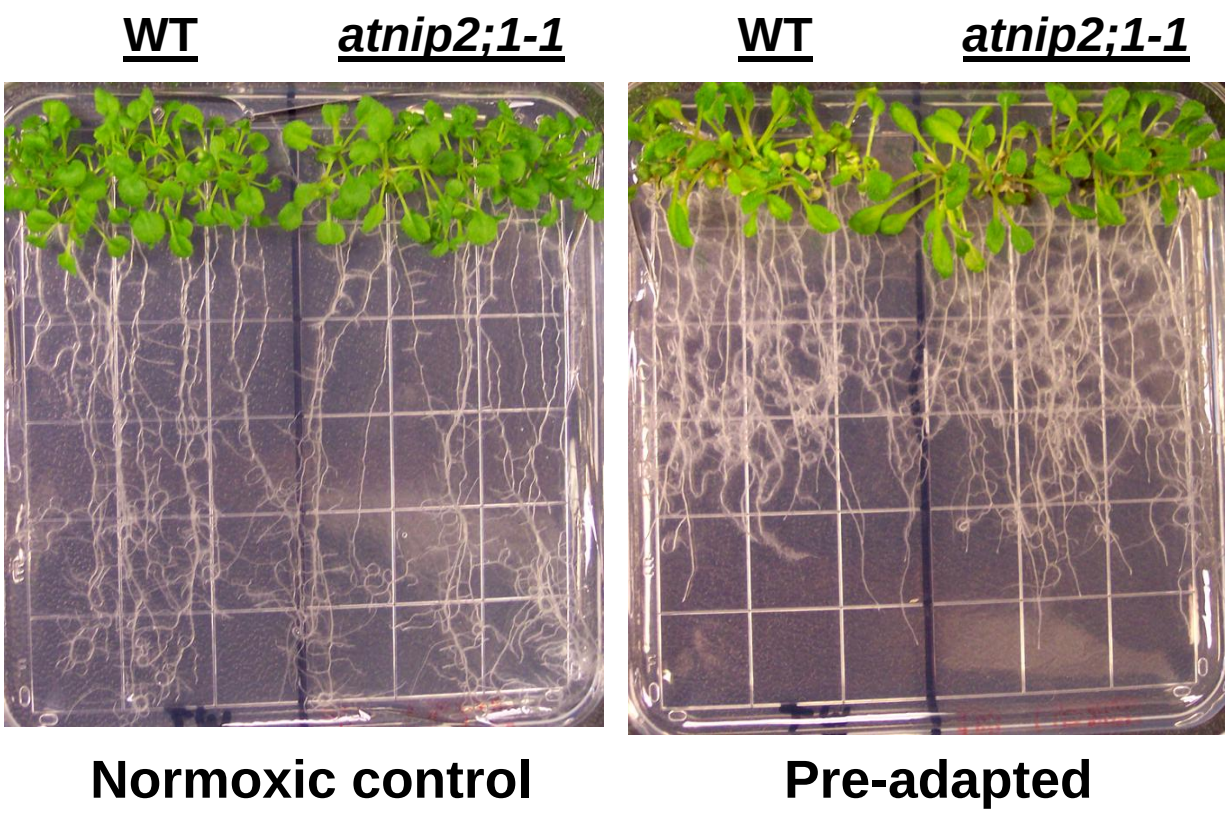

Figure 3.33. Comparison of the survival of wild type and *atnip2;1-1* seedlings after pre-adaptation to mild hypoxia. Seedlings of 2-wk old WT and *atnip2;1-1* were pre-adapted by brief exposure (3 hr) to hypoxic conditions. The seedlings were allowed to recover for 24 hr under normoxic conditions before administering the severe 48 hr hypoxia stress shown in Figure 3.32.

WT and *atnip2;1-1* seedlings subjected to hypoxic conditions as well as from normoxic controls. Prior to performing the microarray experiment, the quality of the isolated total RNA was verified by agarose gel electrophoresis (Fig. 3.34A), and by Q-PCR analysis (Fig. 3.34B and C). Electrophoretic analysis showed the presence of intact 18S and 28S rRNA bands without genomic DNA contamination and verified quantitation of total RNA (Fig. 3.34A). This is supported by Q-PCR analysis of an internal reference *UBQ10* gene (Fig. 3.34B), which shows equivalent expression in all biological samples. To verify the effectiveness of hypoxia-treatment, Q-PCR analysis was done to quantitate *Adh1* gene expression. *Adh1* expression was low in the roots of the normoxic controls, but was stimulated over 100-fold in the roots of the 4 hr hypoxia-treated samples (Fig. 3.34C), confirming successful hypoxic treatment and ANP gene induction.

Microarray analysis of the twelve total RNA samples was done by using Affymetrix Arabidopsis ATH1 chips which contain probe sets representing greater than 24,000 Arabidopsis gene sequences. To verify the quality of the microarray data, the signal for the control genes analyzed by Q-PCR (Fig. 3.34) were compared (Table 3.3 and 3.4). The microarray results show similar reproducibility and precision for the *UBQ10* and *Adh1* test transcripts. Further, the differences from pairwise comparisons of the four data sets reflect the differences observed in the Q-PCR results (c.f., Fig. 3.34 and Table 3.4). Based on these results, the differences in the stimulation of global gene transcription between the microarray data sets were analyzed.

Initial analyses were performed on the normoxic and 4 hr hypoxic wild type root data sets by using the Partek Genome suite™ software to determine which genes are induced by hypoxic stress. The threshold for a significant result was: 1. stimulation of at

Figure 3.34. Analysis of total RNA samples prior to microarray analysis. A. Total RNA (700 ng of each sample) of the roots of 2-wk old wild type Arabidopsis and *atnip2;1-1* was separated on a 1% (w/v) agarose gel to verify total RNA integrity. Lane 1-3, wild type normoxic root total RNA samples (WT_0HT 1, WT_0HT 2, and WT_0HT 3); lane 4-6, wild type 4 hr hypoxia-treated root total RNA samples (WT_4HT 1, WT_4HT 2, and WT_4HT 3); lane 7-9, *atnip2;1-1* normoxic root total RNA samples (KO_0HT 1, KO_0HT 2, and KO_0HT 3); lane 10-12, *atnip2;1-1* 4 hr anoxia-treated root total RNA samples (KO_4HT 1, KO_4HT 2, and KO_4HT 3). **B.** Q-PCR analysis of *UBQ10*. **C.** Q-PCR analysis of *Adh1*. Error bars show SEM of three replicates.

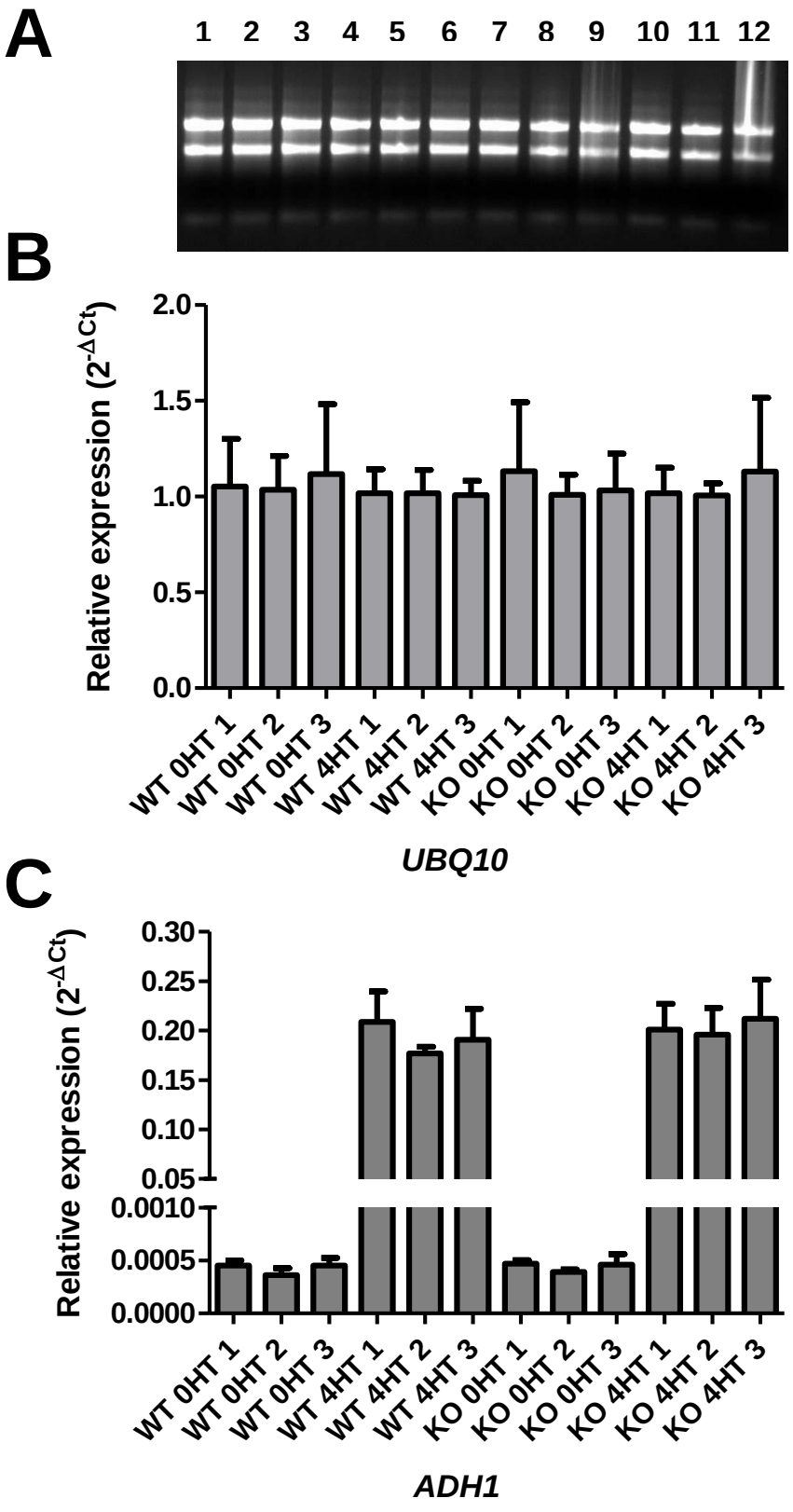
A
1 2 3 4 5 6 7 8 9 10 11 12
B
Relative expression (2-ΔCt)
2.0
1.5
1.0
0.5
0.0
WT 0HT 1
WT 0HT 2
WT 0HT 3
WT 4HT 1
WT 4HT 2
WT 4HT 3
KO 0HT 1
KO 0HT 2
KO 0HT 3
KO 4HT 1
KO 4HT 2
KO 4HT 3
UBQ10
C
Relative expression (2-ΔCt)
0.30
0.25
0.20
0.15
0.10
0.05
0.0010
0.0005
0.0000
WT 0HT 1
WT 0HT 2
WT 0HT 3
WT 4HT 1
WT 4HT 2
WT 4HT 3
KO 0HT 1
KO 0HT 2
KO 0HT 3
KO 4HT 1
KO 4HT 2
KO 4HT 3
ADH1

Table 3.3. Comparison of raw microarray signal intensities of test transcripts

Sample	Replicate[a]	*UBQ10* Raw signal[b] intensity (log_2)	*UBQ10* Mean *(SD)*	*ADH1* Raw signal intensity (log_2)	*ADH1* Mean *(SD)*
WT normoxic	WT 0HT-1	14.06	13.92 *(0.133)*	7.69	7.69 *(0.216)*
	WT 0HT-2	13.91		7.48	
	WT 0HT-3	13.79		7.91	
atnip2;1-1 normoxic	KO 0HT-1	13.80	13.75 *(0.0435)*	7.93	8.06 *(0.139)*
	KO 0HT-2	13.71		8.20	
	KO 0HT-3	13.74		8.05	
WT 4 hr hypoxic	WT 4HT-1	13.97	13.97 *(0.110)*	14.85	14.84 *(0.0496)*
	WT 4HT-2	14.08		14.88	
	WT 4HT-3	13.86		14.79	
atnip2;1-1 4hr hypoxic	KO 4HT-1	14.02	13.94 *(0.0893)*	15.08	15.03 *(0.0815)*
	KO 4HT-2	13.84		14.94	
	KO 4HT-3	13.96		15.07	

[a]Replicate designations are the same as those shown in Figure 3. 33.

[b]The raw signal intensities are given in log_2 values from Microarray data analyzed by using the Affymetrix® Microarray suite software (MAS 5.0). Normalization of the raw data and estimation of signal intensities was done using the GC-Robust Multichip Average (GC-RMA) algorithm (Bolstad et al., 2003).

Table 3.4. Comparison of fold-differences between test transcripts *UBQ10* and *ADH1* from microarray data

Transcript	Fold changes between pairs of microarray[a]			
	WT normoxic vs. *atnip2;1-1* normoxic	WT normoxic vs. WT hypoxic	*atnip2;1* normoxic vs. *atnip2;1-1* hypoxic	WT hypoxic vs. *atnip2;1-1* hypoxic
UBQ10	-1.13 *(0.067)*	1.03 *(0.57)*	1.03 *(0.57)*	-1.02 *(0.72)*
ADH1	1.29 *(0.011)*	142 *(4.1 e^{-12})*	125 *(5.0 e^{-12})*	1.14 *(0.13)*

[a]The mean fold-change based on the ratio of the signals between the indicated pairs of microarrays. The number in parenthesis indicates the calculated *p*-value from one way ANOVA analysis.

least 2-fold by hypoxia treatment; and 2. a *p*-value of less than 0.05 (95% confidence level). By this criteria, 1535 genes (6.7% of the Arabidopsis genome) are upregulated after 4 hr of hypoxia treatment (Fig. 3.35). This result is within the range predicted by various other Arabidopsis anoxia /hypoxia microarray results done by using a wide variety of experimental treatments (629 to 1600 transcripts, Gonzal et al., 2005; Liu et al., 2005; Loreti et al., 2005). A subset of these transcripts that, similar to *AtNIP2;1*, are acutely upregulated (> 20-fold) are listed in Table 3.5. These include some of the classical ANPs involved in carbohydrate breakdown, glycolysis and fermentation including two sucrose synthesis genes, phosphofructokinase, ADH1 and PDC1 (Sachs et al., 1996; Dolferus et al., 1997; Dennis et al., 2000). In addition, other well-established ANPs such as non-symbiotic hemoglobin (GLB1) and the cell wall loosening enzyme xyloglucan endotransglucosylase are also represented in this list (Sachs et al., 1996; Hunt et al., 2002) Other gene networks involved in the hypoxia response including ethylene metabolism and signaling (ETR2, ACC oxidase, ethylene response element binding protein), heat shock proteins, and various transcription factors, that have been observed in other hypoxia microarrays (Klok et al., 2002; Branco-Pice et al., 2005; Gonzal et al., 2005; Liu et al., 2005; Loreti et al., 2005; Baena-Gonzalez et al., 2007) are also apparent (Table 3.5). Of particular interest is the observation of increased transcription of the *CML38* gene. This is a calmodulin-like gene related to rgs CaM, a calcium sensor involved in the regulation of gene silencing (Anandalakshmi et al., 2000). Although, the biochemical and biological functions of CML38 are not yet clear, it is apparent that calcium signaling is an important component of the anoxia

Figure 3.35. Transcript upregulation in wild type Arabidopsis roots in response to hypoxia. Microarray analysis was performed on Affymetrix whole genome Arabidopsis ATH1 chip with the root RNA samples shown in the **Fig. 3.33**. Statistical analysis with one-way ANOVA was done by using Partek Genomics Suite 6.4 software (Partek Inc., Missouri, USA). **A.** Comparison of number of transcripts showing a significant increase in response to 4 hr hypoxic treatment (4HT). **B.** Pie chart of up-regulated genes (> 2-fold) in the roots of 2-wk old wild type Arabidopsis under 4 hr hypoxia/anoxia. The ontology of Arabidopsis genes was assigned by using "ImageAnnotator 3.0.0.RC1" of Mapman software (Thimm et al., 2004; Usadel et al., 2005).

A

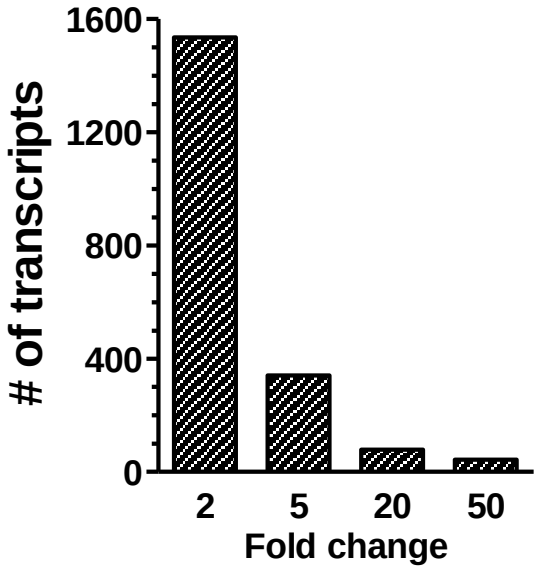

B

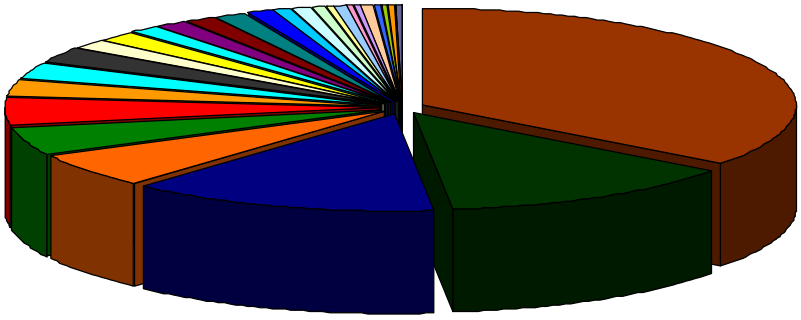

- not assigned (544 genes, 35.4%)
- RNA (206 genes, 12.4%)
- protein (203 genes, 13.2%)
- stress (91 genes, 5.9%)
- misc (75 genes, 4.9%)
- signalling (66 genes, 4.3%)
- development (44 genes, 2.9%)
- hormone metabolism (42 genes, 2.7%)
- transport (42 genes, 2.7%)
- DNA (25 genes, 1.6%)
- cell (24 genes, 1.6%)
- amino acid metabolism (23 genes, 1.5%)
- secondary metabolism (23 genes, 1.5%)
- cell wall (21 genes, 1.4%)
- lipid metabolism (19 genes, 1.2%)
- PS (17 genes, 1.1%)
- redox.regulation (14 genes, 0.9%)
- minor CHO metabolism (11 genes, 0.7%)
- major CHO metabolism (10 genes, 0.7%)
- fermentation (7 genes, 0.5%)
- tetrapyrrole synthesis (6 genes, 0.4%)
- mitochondrial electron transport / ATP synthesis (6 genes, 0.4%)
- nucleotide metabolism (5 genes, 0.3%)
- micro RNA, natural antisense etc (5 genes, 0.3%)
- glycolysis (4 genes, 0.3%)
- gluconeogenese/ glyoxylate cycle (4 genes, 0.3%)
- N-metabolism (2 genes, 0.1%)
- metal handling (2 genes, 0.1%)
- Co-factor and vitamine metabolism (2 genes, 0.1%)
- TCA / org. transformation (2 genes, 0.1%)
- Biodegradation of Xenobiotics (1 genes, 0.1%)
- C1-metabolism (1 genes, 0.1%)
- OPP (1 genes, 0.1%)

Table 3.5. List of transcripts showing 20-fold or greater up-regulation in the roots of wild type Arabidopsis under 4 hr hypoxic/anoxic conditions

AGI	Fold-change	Ontology[a]	Description
AT5G10040	1510.72	not assigned	Similar to unknown protein AT5G65207.1
AT1G43800	1264.20	lipid metabolism	Acyl-(acyl-carrier-protein) desaturase
AT2G17850	1049.88	protein	Similar to unknown protein AT5G66170.2
AT4G24110	929.48	not assigned	Similar to Hypothetical protein AAO17020.1
AT4G10270	898.78	stress	Wound-responsive family protein, similar to AT4G10265.1
AT2G34390	723.87	transport	NOD26-LIKE INTRINSIC PROTEIN 2;1 (NIP2.1)
AT4G33560	701.03	not assigned	Similar to wound-responsive protein-related AT2G14070.1
AT1G76650	658.73	signalling	Calcium-binding EF hand family protein (CML38)
AT3G10040	573.48	RNA	Transcription factor, similar to AT1G21200.1
AT3G29970	553.68	development	Germination protein-related, similar to AT3G48140.1
AT5G39890	448.06	not assigned	Similar to unknown protein AT5G15120.1
AT2G47520	344.14	RNA	AP2 domain-containing transcription factor
AT4G33070	326.81	fermentation	Pyruvate decarboxylase, similar to PDC3
AT1G35140	300.24	signalling	PHI-1 (PHOSPHATE-INDUCED 1)
AT5G62520	298.18	not assigned	SRO5 (SIMILAR TO RCD ONE 5); NAD+ ADP-ribosyltransferase
AT3G46230	233.30	stress	ATHSP17.4 (Arabidopsis thaliana heat shock protein 17.4)
AT3G23150	230.80	hormone metabolism	ETR2, receptor Involved in ethylene perception
AT3G43190	221.66	major CHO metabolism	SUS4, similar to SUS1 (SUCROSE SYNTHASE 1)
AT1G53540	211.22	stress	17.6 kDa class I small heat shock protein (HSP17.6C-CI)
AT2G16060	186.87	redox regulation	Arabidopsis non-symbiotic hemoglobin 1 (GLB1 or AHB1)
AT3G23170	162.87	not assigned	Similar to ATBET12 (AT4G14450.1)
AT4G30380	154.13	cell wall	Expansin-related, identical to putative expansin-like B2 precursor
AT5G12030	153.36	stress	Arabidopsis thaliana heat shock protein 17.6A (AtHSP17.6A)
AT1G59860	144.87	stress	17.6 kDa class I heat shock protein (HSP17.6A-CI)
AT4G01250	144.40	RNA	WRKY22 (WRKY DNA-binding protein 22) transcription factor
AT1G77120	141.75	fermentation	ADH1 (ALCOHOL DEHYDROGENASE 1)
AT3G02550	126.74	RNA	Lateral organ boundaries (LOB) domain protein 41 (LBD41)
AT2G15880	103.59	cell wall	Leucine-rich repeat family protein
AT2G41730	96.45	not assigned	Similar to unknown protein AT5G24640.1
AT3G16150	90.76	amino acid metabolism	L-asparaginase
AT5G26200	89.60	transport	Mitochondrial substrate carrier family protein
AT4G31020	86.62	not assigned	Similar to unknown protein AT2G24320.1
AT5G15120	80.36	not assigned	Similar to unknown protein AT5G39890.1
AT5G12020	78.53	stress	17.6 kDa class II heat shock protein (HSP17.6-CII)
AT4G37710	74.43	not assigned	VQ motif-containing protein, similar to AT2G22880.1
AT3G27220	74.42	RNA	Kelch repeat-containing protein, similar to AT1G51540.1
AT2G44080	71.75	not assigned	ARL (ARGOS-LIKE), similar to ARGOS
AT2G47950	68.74	not assigned	Similar to unknown protein AT3G62990.1
AT1G60750	66.56	hormone metabolism	Pseudogene, aldo/keto reductase family
AT5G44730	65.28	development	Haloacid dehalogenase-like hydrolase family protein

AGI	Fold-change	Ontology	Description
AT2G14210	54.05	RNA	ANR1, transcription factor similar to AGL21 (AGAMOUS-LIKE 21)
AT2G26400	52.56	not assigned	ARD/ATARD3 (ACIREDUCTONE DIOXYGENASE)
AT1G72940	50.14	stress	Disease resistance protein (TIR-NBS class)
AT2G34400	48.14	not assigned	Pentatricopeptide (PPR) repeat-containing protein
AT5G42200	47.79	protein	Zinc finger (C3HC4-type RING finger) family protein, identical to ATL5J
AT4G39675	45.00	not assigned	Unknown protein
AT1G19530	42.57	not assigned	Unknown protein
AT1G54050	39.01	stress	17.4 kDa class III heat shock protein (HSP17.4-CIII)
AT2G44800	38.52	secondary metabolism	Oxidoreductase, 2OG-Fe(II) oxygenase family protein
AT2G26150	37.86	stress and RNA	ATHSFA2 (Arabidopsis thaliana heat shock transcription factor A2)
AT1G28760	34.68	not assigned	Similar to unknown protein AT5G67610.2
AT5G57560	33.58	cell wall	TCH4 (TOUCH 4), identical to Xyloglucan endotransglucosylase
AT4G37370	32.93	misc	CYP81D8 (cytochrome P450, family 81, subfamily D, polypeptide 8)
AT2G39510	32.68	development	Nodulin MtN21 family protein, similar to nodulin AT2G37460.1
AT1G72360	32.37	RNA	Ethylene-responsive element-binding protein
AT2G40340	32.17	RNA	AP2 domain-containing transcription factor
AT3G03270	31.48	development	Universal stress protein (USP) family protein/early nodulin ENOD18
AT4G37240	31.29	not assigned	Similar to unknown protein AT2G23690.1
AT1G76600	30.73	not assigned	Similar to unknown protein AT1G21010.1
AT1G05680	30.73	hormone metabolism	UDP-glucoronosyl/UDP-glucosyl transferase family protein
AT5G10210	30.44	not assigned	Similar to unknown protein AT5G65030.1
AT5G20230	29.96	misc	ATBCB (ARABIDOPSIS BLUE-COPPER-BINDING PROTEIN)
AT2G22880	29.47	not assigned	VQ motif-containing protein, similar to AT4G37710.1
AT5G20830	27.38	major CHO metabolism	SUS1 (SUCROSE SYNTHASE 1)
AT1G72800	27.10	not assigned	nuM1-related, similar to nucleolin AT1G48920.1)
AT4G25810	26.55	cell wall	XTR6 (XYLOGLUCAN ENDOTRANSGLYCOSYLASE 6), hydrolase
AT5G02200	26.48	signalling	Phytochrome A specific signal transduction component-related
AT4G32840	25.04	glycolysis	Phosphofructokinase family protein, similar to AT5G56630.1
AT2G19590	24.34	hormone metabolism	ACO1 (ACC OXIDASE 1), similar to AT1G12010.1
AT5G14470	22.79	not assigned	GHMP kinase-related, similar to AT3G01640.1
AT4G25200	22.60	stress	ATHSP23.6-MITO
AT5G66985	21.46	not assigned	Unknown protein
AT1G59660	21.36	protein	Nucleoporin family protein, similar to transporter AT1G10390.2
AT1G72060	21.23	not assigned	DNAJ heat shock N-terminal domain-containing protein
AT5G22570	21.23	RNA	WRKY38 (WRKY DNA-binding protein 38) transcription factor
AT5G39050	21.08	secondary metabolism	Transferase family protein, similar to AT5G39080.1
AT1G09090	20.85	stress	ATRBOHB (RESPIRATORY BURST OXIDASE HOMOLOG B)
AT3G48520	20.32	misc	CYP94B3 (cytochrome P450, family 94, subfamily B, polypeptide 3)

[a]Ontology is assigned based on analysis with the Mapman software (Thimm et al., 2004; Usadel et al., 2005).

response (Subbaiah and Sachs, 2003) and CML38 may be a mediator of calcium signaling during adaptation to oxygen deprivation.

Effects of the reduction of *AtNIP2;1* expression on transcript changes of genes during anaerobiosis

To investigate differences in the Arabidopsis transcriptome associated with the hypoxia response in the *atnip2;1-1* mutant, a similar analysis as that shown in Figure. 3.35 was performed. By using the same criteria as those used for wild type comparisons (> 2-fold induction, $p < 0.05$), 1480 genes were found to be upregulated by 4 hr of hypoxia stress, suggesting differences between the hypoxia-activated transcriptional response of wild type and *atnip2;1-1* mutant plants. A co-expression analysis was performed (Fig. 3.36) to identify the gene sets that are shared by both as well as those that are unique. This analysis showed that a total of 1306 genes (85% of genes in WT and 88% of genes in *atnip2;1-1*) were found in an intersection of a Venn diagram (Fig. 3.36A), suggesting that most of the genes were co-expressed under hypoxia. However, this analysis also reveals 174 genes that are uniquely upregulated in *atnip2;1-1* and 229 genes that are uniquely upregulated in WT (Fig. 3.26A). Similar comparisons were also done for genes that are repressed at least two fold by hypoxia treatment (Fig. 3.36B). Consistent with previous reports, a greater complement of genes are down regulated in response to oxygen deprivation (Klok et al., 2002). Early work has shown that the expression of most polypeptides are repressed during oxygen deprivation presumably to conserve energy during severe oxygen deficit (Sachs et al., 1980; Dolferus et al., 1985). A full list of the genes uniquely induced or repressed for

Figure 3.36. Co-expression analysis of microarray data sets showing transcript profiles of genes induced or repressed by hypoxia in the roots of wild type and *atnip2;1-1* Arabidopsis. Co-expressed genes showing more than 2-fold increase (*p*-value is less than 0.05) were obtained and analyzed by using Partek Genomics Suite 6.4 software. **A.** Venn diagram showing co-expression of hypoxia-induced genes in the roots of wild type Arabidopsis and *atnip2;1-1*. **B.** Co-expression analysis of downregulated by hypoxia genes in the roots of wild type Arabidopsis and *atnip2;1-1*. A full list of the genes unique for *atnip2;1* or wild type root responses to hypoxia is available in the tables in Appendix 1.

A

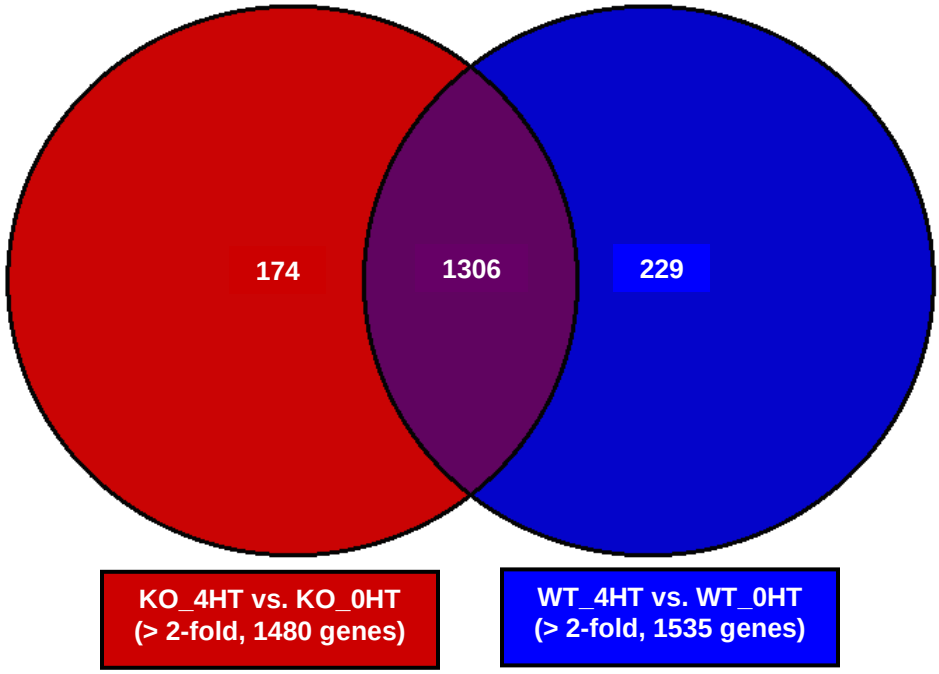
174
1306
229
KO_4HT vs. KO_0HT
(> 2-fold, 1480 genes)
WT_4HT vs. WT_0HT
(> 2-fold, 1535 genes)

B

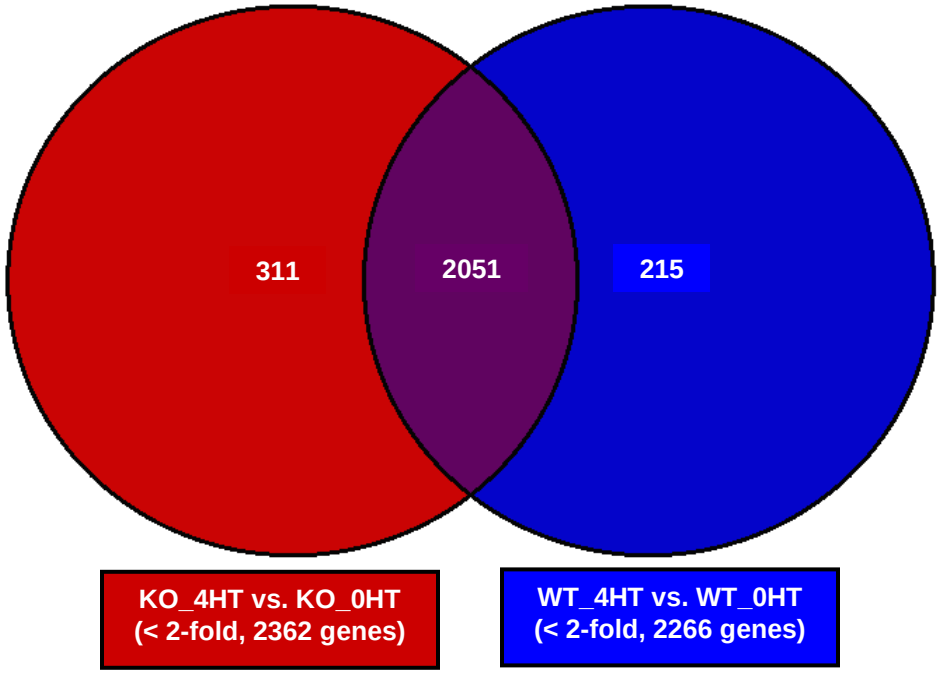
311
2051
215
KO_4HT vs. KO_0HT
(< 2-fold, 2362 genes)
WT_4HT vs. WT_0HT
(< 2-fold, 2266 genes)

atnip2;1-1 or wild type root responses to hypoxia is shown in tables in Appendix 1 (Table A.1; Table A.2; Table A.3; Table A.4).

Among the genes that are uniquely upregulated by hypoxia treatment in *atnip2;1-1*, only 14 show greater than 3-fold upregulation (Table 3.6). Four of these, including the two with the greatest stimulation, are members of heat shock protein family (HSP21, DNAJ proteins) or are involved in the heat shock response (At-HSFA7B). This observation is of interest since the elevation of heat shock proteins during temperature as well as hypoxia stress has been proposed to be involved in Arabidopsis resistance to these stresses (Loreti et al., 2005; Banti et al., 2008).

Effects of the reduction of *AtNIP2;1* expression on gene regulation under normoxic conditions

In order to gain insight into the effects of the *AtNIP2;1* reduction on global transcript regulation of genes under normoxia, the microarray data from normoxic WT and *atnip2;1-1* roots were compared to obtain a list of genes showing a significant increase or decrease in expression in the mutant (a difference of 2-fold, $p < 0.05$). By this criteria, *atnip2;1-1* shows 54 genes that are significantly upregulated and 14 genes that are significantly down regulated. The upregulated genes fall into 15 categories based on ontology analysis using the Mapman software (Fig. 3.37). Among the 15 functional groups, seed developmental genes (10 genes) were the most prevalent (www.arabidopsis.org) (Fig. 3.37 and Table 3.7). Interestingly, several additional genes encoding seed proteins were found in other functional categories showing that 24 total genes (44% of total) are related to seed proteins (highlighted in red in Table 3.7).

Table 3.6. List of transcripts showing significant induction (> 3-fold) only in the roots of *atnip2;1-1* under 4 hr hypoxic conditions

AGI	Fold-change[a]	Ontology[b]	Description
AT4G27670	22.19	stress	HSP21 (HEAT SHOCK PROTEIN 21) chloroplast located small heat shock protein
AT1G71000	8.00	stress	DNAJ heat shock N-terminal domain-containing protein
AT3G49130	7.49	not assigned	RNA binding, similar to SWAP (Suppressor-of-White-APricot)
AT3G63350	5.93	RNA	AT-HSFA7B (Arabidopsis thaliana heat shock transcription factor A7B)
AT1G17870	5.24	protein	S2P-like putative metalloprotease
AT1G60190	4.83	protein	Armadillo/beta-catenin repeat family protein / U-box domain-containing protein
AT5G19100	4.22	not assigned	Extracellular dermal glycoprotein-related / EDGP-related
AT4G19980	3.67	not assigned	Similar to Os06g0666800
AT2G20560	3.33	stress	DNAJ heat shock family protein similar to DNAJ heat shock family protein AT4G28480.1
AT3G17609	3.28	RNA	HYH (HY5-HOMOLOG); DNA binding / transcription factor
AT3G56290	3.22	not assigned	Similar to Os01g0823600
AT5G57345	3.15	not assigned	Similar to unknown protein AT1G54520.1
AT1G66080	3.03	not assigned	Similar to Hypothetical protein AAO06975.1
AT1G07860	3.02	not assigned	Unknown protein

[a]More than 3 fold significantly induced by hypoxia transcripts showing *p*-value < 0.05 only in *atnip2;1-1* root tissues were listed according to fold increase of transcripts under 4 hr hypoxc conditions.

[b]Ontology is assigned based on analysis with the Mapman software (Thimm et al., 2004; Usadel et al., 2005).

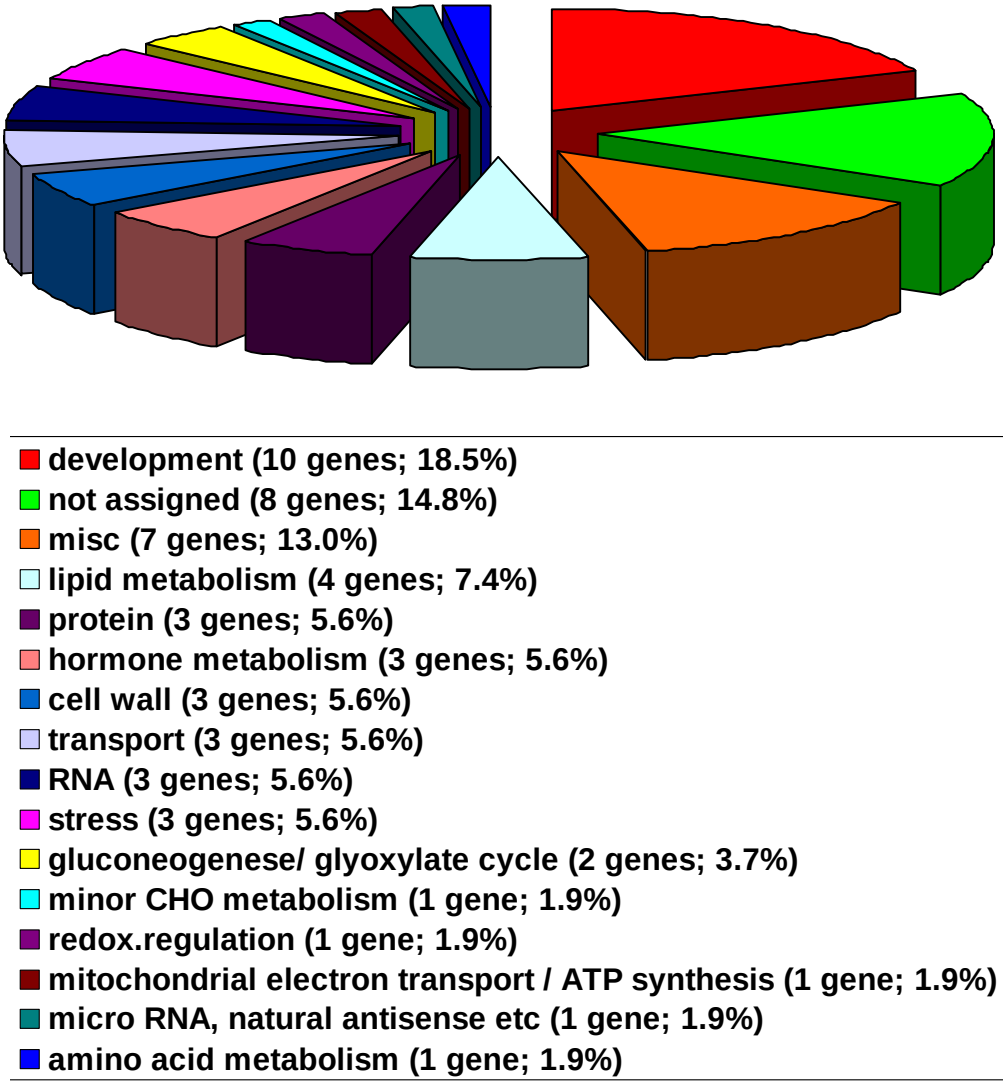

Figure 3.37. Ontology of transcripts showing significant up-regulation in the roots of *atnip2;1-1* under normal growth conditions. Transcripts showing more than 2-fold increase (*p*-value is less than 0.05) in the roots of 2-wk old *atnip2;1-1* compared to the roots of 2-wk old wild type Arabidopsis grown under normoxic growth conditions were obtained and analyzed for ontology by using the Mapman software as described in the **Materials and Methods**.

Table 3.7. List of transcripts showing significant up or down regulation in the roots of *atnip2;1-1* compared to the roots of wild type Arabidopsis under normoxia

AGI	Fold-change[a]	Ontology[b]	Description
AT5G44120	54.60	development	CRA1 (CRUCIFERINA), nutrient reservoir, encodes a 12S seed storage protein
AT4G28520	31.69	development	CRU3 (CRUCIFERIN 3), nutrient reservoir 12S seed storage protein similar to CRA1 (CRUCIFERINA)
AT1G48130	13.43	redox.regulation	ATPER1 (Arabidopsis thaliana 1-cysteine peroxiredoxin 1), antioxidant
AT5G40420	11.42	lipid metabolism	OLEO2 (OLEOSIN 2), a protein found in oil bodies, involved in seed lipid accumulation
AT3G21370	11.38	misc	Glycosyl hydrolase family 1 protein, similar to BGL1 (BETA-GLUCOSIDASE HOMOLOG 1)
AT3G21720	9.71	gluconeogenese/ glyoxylate cycle	Isocitrate lyase, putative
AT2G41260	7.52	development	M17 Late-embryogenesis-abundant gene
AT2G28490	7.17	development	Cupin family protein, similar to probable major protein body membrane protein MP27
AT1G73190	6.10	transport	ALPHA-TIP/TIP3;1 (ALPHA-TONOPLAST INTRINSIC PROTEIN)
AT3G54940	5.87	protein	Cysteine proteinase, putative, similar to cysteine proteinase A494
AT3G02480	4.98	hormone metabolism	ABA-responsive protein-related, similar to unknown protein AT5G38760.1
AT2G31980	4.95	protein	Cysteine proteinase inhibitor-related
AT2G42250	4.94	micro RNA, natural antisense etc	Other RNA Potential natural antisense gene, locus overlaps with AT2G42247
AT5G48485	4.52	misc	DIR1 (DEFECTIVE IN INDUCED RESISTANCE 1), lipid binding encodes a putative apoplastic lipid transfer protein
AT1G04560	4.47	transport	AWPM-19-like membrane family protein, similar to a Lea protein with hydrophobic domain
AT5G59310	4.09	lipid metabolism	LTP4 (LIPID TRANSFER PROTEIN 4)
AT5G10120	4.08	RNA	Ethylene insensitive 3 family protein
AT3G22120	4.01	misc	CWLP (CELL WALL-PLASMA MEMBRANE LINKER PROTEIN)
AT1G52820	3.92	hormone metabolism	2-oxoglutarate-dependent dioxygenase, putative, similar to AOP1
AT2G47770	3.70	not assigned	Benzodiazepine receptor-related
AT3G47340	3.68	amino acid metabolism	ASN1 (DARK INDUCIBLE 6), encodes a glutamine-dependent asparagine synthetase
AT5G52300	3.63	stress	RD29B (RESPONSIVE TO DESSICATION 29B), encodes a protein that is induced in expression in response to water deprivation
AT5G66400	3.46	stress	RAB18 (RESPONSIVE TO ABA 18), belongs to the dehydrin protein family
AT3G20210	3.26	protein	DELTA-VPE (delta vacuolar processing enzyme), cysteine-type endopeptidase
AT3G48740	2.94	development	Nodulin MtN3 family protein
AT1G10640	2.90	cell wall	Polygalacturonase, putative

AGI	Fold-change[a]	Ontology[b]	Description
AT3G15670	2.88	development	Late embryogenesis abundant protein, putative
AT5G51190	2.86	hormone metabolism	AP2 domain-containing transcription factor, putative encodes a member of the ERF
AT4G25140	2.73	lipid metabolism	OLEO1 (OLEOSIN1), a protein found in oil bodies, involved in seed lipid accumulation
AT2G35300	2.69	development	LEA group 1 domain-containing protein
AT3G44260	2.59	RNA	CCR4-NOT transcription complex protein, putative
AT2G36640	2.56	development	ATECP63 (EMBRYONIC CELL PROTEIN 63), ncodes putative phosphotyrosine protein belonging to LEA protein
AT3G53040	2.51	development	Late embryogenesis abundant protein, putative
AT1G52690	2.45	development	Late embryogenesis abundant protein, putative
AT3G51600	2.42	lipid metabolism	LTP5 (LIPID TRANSFER PROTEIN 5)
AT5G57560	2.42	cell wall	TCH4 (TOUCH 4), hydrolase, encodes a cell wall-modifying enzyme
AT1G62560	2.40	misc	Flavin-containing monooxygenase family protein
AT4G37240	2.37	not assigned	Similar to unknown protein AT2G23690.1
AT5G03860	2.35	gluconeogenese/ glyoxylate cycle	Malate synthase, putative, encodes a protein with malate synthase activity
AT3G48520	2.28	misc	CYP94B3 (cytochrome P450, family 94, subfamily B, polypeptide 3), oxygen binding member of CYP94B
AT4G37800	2.27	cell wall	Xyloglucan:xyloglucosyl transferase, putative
AT2G32100	2.26	not assigned	ATOFP16/OFP16 (Arabidopsis thaliana ovate family protein 16)
AT4G11880	2.23	RNA	AGL14 (AGAMOUS-LIKE 14), preferentially expressed in root tissues and therefore represent the only characterized MADS box genes expressed in roots
AT5G38910	2.23	stress	Germin-like protein, putative
AT3G17520	2.22	not assigned	Late embryogenesis abundant domain-containing protein
AT1G48510	2.10	mitochondrial electron transport / ATP synthesis	Cytochrome c oxidase assembly protein surfeit-related, similar to SURF1 (SURFEIT 1)
AT1G69870	2.10	transport	Proton-dependent oligopeptide transport (POT) family protein
AT1G08430	2.10	not assigned	ALMT1/ATALMT1 (AL-ACTIVATED MALATE TRANSPORTER 1), malate transporter
AT3G30350	2.10	not assigned	Unknown protein
AT5G01300	2.05	not assigned	Phosphatidylethanolamine-binding family protein
AT1G07260	2.05	misc	UDP-glucoronosyl/UDP-glucosyl transferase family protein
AT3G50440	2.03	not assigned	Hydrolase, similar to esterase, similar to salicylic acid-binding protein 2 AAR87711.1
AT1G52400	2.02	misc	BGL1 (BETA-GLUCOSIDASE HOMOLOG 1), hydrolase
AT4G39770	2.02	minor CHO metabolism	Trehalose-6-phosphate phosphatase, putative
ATCG00280	-3.70	PS	Chloroplast gene encoding a CP43 subunit of the photosystem II reaction center. promoter contains a blue-light responsive element.
AT5G35940	-2.51	misc	Jacalin lectin family protein similar to jacalin lectin family protein AT5G35950.1
ATCG00520	-2.45	protein	Encodes a protein required for photosystem I assembly and stability.

AGI	Fold-change[a]	Ontology[b]	Description
AT2G22990	-2.38	protein	SNG1 (SINAPOYLGLUCOSE 1); serine carboxypeptidase sinapoylglucose:malate sinapoyltransferase.
AT1G01420	-2.29	secondary metabolism	UDP-glucoronosyl/UDP-glucosyl transferase family protein similar to AT1G01390.1
AT4G04750	-2.22	transport	Carbohydrate transporter/ sugar porter Identical to Sugar transporter ERD6-like14, similar to sugar transporter family protein AT4G04760.1
AT2G07698	-2.16	not assigned	Identical to Hypothetical mitochondrial protein AtMg01200
AT3G23700	-2.13	not assigned	S1 RNA-binding domain-containing protein similar to RPS1 (ribosomal protein S1)
AT5G24850	-2.11	DNA	CRY3 (CRYPTOCHROME 3); DNA binding / DNA photolyase/ FMN binding Binds flavin adenine dinucleotide and DNA.
AT4G28110	-2.09	RNA	AtMYB41 (myb domain protein 41); DNA binding / transcription factor
AT1G03200	-2.06	not assigned	Similar to unknown protein AT1G03240.1
AT2G40530	-2.05	not assigned	Unknown protein
ATCG01100	-2.03	PS	NADH dehydrogenase ND1 Identical to NAD(P)H-quinone oxidoreductase subunit 1
AT5G23350	-2.02	hormone metabolism	GRAM domain-containing protein / ABA-responsive protein-related

[a]List of genes specifically expressed in the roots of *atnip2;1-1* showing significantly up and regulation (2-fold change with *p*-value of < 0.05) under 4 hr hypoxic condition. Genes highlighted in red encode seed and late embryogenesis proteins.

[b]Ontology is assigned based on analysis with the Mapman software (Thimm et al., 2004; Usadel et al., 2005).

Among other notable transcripts are several that are inducible by ABA, several cysteine proteinases, and the induction of genes encoding key enzymes (isocitrate lyase and malate synthase) of the glyoxylate cycle (Table 3.7). These transcripts are consistent with roles in seed physiology and suggest that loss in the ability to express *AtNIP2;1* may result in elevated ABA. In this regard, it should be noted that seed development, particularly late seed development is a naturally hypoxic state in Arabidopsis (Porterfield et al., 1999). One possible explanation is that knockout of *AtNIP2;1* and accumulation of lactic acid may simulate a hypoxic state in normoxic *atnip2;1-1* roots. If this is the case, one might also predict that the transcripts shown in Table 3.7 may be ANPs that are induced in wild type plants during hypoxia. To test this, a comparison of the induction of these genes during hypoxia treatment in wild type plants was performed (Table 3.8). The results show that six of these gene products are induced during wild type hypoxia including enzymes involved in the glyoxylate cycle, a ROS detoxifying peroxidase (AtPER1), an ABA responsive protein, and the AGL14 transcription factor. Whether the elevation of these proteins in the normoxic state leads to “pre-adaptation” of *atnip2;1-1* plants remains an open question.

AtNIP7;1 **is mainly expressed in the flower tissue**

AtNIP7;1 is a representative NIP II protein that is encoded by the At3g06100 gene, and which has an unknown function in Arabidopsis. To investigate the expression of this gene in the *Arabidopsis* tissues, RT-PCR and Q-PCR analyses were performed. Total RNA samples (4 µg of each) isolated from five different tissues (flower, silique, stem, leaf, and root tissues) were reverse transcribed into first strand cDNA and

Table 3.8. Comparison of the transcripts shown in Table 3.7 to hypoxia-induced transcripts in wild type Arabidopsis

AGI	Fold-change[a]	*p*-value	Ontology[b]	Description
AT5G44120	6.75	2.16E-02	development	CRA1 (CRUCIFERINA), nutrient reservoir, encodes a 12S seed storage protein
AT1G48130	8.13	2.94E-02	redox.regulation	ATPER1 (Arabidopsis thaliana 1-cysteine peroxiredoxin 1), antioxidant
AT3G21720	7.81	2.29E-03	gluconeogenese/ glyoxylate cycle	Isocitrate lyase, putative
AT3G02480	3.35	8.83E-03	hormone metabolism	ABA-responsive protein-related, similar to unknown protein AT5G38760.1
AT5G03860	2.06	1.69E-04	gluconeogenese/ glyoxylate cycle	Malate synthase, putative, encodes a protein with malate synthase activity
AT4G11880	2.08	3.02E-02	RNA	AGL14 (AGAMOUS-LIKE 14), preferentially expressed in root tissues and therefore represent the only characterized MADS box genes expressed in roots

[a]Fold chage of transcripts shows hypoxic-induction level in WT root tissues under 4 hr hypoxic conditions. A list of transcripts is also found in the Table 3.7.

[b]Ontology is assigned based on analysis with the Mapman software (Thimm et al., 2004; Usadel et al., 2005).

were used for initial investigation of *AtNIP7;1* expression by semi-quantitative RT-PCR (Fig. 3.38). The RT-PCR result for *AtNIP7;1* showed the expected 638bp amplification product and shows that *AtNIP7;1* was mainly expressed in flower tissue, with much lower amounts of cDNA detected in stem, leaf, and root, and no expression detected in siliques (Fig. 3.38B). To investigate this RT-PCR result in a more quantitative fashion, Q-PCR was performed using the *AtNIP7;1* Q-PCR specific-primers. *UBQ10*, which is constitutively expressed in all *Arabidopsis* tissues, was amplified to monitor amplification efficiency and normalize loading errors in total RNA concentration. The results showed that the expression pattern of *AtNIP7;1* in Arabidopsis tissues was consistent with previous RT-PCR (Fig. 3.38B), with the exception of siliques which showed an elevated expression based on Q-PCR (Fig. 3.39). Regardless of this discrepancy both analyses show that *AtNIP7;1* is expressed at a much higher in flower tissue than other tissues (Fig. 3.39).

To address the question of which floral stage *AtNIP7;1* is predominantly expressed in, analysis of floral developmental microarray data (Genevestigator; www.genevestigator.ethz.ch/) was done. *Arabidopsis* flower development is divided into 12 stages which represent a series of landmark events beginning with flower initiation and ending with the opening of the buds (Smyth et al. 1990; see Fig. 3.40A). Analysis of *AtNIP7;1* on floral development microarray shows high levels of the transcript at stage 9 and then a gradual decline over flower stages 10 to 12 (Fig. 3.40B). The flower stage 9 appears to be one of the most important growth stages since the rapid expansion and growth of all floral parts, occur in this floral stage (Smyth et al., 1990; see Fig. 3.40A).

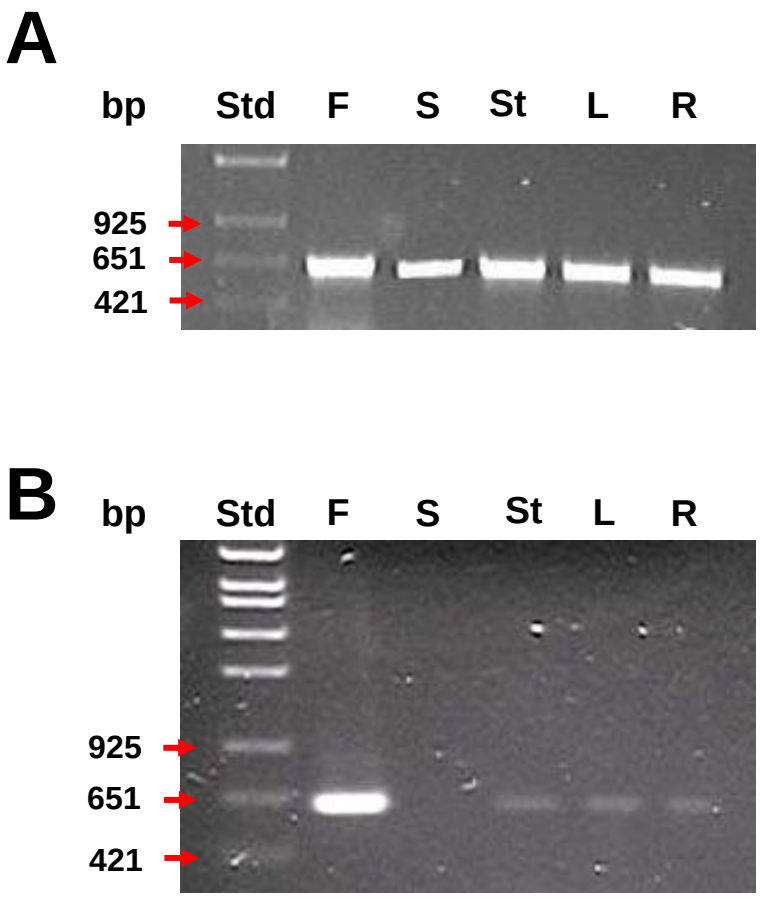

Figure 3.38. Expression of *AtNIP7;1* in the Arabidopsis tissues by RT-PCR. Total RNA (100 ng) isolated from the indicated organs of 6 wk old Arabidopsis plants was used for semi-quantitative RT-PCR. **A.** Amplification of *Arabidopsis Actin 2* (*ACT2*) as a loading control. **B.** Expression of *AtNIP7;1* in the various tissues of 6-wk old Arabidopsis plants. **Std** shows the loading of DNA molecular standard marker and **bp** shows the molecular weight of the standared in base pairs. Abbreviations of **F, S, St, L,** and **R** indicate flower, siliques, stem, leaf, and root, respectively.

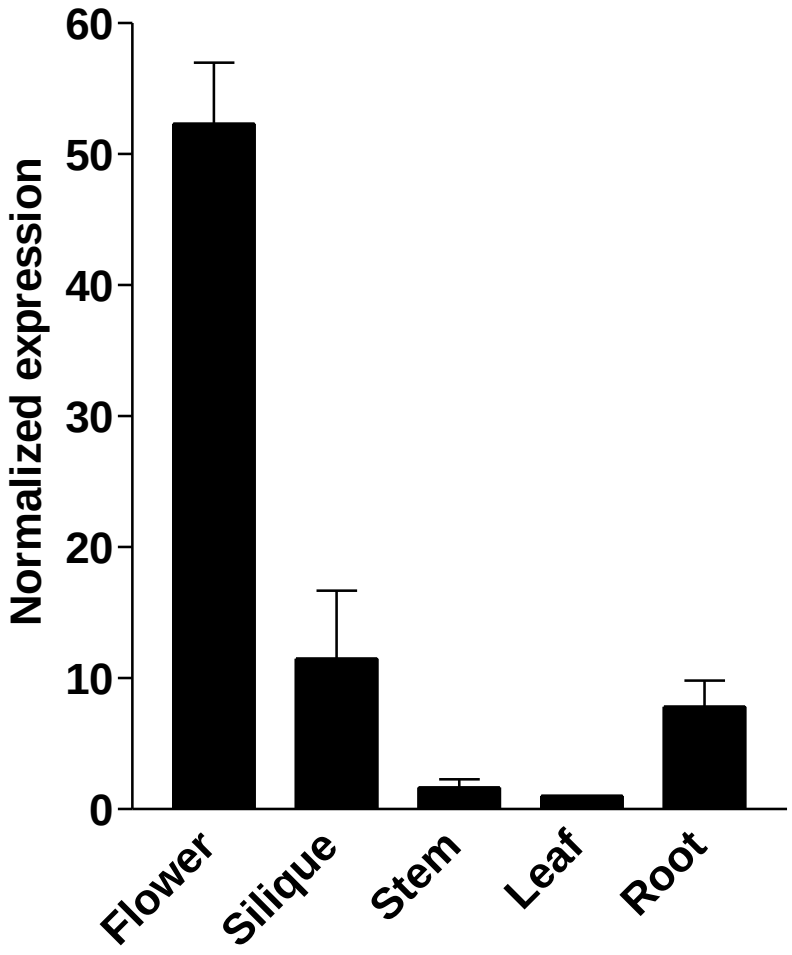

Figure 3.39. Q-PCR analysis for expression of *AtNIP7;1* in Arabidopsis tissues. The same cDNA samples (10 ng of each) described in Figure 3.42 were used for *AtNIP7;1* expression in the various tissues tested by using Q-PCR analysis. The data was normalized to *AtNIP7;1* expression in the leaf. The highest expression signal was detected in flower tissue. Error bars show SEM of two (siliques) to five (flower, stem, leaf and root) biological replicates.

Figure 3.40. AtNIP7;1 expression during flower developmental stages 9 to 15. **A**. Lateral views of the flower stages 9 to 12 taken from Smyth et al. (1990). **B.** Microarray **of *AtNIP7;1* expression using an affy 22K chip in each flower stage (Genevestigator; www.genevestigator.ethz.ch/).** Error bars show standard error of mean (n=3).

A

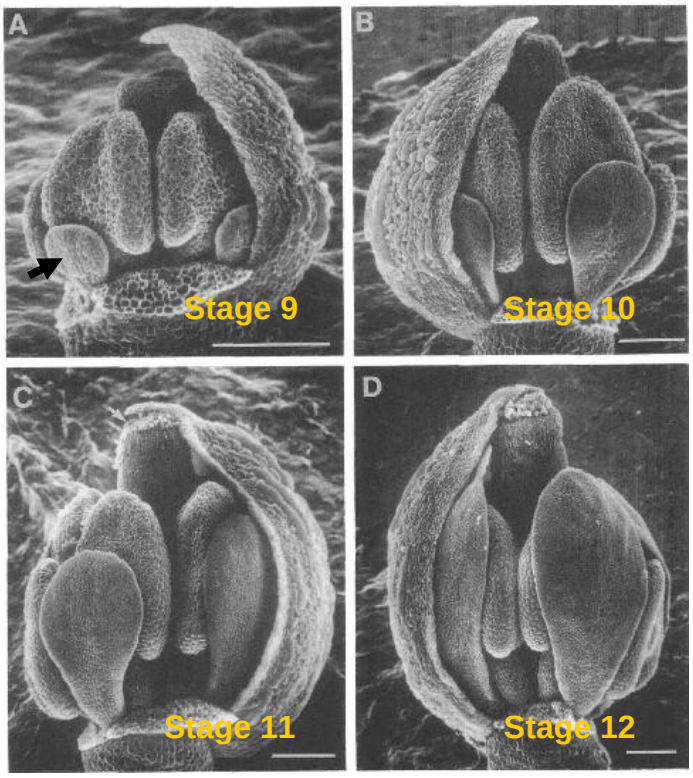

<Smyth et al. 1990>

B

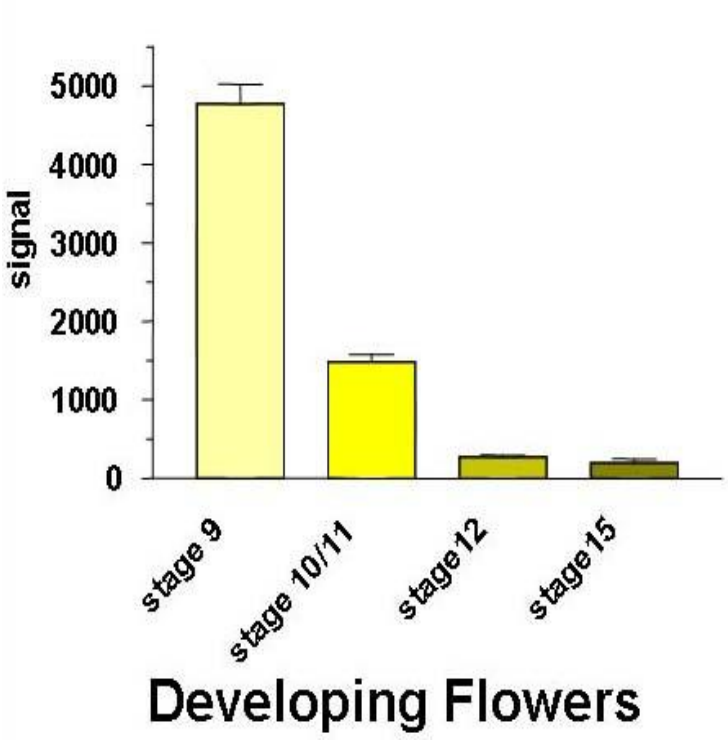

To investigate the cellular localization of *AtNIP7;1* expression in developing Arabidopsis flower, *in situ* hybridization was performed by using a *AtNIP7;1* specific probe. The result showed that *AtNIP7;1* expression signal was strong and was selectively found in pollen granules of early floral buds with anti-sense *AtNIP7;1* probe hybridization (Fig. 3.41B). Specificity is apparent since hybridization with sense *AtNIP7;1* probe hybridization showed no apparent signal (negative control, Fig. 3.41A). The results suggest that *AtNIP7;1* might be involved in pollen development.

Characterization of a *AtNIP7;1* T-DNA knockout mutant line

A *AtNIP7;1* T-DNA KO line (Salk_042590; T4 generation seed) was obtained from the ABRC and was characterized by using RT-PCR and PCR-based genotyping. The T4 generation *AtNIP7;1* mutant line was germinated on the 1/2 strength of Murashige and Skoog (MS) media under the standard LD condition. Harvested T5 generation seeds were then germinated on the 1/2MS+Kan (50 µg/mL) plate, but it was found that they were sensitive to Kanamycin suggesting that the Kan^R gene has been silenced. Therefore, a PCR genotyping approach was taken to determine T-DNA genotype of the mutant line and to verify the location of the T-DNA insert. PCR genotyping was done using the three primers, two gene specific primers and a left border T-DNA primer. The proposed pattern for wild type (WT), heterozygous (HZ), and homozygous (HM) genotypes are shown in Figure 3.46A. As expected, WT. Col-0 showed a single 900bp band corresponding to the wild type *AtNIP7;1* gene (Fig. 3.42A). On the other hand, only the predicted 500bp *T-DNA*/*AtNIP7;1* band was detected in two different T5 *AtNIP7;1* mutant biological samples in lane 2 and 3 (Fig. 3.42A). PCR

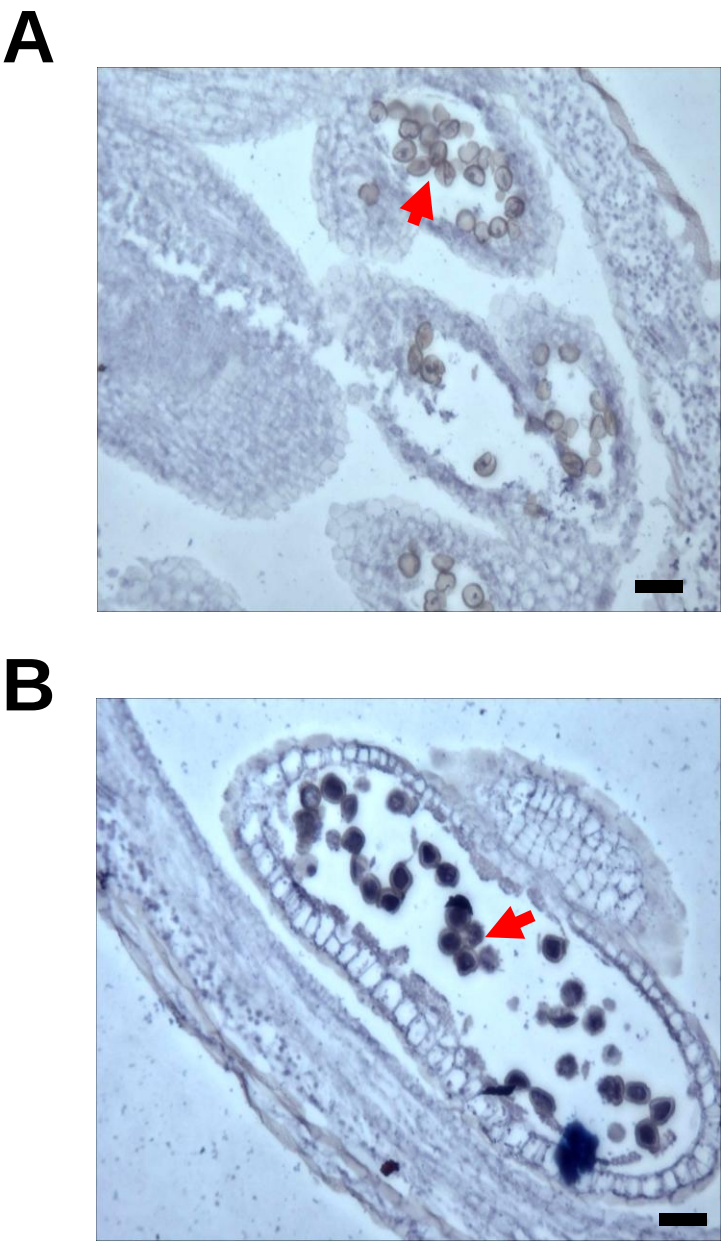

Figure 3.41. *In situ* hybridization analysis of *AtNIP7;1* expression in developing Arabidopsis flowers. Early floral buds were fixed and embedded in paraffin for *in situ* hybridization as described in the **Materials and Methods**. Each tissue section was counter stained with Eosin Y for color contrast. **A.** Early floral stage hybridized with *AtNIP7;1* sense probe. **B.** Early floral bud hybridized with *AtNIP7;1* anti-sense probe showing selective expression of *AtNIP7;1* in pollen granules (arrow heads). Size bars are 20 µm.

Figure 3.42. Characterization of a *AtNIP7;1* mutant line. A. PCR based genotyping analysis of WT. Col-0 and *AtNIP7;1* mutant line (Salk_042590) with the proposed PCR genotyping band patterns for WT, HZ, and HM is shown. Closed arrow heads indicate molecular weight of DNA molecular standard marker. Open arrow heads represent wild type *AtNIP7;1* band and T-DNA inserted *AtNIP7;1* band (T-DNA/*AtNIP7;1*). STD, λEcoT14I/Bgl II DNA molecular marker standard; lane 1, WT. Col-0; lane 2 and 3, two different genomic DNA samples from two separate *nip7;1-1* plants T5 generation. Lower diagram shows predicted patters of PCR for WT (wild type), HZ (heterozygous), and HM (homozygous) genotypes. "N" designates expected nucleotide size between the T-DNA insertion and gene of interest. **B.** A diagram of sequencing of PCR result showing the T-DNA insertion site in the 4th exon of *AtNIP7;1*. T-DNA LBb1 shows T-DNA left border primer of Salk T-DNA. NIP7.1LP and NIP7.1RP represent *AtNIP7;1* specific forward and reverse primers used for PCR genotyping.

A

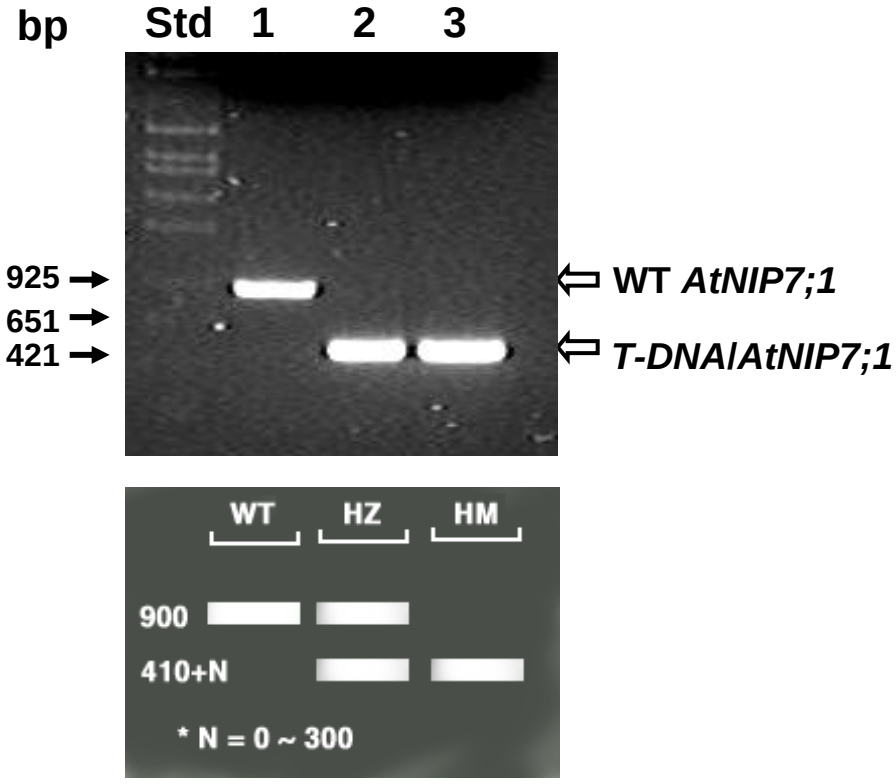
bp
Std
1
2
3
925
651
421
WT AtNIP7;1
T-DNA/AtNIP7;1
WT
HZ
HM
900
410+N
* N = 0 ~ 300

B

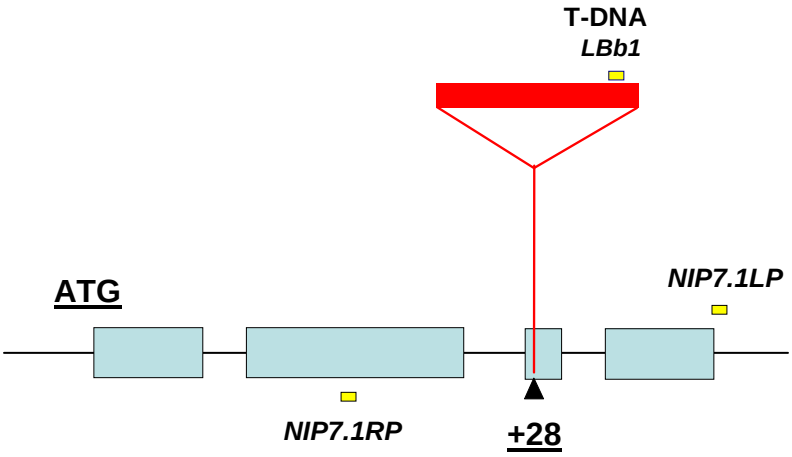
T-DNA
LBb1
ATG
NIP7.1LP
NIP7.1RP
+28

based genotyping for *AtNIP7;1* was done using the 13 different T5 *AtNIP7;1* mutant plants. Only homozygous band pattern was detected from the mutant plants tested. Therefore, this *AtNIP7;1* mutant line (Salk_042590) appears to be homozygous for the T-DNA insertion (Fig. 3.42A). Sequence analysis revealed that the T-DNA is inserted at 28 bp downstream from starting of the 4th exon of *AtNIP7;1* as shown in Figure. 3.41B. We will refer to this KO line as *nip7;1-1*.

In order to verify that mRNA expression was lost in *nip7;1-1*, RT-PCR and Q-PCR was done. Because *NIP7;1* appeared to be mainly expressed in flower (Fig. 3.38; Fig. 3.39; Fig. 3.40), total RNA was isolated from flowers of 6 week old WT. Col-0, and *nip7;1-1* for these analyses. The results show, as expected, that a 650bp *AtNIP7;1* band was amplified from a flower sample of wily type Arabidopsis, but no band was detected for neither a *nip7;1-1* flower sample nor a *nip7;1-1* whole seedling sample (Fig. 3.43B). Additional Q-PCR was also performed to verify RT-PCR result shown in Figure 3.43B. The results are consistent with RT-PCR (Fig. 3.43) showing that high expression of *AtNIP7;1* was detected in flowers of wild type Arabidopsis, but no expression was detected in either *nip7;1-1* flowers or whole seedlings (Fig. 3.43C). Taken together, the data suggest that *AtNIP7;1* gene expression appeared to be knocked out by T-DNA insertion in *nip7;1-1* (Salk_042590) (Fig. 3.43).

Phenotypic analysis of *nip7;1-1*

The inflorescence of both *nip7;1-1* KO and WT. Col-0 plants was harvested from 5 week old plants and analyzed by light microscopy and by scanning electron microscopy (SEM). The flowers appeared normal in both suggesting that *AtNIP7;1* KO

Figure 3.43. Expression analysis of *AtNIP7;1* from 6-wk old Arabidopsis plants. RT-PCR analyses were done on *AtNIP7;1* expression in wild type flower, *nip7;1-1* flower, and *nip7;1-1* whole seedlings as described in the **Materials and Methods**. PCR products were resolved by gel electorphoresis on 0.8% (w/v) agarose gels and were stained with EtBr (panel A and B). **A.** Amplification of *ACT2* as a loading control, showing even amplication of this transcript. **B.** Expression of *AtNIP7;1* in wild type flower, *nip7;1-1* flower, and *nip7;1-1* whole seedlings. The expected 650bp *AtNIP7;1* band was amplified only from WT. flower, but no expression of *AtNIP7;1* was found in *nip7;1-1* flower and whole seedlings. STD, λEcoT14I/Bgl II DNA molecular standard marker; lane 1, WT. flower; lane 2, T5 *nip7;1-1* flower; lane 3, whole seedling of T5 *nip7;1-1*. **C.** Q-PCR analysis of *AtNIP7;1* expression analysis in 6 week old Arabidopsis. The expression data was normalized to *AtNIP7;1* in wild type flowers. Errors show SEM of six biological replicates.

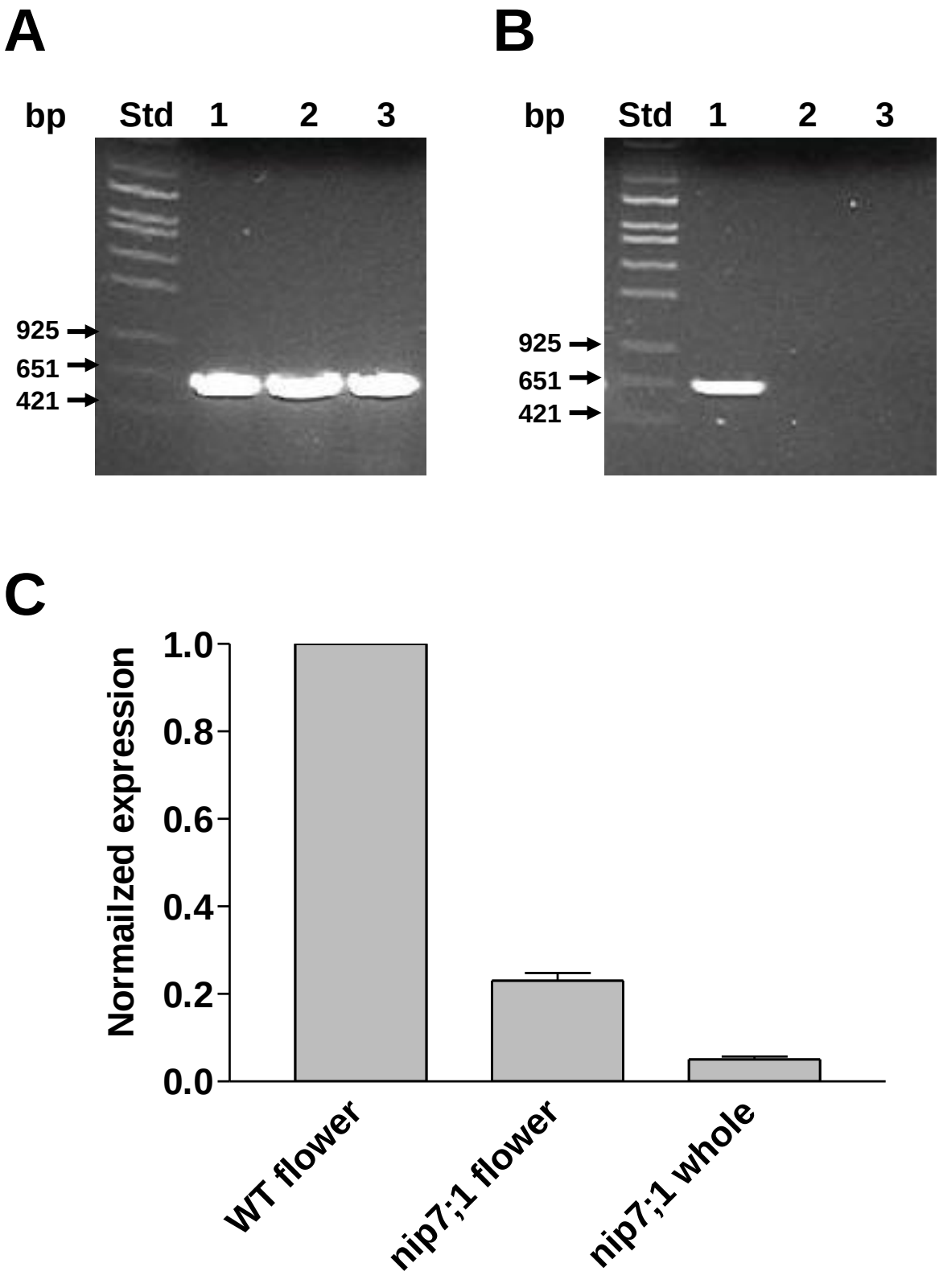
A
bp
Std
1
2
3
925
651
421
B
bp
Std
1
2
3
925
651
421
C
Normailzed expression
1.0
0.8
0.6
0.4
0.2
0.0
WT flower
nip7;1 flower
nip7;1 whole

did not affect the morphology or developmental properties of flowers (Fig. 3.44). Because *AtNIP7;1* appears to be expressed during floral stage 9 (Fig. 3. 40), especially in pollen granules in early floral buds (Fig. 3.41), the possibility that pollen physiology and growth maybe affected was tested. Further, since MIP subgroup II proteins often transport of metalloid compounds, and because boric acid is a critical plant nutrient (Takano et al., 2006; Ma et al., 2007; Bienert et al., 2008; Isayenkov and Maathuis, 2008; Tanaka et al., 2008; Yamaji et al., 2008), we investigated pollen tube growth under conditions of limiting boric acid. Pollen granule dusts were obtained from fully opened flower of WT and *nip7;1-1* and were germinated in a humidity chamber overnight at 22 °C on special pollen tube growth medium (PGM) in the presence or absence of 0.01% (w/v; 1.6 mM) boric acid. Pollen tube growth rate and size were measured by using the 'Image J' software distributed by the National Institutes of Health (NIH). The results show that the *atnip7;1-1* differs only slightly from wild type in pollen tube growth showing mildly reduced growth rate (P value = 0.0134) in the presence of boric acid (Fig. 3.45). However, the size of pollen granules were not significaltly different between *atnip7;1-1* and WT (P value = 0.9309, Fig. 3.45C). However, pollen tube growth rate of *atnip7;1-1* pollen was significantly reduced compared to wild type (P value = <0.0001) in media lacking boric acid (Fig. 3.46).

Taken together, the date suggest that *AtNIP7;1* is a floral specific gene that is selectively expressed in pollen granules. Knockout of the *AtNIP7;1* gene alters pollen germination in the absence of boric acid, which is one of the substrate of the NIP subgroup 2 family. Therefore, a functional property of this channel protein might be to transport boric acid or other uncharged metalloid compounds necessary for cell wall

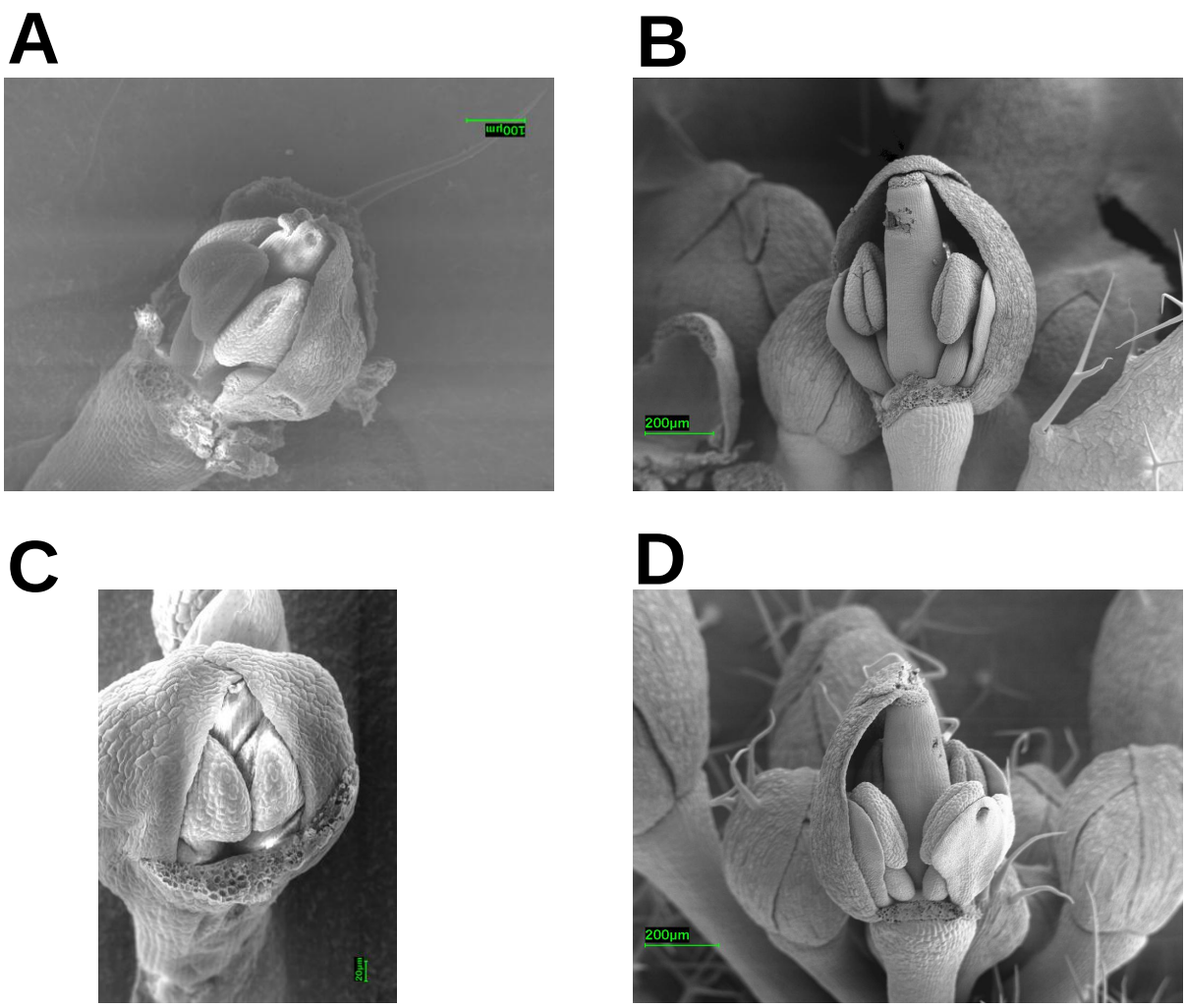

Figure 3.44. Morphological analysis of WT Col-0 and *nip7;1-1* inflorescences by scanning electron microscopy. Floral stage 9 and 10 images of inflorescences were selected under the scanning electron microscope (SEM). Each floral stage was determined according to the criteria of Smyth et al. (1990). **A.** Floral stage 9 of WT. Col-0. **B.** Floral stage 10 of WT. Col-0. **C.** Floral stage 9 of *nip7;1-1*. **D.** Floral stage 10 of *nip7;1-1*. The floral stage 9 and 10 observation of both WT. Col-0 flower and *nip7;1-1* flower was no difference in flower morphology. Size bars (200µm) are shown in white.

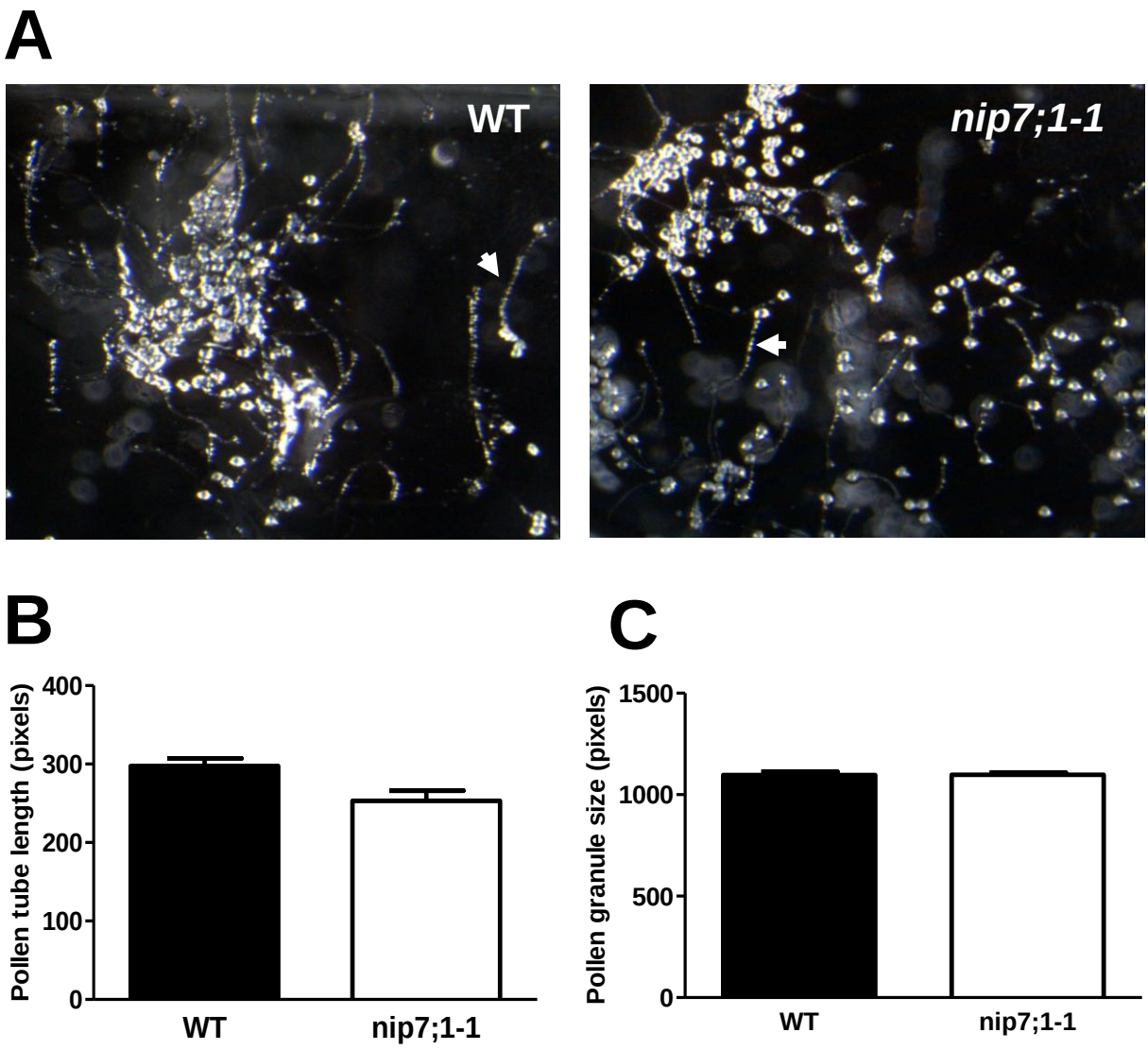

Figure 3.45. Pollen tube germination of WT and *nip7;1-1* pollen in the presence of boric acid. Pollen granules were obtained from fully open flower of WT and *nip7;1-1* and were germinated on pollen tube growth medium (PGM) in the presence of 1.6 mM boric acid as described in the **Materials and Methods**. Pollen tube growth rate was examined from microscope image by using "Image J" software. **A.** Pollen tube growth images of WT and *nip7;1-1* indicated (arrow heads). **B.** Measurement of pollen tube length. Pollen tube growth rate was slightly reduced in *atnip7;1-1* pollen (*p*- value = 0.0134). Error bars are SEM (*n*=10). **C.** Measurement of pollen granules size showing no alteration in size (P value = 0.9309). Error bars are SEM (*n*=20).

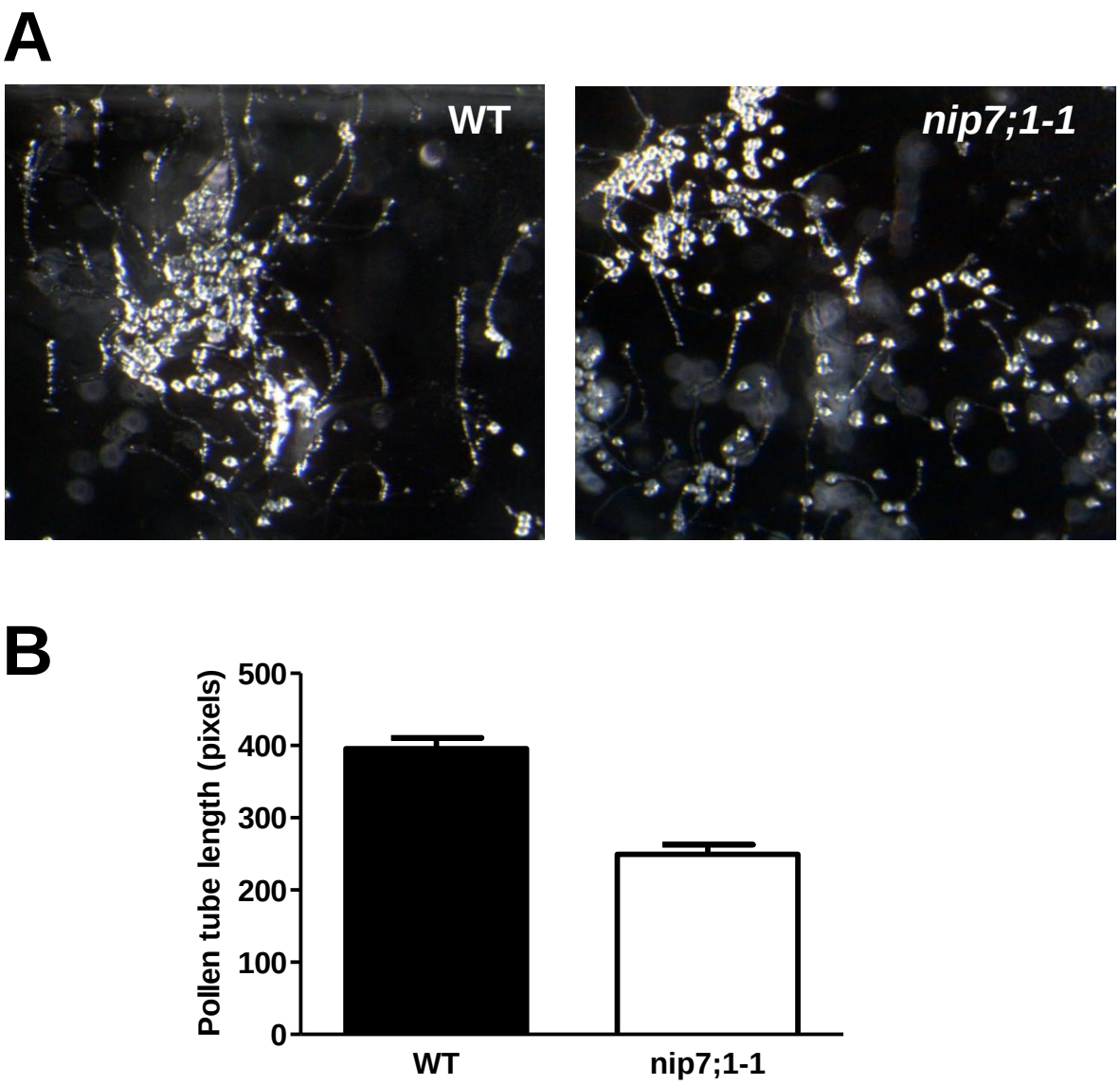

Figure 3.46. Pollen tube germination of WT and *nip7;1-1* in the absence of boric acid. Pollen granules were obtained from fully open flower of WT and *nip7;1-1* and were germinated as described in Figure 3.49. Size of pollen granules and germinated pollen tube length were measured in pixels by using 'Image J' software. **A.** Pollen tube growth images of WT and *nip7;1-1*. **B.** Measurement of pollen tube length of WT and *nip7;1-1* (P value = <0.0001). Error bars are SEM (*n*=10).

growth as has been observed with other NIP subgroup II proteins (Takano et al., 2006; Ma et al., 2007; Bienert et al., 2008; Isayenkov and Maathuis, 2008; Tanaka et al., 2008; Yamaji et al., 2008)

CHAPTER IV

DISCUSSION

The present thesis work with two representative Arabidopsis NIPs, NIP2;1 (NIP subgroup I) and NIP7;1 (NIP subgroup II) led us to new findings regarding the biological roles of this gene family in Arabidopsis. We found that *AtNIP2;1* is selectively expressed in root tissues under normoxic growth conditions, but its expression is rapidly and steeply induced along with other representative anaerobic polypeptide (ANP) genes in response to oxygen deprivation, suggesting that *AtNIP2;1* is an ANP gene. *Xenopus* oocytes expressing AtNIP2;1 showed unique lactic acid transport activity, and AtNIP2;1 may play a role in adaptation to low oxygen stress by serving as a lactic acid channel causing the cytosolic efflux of this fermentation end product.

In addition, we showed that *AtNIP7;1* is selectively expressed in flowers, especially in pollen grains during flower development. Interestingly, a knock-out (*atnip7;1-1*) line of *AtNIP7;1* showed pollen tube germination and growth defects in the absence of boric acid. These observations suggest that AtNIP7;1 might be involved in pollen development and that it might serve as a transporter involved in boric acid uptake similar to other NIP subgroup II proteins. These observations will be discussed in more detail in the following sections below.

Arabidopsis NIP2;1 is an anaerobic polypeptide

As mentioned previously, NIPs are in general expressed at a low level compared to other plant MIPs, but are often selectively expressed in certain types of tissues (Wallace et al., 2006). The present experiments with AtNIP2;1 support this contention. *AtNIP2;1* appears to be a root-specific transcript with basal levels of expression predominantly in the vascular tissues of mature roots as well as in the root tip. Cross section of roots shows that in the mature root, expression is limited to cells within the stele at the core of the root. Expression in leaves represents a minor component of the *AtNIP2;1* expression profile although low expression in vascular tissue in green leaves, and expression in etiolated leaves are observed. The major discovery however is the finding that *AtNIP2;1* gene expression is extremely sensitive to oxygen deprivation, showing a rapid and large increase in transcript levels in response to water logging or hypoxia .

Oxygen deficit resulting from stress such as flooding or water logging leads to severe depression of respiration resulting in reduced adenylate energy charge and the accumulation of toxic metabolites and cytosol acidification (Felle, 2005). Plants adapt to these conditions by employing several short and long term strategies including: 1. Increases in glycolytic flux to provide ATP (the Pasteur Effect); 2. the elevation of fermentation metabolism to regenerate NAD^+ for glycolysis; and 3. ultimately morphological developmental changes (e.g., aerenchyma, adventitious root formation, and root and stem elongation) to elevate O_2 levels in water-logged roots (Drew, 1997). The expression and translation of most genes and mRNAs are generally suppressed under hypoxic conditions due to the need to conserve energy. However a set of genes

encoding “Anaerobic Polypeptides” (ANPs) (Sachs et al., 1980) are induced, that include glycolytic and fermentation enzymes, as well as various signal transduction proteins, transcription factors and other genes involved in the adaptation response to anaerobiosis (Sachs et al., 1996; Klok et al., 2002). Therefore, the results from the present study suggest that AtNIP2;1 is an ANP in Arabidopsis.

The expression of *AtNIP2;1* appears to be regulated tightly with respect to the timing and location of the response. The induction of *AtNIP2;1* expression is extremely rapid in roots peaking between 1 (flooding) to 3 (anaerobiosis) hr after the initiation of stress. GUS staining shows enhanced expression within cells of the stele but also is apparent in cortical and epidermal cells as well as in lateral roots. The other interesting observation is that *AtNIP2;1* expression rapidly decreases to a reduced steady state level by 6 hr. This suggests that the hypoxic response is a coordinated and involves tight regulation of gene expression. This is supported by microarray data of the hypoxia time course in *Arabidopsis* which shows that gene sets induced by hypoxia can be organized into “clusters” that show defined kinetics and duration of induction (Klok et al., 2002; Liu et al., 2005). Another interesting observation is that while *AtNIP2;1* is considered a root-specific transcript, it is induced to a lesser extent in leaf tissues, mainly in the vascular tissue, with a delayed response (peaking after 24 hr of hypoxia), suggesting a secondary role in these tissues.

An interesting parallel is also observed between patterns of AtNIP2;1 expression in plants grown under unstressed “normoxic” conditions and previous observations of the oxygen content of various tissues. For example, root tissues that show high expression of *AtNIP2;1* are also the tissues which have low oxygen tension

even under growth in sufficient O_2. For example, the stele of mature root generally exhibits the metabolic symptoms of hypoxia, likely due to poor radial diffusion of O_2 (Ober and Sharp, 1996; van Dongen et al., 2003). Cellular localization of *AtNIP2;1* expression support this content showing that *AtNIP2;1* expression is limited in the stele under normoxia, indicating that *AtNIP2;1* expression may due to low oxygen stress because the stele tissues are naturally hypoxic due to restricted oxygen diffusion even under growth in the presence of normal atmospheric levels of O_2 (van Dongen et al., 2003). Similarly, the root tip also exhibits low O_2 tension (Ober and Sharp, 1996) presumably due to high metabolic rates and O_2 consumption. Overall, these observations support the results of flooding and anoxia treatments, and suggest that low oxygen concentration is the critical factor inducing AtNIP2;1 expression even in normoxic plants.

AtNIP2;1 is a lactic acid transporter

With respect to transport function, AtNIP2;1-injected oocytes show an extremely low osmotic water permeability. Consistent with this finding, previous light scattering work with microsomes from AtNIP2;1-transformed yeast show only modest increases (50%) in water permeability (Mizutani et al., 2006). These observations, along with the general finding that aquaporin activities in roots are suppressed by flooding stress (Tournaire-Roux et al., 2003), suggest that AtNIP2;1 likely does not function as an aquaporin *in vivo*. In addition, unlike soybean nodulin 26 and other NIP aquaglyceroporins (Dean et al., 1999; Guenther and Roberts, 2000; Weig and Jakob, 2000; Wallace and Roberts, 2005), AtNIP2;1 shows low permeability to glycerol. The

surprising finding is that the protein mediates the flux of lactic acid. Evidence that lactic acid is the likely endogenous substrate for AtNIP2;1 is also apparent from the analysis of *atnip2;1-1* knockout mutants which show increased accumulation of lactic acid in roots compared to wild type controls. A possible function of lactic acid transport emerges when one considers the metabolic changes associated with the onset of oxygen deprivation in roots.

Among the metabolic responses of plant roots to anaerobic stress is the rapid and transient induction of lactic acid fermentation followed by a switch to a sustained ethanolic fermentation (the Davies-Roberts hypothesis [Davies et al., 1974; Roberts et al., 1989; see Fig. 3.16]). This shift to the non-acid producing ethanolic fermentation pathway is proposed to prevent over-acidification of the cytosolic compartment by excess production of lactic acid (Roberts et al., 1984b; Roberts et al., 1984a). Consistent with this observation, lactic acid efflux is observed in hypoxia-challenged roots of certain plant species (Xia and Saglio, 1992; Rivoal and Hanson, 1993; Xia and Roberts, 1994). Moreover, this induction of lactic acid transport is correlated with an increased ability to survive anoxic conditions (Xia and Saglio, 1992; Xia and Roberts, 1994), and could aid in preventing the cytosolic acidification resulting from flooding induced-fermentation.

To decrease cytosolic acidity from lactic acid fermentation, the transport of a proton, either as lactic acid or co-transport of H^+ and lactate, is required. In animal cells engaged in lactic acid fermentation, this role is performed by a proton-coupled monocarboxylic acid transporter which is induced under hypoxic conditions (Halestrap and Price, 1999; Ullah et al., 2006). The mechanism for lactic acid efflux in oxygen-

deprived plant roots is less clear. The transport properties of AtNIP2;1 suggest that it has the potential properties needed for a lactic acid efflux channel. For example, the pH profile of transport strongly suggests that AtNIP2;1 transports only the uncharged protonated form of lactic acid. This is consistent with the general properties of MIPs as transporters of uncharged metabolites which are resistant to permeation by charged species (Agre et al., 2002). Thus, the efflux of lactate would only occur in conjunction with a proton, lowering the acidity of the cytosol in the process. In addition, the rapid time course of expression is consistent with the rapid onset of lactic acid fermentation and accompanying lactic acid release from hypoxic roots which is detectable within the first hour after oxygen deprivation in maize (Xia and Saglio, 1992).

One interesting consideration in regard to its potential transport function is the subcellular localization of AtNIP2;1. In previous work using C-terminal AtNIP2;1-green fluorescence protein fusions and transient expression analysis in Arabidopsis suspension cell cultures, Mizutani et al. (2006) showed predominant localization to an internal membrane compartment proposed to be the endoplasmic reticulum. In contrast, in the present work, using both transient expression in mesophyll protoplasts and transgenic Arabidopsis roots, an AtNIP 2;1 yellow fluorescence protein fusion appears to be localized to the surface of the cell, presumably the plasma membrane. However, similar to Mizutani et al. (2006), observations of fluorescence in internal membrane compartments was sometimes observed with mesophyll protoplasts (data not shown). It is noteworthy that some aquaporins, such as AQP2 in mammalian cells, can be observed both on internal membrane vesicles as well as the plasma membrane, with this localization being subject to regulation by posttranslational phosphorylation on

the C-terminal domain (Noda and Sasaki, 2006). Since AtNIP2;1, like nodulin 26 and certain other NIP I proteins, contains a conserved phosphorylation site within its C-terminal domain (Table 1.1), it will be of interest to determine whether phosphorylation plays a role in the regulation of its activity or in trafficking in planta. Since we have an antibody directed against AtNIP2;1, future work will allow the localization of native AtNIP2;1 under conditions of normoxia and anoxia to determine whether the protein is regulated by intracellular trafficking.

The transport properties of AtNIP2;1 are also noteworthy from a structural and functional perspective of the NIP transport family. As discussed in the **Introduction**, the pore properties and multifunctional transport signature of this subfamily of plant MIPs are unique (Wallace et al., 2006). Based on modeling, there are two general pore subfamilies of Arabidopsis NIPs: NIP I and NIP II (Wallace and Roberts, 2004). NIP I proteins are typified by soybean nodulin 26, and form aquaglyceroporins that transport glycerol as well as water (Rivers et al., 1997; Dean et al., 1999). With respect to pore determinant sequences, AtNIP2;1 resembles the nodulin 26-like NIP I pore group (Wallace and Roberts, 2004), showing the conserved ar/R selectivity sequence of this group. Nevertheless, the results of the present work show that AtNIP2;1 is clearly distinct from nodulin 26, not only in its ability to transport lactic acid instead of glycerol, but also in its unusually low permeability to water. Modeling results using existing crystal structure templates do not provide any apparent leads for this distinction. In this regard, it is important to realize that although the MIP family in general consists of a conserved “hourglass” fold and topology (Agre et al., 2002), each MIP has unique regulatory and transport properties. For example, the structural determination of

SoPIP2;1 from spinach reveals the importance of cytosolic loop and terminal regions in gating the transport through PIP aquaporins (Tornroth-Horsefield et al., 2006), and structures of mammalian aquaporins such as AQP0, which have low water permeability reveal other selectivity constrictions besides the classical NPA and aromatic-arginine pore selectivity regions (Gonen et al., 2004). Further structural analyses of AtNIP2;1 are needed to reveal the molecular basis for its distinct transport selectivity relative to the soybean nodulin 26 archetype.

Characterization of *AtNIP2;1*-promoter T-DNA insertional mutants: Normoxic conditions

Experiments with two T-DNA insertional mutants in the promoter of *AtNIP2;1* show that *AtNIP2;1* expression is affected by the position of T-DNA insertion, relative to the position of *cis*-acting promoter elements “Anaerobic Response Elements (ARE)”. One insertional mutant (*atnip2;1-1*) shows a lost ability to respond to oxygen deprivation because of disruption of all six AREs in the promoter region of *AtNIP2;1*. A second insertional mutant (*atnip2;1-2*) still responds to hypoxia but shows a reduced sensitivity because of disruption of four AREs by T-DNA insertion. Under normal normoxic growth conditions, both mutants grew and set seed normally but showed subtle changes in root morphology and growth. *atnip2;1* mutant plants grown on MS media with sucrose showed increased numbers of lateral roots as well as increased primary root length and mass.

The developmental regulation of lateral root formation is complex and is subject to regulation by a wide number of hormonal, metabolic, and environmental cues

including Carbon/Nitrogen nutrient ratio, Auxin:Cytokinin:Abscisic Acid ratios, and various abiotic stresses including drought, salinity, and nutrient deficiency (Casimiro et al., 2003; Malamy, 2005). This finding that *atnip2;1* mutants exhibit enhanced lateral root growth suggests that one or more of these developmental or environmental cues is altered. The only other property that is altered in *atnip2;1* plants is lactic acid levels which are elevated, which could also potentially alter cytosolic pH or serve as a metabolic signal.

To gain additional insight into other potential changes associated with the normoxic state in *atnip2;1-1* roots, we examined the transcriptional profile of the roots of *atnip2;1-1* and wild type plants grown vertically under LD conditions on MS agar/sucrose plates under normoxic conditions. Global transcript profiling by microarray shows that there are 54 genes that are significantly upregulated in *atnip2;1-1* roots compared to wild type roots under normoxic conditions. The majority of these genes (24) appear to be related to seed or late embryogenesis induced genes. As mentioned previously, seed development, particularly late seed development, is a naturally hypoxic state in Arabidopsis (Porterfield et al., 1999). Therefore it is possible that knockout of *AtNIP2;1* and accumulation of lactic acid may simulate a hypoxic state in normoxic *atnip2;1-1* roots. The top two most highly upregulated genes encode the 12S seed storage proteins (SSP) CRA1 (cruciferina) and CRU 3 (cruciferin 3) which are legumin-type globulins (Sjodahl et al., 1991). These types of SSPs are selectively expressed during late embryogenesis (Pang et al., 1988). In addition, proteomics studies showed that SSPs are also accumulated during early seedling germination states (Gruis et al., 2002; Li et al., 2007). Abscisic acid (ABA) accumulation plays a critical role of

regulation of SSPs in expression (Pang et al., 1988). The accumulation of these transcripts in *atnip2;1-1* roots under normoxic conditions is unusual, and one possibility is that the knockout of *AtNIP2;1* may result in elevated ABA in roots. This is supported by the findings that are number of elevated transcripts in normoxic *atnip2;1-1* roots are ABA-inducible (Table 3.7). This observation makes sense since ABA promotes late seed development and seed dormancy (Zeevaart and Creelman, 1988).

The effects of hormones on lateral root primordia has been extensively studied, and it is clear that auxin is the key signal promoting lateral root formation and growth (Malamy, 2005). However, the role of ABA in the process is complex with both inhibitory and promoting effects observed. On one hand, ABA has been implicated as the endogenous hormone that controls the suppression and dormancy of lateral root meristem growth in response to nitrate and osmotic stress (Signora et al., 2001; Malamy, 2005). However work by Brady et al. (2003) with the ABA insensitive mutant (*abi3*) suggests that ABA is necessary for auxin induced lateral root formation. Whether the changes in *atnip2;1* root development are related to changes in hormone signaling or are due to other factors remains to be determined.

Characterization of *AtNIP2;1*-promoter T-DNA insertional mutants: Hypoxic conditions

A number of studies with ANP mutants (either with defective ANP expression or ANP overexpression) have been investigated in Arabidopsis (Dennis et al., 2000). For example, ADH1 null mutants (Jacobs et al., 1988) show poor survival to hypoxic stress, whereas ectopic overexpression of the fermentation enzymes ADH1 and PDC1

enhance survival to low O_2 stress (Ismond et al., 2003). Hunt et al. (2002) showed when the non symbiotic class 1 hemoglobin (*GLB1*) was overexpressed in Arabidopsis (*35S::GLB1*) under the control of strong CaMV 35S promoter, the plants showed better survival rates than WT plants after 48 hr hypoxic treatment.

Based on our model for AtNIP2;1 as a lactic acid efflux channel, and the proposal that prevention of cytosolic acidification maybe a critical factor in survival to hypoxic stress (Felle, 2005), we predicted that a knockout of this gene would result in: 1. increased lactic acid accumulation and possible cytosolic acidification of root tissues, and 2. decreased survival to hypoxic conditions compared to wild type plants. Whereas the first prediction appears to be supported (although the cellular localization of lactic acid and cytosolic pH were not measured), analysis of the survival of the two *atnip2;1* T-DNA insertional mutants under hypoxic conditions showed that surprisingly these mutants possess greater resistance to severe hypoxia compared to wild type plants. Pre-adaptation of *atnip2;1-1* and WT to brief hypoxic episode showed that both *atnip2;1-1* and WT acquire high resistance to severe hypoxia (100% survival). These findings are also consistent to previous studies showing that pre-adapted ADH1 null mutant plants to brief hypoxia show much greater survival to subsequent severe hypoxia stress (Ismond et al., 2003; Banti et al., 2008). These findings suggest that the pH stat model and the role of AtNIP2;1 shown in Fig. 3.16 may be overly simplified. Further, the nature of the “pre-adaptation” effect of mild hypoxia is not apparently due to increased production of fermentation enzymes. This is also supported by the recent results of Banti et al. (2008), and other adaptive effects need to be considered.

To gain insight into enhanced survival phenotype of *atnip2;1-1* under severe hypoxia, we carefully analyzed transcripts which are significantly upregulated only in *atnip2;1-1* roots. Although most transcripts are present in both hypoxic *atnip2;1-1* roots and hypoxic WT roots, 14 unique genes show upregulation (> 3-fold) in hypoxic *atnip2;1-1* roots. It is notable that among the 14 genes, two members of heat shock protein family (HSP21, DNAJ proteins) show the greatest stimulation and that a third upregulated gene is a transcription factor involved in mediating the heat shock response (At-HSFA7B). This observation is particularly interesting because several hypoxic microarray studies showed that a number of genes encoding heat shock proteins are significantly upregulated during anaerobiosis (Klok et al., 2002; Branco-Price et al., 2005; Liu et al., 2005; Loreti et al., 2005; Baena-Gonzalez et al., 2007). A possible functional role for heat shock proteins comes from recent work by Banti et al. (2008) showing that heat acclimation provides cross tolerance to anoxia stress in Arabidopsis. They showed that a brief pre-exposure to heat shock conditions results in the same effect as hypoxia pre-adaptation with 100% of the heat pre-treated seedlings surviving subsequent severe anoxia shock. This protection was linked to the induction of heat shock protein including *HSP25.3-P* and *HSP70* (Loreti et al., 2005; Banti et al., 2008). A model for heat shock proteins as chaperones to prevent oxidative damage from reactive oxygen species as a mechanism for plant survival was presented (Banti et al., 2008).

Therefore, it is possible that the selective induction of heat shock-related genes in hypoxic *atnip2;1-1* roots could play role of protecting *atnip2;1-1* from severe low oxygen stress damage resulting in enhanced survival during anaerobiosis. In addition,

the finding that the gene encoding the ROS detoxifying peroxidase AtPER1 is elevated in *atnip2;1-1* roots suggests that prevention of ROS accumulation may be part of the increased resistance associated with *atnip2;1-1* plants.

The survival analysis of two T-DNA insertional mutants in response to anaerobic stress is also similar to the phenotype observed by Hunt et al. (2002) when the *GLB1* overexpression (*35S::GLB1*) Arabidopsis was subjected to hypoxic stress. Plants overexpressing the *GLB1* gene showed enhanced early growth rates and an increase in the number of later roots (Hunt et al., 2002). Although there are no differences in *GLB1* expression at 4 hr hypoxia in our microarray, we found that by Q-PCR analysis (Fig. 4.1), there is an increase in expression of the *GLB1* in *atnip2;1-1* roots compared to wild type after 12 hr post hypoxic treatment which might result in enhanced early root development and survival.

Although, the reverse genetic approach and global transcripts analyses in the present study provide interesting findings and suggest new hypothesis for hypoxia adaptation, the exact relationship and mechanism of the *atnip2;1-1* phenotype and its relationship to cellular pH and lactic acid concentrations needs to be investigated further.

AtNIP7;1: A flower specific NIP II protein

As discussed in the **Introduction**, Arabidopsis has three genes, *AtNIP5;1, AtNIP6;1,* and *AtNIP7;1*, which are classified as NIP II proteins. Interestingly, these three genes show tissue-specific expression in Arabidopsis. For example, *AtNIP5;1*

shows root specific expression and is localized in the plasma membrane of root epidermal and cortical cells (Takano et al., 2006). Recent evidence shows that the

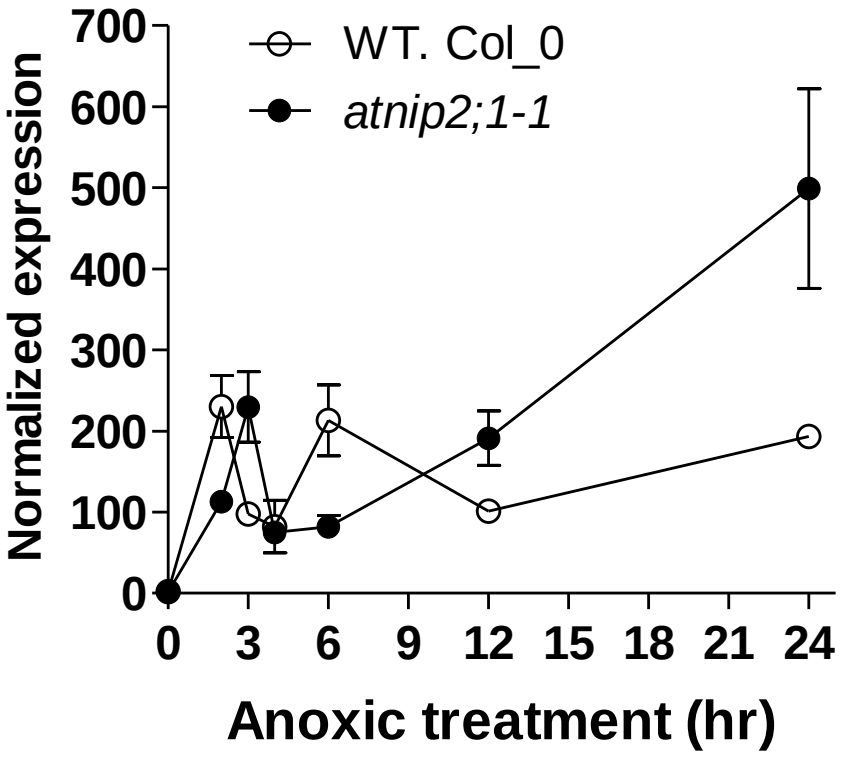

Figure 4.1. Analysis of expression of non-symbiotic hemoglobin (*GLB1*) in wild type and *atnip2;1-1* roots during hypoxia. Expression of *GLB1* was analysis using Q-PCR from 2-wk old WT (open circles) and *atnip2;1-1* (filled circles) plants during the onset of hypoxia. The ΔCt values of *GLB1* expression signal in the roots of WT plants under normoxia (0 hr time point) were used as a calibrator for ΔΔCt and $2^{-\Delta\Delta Ct}$ calculations. Error bars show the SEM of three to six biological replicates.

closely related gene product, AtNIP6;1, is expressed selectively in nodal regions of stems particularly in phloem companion cells (Tanaka et al., 2008). The present work shows that *AtNIP7;1* represents a flower-specific transcript that is particularly prevalent in floral stage 9 of Arabidopsis flower development and appears to be highly expressed in developing pollen grains.

In the case of AtNIP5;1 and AtNIP6;1, insight into their function came from the observation that their transcription is stimulated under boric acid limiting conditions (Takano et al., 2006; Tanaka et al., 2008). Boric acid is a critical plant nutrient that is required for normal plant growth and cell wall biosynthesis (Dell and Huang, 1997; O'Neill et al., 2004; Takano et al., 2008). Boric acid is a weak Lewis acid that exists in an uncharged form ($B(OH)_3$, pKa = 9.3) at physiological pH. Boric acid is incorporated into the rhamnogalacturonan II (RGII) cell wall pectin polysaccharide where it serves to dimerize RGII monomeric units through borate diester linkage between D-apiose saccharide units. This is needed for the assembly of the pectic network of the primary cell wall (O'Neill et al., 2004). Boron deficiencies result in defective cell wall formation and decreased cell expansion and developmental defects (Dell and Huang, 1997).

Expression of AtNIP5;1 and AtNIP6;1 in *Xenopus* oocytes and analysis of their transport activities show that they transport boric acid (Takano et al., 2006; Tanaka et al., 2008). Initial attempts to determine whether AtNIP7;1 is also a boric acid/metalloid transporter by using a similar approach was negative, even through the protein appeared to be folded and trafficked to the oocyte plasma membrane (Choi and Roberts, unpublished observations). However, more recently modeling of AtNIP7;1 by homology modeling showed an unusual tyrosine substitution that is found within the

proposed pore pathway. Substitution of this residue with a cysteine (typical of AtNIP5;1 and AtNIP6;1) for this tyrosine in AtNIP7;1 resulted in the recovery of boric acid transport activity (Li, Wallace and Roberts, unpublished results). One potential model is that boric acid transport in AtNIP7;1 is gated by the tyrosine side chain, and may be regulated by phosphorylation similar to other MIPs (Hedfalk et al., 2006). We have found that the C-terminus of AtNIP7;1 is phosphorylated *in vitro* by Arabidopsis MAP kinase (Wallace et al., 2006), and it will be interesting to see if NIP7;1 is regulated by this enzyme.

Other evidence for AtNIP7;1 transport of metalloid compounds comes from genetic evidence from yeast complementation and selection analyses (Bienert et al., 2008). These analyses are biological in nature and are based on the ability of various NIPs to sensitize yeast to the effects of toxic metalloids such as arsenous acid ($As^{III}(OH)_3$) and antimonous acid ($Sb^{III}(OH)_3$). The study of metalloid transport analysis using a yeast expression system shows that the NIP II proteins AtNIP5;1 and AtNIP6;1 from Arabidopsis, OsNIP2;1 and OsNIP3;2 from rice, and LjNIP5;1 and LjNIP6;1 from *Lotus japonicus* are bi-directional transporters of As(III), a metalloid compound that is similar to boric acid (Bienert et al., 2008). AtNIP7;1, a member of NIP subgroup II from Arabidopsis, also shows transport of metalloids but shows selectivity of SbIII over AsIII (Bienert et al., 2008). All of these metalloid compounds ($As(OH)_3$, $Sb(OH)_3$, and $B(OH)_3$) show a similar chemistry and have similar van der Waal's volumes, and the reason for these discrepancies from the yeast data remain unclear. A detailed biophysical analysis of the transport properties of AtNIP7;1 will be needed to determine more carefully the metalloid selectivity of this protein.

In the case of both AtNIP5;1 (Takano et al., 2006) and AtNIP6;1 (Tanaka et al., 2008), the effects of T-DNA insertion knockouts on plant growth have been documented. Similar to the AtNIP7;1 knockout characterized in this work, knockouts of AtNIP5;1 and AtNIP6;1 show no phenotypes under normal growth conditions. However, under conditions of limiting boron conditions, both AtNIP5;1 and AtNIP6;1 T-DNA knockouts show severe developmental phenotypes. In the case of AtNIP5;1, under boron limiting conditions (0.1 µM boric acid), both root and shoot growth were stunted and cell expansion was inhibited (Takano et al., 2006). In case of AtNIP6;1 plants, growth under limiting boric acid conditions showed preferential stunting of young leaves (Tanaka et al., 2008), which have been shown to be particularly sensitive to boric acid-limiting conditions (Dell and Huang, 1997). Interestingly, AtNIP5;1 and AtNIP6;1 plants show no developmental effects under growth in sufficient boric acid conditions (100 µM). Under these conditions simple diffusion of boric acid is adequate to supply the plant with this nutrient, and the induction of facilitated pathways for boric acid accumulation becomes in necessary (Takano et al., 2008).

In the present work, we provide evidence that AtNIP7;1 may also show a boric acid-dependent phenotype. Both wild type and *atnip7;1-1* pollen grains show normal germination and pollen tube growth in the presence of normal boric acid conditions, but *atnip7;1-1* pollen grains show retarded growth in the absence of boric acid. Further work in necessary to determine whether *atnip7;1-1* plants show reproductive or flower developmental defects under limiting boric acid conditions.

LIST OF REFERENCES

Agre, P., Saboori, A.M., Asimos, A., and Smith, B.L. (1987). Purification and partial characterization of the Mr 30,000 integral membrane protein associated with the erythrocyte Rh(D) antigen. J Biol Chem **262,** 17497-17503.

Agre, P., Preston, G.M., Smith, B.L., Jung, J.S., Raina, S., Moon, C., Guggino, W.B., and Nielsen, S. (1993). Aquaporin CHIP: the archetypal molecular water channel. Am J Physiol **265,** F463-476.

Agre, P., King, L.S., Yasui, M., Guggino, W.B., Ottersen, O.P., Fujiyoshi, Y., Engel, A., and Nielsen, S. (2002). Aquaporin water channels--from atomic structure to clinical medicine. J Physiol **542,** 3-16.

Alexandersson, E., Fraysse, L., Sjovall-Larsen, S., Gustavsson, S., Fellert, M., Karlsson, M., Johanson, U., and Kjellbom, P. (2005). Whole gene family expression and drought stress regulation of aquaporins. Plant Mol Biol **59,** 469-484.

Anandalakshmi, R., Marathe, R., Ge, X., Herr, J.M., Jr., Mau, C., Mallory, A., Pruss, G., Bowman, L., and Vance, V.B. (2000). A calmodulin-related protein that suppresses posttranscriptional gene silencing in plants. Science **290,** 142-144.

Baena-Gonzalez, E., Rolland, F., Thevelein, J.M., and Sheen, J. (2007). A central integrator of transcription networks in plant stress and energy signalling. Nature **448,** 938-942.

Bansal, A., and Sankararamakrishnan, R. (2007). Homology modeling of major intrinsic proteins in rice, maize and Arabidopsis: comparative analysis of transmembrane helix association and aromatic/arginine selectivity filters. BMC Struct Biol **7,** 27.

Banti, V., Loreti, E., Novi, G., Santaniello, A., Alpi, A., and Perata, P. (2008). Heat acclimation and cross-tolerance against anoxia in Arabidopsis. Plant Cell Environ **31,** 1029-1037.

Benga, G. (2009). Water channel proteins (later called aquaporins) and relatives: past, present, and future. IUBMB Life **61,** 112-133.

Bergmeyer, H.U. (1974). Methods of enzymatic analysis. (Weinheim, New York: Verlag Chemie ; Academic Press).

Bienert, G.P., Moller, A.L., Kristiansen, K.A., Schulz, A., Moller, I.M., Schjoerring, J.K., and Jahn, T.P. (2007). Specific aquaporins facilitate the diffusion of hydrogen peroxide across membranes. J Biol Chem **282,** 1183-1192.

Bienert, G.P., Thorsen, M., Schussler, M.D., Nilsson, H.R., Wagner, A., Tamas, M.J., and Jahn, T.P. (2008). A subgroup of plant aquaporins facilitate the bi-directional diffusion of As(OH)3 and Sb(OH)3 across membranes. BMC Biol **6,** 26.

Bolstad, B.M., Irizarry, R.A., Astrand, M., and Speed, T.P. (2003). A comparison of normalization methods for high density oligonucleotide array data based on variance and bias. Bioinformatics **19,** 185-193.

Borgnia, M., Nielsen, S., Engel, A., and Agre, P. (1999a). Cellular and molecular biology of the aquaporin water channels. Annu Rev Biochem **68,** 425-458.

Borgnia, M.J., Kozono, D., Calamita, G., Maloney, P.C., and Agre, P. (1999b). Functional reconstitution and characterization of AqpZ, the *E. coli* water channel protein. J Mol Biol **291,** 1169-1179.

Bradford, M.M. (1976). A rapid and sensitive method for the quantitation of microgram quantities of protein utilizing the principle of protein-dye binding. Anal Biochem **72,** 248-254.

Branco-Price, C., Kawaguchi, R., Ferreira, R.B., and Bailey-Serres, J. (2005). Genome-wide analysis of transcript abundance and translation in Arabidopsis seedlings subjected to oxygen deprivation. Ann Bot (Lond) **96,** 647-660.

Calamita, G. (2000). The *Escherichia coli* aquaporin-Z water channel. Mol Microbiol **37,** 254-262.

Casimiro, I., Beeckman, T., Graham, N., Bhalerao, R., Zhang, H., Casero, P., Sandberg, G., and Bennett, M.J. (2003). Dissecting Arabidopsis lateral root development. Trends Plant Sci **8,** 165-171.

Catalano, C.M., Lane, W.S., and Sherrier, D.J. (2004). Biochemical characterization of symbiosome membrane proteins from Medicago truncatula root nodules. Electrophoresis **25,** 519-531.

Chaumont, F., Moshelion, M., and Daniels, M.J. (2005). Regulation of plant aquaporin activity. Biol Cell **97,** 749-764.

Chaumont, F., Barrieu, F., Herman, E.M., and Chrispeels, M.J. (1998). Characterization of a maize tonoplast aquaporin expressed in zones of cell division and elongation. Plant Physiol **117,** 1143-1152.

Chaumont, F., Barrieu, F., Jung, R., and Chrispeels, M.J. (2000). Plasma membrane intrinsic proteins from maize cluster in two sequence subgroups with differential aquaporin activity. Plant Physiol **122,** 1025-1034.

Chaumont, F., Barrieu, F., Wojcik, E., Chrispeels, M.J., and Jung, R. (2001). Aquaporins constitute a large and highly divergent protein family in maize. Plant Physiol **125,** 1206-1215.

Choi, W.G., and Roberts, D.M. (2007). Arabidopsis NIP2;1, a major intrinsic protein transporter of lactic acid induced by anoxic stress. J Biol Chem **282,** 24209-24218.

Ciavatta, V.T., Morillon, R., Pullman, G.S., Chrispeels, M.J., and Cairney, J. (2001). An aquaglyceroporin is abundantly expressed early in the development of the suspensor and the embryo proper of loblolly pine. Plant Physiol **127,** 1556-1567.

Clough, S.J., and Bent, A.F. (1998). Floral dip: a simplified method for *Agrobacterium*-mediated transformation of *Arabidopsis thaliana*. Plant J **16,** 735-743.

Cohen, B.E. (1975). The permeability of liposomes to nonelectrolytes. I. Activation energies for permeation. J Membr Biol **20,** 205-234.

Czechowski, T., Bari, R.P., Stitt, M., Scheible, W.R., and Udvardi, M.K. (2004). Real-time RT-PCR profiling of over 1400 Arabidopsis transcription factors: unprecedented sensitivity reveals novel root- and shoot-specific genes. Plant J **38,** 366-379.

Daniels, M.J., and Yeager, M. (2005). Phosphorylation of aquaporin PvTIP3;1 defined by mass spectrometry and molecular modeling. Biochemistry **44,** 14443-14454.

Danielson, J.A., and Johanson, U. (2008). Unexpected complexity of the aquaporin gene family in the moss *Physcomitrella patens*. BMC Plant Biol **8,** 45.

de Groot, B.L., Frigato, T., Helms, V., and Grubmuller, H. (2003). The mechanism of proton exclusion in the aquaporin-1 water channel. J Mol Biol **333,** 279-293.

Dean, R.M., Rivers, R.L., Zeidel, M.L., and Roberts, D.M. (1999). Purification and functional reconstitution of soybean nodulin 26. An aquaporin with water and glycerol transport properties. Biochemistry **38,** 347-353.

Deen, P.M., Verdijk, M.A., Knoers, N.V., Wieringa, B., Monnens, L.A., van Os, C.H., and van Oost, B.A. (1994). Requirement of human renal water channel aquaporin-2 for vasopressin-dependent concentration of urine. Science **264,** 92-95.

Dell, B., and Huang, L. (1997). Physiological response of plants to low boron. Plant Soil **193,** 103–120.

Dennis, E.S., Dolferus, R., Ellis, M., Rahman, M., Wu, Y., Hoeren, F.U., Grover, A., Ismond, K.P., Good, A.G., and Peacock, W.J. (2000). Molecular strategies for improving waterlogging tolerance in plants. J Exp Bot **51,** 89-97.

Dolferus, R., Jacobs, M., Peacock, W.J., and Dennis, E.S. (1994). Differential interactions of promoter elements in stress responses of the Arabidopsis Adh gene. Plant Physiol **105,** 1075-1087.

Drew, M.C. (1997). OXYGEN DEFICIENCY AND ROOT METABOLISM: Injury and Acclimation Under Hypoxia and Anoxia. Annu Rev Plant Physiol Plant Mol Biol **48,** 223-250.

Ellis, M.H., Dennis, E.S., and Peacock, W.J. (1999). Arabidopsis roots and shoots have different mechanisms for hypoxic stress tolerance. Plant Physiol **119,** 57-64.

Ellman, G.L. (1959). Tissue sulfhydryl groups. Arch Biochem Biophys **82,** 70-77.

Felle, H.H. (2005). pH regulation in anoxic plants. Ann Bot (Lond) **96,** 519-532.

Fortin, M.G., Morrison, N.A., and Verma, D.P. (1987). Nodulin-26, a peribacteroid membrane nodulin is expressed independently of the development of the peribacteroid compartment. Nucleic Acids Res **15,** 813-824.

Frisch, D.A., Harris-Haller, L.W., Yokubaitis, N.T., Thomas, T.L., Hardin, S.H., and Hall, T.C. (1995). Complete sequence of the binary vector Bin 19. Plant Mol Biol **27,** 405-409.

Fu, D., Libson, A., Miercke, L.J., Weitzman, C., Nollert, P., Krucinski, J., and Stroud, R.M. (2000). Structure of a glycerol-conducting channel and the basis for its selectivity. Science **290,** 481-486.

Gonen, T., Sliz, P., Kistler, J., Cheng, Y., and Walz, T. (2004). Aquaporin-0 membrane junctions reveal the structure of a closed water pore. Nature **429,** 193-197.

Gorin, M.B., Yancey, S.B., Cline, J., Revel, J.P., and Horwitz, J. (1984). The major intrinsic protein (MIP) of the bovine lens fiber membrane: characterization and structure based on cDNA cloning. Cell **39,** 49-59.

Gruis, D.F., Selinger, D.A., Curran, J.M., and Jung, R. (2002). Redundant proteolytic mechanisms process seed storage proteins in the absence of seed-type members of the vacuolar processing enzyme family of cysteine proteases. Plant Cell **14,** 2863-2882.

Guenther, J.F., and Roberts, D.M. (2000). Water-selective and multifunctional aquaporins from *Lotus japonicus* nodules. Planta **210,** 741-748.

Guenther, J.F., Chanmanivone, N., Galetovic, M.P., Wallace, I.S., Cobb, J.A., and Roberts, D.M. (2003). Phosphorylation of soybean nodulin 26 on serine 262

enhances water permeability and is regulated developmentally and by osmotic signals. Plant Cell **15,** 981-991.

Hajdukiewicz, P., Svab, Z., and Maliga, P. (1994). The small, versatile pPZP family of *Agrobacterium* binary vectors for plant transformation. Plant Mol Biol **25,** 989-994.

Halestrap, A.P., and Price, N.T. (1999). The proton-linked monocarboxylate transporter (MCT) family: structure, function and regulation. Biochem J 343 Pt **2,** 281-299.

Harries, W.E., Akhavan, D., Miercke, L.J., Khademi, S., and Stroud, R.M. (2004). The channel architecture of aquaporin 0 at a 2.2-A resolution. Proc Natl Acad Sci U S A **101,** 14045-14050.

Hedfalk, K., Tornroth-Horsefield, S., Nyblom, M., Johanson, U., Kjellbom, P., and Neutze, R. (2006). Aquaporin gating. Curr Opin Struct Biol **16,** 447-456.

Heller, K.B., Lin, E.C., and Wilson, T.H. (1980). Substrate specificity and transport properties of the glycerol facilitator of *Escherichia coli*. J Bacteriol **144,** 274-278.

Henzler, T., and Steudle, E. (1995). Reversible closing of water channels in *Chara* internodes provides evidence for a composite transport model of the plasma membrane. J Exp Bot **46,** 199-209.

Hirayama, T., Fujishige, N., Kunii, T., Nishimura, N., Iuchi, S., and Shinozaki, K. (2004). A novel ethanol-hypersensitive mutant of Arabidopsis. Plant Cell Physiol **45,** 703-711.

Hiroaki, Y., Tani, K., Kamegawa, A., Gyobu, N., Nishikawa, K., Suzuki, H., Walz, T., Sasaki, S., Mitsuoka, K., Kimura, K., Mizoguchi, A., and Fujiyoshi, Y. (2006).

Implications of the aquaporin-4 structure on array formation and cell adhesion. J Mol Biol **355,** 628-639.

Horsefield, R., Norden, K., Fellert, M., Backmark, A., Tornroth-Horsefield, S., Terwisscha van Scheltinga, A.C., Kvassman, J., Kjellbom, P., Johanson, U., and Neutze, R. (2008). High-resolution x-ray structure of human aquaporin 5. Proc Natl Acad Sci U S A **105,** 13327-13332.

Hunt, P.W., Klok, E.J., Trevaskis, B., Watts, R.A., Ellis, M.H., Peacock, W.J., and Dennis, E.S. (2002). Increased level of hemoglobin 1 enhances survival of hypoxic stress and promotes early growth in *Arabidopsis thaliana*. Proc Natl Acad Sci U S A **99,** 17197-17202.

Isayenkov, S.V., and Maathuis, F.J. (2008). The *Arabidopsis thaliana* aquaglyceroporin AtNIP7;1 is a pathway for arsenite uptake. FEBS Lett **582,** 1625-1628.

Ishikawa, F., Suga, S., Uemura, T., Sato, M.H., and Maeshima, M. (2005). Novel type aquaporin SIPs are mainly localized to the ER membrane and show cell-specific expression in Arabidopsis thaliana. FEBS Lett **579,** 5814-5820.

Ismond, K.P., Dolferus, R., de Pauw, M., Dennis, E.S., and Good, A.G. (2003). Enhanced low oxygen survival in Arabidopsis through increased metabolic flux in the fermentative pathway. Plant Physiol **132,** 1292-1302.

Jacobs, M., Dolferus, R., and Van den Bossche, D. (1988). Isolation and biochemical analysis of ethyl methanesulfonate-induced alcohol dehydrogenase null mutants of *Arabidopsis thaliana* (L.) Heynh. Biochem Genet **26,** 105-122.

Jap, B.K., and Li, H. (1995). Structure of the osmo-regulated H_2O-channel, AQP-CHIP, in projection at 3.5 Å resolution. J Mol Biol **251,** 413-420.

Jauh, G.Y., Fischer, A.M., Grimes, H.D., Ryan, C.A., Jr., and Rogers, J.C. (1998). delta-Tonoplast intrinsic protein defines unique plant vacuole functions. Proc Natl Acad Sci U S A **95,** 12995-12999.

Johanson, U., Karlsson, M., Johansson, I., Gustavsson, S., Sjovall, S., Fraysse, L., Weig, A.R., and Kjellbom, P. (2001). The complete set of genes encoding major intrinsic proteins in Arabidopsis provides a framework for a new nomenclature for major intrinsic proteins in plants. Plant Physiol **126,** 1358-1369.

Johansson, I., Karlsson, M., Johanson, U., Larsson, C., and Kjellbom, P. (2000). The role of aquaporins in cellular and whole plant water balance. Biochim Biophys Acta **1465,** 324-342.

Jung, J.S., Preston, G.M., Smith, B.L., Guggino, W.B., and Agre, P. (1994). Molecular structure of the water channel through aquaporin CHIP. The hourglass model. J Biol Chem **269,** 14648-14654.

King, L.S., Kozono, D., and Agre, P. (2004). From structure to disease: the evolving tale of aquaporin biology. Nat Rev Mol Cell Biol **5,** 687-698.

Klok, E.J., Wilson, I.W., Wilson, D., Chapman, S.C., Ewing, R.M., Somerville, S.C., Peacock, W.J., Dolferus, R., and Dennis, E.S. (2002). Expression profile analysis of the low-oxygen response in Arabidopsis root cultures. Plant Cell **14,** 2481-2494.

Lee, J.K., Kozono, D., Remis, J., Kitagawa, Y., Agre, P., and Stroud, R.M. (2005). Structural basis for conductance by the archaeal aquaporin AqpM at 1.68 Å. Proc Natl Acad Sci U S A **102,** 18932-18937.

Legocki, R.P., and Verma, D.P. (1980). Identification of "nodule-specific" host proteins (nodoulins) involved in the development of rhizobium-legume symbiosis. Cell **20,** 153-163.

Li, Q., Wang, B.C., Xu, Y., and Zhu, Y.X. (2007). Systematic studies of 12S seed storage protein accumulation and degradation patterns during Arabidopsis seed maturation and early seedling germination stages. J Biochem Mol Biol **40,** 373-381.

Liu, F., Vantoai, T., Moy, L.P., Bock, G., Linford, L.D., and Quackenbush, J. (2005). Global transcription profiling reveals comprehensive insights into hypoxic response in Arabidopsis. Plant Physiol **137,** 1115-1129.

Liu, L.H., Ludewig, U., Gassert, B., Frommer, W.B., and von Wiren, N. (2003). Urea transport by nitrogen-regulated tonoplast intrinsic proteins in Arabidopsis. Plant Physiol **133,** 1220-1228.

Loque, D., Ludewig, U., Yuan, L., and von Wiren, N. (2005). Tonoplast intrinsic proteins AtTIP2;1 and AtTIP2;3 facilitate NH_3 transport into the vacuole. Plant Physiol **137,** 671-680.

Loreti, E., Poggi, A., Novi, G., Alpi, A., and Perata, P. (2005). A genome-wide analysis of the effects of sucrose on gene expression in Arabidopsis seedlings under anoxia. Plant Physiol **137,** 1130-1138.

Ma, J.F., Yamaji, N., Mitani, N., Tamai, K., Konishi, S., Fujiwara, T., Katsuhara, M., and Yano, M. (2007). An efflux transporter of silicon in rice. Nature **448,** 209-212.

Malamy, J.E. (2005). Intrinsic and environmental response pathways that regulate root system architecture. Plant Cell Environ **28,** 67-77.

Maurel, C. (2007). Plant aquaporins: novel functions and regulation properties. FEBS Lett **581,** 2227-2236.

Maurel, C., and Chrispeels, M.J. (2001). Aquaporins. A molecular entry into plant water relations. Plant Physiol **125,** 135-138.

Maurel, C., Reizer, J., Schroeder, J.I., and Chrispeels, M.J. (1993). The vacuolar membrane protein gamma-TIP creates water specific channels in *Xenopus* oocytes. Embo J **12,** 2241-2247.

Maurel, C., Kado, R.T., Guern, J., and Chrispeels, M.J. (1995). Phosphorylation regulates the water channel activity of the seed-specific aquaporin alpha-TIP. Embo J **14,** 3028-3035.

Maurel, C., Verdoucq, L., Luu, D.T., and Santoni, V. (2008). Plant aquaporins: membrane channels with multiple integrated functions. Annu Rev Plant Biol **59,** 595-624.

Maurel, C., Reizer, J., Schroeder, J.I., Chrispeels, M.J., and Saier, M.H., Jr. (1994). Functional characterization of the *Escherichia coli* glycerol facilitator, GlpF, in Xenopus oocytes. J Biol Chem **269,** 11869-11872.

Mitra, A.K., Yeager, M., van Hoek, A.N., Wiener, M.C., and Verkman, A.S. (1994). Projection structure of the CHIP28 water channel in lipid bilayer membranes at 12-Å resolution. Biochemistry **33,** 12735-12740.

Mizutani, M., Watanabe, S., Nakagawa, T., and Maeshima, M. (2006). Aquaporin NIP2;1 is mainly localized to the ER membrane and shows root-specific accumulation in *Arabidopsis thaliana*. Plant Cell Physiol **47,** 1420-1426.

Mulders, S.M., Bichet, D.G., Rijss, J.P., Kamsteeg, E.J., Arthus, M.F., Lonergan, M., Fujiwara, M., Morgan, K., Leijendekker, R., van der Sluijs, P., van Os, C.H., and Deen, P.M. (1998). An aquaporin-2 water channel mutant which causes autosomal dominant nephrogenic diabetes insipidus is retained in the Golgi complex. J Clin Invest **102,** 57-66.

Murata, K., Mitsuoka, K., Hirai, T., Walz, T., Agre, P., Heymann, J.B., Engel, A., and Fujiyoshi, Y. (2000). Structural determinants of water permeation through aquaporin-1. Nature **407,** 599-605.

Nemeth-Cahalan, K.L., and Hall, J.E. (2000). pH and calcium regulate the water permeability of aquaporin 0. J Biol Chem **275,** 6777-6782.

Niemietz, C.M., and Tyerman, S.D. (1997). Characterization of Water Channels in Wheat Root Membrane Vesicles. Plant Physiol **115,** 561-567.

Niemietz, C.M., and Tyerman, S.D. (2000). Channel-mediated permeation of ammonia gas through the peribacteroid membrane of soybean nodules. FEBS Lett **465,** 110-114.

Noda, Y., and Sasaki, S. (2006). Regulation of aquaporin-2 trafficking and its binding protein complex. Biochim Biophys Acta **1758,** 1117-1125.

O'Neill, M.A., Ishii, T., Albersheim, P., and Darvill, A.G. (2004). Rhamnogalacturonan II: structure and function of a borate cross-linked cell wall pectic polysaccharide. Annu Rev Plant Biol **55,** 109-139.

Ober, E.S., and Sharp, R.E. (1996). A microsensor for direct measurement of O_2 partial pressure within plant tissues. J Exp Bot **47,** 447–454.

Olive, M.R., Walker, J.C., Singh, K., Dennis, E.S., and Peacock, W.J. (1990). Functional properties of the anaerobic responsive element of the maize Adh1 gene. Plant Mol Biol **15,** 593-604.

Pang, P.P., Pruitt, R.E., and Meyerowitz, E.M. (1988). Molecular cloning, genomic organization, expression and evolution of 12S seed storage protein genes of *Arabidopsis thaliana*. Plant Mol Biol **11,** 805-820.

Pfaffl, M.W. (2001). A new mathematical model for relative quantification in real-time RT-PCR. Nucleic Acids Res **29,** e45.

Porterfield, D.M., Kuang, A., Smith, P.J., Crispi, M.L., and Musgrave, M.E. (1999). Oxygen-depleted zones inside reproductive structures of *Brassicaceae*: implications for oxygen control of seed development. Can J Bot **77,** 1439-1446.

Preston, G.M., and Agre, P. (1991). Isolation of the cDNA for erythrocyte integral membrane protein of 28 kilodaltons: member of an ancient channel family. Proc Natl Acad Sci U S A **88,** 11110-11114.

Preston, G.M., Carroll, T.P., Guggino, W.B., and Agre, P. (1992). Appearance of water channels in Xenopus oocytes expressing red cell CHIP28 protein. Science **256,** 385-387.

Preston, G.M., Jung, J.S., Guggino, W.B., and Agre, P. (1993). The mercury-sensitive residue at cysteine 189 in the CHIP28 water channel. J Biol Chem **268,** 17-20.

Preston, G.M., Jung, J.S., Guggino, W.B., and Agre, P. (1994). Membrane topology of aquaporin CHIP. Analysis of functional epitope-scanning mutants by vectorial proteolysis. J Biol Chem **269,** 1668-1673.

Quigley, F., Rosenberg, J.M., Shachar-Hill, Y., and Bohnert, H.J. (2002). From genome to function: the Arabidopsis aquaporins. Genome Biol **3,** RESEARCH0001.

Reizer, J., Reizer, A., and Saier, M.H., Jr. (1993). The MIP family of integral membrane channel proteins: sequence comparisons, evolutionary relationships, reconstructed pathway of evolution, and proposed functional differentiation of the two repeated halves of the proteins. Crit Rev Biochem Mol Biol **28,** 235-257.

Rivers, R.L., Dean, R.M., Chandy, G., Hall, J.E., Roberts, D.M., and Zeidel, M.L. (1997). Functional analysis of nodulin 26, an aquaporin in soybean root nodule symbiosomes. J Biol Chem **272,** 16256-16261.

Rivoal, J., and Hanson, A.D. (1993). Evidence for a large and sustained glycolytic flux to lactate in anoxic roots of some members of the halophytic genus Limonium. Plant Physiol **101,** 553-560.

Roberts, J.K., Callis, J., Wemmer, D., Walbot, V., and Jardetzky, O. (1984a). Mechanisms of cytoplasmic pH regulation in hypoxic maize root tips and its role in survival under hypoxia. Proc Natl Acad Sci U S A **81,** 3379-3383.

Roberts, J.K., Callis, J., Jardetzky, O., Walbot, V., and Freeling, M. (1984b). Cytoplasmic acidosis as a determinant of flooding intolerance in plants. Proc Natl Acad Sci U S A **81,** 6029-6033.

Rojek, A., Praetorius, J., Frokiaer, J., Nielsen, S., and Fenton, R.A. (2008). A current view of the mammalian aquaglyceroporins. Annu Rev Physiol **70,** 301-327.

Saboori, A.M., Smith, B.L., and Agre, P. (1988). Polymorphism in the Mr 32,000 Rh protein purified from Rh(D)-positive and -negative erythrocytes. Proc Natl Acad Sci U S A **85,** 4042-4045.

Sachs, M.M., Freeling, M., and Okimoto, R. (1980). The anaerobic proteins of maize. Cell **20,** 761-767.

Saito, C., Ueda, T., Abe, H., Wada, Y., Kuroiwa, T., Hisada, A., Furuya, M., and Nakano, A. (2002). A complex and mobile structure forms a distinct subregion within the continuous vacuolar membrane in young cotyledons of Arabidopsis. Plant J **29,** 245-255.

Sakurai, J., Ishikawa, F., Yamaguchi, T., Uemura, M., and Maeshima, M. (2005). Identification of 33 rice aquaporin genes and analysis of their expression and function. Plant Cell Physiol **46,** 1568-1577.

Sambrook, J., and Russell, W.D. (2001). Molecular cloning; A Laboratory Manual Third Edition.

Sandal, N.N., and Marcker, K.A. (1988). Soybean nodulin 26 is homologous to the major intrinsic protein of the bovine lens fiber membrane. Nucleic Acids Res **16,** 9347.

Schmittgen, T.D., and Livak, K.J. (2008). Analyzing real-time PCR data by the comparative C(T) method. Nat Protoc **3,** 1101-1108.

Schuurmans, J.A., van Dongen, J.T., Rutjens, B.P., Boonman, A., Pieterse, C.M., and Borstlap, A.C. (2003). Members of the aquaporin family in the developing pea seed coat include representatives of the PIP, TIP, and NIP subfamilies. Plant Mol Biol **53,** 633-645.

Sheen, J. (1995). Methods for mesophyll and bundle sheath cell separation. Methods Cell Biol **49,** 305-314.

Shiels, A., Kent, N.A., McHale, M., and Bangham, J.A. (1988). Homology of MIP26 to Nod26. Nucleic Acids Res **16,** 9348.

Signora, L., De Smet, I., Foyer, C.H., and Zhang, H. (2001). ABA plays a central role in mediating the regulatory effects of nitrate on root branching in Arabidopsis. Plant J **28,** 655-662.

Sjodahl, S., Rodin, J., and Rask, L. (1991). Characterization of the 12S globulin complex of Brassica napus. Evolutionary relationship to other 11-12S storage globulins. Eur J Biochem **196,** 617-621.

Smith, B.L., and Agre, P. (1991). Erythrocyte Mr 28,000 transmembrane protein exists as a multisubunit oligomer similar to channel proteins. J Biol Chem **266,** 6407-6415.

Sorani, M.D., Manley, G.T., and Giacomini, K.M. (2008). Genetic variation in human aquaporins and effects on phenotypes of water homeostasis. Hum Mutat **29,** 1108-1117.

Subramanian, C., Kim, B.H., Lyssenko, N.N., Xu, X., Johnson, C.H., and von Arnim, A.G. (2004). The Arabidopsis repressor of light signaling, COP1, is regulated by nuclear exclusion: mutational analysis by bioluminescence resonance energy transfer. Proc Natl Acad Sci U S A **101,** 6798-6802.

Sui, H., Han, B.G., Lee, J.K., Walian, P., and Jap, B.K. (2001). Structural basis of water-specific transport through the AQP1 water channel. Nature **414,** 872-878.

Sweet, G., Gandor, C., Voegele, R., Wittekindt, N., Beuerle, J., Truniger, V., Lin, E.C., and Boos, W. (1990). Glycerol facilitator of *Escherichia coli*: cloning of glpF and identification of the glpF product. J Bacteriol **172,** 424-430.

Tajkhorshid, E., Nollert, P., Jensen, M.O., Miercke, L.J., O'Connell, J., Stroud, R.M., and Schulten, K. (2002). Control of the selectivity of the aquaporin water channel family by global orientational tuning. Science **296,** 525-530.

Takano, J., Miwa, K., and Fujiwara, T. (2008). Boron transport mechanisms: collaboration of channels and transporters. Trends Plant Sci **13,** 451-457.

Takano, J., Wada, M., Ludewig, U., Schaaf, G., von Wiren, N., and Fujiwara, T. (2006). The Arabidopsis major intrinsic protein NIP5;1 is essential for efficient boron uptake and plant development under boron limitation. Plant Cell **18,** 1498-1509.

Tanaka, M., Wallace, I.S., Takano, J., Roberts, D.M., and Fujiwara, T. (2008). NIP6;1 is a boric acid channel for preferential transport of boron to growing shoot tissues in Arabidopsis. Plant Cell **20,** 2860-2875.

Thimm, O., Blasing, O., Gibon, Y., Nagel, A., Meyer, S., Kruger, P., Selbig, J., Muller, L.A., Rhee, S.Y., and Stitt, M. (2004). MAPMAN: a user-driven tool to display genomics data sets onto diagrams of metabolic pathways and other biological processes. Plant J **37,** 914-939.

Tornroth-Horsefield, S., Wang, Y., Hedfalk, K., Johanson, U., Karlsson, M., Tajkhorshid, E., Neutze, R., and Kjellbom, P. (2006). Structural mechanism of plant aquaporin gating. Nature **439,** 688-694.

Tournaire-Roux, C., Sutka, M., Javot, H., Gout, E., Gerbeau, P., Luu, D.T., Bligny, R., and Maurel, C. (2003). Cytosolic pH regulates root water transport during anoxic stress through gating of aquaporins. Nature **425,** 393-397.

Tyerman, S.D. (1999). Plant aquaporins: their molecular biology, biophysics and significance for plant water relations. J Exp Bot **50,** 1055-1071.

Ullah, M.S., Davies, A.J., and Halestrap, A.P. (2006). The plasma membrane lactate transporter MCT4, but not MCT1, is up-regulated by hypoxia through a HIF-1alpha-dependent mechanism. J Biol Chem **281,** 9030-9037.

Usadel, B., Nagel, A., Thimm, O., Redestig, H., Blaesing, O.E., Palacios-Rojas, N., Selbig, J., Hannemann, J., Piques, M.C., Steinhauser, D., Scheible, W.R., Gibon, Y., Morcuende, R., Weicht, D., Meyer, S., and Stitt, M. (2005). Extension of the visualization tool MapMan to allow statistical analysis of arrays, display of corresponding genes, and comparison with known responses. Plant Physiol **138,** 1195-1204.

van Dongen, J.T., Schurr, U., Pfister, M., and Geigenberger, P. (2003). Phloem metabolism and function have to cope with low internal oxygen. Plant Physiol **131,** 1529-1543.

Van Hoek, A.N., Luthjens, L.H., Hom, M.L., Van Os, C.H., and Dempster, J.A. (1992). A 30 kDa functional size for the erythrocyte water channel determined in situ by radiation inactivation. Biochem Biophys Res Commun **184,** 1331-1338.

van Hoek, A.N., Hom, M.L., Luthjens, L.H., de Jong, M.D., Dempster, J.A., and van Os, C.H. (1991). Functional unit of 30 kDa for proximal tubule water channels as revealed by radiation inactivation. J Biol Chem **266,** 16633-16635.

Van Toai, T.T., Saglio, P., Ricard, B., and Pradet, A. (1995). Developmental regulation of anoxic stress tolerance in maize. Plant Cell Environ **18,** 937–942.

Vokes, T. (1987). Water homeostasis. Annu Rev Nutr **7,** 383-406.

Walker, J.C., Howard, E.A., Dennis, E.S., and Peacock, W.J. (1987). DNA sequences required for anaerobic expression of the maize alcohol dehydrogenase 1 gene. Proc Natl Acad Sci U S A **84,** 6624-6628.

Wallace, I.S., and Roberts, D.M. (2004). Homology modeling of representative subfamilies of Arabidopsis major intrinsic proteins. Classification based on the aromatic/arginine selectivity filter. Plant Physiol **135,** 1059-1068.

Wallace, I.S., and Roberts, D.M. (2005). Distinct transport selectivity of two structural subclasses of the nodulin-like intrinsic protein family of plant aquaglyceroporin channels. Biochemistry **44,** 16826-16834.

Wallace, I.S., Choi, W.G., and Roberts, D.M. (2006). The structure, function and regulation of the nodulin 26-like intrinsic protein family of plant aquaglyceroporins. Biochim Biophys Acta **1758,** 1165-1175.

Wallace, I.S., Wills, D.M., Guenther, J.F., and Roberts, D.M. (2002). Functional selectivity for glycerol of the nodulin 26 subfamily of plant membrane intrinsic proteins. FEBS Lett **523,** 109-112.

Weaver, C.D., and Roberts, D.M. (1992). Determination of the site of phosphorylation of nodulin 26 by the calcium-dependent protein kinase from soybean nodules. Biochemistry **31,** 8954-8959.

Weaver, C.D., Crombie, B., Stacey, G., and Roberts, D.M. (1991). Calcium-Dependent Phosphorylation of Symbiosome Membrane Proteins from Nitrogen-Fixing Soybean Nodules : Evidence for Phosphorylation of Nodulin-26. Plant Physiol **95,** 222-227.

Weig, A., Deswarte, C., and Chrispeels, M.J. (1997). The major intrinsic protein family of Arabidopsis has 23 members that form three distinct groups with functional aquaporins in each group. Plant Physiol **114,** 1347-1357.

Weig, A.R., and Jakob, C. (2000). Functional identification of the glycerol permease activity of *Arabidopsis thaliana* NLM1 and NLM2 proteins by heterologous expression in *Saccharomyces cerevisiae*. FEBS Lett **481,** 293-298.

Xia, J.H., and Saglio, P.H. (1992). Lactic Acid Efflux as a Mechanism of Hypoxic Acclimation of Maize Root Tips to Anoxia. Plant Physiol **100,** 40-46.

Xia, J.H., and Roberts, J. (1994). Improved Cytoplasmic pH Regulation, Increased Lactate Efflux, and Reduced Cytoplasmic Lactate Levels Are Biochemical Traits Expressed in Root Tips of Whole Maize Seedlings Acclimated to a Low-Oxygen Environment. Plant Physiol **105,** 651-657.

Yamaji, N., Mitatni, N., and Ma, J.F. (2008). A transporter regulating silicon distribution in rice shoots. Plant Cell **20,** 1381-1389.

Yoo, S.D., Cho, Y.H., and Sheen, J. (2007). Arabidopsis mesophyll protoplasts: a versatile cell system for transient gene expression analysis. Nat Protoc **2,** 1565-1572.

Zampighi, G.A., Kreman, M., Boorer, K.J., Loo, D.D., Bezanilla, F., Chandy, G., Hall, J.E., and Wright, E.M. (1995). A method for determining the unitary functional capacity of cloned channels and transporters expressed in Xenopus laevis oocytes. J Membr Biol **148,** 65-78.

Zeevaart, J.A.D., and Creelman, R.A. (1988). Metabolism and physiology of abscisic acid. Annu Rev Plant Phys Plant Mol Biol **39,** 439-473.

Zelazny, E., Miecielica, U., Borst, J.W., Hemminga, M.A., and Chaumont, F. (2009). An N-terminal diacidic motif is required for the trafficking of maize aquaporins ZmPIP2;4 and ZmPIP2;5 to the plasma membrane. Plant J **57,** 346-355.

Zelazny, E., Borst, J.W., Muylaert, M., Batoko, H., Hemminga, M.A., and Chaumont, F. (2007). FRET imaging in living maize cells reveals that plasma membrane aquaporins interact to regulate their subcellular localization. Proc Natl Acad Sci U S A **104,** 12359-12364.

Zhang, R., van Hoek, A.N., Biwersi, J., and Verkman, A.S. (1993). A point mutation at cysteine 189 blocks the water permeability of rat kidney water channel CHIP28k. Biochemistry **32,** 2938-2941.

Zhang, R.B., Logee, K.A., and Verkman, A.S. (1990). Expression of mRNA coding for kidney and red cell water channels in Xenopus oocytes. J Biol Chem **265,** 15375-15378.

APPENDIX

Table A.1. List of transcripts showing > 2-fold increase only in WT root tissues under 4 hr hypoxia compared to normoxic WT

bin	# of genes	%	name
35	82	35.8	not assigned
29	28	12.2	protein
27	18	7.9	RNA
20	13	5.7	stress
26	13	5.7	misc
34	12	5.2	transport
30	12	5.2	signalling
33	8	3.5	development
17	6	2.6	hormone metabolism
28	6	2.6	DNA
31	5	2.2	cell
16	4	1.7	secondary metabolism
11	3	1.3	lipid metabolism
13	2	0.9	amino acid metabolism
32	2	0.9	micro RNA, natural antisense etc
9	2	0.9	mitochondrial electron transport / ATP synthesis
10	2	0.9	cell wall
19	2	0.9	tetrapyrrole synthesis
6	2	0.9	gluconeogenese/ glyoxylate cycle
1	2	0.9	PS
21	1	0.4	redox.regulation
5	1	0.4	fermentation
18	1	0.4	Co-factor and vitamine metabolism
23	1	0.4	nucleotide metabolism
3	1	0.4	minor CHO metabolism
7	1	0.4	OPP
2	1	0.4	major CHO metabolism

#	bin	AGI	Fold-Change	Description
1	34	AT2G29870 /// AT2G34390	723.87	(aNIP2;1/NLM4 (NOD26-LIKE INTRINSIC PROTEIN 2;1)
2	21	AT1G48130	8.13	ATPER1 (Arabidopsis thaliana 1-cysteine peroxiredoxin 1); antioxidant
3	6	AT3G21720	7.81	isocitrate lyase, putative
4	33	AT5G44120	6.75	CRA1 (CRUCIFERINA); nutrient reservoir Encodes a 12S seed storage protein
5	26	AT3G53160	4.10	UGT73C7 (UDP-glucosyl transferase 73C7)
6	27	AT2G43500	3.64	RWP-RK domain-containing protein
7	35	AT5G59510	3.50	DVL18/RTFL5 (ROTUNDIFOLIA LIKE 5)
8	17	AT3G02480	3.35	ABA-responsive protein-related
9	35	AT2G14560	3.29	similar to unknown protein AT1G33840.1
10	20	AT1G72070	3.25	DNAJ heat shock N-terminal domain-containing protein
11	34	AT5G19700	3.16	MATE efflux protein-related
12	17	AT1G17990 /// AT1G18020	3.11	2-oxophytodienoate reductase, putative
13	27	AT4G16680	3.02	RNA helicase, putative similar to MEE29 (maternal effect embryo arrest 29)
14	34	AT5G46040	2.99	proton-dependent oligopeptide transport (POT) family protein
15	35	AT5G64450	2.98	similar to unknown protein AT3G62200.1

16	35	AT1G79160	2.98	similar to unknown protein AT1G16500.1
17	26	AT2G15480	2.94	UGT73B5 (UDP-glucosyl transferase 73B5)
18	20	AT5G25910	2.94	disease resistance family protein putative disease resistance protein induced by chitin oligomers
19	27	AT3G01970 /// AT3G01980	2.86	WRKY45 (WRKY DNA-binding protein 45); transcription factor member of WRKY Transcription Factor
20	20	AT1G75830	2.82	LCR67/PDF1.1 (Low-molecular-weight cysteine-rich 67)
21	30	AT5G25930	2.79	leucine-rich repeat family protein / protein kinase family protein
22	35	AT4G27652	2.74	similar to unknown protein AT4G27657.1
23	29	AT3G12700	2.62	aspartyl protease family protein
24	35	AT3G11620	2.61	BAS1 similar to Os01g0958800
25	16	AT1G33030	2.61	O-methyltransferase family 2 protein similar to ATOMT1 (O-METHYLTRANSFERASE 1)
26	34	AT2G37920	2.60	EMB1513 (EMBRYO DEFECTIVE 1513); copper ion transporter
27	34	AT2G33820	2.59	mitochondrial substrate carrier family protein (BAC1) encodes a mitochondrial ornithine transporter which exports ornithine from the mitochondrion to the cytosol
28	29	AT5G03020	2.58	kelch repeat-containing F-box family protein
29	20	AT3G46730	2.57	disease resistance protein (CC-NBS class), putative
30	35	AT5G58960	2.52	GIL1 (GRAVITROPIC IN THE LIGHT) Mutant plants display impaired light-regulation of the hypocotyl randomization response
31	35	AT3G25210	2.52	pentatricopeptide (PPR) repeat-containing protein
32	27	AT4G17785	2.50	myb family transcription factor (MYB39)
33	27	AT5G17490	2.47	RGL3 (RGA-LIKE 3); transcription factor DELLA subfamily member involved in GA signal transduction
34	26	AT1G69930	2.47	ATGSTU11 (Arabidopsis thaliana Glutathione S-transferase (class tau) 11)
35	35	AT5G13590	2.46	similar to unnamed protein product; gene_id:MSH12.5
36	35	AT2G14160	2.45	nucleic acid binding similar to RNA-binding protein, putative AT2G21690.1
37	35	AT5G22555	2.43	unknown protein
38	33	AT4G22530	2.42	embryo-abundant protein-related
39	35	AT1G70700	2.38	similar to unknown protein AT1G48500.1
40	35	AT4G25070	2.37	similar to unknown protein AT3G48860.2
41	35	AT4G17130	2.37	NO MATCH
42	30	AT1G50300	2.36	zinc finger (Ran-binding) family protein / RNA recognition motif (RRM)-containing protein
43	35	AT5G56980	2.35	similar to unknown protein AT4G26130.1
44	17	AT4G19230	2.34	CYP707A1 (cytochrome P450, family 707, subfamily A, polypeptide 1); oxygen binding Encodes a protein with ABA 8'-hydroxylase activity, involved in ABA catabolism
45	35	AT4G25830	2.34	integral membrane family protein
46	35	AT1G16850	2.34	similar to unknown protein AT5G64820.1
47	35	AT4G33140	2.34	similar to tac7077 [Zea mays] AAV64220.1
48	20	AT4G15740	2.33	C2 domain-containing protein
49	35	AT3G03420	2.32	Ku70-binding family protein
50	29	AT1G71530	2.32	protein kinase family protein
51	32 and 33	AT2G33810	2.32	SPL3 (SQUAMOSA PROMOTER BINDING PROTEIN-LIKE 3)
52	35	AT3G61190	2.31	BAP1 (BON ASSOCIATION PROTEIN 1) Encodes a protein with a C2 domain that binds to BON1 in yeast two hybrid analyses
53	29	AT1G67470	2.31	protein kinase family protein similar to wall-associated kinase 1 AAY34780.1
54	10	AT2G47550	2.31	pectinesterase family protein
55	27	AT5G06080	2.31	LOB domain protein 33 / lateral organ boundaries domain protein 33 (LBD33)
56	35	AT3G03880	2.31	similar to unknown protein AT1G55340.1
57	33	AT4G00650	2.31	FRI (FRIGIDA) Encodes a major determinant of natural variation in Arabidopsis flowering time
58	20	AT1G63730	2.30	disease resistance protein (TIR-NBS-LRR class), putative
59	33	AT1G66660	2.29	seven in absentia (SINA) protein, putative
60	26	AT1G14550	2.28	anionic peroxidase, putative

61	29	AT1G21410	2.27	F-box family protein AtSKP2;1 is a homolog of human SKP2, the human F-box protein that recruits E2F1
62	35	AT1G25290	2.27	rhomboid family protein
63	35	AT4G36030	2.27	armadillo/beta-catenin repeat family protein
64	34	AT3G13320	2.27	CAX2 (CATION EXCHANGER 2); calcium:hydrogen antiporter low affinity calcium antiporter CAX2
65	35	AT4G11980	2.26	ATNUDT14 (Arabidopsis thaliana Nudix hydrolase homolog 14)
66	26	AT3G20020	2.26	protein arginine N-methyltransferase family protein
67	3	AT5G11920	2.26	ATCWINV6 (6-&1-FRUCTAN EXOHYDROLASE); hydrolase
68	35	AT4G33310	2.26	unknown protein
69	35	AT3G11390	2.25	DC1 domain-containing protein
70	29	AT1G17960	2.25	threonyl-tRNA synthetase, putative
71	35	AT1G08315	2.25	armadillo/beta-catenin repeat family protein
72	29	AT4G38940	2.24	kelch repeat-containing F-box family protein
73	29	AT3G23260	2.24	F-box family protein
74	29	AT5G59270	2.24	lectin protein kinase family protein
75	35	AT5G54090	2.23	DNA mismatch repair MutS family protein
76	35	AT5G15330	2.23	SPX (SYG1/Pho81/XPR1) domain-containing protein
77	35	AT4G34120	2.23	LEJ1 (LOSS OF THE TIMING OF ET AND JA BIOSYNTHESIS 1)
78	35	AT5G27760	2.23	hypoxia-responsive family protein
79	30	AT3G07520	2.23	ATGLR1.4 (Arabidopsis thaliana glutamate receptor 1.4) member of Putative ligand-gated ion channel subunit family Identical to Glutamate receptor 1.4 precursor (Ligand-gated ion channel 1.4) (GLR1.4)
80	35	AT3G16330	2.23	similar to unknown protein AT1G52140.1
81	30	AT1G51820	2.22	leucine-rich repeat protein kinase, putative
82	30	AT5G49770	2.22	leucine-rich repeat transmembrane protein kinase, putative
83	29	AT4G33160	2.22	ubiquitin-protein ligase Identical to F-box only protein 13 (FBX13) Q9SMZ3
84	35	AT1G68450	2.22	VQ motif-containing protein
85	35	AT4G15120	2.21	VQ motif-containing protein
86	17	AT5G08350	2.21	GRAM domain-containing protein / ABA-responsive protein-related
87	35	AT3G27570	2.21	similar to unknown protein AT5G40510.1
88	29	AT5G65600	2.20	legume lectin family protein / protein kinase family protein
89	34	AT2G24520	2.20	AHA5 (ARABIDOPSIS H(+)-ATPASE 5); ATPase Identical to ATPase 5
90	28	AT3G43690	2.20	copia-like retrotransposon family protein
91	27	AT3G01080	2.20	WRKY58 (WRKY DNA-binding protein 58); transcription factor member of WRKY Transcription Factor
92	27	AT4G38620	2.20	MYB4 (myb domain protein 4); transcription factor Encodes a R2R3 MYB protein which is involved in the response to UV-B
93	35	AT4G28703	2.19	similar to unknown protein AT3G04300.1
94	10 and 32	AT5G06860	2.19	PGIP1 (POLYGALACTURONASE INHIBITING PROTEIN 1)
95	26	AT1G02850	2.19	glycosyl hydrolase family 1 protein
96	35	AT2G26530	2.19	AR781 unknown function similar to calmodulin-binding protein AT2G15760.1
97	35	AT3G60410	2.19	similar to unknown protein AT1G25370.1
98	29	AT1G01540	2.19	protein kinase family protein
99	28	AT2G13840	2.19	PHP domain-containing protein similar to Os03g0192000 NP_001049236.1
100	29	AT3G06190	2.18	ATBPM2; protein binding
101	7	AT5G24410	2.18	glucosamine/galactosamine-6-phosphate isomerase-related
102	29	AT3G17280	2.17	F-box family protein
103	27	AT4G33450	2.17	AtMYB69 (myb domain protein 69); DNA binding / transcription factor Member of the R2R3 factor gene family
104	35	AT4G32630	2.17	similar to human Rev interacting-like protein-related AT4G13350.2
105	35	AT1G32920	2.17	similar to unknown protein AT1G32928.1
106	17	AT4G34000	2.17	ABF3/DPBF5 (ABSCISIC ACID RESPONSIVE ELEMENTS-BINDING FACTOR 3); DNA binding / protein binding / transcription factor/ transcriptional activator
107	34	AT1G76520	2.17	auxin efflux carrier family protein

108	2	AT1G43670	2.17	fructose-1,6-bisphosphatase, putative
109	28	AT1G18680	2.17	HNH endonuclease domain-containing protein
110	35	AT2G32900	2.16	ATZW10 homologous to Drosophila ZW10, a centromere/kinetochore protein involved in chromosome segregation
111	30	AT5G16900	2.16	leucine-rich repeat protein kinase, putative
112	16	AT3G59530	2.16	strictosidine synthase family protein
113	27	AT3G03750	2.16	SET domain-containing protein Identical to Histone-lysine N-methyltransferase SUVR3
114	35	AT1G59590	2.15	ZCF37 ZCF37 mRNA, complete cds similar to unknown protein AT1G10220.1
115	26	AT1G17170	2.15	ATGSTU24 (Arabidopsis thaliana Glutathione S-transferase (class tau) 24)
116	20	AT5G37380	2.15	DNAJ heat shock N-terminal domain-containing protein
117	1	AT1G45474	2.15	LHCA5 (Photosystem I light harvesting complex gene 5) Encodes a component of the light harvesting complex of photosystem I
118	1	AT1G08380	2.15	PSAO (photosystem I subunit O) Encodes subunit O of photosystem I
119	35	AT3G11290	2.15	similar to unknown protein AT3G11310.1
120	35	AT1G19020	2.14	similar to unknown protein AT3G48180.1
121	26	AT4G13180	2.14	short-chain dehydrogenase/reductase (SDR) family protein
122	34	AT2G16380	2.14	SEC14 cytosolic factor family protein / phosphoglyceride transfer family protein similar to transporterAT4G34580.1
123	35	AT1G05750	2.14	PDE247 (PIGMENT DEFECTIVE 247); binding similar to pentatricopeptide (PPR) repeat-containing protein AT2G20540.1
124	30	AT4G27280	2.14	calcium-binding EF hand family protein similar to PBP1 (PINOID-BINDING PROTEIN 1), calcium ion binding AT5G54490.1
125	9	---	2.14	cytochrome c oxidase subunit 2
126	35	AT5G25630	2.14	pentatricopeptide (PPR) repeat-containing protein similar to protein kinase family protein AT5G21222.1
127	16	AT5G07860	2.13	transferase family protein similar to AT5G07870.1
128	35	AT3G46810	2.13	DC1 domain-containing protein
129	35	AT4G40020	2.13	similar to unknown protein AT5G16730.1
130	31	AT5G56600	2.13	PFN3/PRF3 (PROFILIN 3); actin binding Encodes profilin3, a low-molecular weight, actin monomer-binding protein that regulates the organization of actin cytoskeleton
131	35	AT3G52570	2.13	similar to hydrolase, alpha/beta fold family protein AT4G10030.1
132	29	AT3G57190	2.12	peptide chain release factor, putative similar to HCF109 (HIGH CHLOROPHYLL FLUORESCENT 109), translation release factor AT5G36170.1
133	35	AT5G64190	2.12	similar to unknown protein AT2G40390.1
134	35	AT5G66810	2.12	similar to unknown protein AT1G61150.6
135	35	AT1G12970	2.12	leucine-rich repeat family protein
136	35	AT5G13310	2.11	similar to unknown protein AT5G13970.1
137	27	AT5G13330	2.11	RAP2.6L (related to AP2 6L); DNA binding / transcription factor encodes a member of the ERF (ethylene response factor) subfamily B-4 of ERF/AP2 transcription factor family
138	20	AT1G74180	2.11	leucine-rich repeat family protein
139	31	AT3G43210	2.11	TES (TETRASPORE); microtubule motor Required for cytokinesis in pollen
140	35	AT5G23340	2.11	protein binding similar to F-box family protein (FBL4) AT4G15475.1
141	35	AT5G19630	2.10	similar to Esterase/lipase/thioesterase ABE92731.1
142	29	AT5G01980	2.10	zinc finger (C3HC4-type RING finger) family protein
143	19	AT1G09940	2.10	HEMA2; glutamyl-tRNA reductase Encodes glutamyl-tRNA reductase
144	35	AT2G31150	2.10	NO MATCH
145	35	AT1G15330	2.10	CBS domain-containing protein
146	19	AT2G26540	2.10	HEMD; uroporphyrinogen-III synthase
147	33	AT3G54320	2.09	WRI1 (WRINKLED 1); DNA binding / transcription factor WRINKLED1 encodes transcription factor of the AP2/ERWEBP class
148	35	AT1G15900	2.09	similar to hypothetical protein BAD45781.1
149	17	AT5G15230	2.09	GASA4 (GAST1 PROTEIN HOMOLOG 4) gibberellin-regulated (GASA4) Identical to Gibberellin-regulated protein 4 precursor (GASA4) P46690;GB:O49593
150	29	AT2G38000	2.09	chaperone protein dnaJ-related
151	35	AT3G48020	2.09	similar to F-box family protein-related AT5G62860.1

152	16	AT5G42830	2.09	transferase family protein
153	35	AT4G10090	2.09	similar to unknown protein AAN64485.1
154	28	AT5G07460	2.09	PMSR2 (PEPTIDEMETHIONINE SULFOXIDE REDUCTASE 2); protein-methionine-S-oxide reductase ubiquitous enzyme that repairs oxidatively damaged proteins
155	27	AT1G60200	2.09	splicing factor PWI domain-containing protein / RNA recognition motif (RRM)-containing protein
156	31	AT3G33520	2.08	ATARP6; structural constituent of cytoskeleton Encodes ACTIN-RELATED PROTEIN6 (ARP6), a putative component of a chromatin-remodeling complex
157	29	AT4G17300	2.08	NS1 (OVULE ABORTION 8) Asparaginyl-tRNA synthetase protein involved in amino acid activation/protein synthesis
158	20	AT5G61560	2.08	protein kinase family protein
159	35	---	2.08	Identical to Hypothetical mitochondrial protein AtMg01180 (ORF111b) P92548
160	27	AT4G11880	2.08	AGL14 (AGAMOUS-LIKE 14); DNA binding / transcription factor
161	30	AT5G06740	2.08	lectin protein kinase family protein
162	20	AT1G59980	2.07	DNAJ heat shock N-terminal domain-containing protein
163	26	AT1G13100	2.07	CYP71B29 (cytochrome P450, family 71, subfamily B, polypeptide 29); oxygen binding putative cytochrome P450 Identical to Cytochrome P450 71B29 (EC 1.14.-.-) (CYP71B29) Q9SAE4
164	11	AT1G01710	2.07	acyl-CoA thioesterase family protein
165	29	AT4G05000	2.07	vacuolar protein sorting-associated protein 28 family protein
166	29	AT2G07675	2.07	similar to ribosomal protein S12 mitochondrial family protein AT2G07675.1
167	35	AT5G60680	2.06	similar to unknown protein AT3G45210.1
168	29	AT1G77000	2.06	ATSKP2;2 (ARABIDOPSIS HOMOLOG OF HOMOLOG OF HUMAN SKP2 2)
169	20	AT4G16860	2.06	RPP4 (RECOGNITION OF PERONOSPORA PARASITICA 4) Confers resistance to Peronospora parasitica
170	35	AT5G51130	2.06	similar to Os08g0540500 NP_001062384.1
171	35	AT5G38660	2.06	APE1 (ACCLIMATION OF PHOTOSYNTHESIS TO ENVIRONMENT) mutant has Altered acclimation responses
172	27	AT1G22190	2.06	AP2 domain-containing transcription factor
173	6	AT5G03860	2.06	malate synthase, putative Encodes a protein with malate synthase activity
174	34	AT2G04040	2.06	ATDTX1; antiporter/ multidrug efflux pump/ multidrug transporter/ transporter AtDTX1 (At2g04040)
175	13	AT2G35500	2.05	shikimate kinase-related
176	35	AT1G70180	2.05	sterile alpha motif (SAM) domain-containing protein
177	20	AT1G17250	2.05	leucine-rich repeat family protein
178	11	AT2G28630	2.05	beta-ketoacyl-CoA synthase family protein
179	35	---	2.05	Identical to Hypothetical mitochondrial protein AtMg01220 (ORF113) P92552
180	11	AT5G14180	2.05	lipase family protein
181	35	AT4G36500	2.05	similar to unknown protein AT2G18210.1
182	33	AT3G54150	2.05	embryo-abundant protein-related
183	31	AT1G80480	2.05	PTAC17 (PLASTID TRANSCRIPTIONALLY ACTIVE17) similar to PRLI-interacting factor L
184	29	AT5G02910	2.05	F-box family protein
185	35	AT1G12650	2.04	similar to PREDICTED: hypothetical protein [Strongylocentrotus purpuratus] XP_783665.2
186	35	AT1G51580	2.04	KH domain-containing protein
187	35	AT4G14820	2.04	pentatricopeptide (PPR) repeat-containing protein
188	26	AT5G61510	2.04	NADP-dependent oxidoreductase
189	9	AT2G07731	2.03	NADH dehydrogenase subunit 6 similar to cytochrome b, putative AT2G07718.1
190	29	AT4G15410	2.03	ATB' GAMMA (Arabidopsis thaliana serine/threonine protein phosphatase 2A 55 kDa regulatory subunit B prime gamma) B' regulatory subunit of PP2A (AtB'gamma) mRNA, complete Identical to UBA and UBX domain-containing protein At4g15410
191	29	AT3G45630	2.03	RNA recognition motif (RRM)-containing protein
192	23	AT3G10030	2.03	aspartate/glutamate/uridylate kinase family protein
193	35	AT5G49440	2.03	unknown protein
194	35	AT1G30540	2.03	ATPase, BadF/BadG/BcrA/BcrD-type family
195	30	AT4G04960	2.02	lectin protein kinase, putative

196	34	AT2G02020	2.02	proton-dependent oligopeptide transport (POT) family protein
197	35	AT2G38780	2.02	binding similar to IMP dehydrogenase/GMP reductase ABE88378.1
198	35	AT5G63620	2.02	oxidoreductase, zinc-binding dehydrogenase family protein
199	35	AT4G17540	2.02	similar to Os10g0563400 NP_001065401.1
200	31	AT1G15730	2.02	PRLI-interacting factor L, putative
201	27	AT5G38140	2.02	histone-like transcription factor (CBF/NF-Y) family protein
202	30	AT1G78010	2.02	tRNA modification GTPase, putative
203	20	AT5G40100	2.02	disease resistance protein (TIR-NBS-LRR class), putative similar to ATP binding / protein binding / transmembrane receptor AT1G72840.1
204	29	AT5G02800	2.02	protein kinase family protein
205	29	AT5G60710	2.02	zinc finger (C3HC4-type RING finger) family protein
206	28	AT4G08220	2.01	Mutator-like transposase family
207	28	AT3G18035	2.01	HON4; DNA binding A linker histone like protein similar to histone H1/H5 family protein AT1G48620.1
208	33	AT4G14110	2.01	COP9 (CONSTITUTIVE PHOTOMORPHOGENIC 9) Represses photomorphogenesis and induces skotomorphogenesis in the dark
209	5	AT5G17380	2.01	pyruvate decarboxylase family protein similar to CSR1 (CHLORSULFURON/IMIDAZOLINONE RESISTANT 1) AT3G48560.1
210	18	AT5G64300	2.01	ATGCH (Arabidopsis thaliana GTP cyclohydrolase II)
211	27	AT2G36080	2.01	DNA-binding protein, putative
212	26	AT3G17790	2.01	ATACP5 (acid phosphatase 5); acid phosphatase/ protein serine/threonine phosphatase
213	27	AT1G77080	2.01	
214	29	AT5G03470	2.01	ATB' ALPHA (PP2A, B' subunit, alpha isoform); protein phosphatase type 2A regulator Encodes B' regulatory subunit of PP2A (AtB'alpha)
215	35	AT2G45320	2.01	similar to conserved hypothetical protein ABE93197.1
216	35	AT3G18350	2.01	similar to unknown protein AT1G48840.1
217	35	AT4G28020	2.01	similar to Protein of unknown function UPF0066 ABE81280.1
218	30	AT1G70530	2.01	protein kinase family protein
219	27	AT5G63830	2.01	zinc finger (HIT type) family protein
220	26	AT4G15260	2.01	UDP-glucoronosyl/UDP-glucosyl transferase family protein
221	35	AT3G62920	2.01	similar to Os05g0371500 [Oryza sativa (japonica cultivar-group)] NP_001055356.1
222	35	AT3G54680	2.01	proteophosphoglycan-related
223	26	AT2G32030	2.00	GCN5-related N-acetyltransferase (GNAT) family protein
224	35	AT4G03410	2.00	peroxisomal membrane protein-related
225	13	AT2G24580	2.00	sarcosine oxidase family protein
226	30	AT5G58350	2.00	WNK4 (Arabidopsis WNK kinase 4); kinase Encodes a member of the WNK family (9 members in all) of protein kinases
227	29	AT3G17410	2.00	serine/threonine protein kinase, putative
228	34	AT1G02520 /// AT1G02530	2.00	PGP12 (P-GLYCOPROTEIN 12); ATPase, coupled to transmembrane movement of substances Identical to Multidrug resistance protein 16 (P-glycoprotein 12) (MDR16) Q9FWX8
229	35	AT3G57860	2.00	(UV-B-INSENSITIVE 4-LIKE); unknown protein Plant specific-protein of unknown function, shares 62% homology with UVI4 at aa level

Table A.2. List of transcripts showing > 2-fold increase only in *atnip2;1-1* root tissues under 4 hr hypoxia compared to normoxic *atnip2;1-1*

bin	# of genes	%	name
35	69	39.7	not assigned
29	33	19.0	protein
27	26	14.9	RNA
20	10	5.7	stress
30	9	5.2	signalling
26	5	2.9	misc
21	4	2.3	redox.regulation
34	4	2.3	transport
31	2	1.1	cell
17	2	1.1	hormone metabolism
33	2	1.1	development
32	1	0.6	micro RNA, natural antisense etc
10	1	0.6	cell wall
13	1	0.6	amino acid metabolism
1	1	0.6	PS
19	1	0.6	tetrapyrrole synthesis
3	1	0.6	minor CHO metabolism
9	1	0.6	mitochondrial electron transport / ATP synthesis
15	1	0.6	metal handling
16	1	0.6	secondary metabolism
11	1	0.6	lipid metabolism

#	bin	AGI	Fold-Change	Description
1	20	AT4G27670	22.19	HSP21 (HEAT SHOCK PROTEIN 21) chloroplast located small heat shock protein
2	20	AT1G71000	8.00	DNAJ heat shock N-terminal domain-containing protein
3	35	AT3G49130	7.49	RNA binding similar to SWAP (Suppressor-of-White-APricot)/surp domain-containing protein AT5G06520.1
4	35	AT3G63350	5.93	Similar to S locus F-box-related / SLF-related AT1G71320.1
5	29	AT1G17870	5.24	S2P-like putative metalloprotease, also contain transmembrane helices near their C-termini and many of them, five of seven, contain a conserved zinc-binding motif HEXXH. Homolog of EGY1
6	29	AT1G60190	4.83	Armadillo/beta-catenin repeat family protein / U-box domain-containing protein
7	35	AT5G19100	4.22	Extracellular dermal glycoprotein-related / EDGP-related
8	35	AT4G19980	3.67	Similar to Os06g0666800
9	20	AT2G20560	3.33	DNAJ heat shock family protein similar to DNAJ heat shock family protein AT4G28480.1
10	27	AT3G17609	3.28	HYH (HY5-HOMOLOG); DNA binding / transcription factor
11	35	AT3G56290	3.22	Similar to Os01g0823600
12	35	AT5G57345	3.15	Similar to unknown protein AT1G54520.1
13	35	AT1G66080	3.03	Similar to Hypothetical protein AAO06975.1
14	35	AT1G07860	3.02	Unknown protein
15	35	AT4G33930 /// AT4G34300	2.94	glycine-rich protein Encodes protein with 14.7% glycine residues, similar to auxin response factor 30 AT4G33930.1
16	35	AT3G56160	2.86	Bile acid:sodium symporter similar to bile acid:sodium symporter family protein TAIR:AT2G26900.1
17	26	AT2G29450	2.84	ATGSTU5 (Arabidopsis thaliana Glutathione S-transferase (class tau) 5)
18	20	AT5G37440 /// AT5G37750	2.76	Heat shock protein binding / unfolded protein binding similar to DNAJ heat shock N-terminal domain-containing protein AT5G37440.1

19	35	AT2G35450	2.71	hydrolase similar to Os04g0391900
20	27	AT5G02580	2.71	EMB2730 (EMBRYO DEFECTIVE 2730); RNA binding / ribonuclease
21	27	AT1G77640	2.69	AP2 domain-containing transcription factor, putative encodes a member of the DREB subfamily A-5 of ERF/AP2 transcription factor family
22	35	AT1G03620	2.64	phagocytosis and cell motility protein ELMO1-related
23	35	AT1G21350	2.63	electron carrier similar to hypothetical protein RB2501_11257
24	29	AT3G11240	2.62	arginine-tRNA-protein transferase
25	29	AT5G05220	2.62	inositol or phosphatidylinositol phosphatase/ phosphoric monoester hydrolase
26	29	AT4G39560	2.62	kelch repeat-containing F-box family protein
27	27	AT3G09370	2.58	MYB3R-3 (myb domain protein 3R-3); DNA binding / transcription factor putative c-myb-like transcription factor (MYB3R3) mRNA
28	27	AT2G37590	2.56	Dof-type zinc finger domain-containing protein Identical to Dof zinc finger protein DOF2.4 (AtDOF2.4)
29	27	AT3G15510	2.51	ATNAC2 (Arabidopsis thaliana NAC domain containing protein 2); transcription factor
30	35	AT5G66930	2.51	similar to Os12g0446700
31	35	AT1G56260	2.51	similar to hypothetical protein MtrDRAFT_AC144513g16v1
32	35	AT5G58770	2.48	dehydrodolichyl diphosphate synthase, putative / DEDOL-PP synthase
33	27	AT2G45050	2.48	zinc finger (GATA type) family protein
34	17	AT4G36110	2.46	auxin-responsive protein, putative
35	29	AT3G61210	2.45	serine/threonine protein kinase, putative
36	35	AT2G43160	2.45	epsin N-terminal homology (ENTH) domain-containing protein similar to (EPSIN3)
37	35	AT1G52870	2.43	peroxisomal membrane protein-related
38	27	AT1G75540	2.43	zinc finger (B-box type) family protein Identical to Putative salt tolerance-like protein At1g75540
39	26	AT4G19880	2.43	similar to Glutathione S-transferase
40	34	AT1G72660	2.42	developmentally regulated GTP-binding protein, putative similar to ATDRG1 (ARABIDOPSIS THALIANA DEVELOPMENTALLY REGULATED G-PROTEIN 1)
41	35	AT2G30480	2.39	similar to Os01g0167700
42	13	AT5G14760	2.39	AO (L-ASPARTATE OXIDASE); L-aspartate oxidase At5g14760 encodes for L-aspartate oxidase involved in the early steps of NAD biosynthesis
43	29	AT3G57470	2.39	peptidase M16 family protein / insulinase family protein
44	30	AT3G55020	2.38	RabGAP/TBC domain-containing protein
45	30	AT2G18750	2.37	calmodulin-binding protein
46	1	AT4G20130	2.37	PTAC14 (PLASTID TRANSCRIPTIONALLY ACTIVE14)
47	27	AT2G22630	2.37	AGL17 (AGAMOUS-LIKE 17); transcription factor encodes a root-specific MADS-box protein, expressed in the root
48	35	AT1G18380	2.35	similar to unknown protein similar to Ser/Thr protein kinase
49	20	AT5G18360	2.35	disease resistance protein (TIR-NBS-LRR class)
50	29	AT5G57630	2.32	CIPK21 (CBL-INTERACTING PROTEIN KINASE 21)
51	35	AT1G31540	2.32	NO MATCH
52	35	AT5G12050	2.32	similar to ATP-dependent DNA helicase, putative NP_702167.1
53	35	AT3G26990	2.31	similar to unknown protein AT5G10060.1
54	35	AT2G39080	2.31	similar to Os01g0367100; contains domain NAD(P)-binding Rossmann-fold domains (SSF51735)
55	29	AT1G03770	2.31	protein binding / zinc ion binding similar to putative ring finger protein 1 BAD53026.1
56	35	AT1G17665	2.30	similar to Os01g0197400
57	19	AT4G18480	2.30	CHLI1 (CHLORINA 42); magnesium chelatase Encodes the CHLI subunit of magnesium chelatase which is required for chlorophyll biosynthesis
58	35	AT5G51110	2.29	similar to dehydratase family AT1G29810.1
59	29	AT3G58630	2.26	peptidase M16 family protein / insulinase family protein; similar to putative insulin degrading enzyme BAD52843.1
60	35	AT1G55820	2.26	similar to GIP1 (GBF-INTERACTING PROTEIN 1)
61	27	AT2G46410	2.25	CPC (CAPRICE); DNA binding / transcription factor Nuclear-localized R3-type MYB transcription factor
62	35	AT5G05140	2.25	unknown protein
63	29	ATCG00520	2.24	Encodes a protein required for photosystem I assembly and stability

64	9	AT2G07711	2.24	Mitochondrial NADH dehydrogenase subunit 5
65	15	AT1G22990	2.24	heavy-metal-associated domain-containing protein / copper chaperone (CCH)-related
66	29	AT5G16140	2.24	peptidyl-tRNA hydrolase family protein
67	35	AT1G63950	2.24	heavy-metal-associated domain-containing protein
68	27	AT5G08190	2.23	transcription elongation factor-related
69	35	AT4G15030	2.23	similar to unknown protein AT1G56660.1
70	29	AT2G22990	2.23	SNG1 (SINAPOYLGLUCOSE 1); serine carboxypeptidase sinapoylglucose:malate sinapoyltransferase
71	35	AT2G25320 /// AT2G25330	2.22	meprin and TRAF homology domain-containing protein / MATH domain-containing protein
72	35	AT1G11070	2.21	hydroxyproline-rich glycoprotein family protein
73	29	AT2G44950	2.20	HUB1 (HISTONE MONO-UBIQUITINATION 1); protein binding / zinc ion binding
74	35	AT1G54680	2.20	similar to unknown protein AT5G27290.1)
75	35	AT1G52140	2.20	similar to unknown protein AT3G16330.1
76	27	AT3G47675 /// AT3G47680	2.20	DNA binding similar to unknown protein AT2G16140.1
77	35	AT1G04300	2.20	similar to meprin and TRAF homology domain-containing protein / MATH domain-containing protein
78	35	AT4G21090	2.19	adrenodoxin-like ferredoxin 1
79	35	AT2G07698	2.19	Identical to Hypothetical mitochondrial protein AtMg01200
80	29	AT4G33940	2.18	zinc finger (C3HC4-type RING finger) family protein
81	35	AT1G03220 /// AT1G03230	2.18	extracellular dermal glycoprotein, putative / EDGP, putative
82	27	AT4G37180	2.18	myb family transcription factor myb family transcription factor
83	35	AT2G47960	2.18	similar to unknown protein AAM93677.1
84	20	AT1G63740	2.18	disease resistance protein (TIR-NBS-LRR class)
85	17	AT1G05160	2.17	CYP88A3 (ENT-KAURENOIC ACID HYDROXYLASE 1); oxygen binding Encodes an ent-kaurenoic acid hydroxylase
86	21	AT4G18260	2.16	cytochrome B561-related
87	35	AT1G27510	2.16	similar to EX1 (EXECUTER1) AT4G33630.2
88	34	AT5G60800	2.16	heavy-metal-associated domain-containing protein
89	27	AT3G42860	2.16	zinc knuckle (CCHC-type) family protein
90	35	AT1G21000	2.16	zinc-binding family protein
91	29	AT5G45360	2.16	F-box family protein
92	26	AT3G14660	2.15	CYP72A13 (cytochrome P450, family 72, subfamily A, polypeptide 13); oxygen binding putative cytochrome P450
93	11	AT3G16785	2.15	PLDP1 (PHOSPHOLIPASE D ZETA1); phospholipase D Encodes a member of the PXPH-PLD subfamily of phospholipase D proteins
94	35	AT4G14600	2.15	Identical to Bet1-like protein At4g14600
95	29	AT4G13190	2.15	kinase similar to kinase; similar to putative serine/threonine protein kinase AAT58829.1
96	29	AT4G01800	2.15	preprotein translocase secA subunit
97	16	AT3G02780	2.14	IPP2 (ISOPENTENYL PYROPHOSPHATE:DIMETHYLLALLYL PYROPHOSPHATE ISOMERASE 2)
98	35	AT1G60010	2.14	similar to unknown protein AT1G10530.1
99	26	AT5G44410	2.13	FAD-binding domain-containing protein
100	29	AT2G45770	2.13	CPFTSY (ferric reductase deficient 4); GTP binding chloroplast SRP receptor homolog, alpha subunit CPFTSY
101	27	AT5G64390	2.12	HEN4 (HUA ENHANCER 4); nucleic acid binding encodes a K homology (KH) domain-containing, putative RNA binding protein that interacts with HUA1, a CCCH zinc finger RNA binding protein in the nucleus
102	27	AT5G08650	2.12	TATA-binding protein-associated phosphoprotein Dr1 protein
103	29	AT1G04130	2.12	binding similar to serine/threonine protein phosphatase-related 1G56440.1
104	20	AT1G11310	2.11	MLO2 (MILDEW RESISTANCE LOCUS O 2); calmodulin binding A member of a large family of seven-transmembrane domain proteins specific to plants
105	20	AT4G33720	2.11	pathogenesis-related protein
106	29	AT5G14420	2.11	copine-related

107	30	AT4G00960	2.11	protein kinase family protein similar to putative receptor-like serine-threonine protein kinase CAC84518.1
108	20	AT1G21610	2.11	wound-responsive family protein
109	30	AT4G35750	2.11	Rho-GTPase-activating protein-related
110	29	AT2G45170	2.10	AtATG8e (AUTOPHAGY 8E); microtubule binding Involved in autophagy.
111	35	AT3G21360	2.10	oxidoreductase Identical to Clavaminate synthase-like protein At3g21360
112	35	AT3G27610	2.10	similar to nucleotidyltransferase AT2G01220.2
113	33	AT3G61210	2.10	embryo-abundant protein-related
114	21	AT5G08410	2.10	FTRA2 (ferredoxin/thioredoxin reductase subunit A (variable subunit) 2)
115	27	AT4G36730	2.10	GBF1 (G-box binding factor 1); transcription factor member of a gene family encoding basic leucine zipper proteins
116	27	AT3G58630	2.09	transcription factor
117	27	AT1G51600	2.09	ZML2 (ZIM-LIKE 2); transcription factor member of a novel family of plant-specific GATA-type transcription factors
118	3	AT3G59100	2.08	ATGSL11 (GLUCAN SYNTHASE-LIKE 11); 1,3-beta-glucan synthase/ transferase
119	21	AT1G06650	2.08	2-oxoglutarate-dependent dioxygenase
120	35	AT1G27150	2.08	binding similar to binding AT1G27110.1
121	35	AT3G55560	2.07	DNA-binding protein-related
122	35	AT1G29180	2.07	DC1 domain-containing protein
123	29	AT3G20630	2.07	UBP14 (UBIQUITIN-SPECIFIC PROTEASE 14)
124	27	AT2G19810	2.07	zinc finger (CCCH-type) family protein
125	35	AT5G02580	2.06	similar to unknown protein AT3G55240.1
126	35	AT1G68910	2.06	similar to unknown protein AT5G11390.1
127	29	AT3G61390	2.06	U-box domain-containing protein
128	30	AT5G20010 /// AT5G20020	2.06	RAN-1 (Ras-related GTP-binding nuclear protein 1)
129	35	AT1G21580	2.06	hydroxyproline-rich glycoprotein family protein
130	35	AT5G13240	2.06	similar to conserved hypothetical protein ABE92223.1
131	29	AT5G47190	2.05	Identical to 50S ribosomal protein L19-2, chloroplast precursor Q8RXX5;Q8LBV7;Q9LVU0
132	30	AT4G13730	2.05	RabGAP/TBC domain-containing protein
133	30	AT5G08650	2.05	GTP-binding protein LepA, putative
134	29	AT3G54850	2.05	armadillo/beta-catenin repeat family protein / U-box domain-containing family protein
135	29	AT2G17830 /// AT5G42460	2.05	F-box family protein
136	29	AT1G71980	2.04	protease-associated zinc finger (C3HC4-type RING finger) family protein
137	27	AT1G66160	2.04	U-box domain-containing protein
138	35	AT2G05310 /// AT4G13500	2.04	similar to unknown protein AT2G05310.1
139	29	AT1G11870	2.04	AtSRS (OVULE ABORTION 7); serine-tRNA ligase Seryl-tRNA synthetase targeted to chloroplasts and mitochondria
140	21	AT5G51010	2.04	rubredoxin family protein
141	27	AT3G63350	2.04	AT-HSFA7B (Arabidopsis thaliana heat shock transcription factor A7B); DNA binding / transcription factor member of Heat Stress Transcription Factor (Hsf) family
142	35	AT2G30600	2.04	BTB/POZ domain-containing protein
143	27	AT1G07840	2.04	leucine zipper factor-related
144	29	AT1G03740	2.03	protein kinase family protein similar to AT5G44290.4
145	29	AT3G07370	2.03	ATCHIP/CHIP (CARBOXYL TERMINUS OF HSC70-INTERACTING PROTEIN); ubiquitin-protein ligase
146	30	AT5G50120	2.03	transducin family protein / WD-40 repeat family protein
147	33	AT1G67440	2.03	EMB1688 (EMBRYO DEFECTIVE 1688); GTP binding / GTPase
148	29	AT1G05840	2.03	aspartyl protease family protein
149	35	AT5G42310	2.03	pentatricopeptide (PPR) repeat-containing protein
150	35	AT2G37750	2.03	unknown protein
151	35	AT3G13760	2.03	DC1 domain-containing protein
152	27	AT1G75410	2.02	BLH3 (BLH3); DNA binding / transcription factor BEL1-like homeodomain 3 (BLH3)

153	30	AT1G31930	2.02	XLG3 (extra-large GTP-binding protein 3); signal transducer
154	35	AT3G20930	2.02	RNA recognition motif (RRM)-containing protein
155	35	AT5G52760	2.02	heavy-metal-associated domain-containing protein
156	35	AT3G14750	2.02	similar to unknown protein AT1G67170.1
157	10	AT1G48100	2.02	glycoside hydrolase family 28 protein / polygalacturonase (pectinase) family protein
158	29	AT2G35635	2.02	UBQ7 (RELATED TO UBIQUITIN 2) encodes a ubiquitin-like protein
159	34	AT5G27520	2.02	mitochondrial substrate carrier family protein
160	35	AT2G32235 /// AT2G32240	2.02	similar to unknown protein AT1G05320.3
161	26	AT2G23590 /// AT2G23600	2.02	hydrolase, alpha/beta fold family protein
162	35	AT2G32190 /// AT2G32210	2.02	similar to unknown protein AT2G32210.1
163	35	AT2G29670	2.02	binding similar to binding AT1G07280.2
164	35	AT1G26160	2.01	metal-dependent phosphohydrolase HD domain-containing protein
165	35	AT5G02710	2.01	similar to Uncharacterised protein family containing protein, expressed [Oryza sativa (japonica cultivar-group)] ABF96102.1
166	27	AT3G25440	2.01	similar to group II intron splicing factor CRS1-related AT4G13070.1
167	34	AT1G79520	2.01	cation efflux family protein
168	35	AT3G14160	2.01	oxidoreductase, 2OG-Fe(II) oxygenase family protein
169	20 and 32	AT4G26090	2.01	RPS2 (RESISTANT TO P. SYRINGAE 2) Encodes a plasma membrane protein with leucine-rich repeat, leucine zipper, and P loop domains
170	27	AT3G54390	2.01	transcription factor
171	29	AT4G34370	2.01	IBR domain-containing protein similar to zinc finger protein-related
172	35	AT2G02570	2.00	nucleic acid binding similar to Os08g0109900
173	35	AT3G17365	2.00	catalytic
174	35	AT1G71460	2.00	pentatricopeptide (PPR) repeat-containing protein

Table A.3. List of transcripts showing ≤ 2-fold decrease only in WT root tissues under 4 hr hypoxia compared to normoxic WT

bin	# of genes	%	name
35	67	31.16	not assigned
27	25	11.63	RNA
29	18	8.37	protein
30	15	6.98	signalling
26	15	6.98	misc
34	12	5.58	transport
20	10	4.65	stress
31	10	4.65	cell
28	8	3.72	DNA
33	8	3.72	development
17	7	3.26	hormone metabolism
10	7	3.26	cell wall

#	bin	AGI	Fold-Change	Description
1	20	AT4G16660	-2.00	heat shock protein 70, putative
2	29	AT4G16640	-2.76	matrix metalloproteinase, putative
3	34	AT4G17340	-2.04	DELTA-TIP2/TIP2;2 (tonoplast intrinsic protein 2;2); water channel
4	4	AT5G04120	-2.24	phosphoglycerate/bisphosphoglycerate mutase family protein
5	35	AT1G26130	-2.10	haloacid dehalogenase-like hydrolase family protein
6	23	AT1G26190	-2.22	phosphoribulokinase/uridine kinase family protein
7	33	AT4G36920	-2.30	AP2 (APETALA 2); transcription factor Encodes a floral homeotic gene
8	34	AT1G77380	-2.21	AAP3 (amino acid permease 3)
9	17	AT1G77330	-2.04	1-aminocyclopropane-1-carboxylate oxidase, putative
10	29	AT5G17600	-2.03	zinc finger (C3HC4-type RING finger) family protein Identical to Probable RING-H2 finger protein ATL5G (ATL5G) Q9LF64
11	35	AT5G16220	-2.32	octicosapeptide/Phox/Bem1p (PB1) domain-containing protein
12	10	AT5G15630	-2.01	COBL4/IRX6 (COBRA-LIKE4); hydrolase, hydrolyzing O-glycosyl compounds / polysaccharide binding Encodes a member of the COBRA family
13	35	AT5G28150	-2.27	similar to unknown protein AT3G04860.1
14	35	AT5G24880	-2.34	similar to calmodulin-binding protein-related AT5G10660.1
15	35	AT5G67470	-2.06	formin homology 2 domain-containing protein
16	28	AT5G67100	-2.19	DNA-directed DNA polymerase alpha catalytic subunit, putative
17	26	AT5G67230	-2.35	glycosyl transferase family 43 protein
18	31	AT5G66310	-2.10	kinesin motor family protein
19	33	AT5G65040	-2.07	senescence-associated protein-related
20	10	AT5G64740	-2.16	CESA6 (CELLULASE SYNTHASE 6); transferase, transferring glycosyl groups Encodes a cellulase synthase
21	26	AT5G64120	-2.04	peroxidase, putative
22	26	AT5G63450	-2.17	CYP94B1 (cytochrome P450, family 94, subfamily B, polypeptide 1); oxygen binding member of CYP94B similar to CYP94B3 (cytochrome P450, family 94, subfamily B, polypeptide 3), oxygen binding AT3G48520.1
23	34	AT5G63060	-2.51	transporter similar to SEC14 cytosolic factor family protein / phosphoglyceride transfer family protein AT4G08690.1
24	33	AT5G62380	-2.22	VND6 (VASCULAR-RELATED NAC-DOMAIN 6); transcription factor Encodes a NAC-domain transcription factor involved in xylem formation

25	9	AT5G61310		-2.01	cytochrome c oxidase subunit Vc, putative / COX5C, putative Identical to Probable cytochrome c oxidase polypeptide Vc-3 (EC 1.9.3.1) (Cytochrome c oxidase subunit 5c-3) Q9FLK2
26	27	AT5G60100		-2.35	APRR3 (PSEUDO-RESPONSE REGULATOR 3); transcription regulator Encodes pseudo-response regulator 3 (APRR3)
27	27	AT5G59780		-2.18	MYB59 (myb domain protein 59); DNA binding / transcription factor Encodes a putative transcription factor (MYB59)
28	17	AT5G59220		-2.20	protein phosphatase 2C, putative / PP2C, putative
29	35	AT5G59410		-2.17	similar to Rab5-interacting family protein AT2G29020.1
30	27	AT5G57140 AT5G57150	///	-2.35	basic helix-loop-helix (bHLH) family protein
31	11	AT5G55480		-2.19	glycerophosphoryl diester phosphodiesterase family protein
32	20	AT5G54660		-2.06	heat shock protein-related similar to 17.6 kDa class I small heat shock protein (HSP17.6C-CI) (AA 1-156) AT1G53540.1
33	35	AT5G54300		-2.93	similar to unknown protein AT1G61260.1
34	35	AT5G52180		-2.04	similar to hypothetical protein [Oryza sativa (japonica cultivar-group)] BAD44788.1
35	10	AT5G51500		-2.53	pectinesterase family protein
36	26	AT5G51260		-2.25	acid phosphatase, putative
37	13	AT5G48060		-2.06	C2 domain-containing protein
38	30	AT5G44700		-2.22	EDA23 (embryo sac development arrest 23); ATP binding / protein serine/threonine kinase
39	35	AT5G44780		-2.64	similar to unknown protein AT4G20020.2
40	10	AT5G44480		-2.05	DUR (DEFECTIVE UGE IN ROOT); catalytic mutant has Altered lateral root; UDP Glucose Epimerase Identical to Putative UDP-arabinose 4-epimerase 4 (EC 5.1.3.5) (UDP-D-xylose 4- epimerase 4) Q9FI17
41	33	AT5G43270		-2.75	SPL2 (SQUAMOSA PROMOTER BINDING PROTEIN-LIKE 2); DNA binding / transcription factor member of the SPL (squamosa-promoter binding protein-like) gene family
42	35	AT5G43390 AT5G43400	///	-2.04	similar to unknown protein AT5G13210.1
43	35	AT5G43030		-2.51	DC1 domain-containing protein
44	35	AT5G42280		-2.33	DC1 domain-containing protein
45	35	AT5G40860		-2.15	NO MATCH
46	35	AT5G40640		-2.07	similar to unknown protein AT3G27390.1
47	29	AT5G40140		-2.17	armadillo/beta-catenin repeat family protein / U-box domain-containing protein
48	27	AT5G39840		-2.43	ATP-dependent RNA helicase, mitochondrial, putative similar to ATSUV3 (embryo sac development arrest 15) AT4G14790.1
49	34	AT5G38820		-2.25	amino acid transporter family protein
50	26	AT5G38450		-2.25	CYP735A1 (cytochrome P450, family 735, subfamily A, polypeptide 1); oxygen binding member of CYP709A similar to CYP735A2 (cytochrome P450, family 735, subfamily A, polypeptide 2), oxygen binding AT1G67110.1
51	27	AT5G37020		-2.02	ARF8 (AUXIN RESPONSE FACTOR 8); transcription factor Encodes a member of the auxin response factor family
52	35	AT5G23840		-2.55	MD-2-related lipid recognition domain-containing protein / ML domain-containing protein
53	17	AT5G23350 AT5G23360	///	-2.63	GRAM domain-containing protein / ABA-responsive protein-related
54	27	AT5G23420		-2.16	HMGB6 (High mobility group B 6); transcription factor Encodes a protein belonging to the subgroup of HMGB (high mobility group B) proteins
55	35	AT5G17980		-2.31	C2 domain-containing protein
56	17	AT5G16530		-2.45	PIN5 (PIN-FORMED 5); auxin:hydrogen symporter/ transporter
57	31	AT5G13990		-2.40	ATEXO70C2 (exocyst subunit EXO70 family protein C2); protein binding A member of EXO70 gene family, putative
58	35	AT5G12080		-2.18	mechanosensitive ion channel domain-containing protein / MS ion channel domain-containing protein
59	35	AT5G11560		-2.31	catalytic similar to hypothetical protein LOC419470 [Gallus gallus] NP_001012856.1
60	27	AT5G10280		-2.00	MYB92 (myb domain protein 92); DNA binding / transcription factor Encodes a putative transcription factor (MYB92)

61	17	AT5G08130	-2.39	BIM1 (BES1-interacting Myc-like protein 1); DNA binding / transcription factor Arabidopsis thaliana basic helix-loop-helix (bHLH) family protein involved in brassinosteroid signaling
62	35	AT5G02590	-2.08	chloroplast lumen common family protein
63	35	AT5G01730	-2.15	WAVE3 putative WAVE homolog Identical to Protein SCAR4 (AtSCAR4) (Protein WAVE3) (SCAR4) Q5XPJ6;Q9LCZ7
64	16	AT5G01190	-2.54	LAC10 (laccase 10); copper ion binding / oxidoreductase putative laccase, a member of laccase family of genes (17 members in Arabidopsis)
65	27	AT3G60800	-2.02	zinc finger (DHHC type) family protein
66	27	AT3G60110	-2.44	DNA-binding bromodomain-containing protein
67	26	AT3G59710	-2.04	short-chain dehydrogenase/reductase (SDR) family protein
68	35	AT3G58840	-2.04	similar to myosin heavy chain-related AT1G06530.1
69	35	AT3G57780	-2.01	similar to nucleolar protein gar2-related AT2G42320.2
70	35	AT3G56640	-2.12	exocyst complex subunit Sec15-like family protein
71	35	AT3G55690	-2.33	similar to unknown protein AT2G39870.1
72	16	AT3G55120	-4.49	TT5 (TRANSPARENT TESTA 5); chalcone isomerase Catalyzes the conversion of chalcones into flavanones
73	10 and 30	AT3G54590	-2.56	ATHRGP1; structural constituent of cell wall Encodes a hydroxyproline-rich glycoprotein
74	34	AT3G53960	-2.03	proton-dependent oligopeptide transport (POT) family protein
75	28	AT3G52900	-2.03	similar to unknown protein AT2G36355.1
76	30	AT3G51990	-3.00	protein kinase family protein
77	35	AT3G49720	-2.25	similar to unknown protein AT5G65810.1
78	31	AT3G44730	-3.00	kinesin motor protein-related similar to microtubule motor AT2G47500.1
79	26	AT3G43670	-2.04	copper amine oxidase, putative
80	10	AT4G40090	-2.56	AGP3 (ARABINOGALACTAN-PROTEIN 3) similar to AGP2 (ARABINOGALACTAN-PROTEIN 2) AT2G22470.1
81	35	AT4G39050	-2.18	NO MATCH
82	35	AT4G39190	-2.05	similar to unknown protein AT2G21560.1
83	27	AT4G37850	-2.85	basic helix-loop-helix (bHLH) family protein
84	35	AT4G35510	-2.07	similar to unknown protein AT2G17540.1
85	35	AT4G35270	-2.77	NO MATCH
86	30	AT4G32710	-2.22	kinase similar to ATPERK1 (PROLINE EXTENSIN-LIKE RECEPTOR KINASE 1), ATP binding / protein kinase AT3G24550.1
87	29	AT4G30960	-2.16	CIPK6 (CBL-INTERACTING PROTEIN KINASE 6); kinase Encodes CBL-interacting protein kinase 6 (CIPK6)
88	30	AT4G31100	-2.45	wall-associated kinase, putative Identical to Wall-associated receptor kinase-like 17 precursor (EC 2.7.11.-) (WAKL17) Q9M092
89	20	AT4G30660	-2.12	hydrophobic protein, putative / low temperature and salt responsive protein, putative Identical to UPF057 membrane protein At4g30660 Q9SUI0
90	27	AT4G28110	-2.98	AtMYB41 (myb domain protein 41); DNA binding / transcription factor Member of the R2R3 factor gene family
91	29	AT4G27050	-2.05	F-box family protein
92	34	AT4G25350	-2.15	SHB1 (SHORT HYPOCOTYL UNDER BLUE1) SHB1 encodes a nuclear and cytosolic protein that has motifs homologous with SYG1 protein family members
93	29	AT4G25160	-2.12	protein kinase family protein
94	29	AT4G23940	-2.17	FtsH protease, putative similar to VAR2 (VARIEGATED 2), ATP-dependent peptidase/ ATPase/ metallopeptidase/ zinc ion binding AT2G30950.1
95	30	AT4G23130	-2.23	CRK5 (CYSTEINE-RICH RLK5); kinase Encodes a receptor-like protein kinase
96	35	AT4G21780	-2.01	similar to hypothetical protein MtrDRAFT_AC152499g5v1 [Medicago truncatula] ABE77785.1
97	28	AT4G21600	-2.07	bifunctional nuclease, putative
98	17	AT4G21340	-3.12	B70; transcription factor similar to DNA binding / transcription factor AT4G05170.1
99	17	AT4G21200	-2.04	ATGA2OX8 (GIBBERELLIN 2-OXIDASE 8); gibberellin 2-beta-dioxygenase Encodes a protein with gibberellin 2-oxidase activity which acts specifically on C-20 gibberellins
100	30	AT4G13440	-2.04	calcium-binding EF hand family protein contains InterPro domain EF-Hand type; (InterPro:IPR011992)

101	29	AT4G12910		-2.13	SCPL20 (serine carboxypeptidase-like 20); serine carboxypeptidase
102	30	AT4G12640		-2.14	RNA recognition motif (RRM)-containing protein similar to FPA (FPA) AT2G43410.4
103	29	AT4G11310 /// AT4G11320		-2.09	cysteine proteinase, putative Identical to Probable cysteine proteinase At4g11320 precursor (EC 3.4.22.-) Q9SUS9
104	34	AT4G08620		-3.12	SULTR1;1 (sulfate transporter 1;1); sulfate transporter High affinity sulfate transporter
105	27	AT4G05100		-2.37	AtMYB74 (myb domain protein 74); DNA binding / transcription factor Member of the R2R3 factor gene family
106	31	AT4G03480		-2.55	ankyrin repeat family protein
107	20	AT4G01700		-2.06	chitinase, putative
108	35	AT1G31940		-2.05	similar to unknown protein AT2G35585.1
109	35	AT1G25520		-2.24	similar to unknown protein AT1G68650.1
110	26	AT1G18580		-2.28	GAUT11 (Galacturonosyltransferase 11); polygalacturonate 4-alpha-galacturonosyltransferase Encodes a protein with putative galacturonosyltransferase activity
111	35	AT1G18090		-2.85	E12A11; phosphatidylethanolamine binding E12A11 protein (E12A11) Identical to Protein MOTHER of FT and TF1 (MFT) Q9XFK7
112	28	AT1G55130		-2.14	endomembrane protein 70, putative
113	26	AT3G02350		-2.15	GAUT9 (Galacturonosyltransferase 9); polygalacturonate 4-alpha-galacturonosyltransferase/ transferase, transferring glycosyl groups / transferase, transferring hexosyl groups Encodes a protein with putative galacturonosyltransferase activity
114	33	AT1G54890		-2.15	late embryogenesis abundant protein-related / LEA protein-related
115	27	AT1G66140		-2.04	ZFP4 (ZINC FINGER PROTEIN 4); nucleic acid binding / transcription factor/ zinc ion binding
116	30	AT3G21340		-3.30	leucine-rich repeat protein kinase, putative
117	26	AT3G26330		-2.25	CYP71B37 (cytochrome P450, family 71, subfamily B, polypeptide 37); oxygen binding putative cytochrome P450 Identical to Cytochrome P450 71B37 (EC 1.14.-.-) (CYP71B37) Q9LIP3
118	20	AT3G26460		-2.29	major latex protein-related / MLP-related
119	35	AT3G12870		-2.04	similar to unknown protein AT5G56120.1
120	35	AT3G27210		-2.08	similar to unknown protein AT5G40860.1
121	11	AT3G23510 /// AT3G23530		-2.03	cyclopropane fatty acid synthase, putative
122	27	AT3G20280		-2.15	PHD finger family protein
123	27	AT3G25710		-2.23	basic helix-loop-helix (bHLH) family protein
124	27	AT3G12720		-2.23	AtMYB67/AtY53 (myb domain protein 67); DNA binding / transcription factor Member of the R2R3 factor gene family
125	35	AT3G25400		-2.02	similar to hypothetical protein TTHERM_00522540 [Tetrahymena thermophila SB210] XP_001014432.1
126	26	AT3G15820 /// AT3G15830		-2.01	phosphatidic acid phosphatase-related / PAP2-related
127	35	AT3G26750		-2.87	similar to hypothetical protein MtrDRAFT_AC125480g17v1 [Medicago truncatula] ABE84077.1
128	27	AT3G22780		-2.02	TSO1 (CHINESE FOR 'UGLY'); transcription factor putative DNA binding protein (tso1) mRNA, tso1-3 allele
129	30	AT3G14350		-2.16	leucine-rich repeat transmembrane protein kinase, putative
130	30	AT3G07050		-2.14	GTP-binding family protein
131	29	AT3G02760		-2.01	histidyl-tRNA synthetase, putative
132	27	AT3G02940		-2.36	MYB107 (myb domain protein 107); DNA binding / transcription factor Encodes a putative transcription factor (MYB107)
133	35	AT3G02930		-2.21	similar to unknown protein AT5G16730.1
134	10	AT3G10720		-2.30	pectinesterase, putative
135	35	AT3G03680		-2.06	C2 domain-containing protein
136	30	AT3G11490		-2.14	rac GTPase activating protein, putative
137	35	AT3G05320		-2.16	similar to unnamed protein product [Vitis vinifera] CAO44440.1
138	35	AT1G69150 /// AT3G43890		-3.71	DC1 domain-containing protein
139	35	AT1G13910		-2.99	leucine-rich repeat family protein similar to protein binding AT5G61240.1
140	16	AT1G55290		-2.39	oxidoreductase, 2OG-Fe(II) oxygenase family protein encodes a protein whose sequence is similar to oxidoreductase, 2OG-Fe(II) oxygenase

141	29	AT1G71020	-2.28	armadillo/beta-catenin repeat family protein / U-box domain-containing protein
142	35	AT1G72240	-2.44	similar to unknown protein AT1G22470.1
143	35	AT1G67880	-2.23	glycosyl transferase family 17 protein
144	31	AT1G68060	-2.02	ATMAP70-1 (MICROTUBULE-ASSOCIATED PROTEINS 70-1); microtubule binding Encodes a microtubule associated protein (MAP70-1)
145	29	AT1G78100	-2.01	F-box family protein
146	26	AT1G73610	-2.11	GDSL-motif lipase/hydrolase family protein
147	29	AT1G73310	-2.24	SCPL4 (serine carboxypeptidase-like 4); serine carboxypeptidase
148	29	AT1G73290	-5.52	SCPL5 (serine carboxypeptidase-like 5); serine carboxypeptidase
149	35	AT1G36380	-2.07	similar to unknown protein [Oryza sativa (japonica cultivar-group)] BAD15488.1
150	33	AT1G71930	-2.21	VND7 (VASCULAR RELATED NAC-DOMAIN PROTEIN 7); transcription factor Encodes a NAC-domain transcription factor involved in xylem formation
151	35	AT1G67620	-2.13	similar to AGR_C_5039p, putative, expressed [Oryza sativa (japonica cultivar-group)] ABG21940.1
152	11	AT1G74210	-2.12	glycerophosphoryl diester phosphodiesterase family protein
153	35	AT1G73885	-2.15	NO MATCH
154	20	AT1G62320	-2.04	early-responsive to dehydration protein-related / ERD protein-related
155	16	AT1G01420	-3.66	UDP-glucoronosyl/UDP-glucosyl transferase family protein
156	34	AT1G07290	-2.55	nucleotide-sugar transporter family protein similar to GONST1 (GOLGI NUCLEOTIDE SUGAR TRANSPORTER 1) AT2G13650.2
157	35	AT1G20230	-2.08	pentatricopeptide (PPR) repeat-containing protein
158	28	AT1G44900	-2.03	ATP binding / DNA binding / DNA-dependent ATPase similar to DNA replication licensing factor, putative AT2G16440.1
159	35	AT1G44790	-2.04	ChaC-like family protein
160	30	AT1G14280	-2.14	PKS2 (PHYTOCHROME KINASE SUBSTRATE 2) Encodes phytochrome kinase substrate 2
161	35	AT1G49750	-2.02	leucine-rich repeat family protein
162	27	AT1G35560	-2.03	TCP family transcription factor, putative
163	27	AT1G80070	-2.07	SUS2 (ABNORMAL SUSPENSOR 2) a genetic locus involved in embryogenesis
164	30	AT1G02900	-2.25	RALFL1 (RALF-LIKE 1) Member of a diversely expressed predicted peptide family showing sequence similarity to tobacco Rapid Alkalinization Factor (RALF), and is believed to play an essential role in the physiology of Arabidopsis
165	27	AT1G53910	-2.05	RAP2.12; DNA binding / transcription factor encodes a member of the ERF (ethylene response factor) subfamily B-2 of ERF/AP2 transcription factor family (RAP2.12)
166	20	AT1G70880	-2.10	Bet v I allergen family protein similar to MLP34 (MLP-LIKE PROTEIN 34) AT1G70850.3
167	20	AT1G64160	-3.65	disease resistance-responsive family protein / dirigent family protein
168	35	AT1G73020	-2.96	similar to PREDICTED: similar to CG15270-PA, isoform A, partial [Bos taurus] XP_614009.2
169	31	AT1G11160	-2.40	nucleotide binding similar to WD-40 repeat family protein / katanin p80 subunit, putative AT1G61210.1
170	35	AT1G21790	-2.19	similar to Os01g0869600 [Oryza sativa (japonica cultivar-group)] NP_001044928.1
171	33	AT1G13980	-2.04	GN (GNOM) Encodes a GDP/GTP exchange factor for small G-proteins of the ADP ribosylation factor (RAF) class, and as regulator of intracellular trafficking
172	35	AT1G75730	-3.67	unknown protein
173	11	AT2G31360	-2.04	ADS2 (16:0DELTA9 ARABIDOPSIS DESATURASE 2); oxidoreductase homologous to delta 9 acyl-lipid desaturases of cyanobacteria and acyl-CoA desaturases of yeast and mammals
174	31	AT2G28620	-3.02	kinesin motor protein-related
175	35	AT2G22125	-2.04	binding similar to C2 domain-containing protein / armadillo/beta-catenin repeat family protein AT1G77460.1
176	31	AT2G31900	-2.05	XIF (Myosin-like protein XIF) Encodes an novel myosin isoform
177	20	AT2G17050	-2.39	disease resistance protein (TIR-NBS-LRR class), putative similar to SLH1 (sensitive to low humidity 1) AT5G45260.2
178	35	AT2G16270	-2.14	similar to unknown protein AT1G16630.1
179	35	AT1G04330	-2.14	similar to unknown protein AT3G23170.1
180	27	AT1G04240	-2.80	SHY2 (SHORT HYPOCOTYL 2); transcription factor SHY2/IAA3 regulates multiple auxin responses in roots

181	13	AT1G31180 /// AT5G14200	-2.11	3-isopropylmalate dehydrogenase, chloroplast, putative
182	29	AT2G20630	-2.01	protein phosphatase 2C, putative / PP2C, putative
183	28 and 34	AT2G21520	-2.08	similar to SEC14 cytosolic factor, putative phosphoglyceride transfer protein, putative AT4G39170.1
184	35	AT2G36290	-2.09	hydrolase, alpha/beta fold family protein similar to esterase/lipase/thioesterase family protein AT1G74300.1
185	35	AT2G35990	-2.27	similar to carboxy-lyase AT5G06300.1
186	30	AT2G42880	-2.16	ATMPK20 (Arabidopsis thaliana MAP kinase 20); MAP kinase member of MAP Kinase Identical to Mitogen-activated protein kinase 20 (EC 2.7.11.24) (MAP kinase 20) (AtMPK20) (MPK20) Q9SJG9;Q945L8
187	35	AT2G22510	-2.09	hydroxyproline-rich glycoprotein family protein
188	23 and 34	AT2G03590 /// AT2G03600	-2.13	ATUPS3 (Arabidopsis thaliana ureide permease 3)
189	16	AT1G78950	-3.18	beta-amyrin synthase, putative similar to LUP1 (LUPEOL SYNTHASE 1), lupeol synthase AT1G78970.1
190	26	AT1G61820	-2.22	BGLU46; hydrolase, hydrolyzing O-glycosyl compounds
191	31	AT1G62020	-2.13	coatomer protein complex, subunit alpha, putative
192	35	AT1G12080	-2.21	similar to unknown protein AT3G59370.1
193	26	AT1G12090	-2.07	ELP (EXTENSIN-LIKE PROTEIN); lipid binding extensin-like protein (ELP) similar to protease inhibitor/seed storage/lipid transfer protein (LTP) family protein AT1G62510.1
194	20	AT1G11960	-2.26	early-responsive to dehydration protein-related / ERD protein-related
195	34	AT1G43310 /// AT5G33320	-2.08	triose phosphate/phosphate translocator-related similar to CUE1 (CAB UNDEREXPRESSED 1), antiporter/ triose-phosphate transporter AT5G33320.1
196	29	AT1G04700	-2.55	protein kinase family protein similar to Octicosapeptide/Phox/Bem1p; Protein kinase [Medicago truncatula] ABE86676.1
197	35	AT1G09980 /// AT1G58350	-2.03	ZW18 similar to unknown protein AT1G09980.1
198	34	AT1G62280	-2.85	C4-dicarboxylate transporter/malic acid transport family protein
199	26	AT2G43020	-2.25	ATPAO2 (POLYAMINE OXIDASE 2); amine oxidase similar to ATPAO3 (POLYAMINE OXIDASE 3), oxidoreductase AT3G59050.1
200	31	AT2G37080	-2.03	myosin heavy chain-related similar to cytoplasmic linker protein-related AT5G60210.1
201	35	AT2G28305	-2.13	similar to unknown protein AT2G37210.1
202	35	AT2G27285	-2.04	similar to unknown protein AT2G27280.1
203	28	AT2G18050	-2.43	HIS1-3 (HISTONE H1-3); DNA binding encodes a structurally divergent linker histone whose gene expression is induced by dehydration and ABA
204	35	AT2G39050	-2.01	hydroxyproline-rich glycoprotein family protein similar to PLDBETA1 (PHOSPHOLIPASE D BETA 1), phospholipase D AT2G42010.1
205	35	AT2G29190	-2.15	APUM2 (ARABIDOPSIS PUMILIO 2); RNA binding similar to APUM4 (ARABIDOPSIS PUMILIO 4), RNA binding AT3G10360.1
206	35	AT2G29590	-2.01	thioesterase family protein
207	27	AT2G22750	-2.64	basic helix-loop-helix (bHLH) family protein
208	27	AT2G46130	-2.02	WRKY43 (WRKY DNA-binding protein 43); transcription factor member of WRKY Transcription Factor; Group II-c Identical to Probable WRKY transcription factor 43 (WRKY DNA-binding protein 43) (WRKY43) Q8GY11;O82356;Q8VWZ0
209	27	AT2G38090	-2.27	myb family transcription factor
210	33	AT2G37650	-2.07	scarecrow-like transcription factor 9 (SCL9)
211	25	AT2G44160 /// AT3G59970	-2.38	MTHFR1 (METHYLENETETRAHYDROFOLATE REDUCTASE 1)
212	28	AT2G02480	-2.36	STI (STICHEL); ATP binding / DNA-directed DNA polymerase STICHEL mutant shows trichomes with fewer than normal branches
213	29	AT2G22980	-2.55	SCPL13; serine carboxypeptidase
214	29	AT2G35000	-2.02	zinc finger (C3HC4-type RING finger) family protein E3 ligase-like protein induced by chitin oligomers
215	35	AT2G41950	-2.05	similar to Os03g0226700 [Oryza sativa (japonica cultivar-group)] NP_001049441.1

Table A.4. List of transcripts showing ≤ 2-fold decrease only in the roots of *atnip2;1-1* under 4 hr hypoxic conditions compared to normoxic *atnip2;1-1*

bin	# of genes	%	name
35	87	28.0	not assigned
29	37	11.9	protein
27	31	10.0	RNA
26	26	8.4	misc
34	22	7.1	transport
30	21	6.8	signalling
31	14	4.5	cell
33	13	4.2	development
20	12	3.9	stress
10	11	3.5	cell wall
11	8	2.6	lipid metabolism
17	7	2.3	hormone metabolism
28	6	1.9	DNA
13	5	1.6	amino acid metabolism
32	4	1.3	micro RNA, natural antisense etc
23	3	1.0	nucleotide metabolism
16	3	1.0	secondary metabolism
3	2	0.6	minor CHO metabolism
15	1	0.3	metal handling
9	1	0.3	mitochondrial electron transport / ATP synthesis
7	1	0.3	OPP
21	1	0.3	redox.regulation
14	1	0.3	S-assimilation

#	bin	AGI	Fold-Change	Description
1	35	AT3G21520	-7.04	similar to unknown protein AT3G21550.1
2	29	AT2G31980	-5.41	cysteine proteinase inhibitor-related
3	15	AT5G56080	-5.25	nicotianamine synthase, putative
4	26 and 32	AT2G42250	-4.25	CYP712A1 (cytochrome P450, family 712, subfamily A, polypeptide 1); oxygen binding member of CYP712A
5	35	AT2G25150	-4.22	transferase family protein
6	34	AT1G04560	-4.20	AWPM-19-like membrane family protein
7	35	AT5G15290	-4.15	integral membrane family protein
8	11	AT3G51600	-4.01	LTP5 (LIPID TRANSFER PROTEIN 5)
9	29	AT3G54940	-3.71	cysteine proteinase, putative
10	27	AT5G10120	-3.66	ethylene insensitive 3 family protein
11	26	AT1G07260	-3.32	UDP-glucoronosyl/UDP-glucosyl transferase family protein
12	26	AT5G06730	-3.29	peroxidase, putative Identical to Peroxidase 54 precursor (EC 1.11.1.7) (Atperox P54) (ATP29a) (PER54) Q9FG34;P93729
13	26	AT1G73160	-3.24	glycosyl transferase family 1 protein
14	35	AT1G09310	-3.20	similar to unknown protein AT1G56580.1
15	35	AT1G10530	-3.19	similar to unknown protein AT1G60010.1
16	35	AT1G28190	-3.17	similar to unknown protein AT5G12340.1
17	34	AT1G73220	-3.13	sugar transporter family protein similar to transporter-related AT1G79360.1
18	34	AT2G47160	-3.11	BOR1 (REQUIRES HIGH BORON 1); anion exchanger Boron transporter
19	17	AT4G30610	-3.09	BRS1 (BRI1 SUPPRESSOR 1) Encodes a secreted glycosylated serine carboxypeptidase with broad substrate preference that is involved in brassinosteroid signalling via BRI1

20	27	AT5G61030	-3.05	GR-RBP3 (glycine-rich RNA-binding protein 3); RNA binding encodes a glycine-rich RNA binding protein
21	27	AT2G23760	-2.99	BLH4 (BLH4); DNA binding / transcription factor BEL1-like homeobox 4 (BLH4)
22	11	AT1G27950	-2.95	lipid transfer protein-related Identical to Uncharacterized GPI-anchored protein At1g27950 precursor Q9C7F7;Q570M7;Q8LEI0
23	7	AT1G71100	-2.92	RSW10 (RADIAL SWELLING 10); ribose-5-phosphate isomerase
24	35	AT5G53280	-2.91	PDV1 (PLASTID DIVISION1) An integral outer envelope membrane protein (as its homolog PDV2), component of the plastid division machinery
25	33	AT4G08300	-2.91	nodulin MtN21 family protein
26	34	AT3G54820	-2.85	PIP2;5/PIP2D (plasma membrane intrinsic protein 2;5); water channel
27	30	AT4G23180	-2.84	CRK10 (CYSTEINE-RICH RLK10); kinase Encodes a receptor-like protein kinase
28	10	AT1G10640	-2.81	polygalacturonase, putative / pectinase, putative
29	35	AT4G29020	-2.81	glycine-rich protein
30	10	AT1G02460	-2.80	glycoside hydrolase family 28 protein / polygalacturonase (pectinase) family protein
31	35	AT4G13750	-2.76	ATP binding similar to unknown protein AT1G08300.1
32	35	AT4G23440	-2.74	transmembrane receptor
33	28	AT3G12860	-2.74	nucleolar protein Nop56, putative
34	17	AT5G12270	-2.74	oxidoreductase, 2OG-Fe(II) oxygenase family protein
35	35	AT1G16500	-2.73	similar to unknown protein AT1G79160.1
36	20	AT2G17060	-2.73	disease resistance protein (TIR-NBS-LRR class), putative
37	29	AT1G80640	-2.73	protein kinase family protein
38	35	AT1G08430	-2.73	ALMT1/ATALMT1 (AL-ACTIVATED MALATE TRANSPORTER 1); malate transporter Encodes a Al-activated malate efflux transporter
39	29	AT4G22250	-2.71	zinc finger (C3HC4-type RING finger) family protein similar to protein binding / zinc ion binding AT4G03965.1
40	35	AT1G49000	-2.69	similar to unknown protein AT3G18560.1
41	33	AT5G50570 /// AT5G50670	-2.67	squamosa promoter-binding protein, putative
42	33	AT3G15670	-2.64	late embryogenesis abundant protein, putative
43	16	AT1G74010	-2.64	strictosidine synthase family protein
44	35	AT5G07830	-2.64	glycosyl hydrolase family 79 N-terminal domain-containing protein Identical to Heparanase-like protein 1 precursor (EC 3.2.-.-) Q9FF10;GB:Q9SDA1
45	29	AT4G20430	-2.63	subtilase family protein
46	35	AT1G29195	-2.62	similar to unknown protein AT2G30230.1
47	35	AT5G06480	-2.61	MD-2-related lipid recognition domain-containing protein / ML domain-containing protein
48	35	AT5G48360	-2.60	formin homology 2 domain-containing protein / FH2 domain-containing protein
49	30	AT3G28040	-2.58	leucine-rich repeat transmembrane protein kinase, putative
50	35	AT5G45560	-2.58	pleckstrin homology (PH) domain-containing protein / lipid-binding START domain-containing protein similar to EDR2 (enhanced disease resistance 2), lipid binding AT4G19040.1
51	29	AT1G07430	-2.57	protein phosphatase 2C, putative / PP2C, putative
52	31	AT5G48330	-2.57	regulator of chromosome condensation (RCC1) family protein similar to UVR8 (UVB-RESISTANCE 8) AT5G63860.1
53	10	AT4G24430	-2.56	lyase similar to lyase AT1G09880.1
54	27	AT4G20910	-2.56	hen1 (hua enhancer 1) encodes an enhancer of hua1 and hua2 tha acts to specify reproductive organ identities and to repress a gene function
55	35	AT5G43790	-2.55	pentatricopeptide (PPR) repeat-containing protein
56	26	AT5G45670	-2.55	GDSL-motif lipase/hydrolase family protein
57	33	AT2G36640	-2.54	ATECP63 (EMBRYONIC CELL PROTEIN 63) Encodes putative phosphotyrosine protein belonging to late embryogenesis abundant (LEA) protein in group 3 that might be involved in maturation and desiccation tolerance of seeds
58	26	AT5G18470	-2.54	curculin-like (mannose-binding) lectin family protein similar to lectin protein kinase family protein AT1G67520.1
59	17	AT1G28370	-2.51	ATERF11/ERF11 (ERF domain protein 11); DNA binding / transcription factor/ transcriptional repressor encodes a member of the ERF (ethylene response factor) subfamily B-1 of ERF/AP2 transcription factor family
60	33	AT3G53040	-2.51	late embryogenesis abundant protein, putative
61	33	AT1G75900	-2.51	family II extracellular lipase 3 (EXL3)
62	26	AT3G26830	-2.50	PAD3 (PHYTOALEXIN DEFICIENT 3); oxygen binding Mutations in pad3 are defective in biosynthesis of the indole derived phytoalexin camalexin
63	29	AT2G19720	-2.50	Identical to 40S ribosomal protein S15a-2 (RPS15AB) O82205
64	26	AT1G26380	-2.48	FAD-binding domain-containing protein
65	17	AT1G10810	-2.48	aldo/keto reductase family protein
66	31	AT1G77580	-2.47	myosin heavy chain-related
67	35	AT1G73930	-2.47	similar to Os03g0259700 [Oryza sativa (japonica cultivar-group)] NP_001049615.1

68	10	AT4G38770	-2.46	PRP4 (PROLINE-RICH PROTEIN 4) Encodes one of four proline-rich proteins in Arabidopsis which are predicted to localize to the cell wall
69	35	AT5G26790	-2.45	similar to unknown protein AT1G06475.1
70	29	AT3G53380	-2.45	lectin protein kinase family protein
71	27	AT5G14750	-2.45	WER (WEREWOLF 1); DNA binding / transcription factor Encodes a MyB-related protein involved in root and hypocotyl epidermal cell fate determination
72	35	AT1G48460	-2.44	similar to unknown protein AT5G63040.2
73	35	AT1G21710	-2.43	OGG1 (8-oxoguanine-DNA glycosylase 1) Encodes 8-oxoguanine-DNA glycosylase
74	33	AT4G18510	-2.42	CLE2 (CLAVATA3/ESR-RELATED); receptor binding CLE2, putative ligand, member of large gene family homologous to Clavata3
75	29	AT4G17480	-2.41	palmitoyl protein thioesterase family protein
76	27	AT3G19360	-2.41	zinc finger (CCCH-type) family protein
77	35	AT5G04930	-2.40	ALA1 (AMINOPHOSPHOLIPID ATPASE1); ATPase, coupled to transmembrane movement of ions, phosphorylative mechanism Encodes a putative aminophospholipid translocase (p-type ATPase) involved in chilling response
78	34	AT2G03240	-2.40	EXS family protein / ERD1/XPR1/SYG1 family protein
79	3	AT1G78090	-2.40	ATTPPB (TREHALOSE-6-PHOSPHATE PHOSPHATASE) homologous to the C-terminal part of microbial trehalose-6-phosphate phosphatases
80	11	AT1G13430 /// AT2G14920	-2.40	sulfotransferase family protein
81	35	AT5G01030	-2.39	similar to unknown protein AT2G37930.1
82	29	AT5G45650	-2.39	subtilase family protein
83	10	AT3G02570	-2.39	MEE31 (maternal effect embryo arrest 31); mannose-6-phosphate isomerase
84	35	AT1G23040	-2.38	hydroxyproline-rich glycoprotein family protein similar to proline-rich family protein AT1G70990.1
85	28	AT3G56270	-2.38	similar to unknown protein AT2G40480.1
86	10	AT4G23920	-2.37	UGE2 (UDP-D-glucose/UDP-D-galactose 4-epimerase 2); UDP-glucose 4-epimerase/ protein dimerization Encodes a protein with UDP-D-glucose 4-epimerase activity
87	35	AT5G12970	-2.37	C2 domain-containing protein
88	29	AT2G20650	-2.37	zinc finger (C3HC4-type RING finger) family protein similar to zinc ion binding AT4G28370.1
89	33	AT3G60630	-2.37	scarecrow transcription factor family protein
90	26	AT5G52320	-2.36	CYP96A4 (cytochrome P450, family 96, subfamily A, polypeptide 4); oxygen binding member of CYP96A
91	34	AT1G19650	-2.36	SEC14 cytosolic factor, putative / phosphoglyceride transfer protein, putative
92	26	AT1G55260	-2.36	lipid binding similar to lipid transfer protein-related AT2G44300.1
93	33	AT5G23730	-2.36	nucleotide binding similar to transducin family protein / WD-40 repeat family protein AT5G52250.1
94	35	AT1G69260	-2.36	similar to unknown protein AT1G13740.1
95	23	AT5G63980	-2.35	SAL1 (FIERY1); 3'(2'),5'-bisphosphate nucleotidase/ inositol or phosphatidylinositol phosphatase encodes a bifunctional protein that has 3'(2'),5'-bisphosphate nucleotidase and inositol polyphosphate 1-phosphatase activities and rescues sulfur assimilation mutants in yeast
96	35	AT5G11890	-2.35	similar to unknown protein AT1G17620.1
97	27	AT3G44260	-2.34	CCR4-NOT transcription complex protein, putative
98	30	AT4G17615	-2.34	CBL1 (CALCINEURIN B-LIKE PROTEIN 1); calcium ion binding member of AtCBLs (Calcineurin B-like Calcium Sensor Proteins)
99	35	AT1G50590	-2.34	pirin, putative Identical to Putative pirin-like protein At1g50590 Q9LPS9;GB:Q9C6P9
100	31	AT4G39920	-2.33	POR (PORCINO) Microtubule-folding cofactor, produces assembly-competent alpha-/beta-tubulin heterodimers
101	30	AT1G30570	-2.33	protein kinase family protein
102	35	AT5G15860	-2.32	ATPCME (PRENYLCYSTEINE METHYLESTERASE); prenylcysteine methylesterase
103	35	AT4G17430	-2.32	similar to hypothetical protein 31.t00055 [Brassica oleracea] ABD65093.1
104	29	AT2G25880	-2.32	ATAUR2 (ATAURORA2); histone serine kinase(H3-S10 specific) / kinase Encodes a member of a family of Ser/Thr kinases whose activities peak during cell division
105	34	AT5G03280	-2.31	EIN2 (ETHYLENE INSENSITIVE 2); transporter Involved in ethylene signal transduction
106	35	AT5G03190	-2.31	similar to unknown protein AT3G53400.1
107	34	AT1G29520	-2.31	AWPM-19-like membrane family protein
108	35	AT3G18500	-2.31	similar to endonuclease/exonuclease/phosphatase family protein AT1G73875.1
109	20	AT5G38910	-2.31	germin-like protein, putative
110	17	AT1G75450	-2.30	CKX5 (CYTOKININ OXIDASE 5); cytokinin dehydrogenase
111	29	AT3G48350	-2.30	cysteine proteinase, putativeterPro domain Peptidase C1A, papain C-terminal; (InterPro:IPR000668)

112	10	AT3G62060	-2.30	pectinacetylesterase family protein
113	35	AT2G39370	-2.30	similar to unknown protein AT2G37380.1
114	13	AT3G61300	-2.30	C2 domain-containing protein
115	28	AT1G27880	-2.29	ATP-dependent DNA helicase, putative similar to RecQl3 (Recq-like 3), ATP binding / ATP-dependent helicase AT4G35740.1
116	35	AT3G49880	-2.29	glycosyl hydrolase family protein 43
117	33	AT2G44670	-2.29	senescence-associated protein-related
118	27	AT2G35160	-2.29	SUVH5 (SU(VAR)3-9 HOMOLOG 5) Encodes SU(var)3-9 homologue 5 (SUVH5)
119	20	AT4G14630	-2.28	GLP9 (GERMIN-LIKE PROTEIN 9); manganese ion binding / metal ion binding / nutrient reservoir germin-like protein with N-terminal signal sequence that may target it to the vacuole, plasma membrane and/or outside the cell
120	30	AT3G47480	-2.28	calcium-binding EF hand family protein
121	35	AT4G28085	-2.27	unknown protein
122	20	AT2G19990	-2.27	PR-1-LIKE (PATHOGENESIS-RELATED PROTEIN-1-LIKE) Encodes a PR-1-like protein homolog that is differentially expressed in resistant compared to susceptible cultivars by powdery mildew infection
123	35	AT5G40460	-2.26	similar to unknown protein AT3G27630.1
124	27	AT1G56110	-2.26	NOP56 (ARABIDOPSIS HOMOLOG OF NUCLEOLAR PROTEIN NOP56)
125	13	AT5G06300	-2.26	carboxy-lyase similar to unknown protein AT2G37210.1
126	35	AT5G44370	-2.26	transporter-related similar to ANTR2 (anion transporter 2), organic anion transporter AT4G00370.1
127	35	AT4G12700	-2.25	similar to unknown protein AT2G04280.1
128	30	AT5G65830	-2.25	leucine-rich repeat family protein
129	26	AT3G16530	-2.25	legume lectin family protein Lectin like protein whose expression is induced upon treatment with chitin oligomers
130	35	AT2G28650	-2.25	ATEXO70H8 (exocyst subunit EXO70 family protein H8); protein binding A member of EXO70 gene family, putative exocyst subunits, conserved in land plants
131	13	AT2G04400	-2.25	indole-3-glycerol phosphate synthase (IGPS) Identical to Indole-3-glycerol phosphate synthase, chloroplast precursor (EC 4.1.1.48) (IGPS) P49572;GB:Q8LBV5;GB:Q9SJC9
132	29	AT4G02390	-2.25	APP (ARABIDOPSIS POLY(ADP-RIBOSE) POLYMERASE); NAD+ ADP-ribosyltransferase Encodes a DNA dependent nuclear poly (ADP-ribose) polymerase (E.C.2.4.2.30), thought to be involved in post-translational modification
133	11	AT3G11430	-2.24	ATGPAT5/GPAT5 (GLYCEROL-3-PHOSPHATE ACYLTRANSFERASE 5); 1-acylglycerol-3-phosphate O-acyltransferase/ acyltransferase/ organic anion transporter Encodes a protein with glycerol-3-phosphate acyltransferase activity, involved in the biosynthesis of suberin polyester
134	10	AT5G55730	-2.24	FLA1 (FLA1) fasciclin-like arabinogalactan-protein 1 (Fla1) Identical to Fasciclin-like arabinogalactan protein 1 precursor (FLA1) Q9FM65;Q8L8T1
135	27	AT1G75710	-2.24	zinc finger (C2H2 type) family protein
136	29	AT5G26960	-2.24	kelch repeat-containing F-box family protein
137	31	AT5G14230	-2.23	ankyrin repeat family protein similar to XBAT32 (XB3 ortholog 2 in Arabidopsis thaliana 32), protein binding / zinc ion binding AT5G57740.1
138	27	AT5G51590	-2.23	DNA-binding protein-related
139	27	AT4G14770	-2.22	(at4g14770); tesmin/TSO1-like CXC domain-containing protein similar to TSO1 (CHINESE FOR 'UGLY'), transcription factor [Arabidopsis thaliana] (TAIR:AT3G22780.1); similar to Calcium-binding EF-hand; Tesmin/TSO1-like, CXC [Medicago truncatula] (GB:ABE82953.1); contains InterPro domain Tesmin/TSO1-like, CXC; (InterPro:IPR005172)
140	30	AT3G13720	-2.22	prenylated rab acceptor (PRA1) family protein
141	26	AT1G62540	-2.22	flavin-containing monooxygenase family protein / FMO family protein
142	30	AT1G34110	-2.22	leucine-rich repeat transmembrane protein kinase, putative
143	3 and 21	AT3G02870	-2.22	chr3:627749-629689 REVERSEhighly similar to (511)AT3G02870| Symbols: VTC4 | VTC4; 3'(2'),5'-bisphosphate nucleotidase/ inositol or phosphatidylinositol phosphatase
144	34	AT2G26910	-2.21	ATPDR4/PDR4 (PLEIOTROPIC DRUG RESISTANCE 4); ATPase, coupled to transmembrane movement of substances
145	30	AT5G11100	-2.21	ATSYTD/NTMC2T2.2/NTMC2TYPE2.2/SYTD
146	34	AT1G22570	-2.21	proton-dependent oligopeptide transport (POT) family protein
147	14	AT2G14750	-2.21	ATP binding / kinase/ transferase, transferring phosphorus-containing groups
148	35	AT3G13590	-2.21	DC1 domain-containing protein
149	26	AT4G14940	-2.21	ATAO1 (Arabidosis thaliana amine oxidase 1); copper ion binding atao1 gene of Arabidopsis thaliana
150	26	AT1G52400	-2.21	BGL1 (BETA-GLUCOSIDASE HOMOLOG 1); hydrolase, hydrolyzing O-glycosyl compounds encodes a member of glycosyl hydrolase family 1
151	33	AT1G04770	-2.20	male sterility MS5 family protein
152	34	AT5G27150	-2.20	NHX1 (NA+/H+ EXCHANGER); sodium:hydrogen antiporter

153	26	AT2G35100	-2.20	ARAD1 (ARABINAN DEFICIENT 1); catalytic Putative glycosyltransferase
154	29	AT3G16290	-2.19	EMB2083 (EMBRYO DEFECTIVE 2083); ATPase/ metallopeptidase
155	35	AT4G24380	-2.19	hydrolase, acting on ester bonds s
156	29	AT3G14370	-2.19	WAG2; kinase The WAG2 and its homolog, WAG1 each encodes protein-serine/threonine kinase that are nearly 70% identical to PsPK3 protein
157	35	AT1G65180	-2.19	DC1 domain-containing protein
158	30	AT5G55830	-2.19	lectin protein kinase, putative
159	35	AT5G11870	-2.19	similar to SAG18 (Senescence associated gene 18)
160	35	AT5G02230	-2.18	haloacid dehalogenase-like hydrolase family protein
161	26	AT3G01510	-2.18	5'-AMP-activated protein kinase beta-1 subunit-related
162	35	AT3G50640	-2.18	similar to unknown protein AT5G66800.1
163	27	AT3G25990	-2.18	DNA-binding protein GT-1-related
164	35	AT1G63130	-2.18	pentatricopeptide (PPR) repeat-containing protein
165	20	AT5G52300	-2.18	RD29B (RESPONSIVE TO DESSICATION 29B) encodes a protein that is induced in expression in response to water deprivation such as cold, high-salt, and dessication
166	35	AT1G21560	-2.18	similar to unknown protein AT4G01170.1
167	29	AT3G02110	-2.17	SCPL25 (serine carboxypeptidase-like 25); serine carboxypeptidase
168	26	AT2G47140	-2.17	short-chain dehydrogenase/reductase (SDR) family protein s
169	35	AT3G13674	-2.17	similar to unknown protein AT1G55205.1
170	35	AT3G63290	-2.17	similar to unknown protein AT4G13400.1
171	31	AT4G22540	-2.17	oxysterol-binding family protein
172	11 and 32	AT5G16230	-2.16	acyl-(acyl-carrier-protein) desaturase, putative / stearoyl-ACP desaturase, putative
173	29	AT3G17750	-2.16	protein kinase family protein
174	29	AT5G40540	-2.16	protein kinase, putative similar to ATN1, kinase/ protein threonine/tyrosine kinase AT3G27560.1
175	23	AT5G63990	-2.16	3'(2'),5'-bisphosphate nucleotidase, putative / inositol polyphosphate 1-phosphatase, putative
176	35	AT4G21720	-2.16	similar to Os04g0680300
177	35	AT2G17550	-2.16	similar to unknown protein AT2G20240.1
178	35	AT2G26110	-2.16	similar to unknown proteinAT4G26130.1
179	27 and 33	AT4G28530	-2.16	ANAC074 (Arabidopsis NAC domain containing protein 74)
180	35	AT3G17520	-2.16	late embryogenesis abundant domain-containing protein
181	35	AT4G17215	-2.15	similar to unknown protein AT5G47635.1
182	35	AT4G37110	-2.15	protein binding / zinc ion binding
183	27	AT1G18570	-2.15	MYB51 (myb domain protein 51); DNA binding / transcription factor putative transcription factor
184	35	AT1G32690	-2.15	similar to unknown proteinAT2G35200.1
185	27	AT3G51960	-2.15	bZIP family transcription factor
186	35	AT3G27470	-2.15	similar to unknown protein AT1G67850.2
187	20	AT4G38680	-2.15	GRP2 (COLD SHOCK DOMAIN PROTEIN 2)
188	35	AT1G27100	-2.15	similar to Cytosolic fatty-acid binding; Actin-crosslinking proteins ABE82702.1
189	13	AT1G15410	-2.14	aspartate-glutamate racemase family
190	35	AT4G03820	-2.14	similar to unknown proteinAT4G22270.1)
191	30	AT2G18470	-2.14	protein kinase family protein similar to ATPERK1 (PROLINE EXTENSIN-LIKE RECEPTOR KINASE 1)
192	10	AT4G00110	-2.14	GAE3 (UDP-D-GLUCURONATE 4-EPIMERASE 3); catalytic
193	35	AT5G26731	-2.14	similar to unknown proteinAT3G05937.1
194	34	AT3G24840	-2.13	SEC14 cytosolic factor, putative / phosphoglyceride transfer protein, putative
195	35	AT5G43040	-2.13	DC1 domain-containing protein
196	20	AT5G66590	-2.13	allergen V5/Tpx-1-related family protein
197	31	AT3G54870	-2.13	MRH2 (morphogenesis of root hair 2); microtubule motor Armadillo-repeat containing kinesin-related protein
198	31	AT5G60930	-2.13	chromosome-associated kinesin, putative
199	35	AT1G78650	-2.13	similar to unknown proteinAT2G22795.1
200	28	AT1G74560	-2.12	NRP1 (NAP1-RELATED PROTEIN 1); DNA binding / chromatin binding / histone binding Double nrp1-1 nrp2-1 mutants show arrest of cell cycle progression at G2/M and disordered cellular organization occurred in root tips
201	34	AT5G10180	-2.12	AST68 (Sulfate transporter 2.1)
202	16	AT2G41300	-2.12	strictosidine synthase
203	35	AT2G29050	-2.12	ATRBL1 (ARABIDOPSIS THALIANA RHOMBOID-LIKE 1)
204	29	AT2G27920	-2.12	SCPL51; serine carboxypeptidase
205	35	AT4G37680 /// AT4G38320	-2.12	HHP4 (heptahelical protein 4); receptor heptahelical transmembrane protein HHP4
206	35	AT4G27010	-2.11	binding similar to unknown protein AT1G72270.1
207	30	AT5G61570	-2.11	protein kinase family protein similar to protein kinase family protein AT5G07620.1
208	35	AT2G35155	-2.11	similar to unknown proteinAT5G45030.2)

209	35	AT5G15600	-2.11	SP1L4 (SPIRAL1-LIKE4) SPIRAL1-LIKE4 belongs to a six-member gene family in Arabidopsis
210	34	AT3G47780	-2.11	ATATH6 (ABC2 homolog 6); ATPase, coupled to transmembrane movement of substances member of ATH subfamily
211	30	AT5G46080	-2.11	protein kinase family protein
212	31	AT1G52080	-2.11	actin binding unknown function
213	27	AT2G40260	-2.10	myb family transcription factor
214	26	AT3G46650	-2.10	UDP-glucoronosyl/UDP-glucosyl transferase family protein
215	28	AT3G50900	-2.10	similar to unknown protein AT5G66490.1
216	29	AT3G06030	-2.10	ANP3 (Arabidopsis NPK1-related protein kinase 3)
217	35	AT3G60040 /// AT3G60050	-2.10	F-box family protein
218	35	AT3G60380	-2.10	similar to hydroxyproline-rich glycoprotein family protein AT4G16790.1
219	27	AT5G22250	-2.10	CCR4-NOT transcription complex protein, putative
220	33	AT1G76800	-2.10	nodulin, putative similar to nodulin, putativeAT3G43660.1
221	29	AT2G17030	-2.10	F-box family protein
222	30	AT4G00460	-2.10	ATROPGEF3/ROPGEF3 (KINASE PARTNER PROTEIN-LIKE)
223	27	AT3G57660	-2.10	NRPA1 (nuclear RNA polymerase A 1); DNA binding / DNA-directed RNA polymerase
224	29	AT1G22050	-2.10	ubiquitin family protein
225	17	AT5G57090	-2.10	EIR1 (ETHYLENE INSENSITIVE ROOT 1); auxin:hydrogen symporter/ transporter
226	35	AT2G28870	-2.10	similar to unknown protein AT5G59360.1
227	26	AT3G24040	-2.10	glycosyltransferase family 14 protein / core-2/I-branching enzyme family protein
228	20	AT2G43620	-2.09	chitinase, putative
229	29	AT1G76360	-2.09	protein kinase, putative
230	31	AT4G29340	-2.09	PRF4 (PROFILIN 4); actin binding Profilin is a low-molecular weight, actin monomer-binding protein that regulates the organization of actin cytoskeleton in eukaryotes, including higher plants
231	29	AT3G17340	-2.09	protein transporter similar to protein transporter AT3G59020.2
232	34	AT4G17550	-2.09	transporter-related similar to glycerol-3-phosphate transporter
233	30	AT5G41180	-2.09	leucine-rich repeat protein kinase, putative
234	17	AT2G22830	-2.08	squalene monooxygenase, putative / squalene epoxidase, putative
235	11	AT3G25540	-2.08	LAG1 (Longevity assurance gene 1) LAG1 homolog 1
236	34	AT1G16000 /// AT1G16010	-2.08	magnesium transporter CorA-like family protein (MRS2-1)
237	29	AT2G22010	-2.08	zinc finger (C3HC4-type RING finger) family protein
238	32	AT2G44260	-2.08	other RNA Potential natural antisense gene, locus overlaps with AT2G44260
239	11	AT5G59320	-2.07	LTP3 (LIPID TRANSFER PROTEIN 3); lipid binding lipid transfer protein 3
240	26	AT5G63840	-2.07	RSW3 (RADIAL SWELLING 3); hydrolase, hydrolyzing O-glycosyl compounds radial swelling mutant shown to be specifically impaired in cellulose production
241	35	AT2G42560	-2.07	late embryogenesis abundant domain-containing protein / LEA domain-containing protein
242	29	AT5G10790	-2.07	UBP22 (UBIQUITIN-SPECIFIC PROTEASE 22)
243	34	AT1G21070	-2.07	transporter-related
244	27	AT5G50020	-2.07	zinc finger (DHHC type) family protein
245	35	AT3G07080	-2.06	membrane protein
246	27	AT5G56200	-2.06	zinc finger (C2H2 type) family protein
247	20	AT5G45210	-2.06	disease resistance protein (TIR-NBS-LRR class), putative
248	29	AT2G45270	-2.06	glycoprotease M22 family protein
249	29	AT1G33940 /// AT5G18700	-2.06	EMB3013 (EMBRYO DEFECTIVE 3013); kinase
250	35	AT4G28220 /// AT4G28230	-2.06	unknown protein
251	35	AT2G39795	-2.06	mitochondrial glycoprotein family protein / MAM33 family protein
252	27	AT5G13910	-2.06	LEP (LEAFY PETIOLE); DNA binding / transcription factor Encodes a member of the ERF (ethylene response factor) subfamily B-1 of ERF/AP2 transcription factor family (LEAFY PETIOLE)
253	31	AT3G27960	-2.06	kinesin light chain-related
254	34	AT2G39350	-2.06	ABC transporter family protein
255	11	AT4G04870	-2.06	CLS (CARDIOLIPIN SYNTHASE); cardiolipin synthase/ phosphatidyltransferase Cardiolipin synthase
256	26	AT1G69920	-2.05	ATGSTU12 (Arabidopsis thaliana Glutathione S-transferase (class tau) 12); glutathione transferase
257	34	AT3G26520	-2.05	TIP2 (TONOPLAST INTRINSIC PROTEIN 2); water channel gamma tonoplast intrinsic protein 2 (TIP2)
258	34	AT3G55320	-2.05	PGP20 (P-GLYCOPROTEIN 20); ATPase, coupled to transmembrane movement of substances
259	35	AT2G04280	-2.05	similar to unknown protein AT4G12700.1

260	35	AT1G68490	-2.05	similar to unknown protein AT1G13390.2
261	31 and 32	AT3G54630	-2.05	similar to unknown protein AT5G27330.1
262	29	AT3G20620	-2.05	F-box family protein-related
263	30	AT5G48940	-2.05	leucine-rich repeat transmembrane protein kinase, putative
264	29	AT5G52880	-2.05	F-box family protein similar to Cyclin-like F-box ABE83073.1
265	31	AT2G29550	-2.05	TUB7 (tubulin beta-7 chain)
266	29	AT3G19440	-2.05	pseudouridine synthase family protein
267	35	AT3G54980	-2.04	pentatricopeptide (PPR) repeat-containing protein
268	35	AT3G20430	-2.04	similar to Os01g0559200
269	13	AT5G49810	-2.04	MMT (methionine S-methyltransferase)
270	27	AT1G03530	-2.04	similar to unknown protein AT5G66540.1
271	35	AT2G19660	-2.04	DC1 domain-containing protein
272	30	AT1G48630	-2.04	guanine nucleotide-binding family protein / activated protein kinase C receptor, putative
273	23	AT5G03300	-2.04	ADK2 (ADENOSINE KINASE 2); kinase
274	27	AT3G05690	-2.04	HAP2B (Heme activator protein (yeast) homolog 2B, unfertilized embryo sac 8); transcription factor
275	16	AT3G21420	-2.04	oxidoreductase, 2OG-Fe(II) oxygenase family protein
276	26	AT4G26940	-2.04	galactosyltransferase family protein
277	27	AT1G68990	-2.03	DNA-directed RNA polymerase, mitochondrial (RPOMT)
278	29	AT1G33360	-2.03	ATP-dependent Clp protease ATP-binding subunit ClpX, putative
279	35	AT5G60840	-2.03	unknown protein
280	20	AT5G40020	-2.03	pathogenesis-related thaumatin family protein
281	31	AT4G37630	-2.03	CYCD5;1 (CYCLIN D5;1); cyclin-dependent protein kinase core cell cycle genes
282	26	AT2G18140 /// AT2G18150	-2.03	peroxidase, putative
283	26	AT2G02850	-2.03	ARPN (PLANTACYANIN); copper ion binding
284	20	AT4G19720	-2.03	glycosyl hydrolase family 18 protein
285	26	AT5G63800	-2.02	BGAL6 (beta-galactosidase 6)
286	27	AT4G02820	-2.02	pentatricopeptide (PPR) repeat-containing protein
287	29	AT5G64580	-2.02	AAA-type ATPase family protein
288	27	AT3G14740	-2.02	PHD finger family protein
289	34	AT1G59740	-2.02	proton-dependent oligopeptide transport (POT) family protein
290	35	AT4G38710	-2.02	glycine-rich protein
291	28	AT2G24490	-2.02	ATRPA2/ROR1/RPA2 (REPLICON PROTEIN A); protein binding
292	30	AT4G31250	-2.02	leucine-rich repeat transmembrane protein kinase, putative
293	27	AT2G33860	-2.02	ETT (ETTIN); transcription factor ettin (ett) mutations have pleiotropic effects on Arabidopsis flower development, causing increases in perianth organ number, decreases in stamen number and anther formation, and apical-basal patterning defects in the gynoecium
294	30	AT5G22400	-2.02	rac GTPase activating protein, putative similar to rac GTPase activating protein, putative AT3G11490.1
295	31	AT1G50360	-2.02	VIIIA (Myosin-like protein VIIA); motor member of Myosin-like proteins
296	9	AT1G57600	-2.02	membrane bound O-acyl transferase (MBOAT) family protein
297	26	AT3G61130	-2.02	GAUT1/LGT1 (Galacturonosyltransferase 1); polygalacturonate 4-alpha-galacturonosyltransferase/ transferase, transferring glycosyl groups
298	20	AT1G28290	-2.02	pollen Ole e 1 allergen and extensin family protein
299	30	AT3G21510	-2.01	AHP1 (HISTIDINE-CONTAINING PHOSPHOTRANSMITTER 3); histidine phosphotransfer kinase Encodes AHP1, one of the six Arabidopsis thaliana histidine phosphotransfer proteins (AHPs)
300	35	AT2G37560 /// AT2G37570	-2.01	ATORC2/ORC2 (ORIGIN RECOGNITION COMPLEX SECOND LARGEST SUBUNIT); DNA replication origin binding / protein binding Origin Recognition Complex subunit 2
301	34	AT1G16780	-2.01	vacuolar-type H+-translocating inorganic pyrophosphatase, putative
302	29	AT1G17550	-2.01	HAB2 (Homology to ABI2); protein phosphatase type 2C Protein Phosphatase 2C
303	35	AT5G61660	-2.01	glycine-rich protein similar to glycine-rich protein AT5G46730.1
304	29	AT1G20140 /// AT2G25700	-2.01	ASK3 (ARABIDOPSIS SKP1-LIKE 3); protein binding / ubiquitin-protein ligase E3 ubiquitin ligase SCF complex subunit SKP1/ASK1 (At3), putative, E3 ubiquitin ligase
305	35	AT3G01780	-2.01	similar to unknown protein AT4G08710.1
306	27	AT1G71692	-2.00	AGL12 (AGAMOUS-LIKE 12); transcription factor AGL12, AGL14, and AGL17 are all preferentially expressed in root tissues and therefore represent the only characterized MADS box genes expressed in roots
307	10	AT2G24630	-2.00	ATCSLC08 (Cellulose synthase-like C8); transferase, transferring glycosyl groups encodes a gene
308	10	AT4G20460	-2.00	NAD-dependent epimerase/dehydratase family protein
309	27	AT3G28920	-2.00	ATHB34 (ARABIDOPSIS THALIANA HOMEOBOX PROTEIN 34); DNA binding / transcription factor

310	27	AT1G63650	-2.00	EGL3 (ENHANCER OF GLABRA3); DNA binding / transcription factor Mutant has reduced trichomes, anthocyanin, and seed coat mucilage and abnormally patterned stomates
311	30	AT1G11130	-2.00	SUB (STRUBBELIG); protein binding Encodes a receptor-like kinase protein with a predicted extracellular domain of six leucine-rich repeats and an intracellular serine-threonine kinase domain expressed throughout the developing root

VITA

Won-Gyu Choi was born in Muju, Jeonbuk, South Korea on May 5, 1974. He entered the Woosuk University, Jeonbuk, South Korea in March of 1993 and graduated with a Bachelor of Science degree in Biotechnology in February of 2000. In the middle of his undergraduate career, he served mandatory military service for 3 years in South Korea. After graduation with a BS degree, he continued study in graduate school at the Woosuk University and graduated with a Maters of Science degree in Biotechnology in February of 2002. After graduation with a MS degree, he moved to the United States of America and entered the University of Tennessee, Knoxville in the Department of Biochemistry and Cellular and Molecular Biology in August of 2003. During his tenure at the University of Tennessee, he was employed as a graduate teaching assistant (GTA) from August 2003 to May 2009.

He joined and began his Ph.D training in Dr. Daniel Roberts' laboratory at the University of Tennessee, Knoxville in August of 2004. During his graduate work he worked on the two soybean nodulin 26 ortholog Arabidopsis nodulin 26-like intrinsic proteins (NIPs), NIP2;1 and NIP7;1, and contributed new discoveries on their functional properties and roles of adaptation to low oxygen stress, and development. As a result of his graduate studies in both Korea and USA, he published and presented his research (see below for details).

He was married to Su-Hwa Kim in 2005 and they have a son, Alexander Choi.